Linear Polymers to Target *Vibrio cholerae* Adhesion and Physiology

by

Oliver Creese

UNIVERSITY OF BIRMINGHAM

A thesis submitted to the University of Birmingham for the degree of

DOCTOR OF PHILOSOPHY

School of Chemistry

College of Engineering and Physical Sciences

University of Birmingham

October 2019

Abstract of the Thesis

Linear Polymers to Target *Vibrio cholerae* Adhesion and Physiology

Oliver Creese

A key stage in bacterial pathogenesis is the ability of bacteria to adhere strongly and specifically to the host. Bacterial adhesion to host cells is a prerequisite for infection and disease, and with this in mind, synthetic polymers rationally designed to incorporate side-chain functionality targeting bacterial adhesion mechanisms have been reported to cluster bacteria *via* specific and non-specific multivalent interactions. Targeting bacteria in this way may have therapeutic value towards controlling drug resistant pathogens. However, progress in this area has been slow due to an incomplete understanding of polymer-bacteria interactions as well as technical difficulties in screening large libraries of polymers efficiently under standardised chemical and biological conditions in order to assess structure-activity relationships of these macromolecules.

Here, poly(acryloyl hydrazide) is employed as a polymer scaffold capable of undergoing highly efficient post-polymerisation modifications of the side-chain under physiologically relevant conditions to facilitate the synthesis and *in situ* screening of a range of unexplored polymer chemistries towards sequestering *V. cholerae*. In particular, it was found that imidazole-functionalised polymers dramatically sequestered *V. cholerae* at sub-inhibitory concentrations, and suppressed the production of the Cholera toxin (Chapter 2), while glycopolymers resulted in accelerated biofilm production in a sugar-dependent manner (Chapter 3).

Lastly, improved RAFT polymerisation of poly(Boc-acryloyl hydrazide) by choice of polymerisation temperature is reported (Chapter 1), as well as a synthetic route towards controlled end group fluorescent labelling (Chapter 4).

Acknowledgements

A thesis is a “tip of the iceberg” in the life and work of a PhD student and the sum of many parts often not reflected in the final text. In particular, the training, collaboration or encouragement of many friends and colleagues who have made the work documented here possible, as well as invaluable contributions outside of work. With this in mind, one of the most satisfying and important parts to writing this thesis is in acknowledging and reflecting on the impact and influence of co-workers and friends (often the same) over my four years as a PhD student.

Firstly, to my primary supervisor Dr. Francisco Fernandez-Trillo (Paco) without whom, this work would not have been possible and who has had an immeasurably positive impact on my development as a researcher but also as a person. His mentoring and guidance have challenged me to achieve my best, within and outside of scientific research. I would like to take this opportunity to thank you sincerely for your time and effort in training me.

I would also like to express my gratitude to my secondary supervisor, Professor Anne-Marie Krachler, who took me in as a chemistry student with no prior experience working in biology, and has guided and trained me to conduct the microbiological research which is presented within this thesis. – thank you.

I would like to thank the University of Birmingham as a whole, but especially the academic and technical staff of the School of Chemistry and the School of biosciences. In particular, a special mention to Allen Bowden and Cécile Le Duff, responsible for the excellent running of the HPLC and NMR facility respectively, and for their individual unreserved patience and guidance when running GPCs and NMRs. From the School of Biosciences, I would like to thank sincerely the fantastic members of the Host And Pathogen Interaction (HAPI) lab for accommodating and involving me with their

research. Their support and inclusion have been invaluable, which I cannot stress enough here. A special mention goes to Dr. João Correia who patiently trained me in optical imaging techniques.

Next, I would like to sincerely thank previous members of the BioMedNano lab; Dr. Nicholas Perez-Soto (Nico) who patiently shared his microbiology knowledge with me, to Dr. Ignacio Insua (Nacho) and Dr. Daniel Crisan, for their continued friendship and huge help throughout the beginning of my project, and to Guanlong Su.

To the current members of the Paco lab; Dr. Andrey Romanyuk ,Pavan Adoni, Jose (Zelu) Brioso Jimenez, Andrew Wilkinson, Krystian Ubych, Dr. Sameh Al Sayed, Charlotte Farrow, Carlos Guillen Posteguillo, Tom Leigh, and Manal Alanzi, your help and friendship has made my time as a PhD student one that I will remember fondly, either in the lab, at conferences or on a Friday evening discussing “science” over a beer in staff house. I would also like to thank everyone who has helped me proof-read chapters (you know who you are!) in particular, to Lizzie Sargeant.

I would like to thank Professor Mathew Gibson for his impactful supervision and guidance during my first training year project, and the whole of the Gibson lab with special mentions going to Dr Sarah-Jane Richards and Dr. Ben Martyn for their help during this time.

I am particularly indebted to and would like to thank the Midlands Integrative Biosciences Training Partnership (MIBTP) who made this work possible by providing training and funding. Finally, I would like to thank my family for their unconditional support and encouragement during this time, in particular my parents, Marian and Jos, and my sister Georgie.

Table of Contents

List of Figures, Schemes and Tables

List of Abbreviations

2A3FP	2-amino-3-formyl pyridine
AcOH	Acetic Acid
AMR	Antimicrobial resistance
ATRP	Atom transfer radical polymerisation
cAMP	Cyclic adenosine monophosphate
CFU	Colony forming units
ConA	Concanavalin A
CTA	Chain transfer agent
CuAAC	Copper(I)-catalysed alkyne-azide cycloaddition
CV	Crystal violet
DA	Degree of acetylation
DIC	Differential interference contrast
DIPEA	*N*,*N*-Diisopropylethylamine
$Đ_M$	Molar mass dispersity
DMF	Dimethylformamide
DMSO	Dimethyl sulfoxide
DP	Degree of polymerisation
EDA	1,2-ethylenediamine
eq.	Molar equivalence
FITC	fluorescein isothiocyanate
FRP	Free radical polymerisation
GFP	Green fluorescent protein
GlcNAc	N-acetyl-D-glucosamine
GPC	Gel permeation chromatography
h	Hour
HOMO	Highest occupied molecular orbital
IMI	Imidazole-4-carbaldehyde
MCCA	7-methoxycoumarin-3-carboxylic acid
mg	Milligram
MHz	Megahertz

MIC	Minimum inhibitory concentration
min	Minutes
mL	Millilitres
M_n	Number average molecular mass
mol	Moles
MSHA	Mannose sensitive hemagglutinin
M_w	Weight averaged molecular mass
NHS	N-Hydroxysuccinimide
NIPAM	N-Isopropylacrylamide
NMR	Nuclear magnetic resonance
OD600	Optical density at 600 nm
PEG	Polyethylene glycol
PEO	Polyethylene oxide
PFP	Pentafluorophenol
RT	Room temperature
RAFT	Reversible addition-fragmentation chain transfer
RIU	Refractive index units
ROMP	Ring-opening metathesis polymerization
SEC	Size exclusion chromatography
SPAAC	Strain-promoted azide-alkyne cycloaddition
TCP	Toxin coregulated pilus
TFA	Trifluoroacetic acid
VPS	*Vibrio* polysaccharide
μM	Micro molar
μmol	Micro moles

Introduction

i. The rise of antibiotic resistance: the causes, consequences and solutions

Resistance to antibiotics through their misuse has been predicted since the discovery of the first antibiotic 'penicillin' by Alexander Fleming.[1] Development of resistance to antibiotics often relates to the specific nature of their mechanism against bacteria. Traditional antibiotics interfere with bacterial processes in a highly specific and selective manner, meaning that what works for one species of bacteria may not work for another. Antibiotics are classed based on their mechanism of action (**Table 1**), which generally involves the disruption of biosynthesis within the cell. However exceptions to this include antibiotics such as Polymyxin B, which interferes with the cell membrane resulting in the formation of pores.[2]

Table 1. Common antibiotics listed by their mechanism of action

Target	Classes	Examples
Cell Wall Synthesis	*Beta Lactams*	Penicillins
		Cephalosporins
		Carbapenoems
		Monobactams
	Vancomycin	
	Bacitracin	
	Cell Membrane	Polymyxins
Nucleic Acid Synthesis	*Folate synthesis*	Sulfonamides
		Trimethoprim
	DNA Gyrase	Quinolones
	RNA Polymerase	Rifampin
Protein Synthesis	*Ribosomal 50S subunit*	Macrolides
		Clidamycin
		Linezolid
		Chloramphenicol
		Streptogramins
	Ribosomal 30S subunit	Tetracyclines
		Aminoglycosides

Bacteria constantly mutate to gain evolutionary advantage,[1] and these mutations can lead to changes in crucial processes targeted by antibiotics, or can render the antibiotic non-effective. Mutated genes which advantage the bacteria are

selected for and passed to the next generation. This process is known as evolutionary pressure, and is the main cause of antimicrobial resistance. Misuse of antibiotics, for example failing to complete a prescribed course resulting in incomplete eradication of the bacteria, speeds up this process. The three major ways resistance to antibiotics is conferred are:[1]

1. Efflux pumps; membrane transport proteins which can remove or lower the concentration of the antibiotic within the bacterial cells.
2. Inactivation by enzymes which can degrade or modify the antibiotic, rendering it ineffective (β-lactamases on β-lactam antibiotics).[3,4]
3. Modification of molecular targets; random mutations can inactivate the binding site for certain antibiotics.

The increasing occurrence of multi-drug resistant microbes, coupled with a significant slowdown in new antibiotics coming to market, may result in a "post-antibiotic era" where common infections which were previously easily treatable may become life threatening. Worryingly, a review published by the World Health Organisation in 2017 highlighted that the vast majority of new drugs are modifications of existing classes of antibiotics, and thus expected to only offer a short-term solution to treating pathogenic bacteria.[5] Indeed there have been no new classes of antibiotics discovered to treat Gram-negative bacteria since 1962, and no approved drug class since 1980 (Wellcome trust 2018). Antibiotic resistance is thought to be currently responsible for over 50,000 deaths per year in the US and Europe,[6] and over 700,000 globally, with that number predicted to rise to 10 million by 2050.[7]

i. a. Anti-adhesion therapy towards controlling pathogens

There is an urgent need for new and innovative ways to combat and control microbial infection, and unsurprisingly research in this area is extensive. A key consideration for new therapies, is targeting pathogenic bacteria or bacterial processes in such a way that limits evolutionary pressure (i.e. resistant bacteria are not selected for by "survival of the fittest"). For this reason, one method proposed involves "disarming" rather than killing pathogens by targeting virulence factors.[8,9] Understanding why certain bacteria pose a threat to our health while others benefit it and the driving force behind a bacterium's "switch" from a non-pathogenic to a pathogenic is key to designing new drugs or better control practices.[10]

Bacterial adhesion to surfaces, inside and outside the body is a key process in microbial colonisation, infection and in particular is a prerequisite for many pathogens to deploy virulence factors such as toxins.[11] Common examples of such pathogens include *Escherichia coli, Pseudomonas, salmonella, Klebsiella* and *Vibrio Cholerae*.[11] As such, designing compounds that interfere with this process is a promising antimicrobial strategy.[11-13] Bacteria adhere to surfaces initially through weak non-specific interactions, which can allow them to "sample" the surface,[12] followed by much stronger receptor-mediated interactions which can include recognition of moieties such as sugars, lipids and proteins on both the bacteria and the host.[11] One of the most studied examples of a pathogen binding to a receptor is that of *E. coli* binding to mannose residues displayed on host cells *via* the bacterial adhesin FimH.[11]

Strategies targeting bacterial adhesion include the use of anti-fouling surfaces,[13,14] disruption of the bacterial or host surface receptor biogenesis,[15-17] competition-based receptor binding antagonists,[18,19] and anti-adhesion antibodies and vaccines.[20,21]

i. b Artificial bacterial adhesion antagonists

Targeting bacterial adhesion with materials which mimic natural binding sites for bacteria can offer a pathway to out-compete bacterial binding to surfaces and host cells.[22] The advantage of this particular approach is that, although mutations would be expected to occur which could affect the binding to the antagonist, these mutations would also interfere with the bacteria's ability to bind to the host, and therefore would likely be selected against.[11] One of the major hurdles in designing anti-adhesion materials or biological inhibitors in general, which may contain ligands capable of binding to bacterial receptors, is to maintain a high enough affinity to be able to compete for the target. One method of increasing affinity is through multivalency; by presenting a target receptor with many copies of a ligand covalently linked together by means of a backbone or scaffold, the overall binding affinity to the receptor is greater than that of an equal concentration of monovalent ligands.[23] The potential of highly potent multivalent biological inhibitors has driven research towards the synthesis of macromolecular architectures such as polymers, dendrimers,[24,25] and nanoparticles.[26,27]

i. c. Polymers for bacterial anti-adhesion applications

Ability to take part in non-specific binding, long range and multivalent interactions make polymers very attractive as synthetic multivalent materials to target many biological functions, including bacterial adhesion.[28] Compared with single molecules, multivalent compounds can cooperate in many different binding mechanisms, such as chelation, statistical (increasing the effective concentration at the active site) and steric stabilisation (**Figure 1**).[23,29]

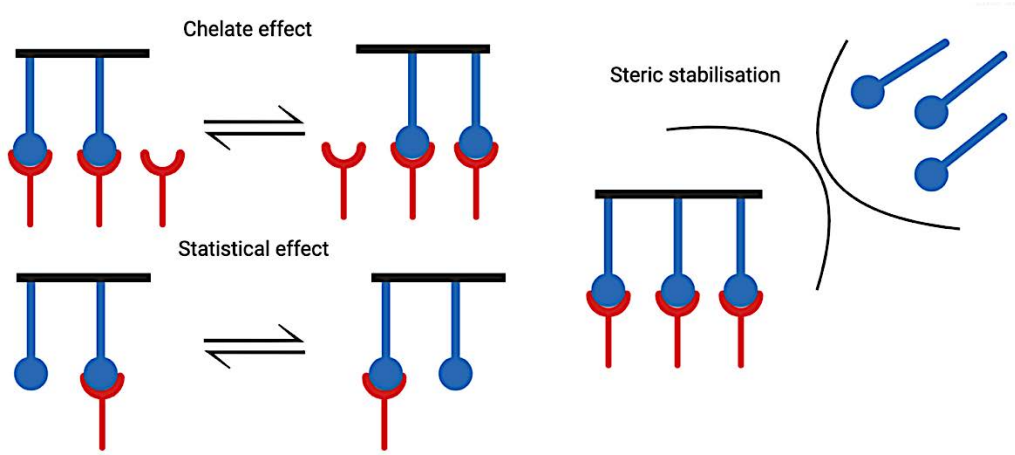

Figure 1. Example of ligands (blue) binding to a receptor (red) *via* different binding modes available to multivalent materials resulting in greater receptor affinity over that of monovalent ligands.

Increased affinity for a multivalent compound compared to its monovalent counterpart, often on orders of magnitude, is known as the "cluster glycoside effect", for example the interaction between a protein (lectin) and carbohydrate is strengthened due to presentation of multiple copies of the carbohydrate to the protein. Protein-carbohydrate interactions are one of the most important recognition motifs in biological systems and can be greatly strengthened if the carbohydrate ligand has multivalence.[23,30]

In this regard, polymers have the potential to competitively block bacterial adhesion, for example, to host cells by displaying repeat units of chemical groups mimicking binding sites for bacterial adhesion (for example, a mannose-displaying polymer as an inhibitor of *E. coli* adhesion).

i. d. Polymer-mediated bacterial aggregation

Bacteria are already known to form aggregates in the presence of polymers in nature, *via* two proposed mechanisms; bridging,[31] whereby bacteria aggregate *via* interactions between cell and polymer, dominated by multivalent interactions, and depletion aggregation, which is entropically driven. Depletion aggregation is an effect

whereby bacteria aggregate together due to osmotic forces between a non-adsorbent polymer and the bacterial cells to maximise the space available for the polymer to move (**Figure 2**).[31]

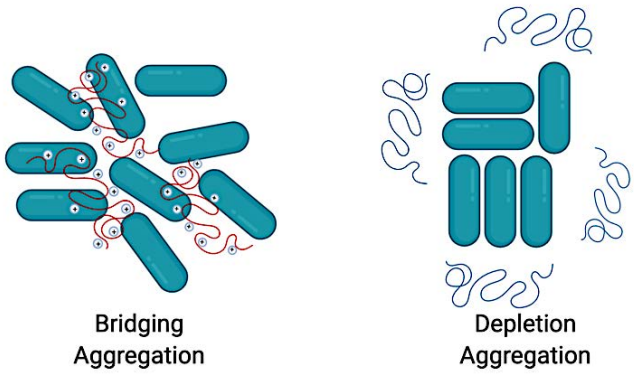

Figure 2. Types of bacterial aggregation modes as a result of interactions with polymers. Bridging aggregation is mediated by multivalent "cross-linking" interactions with the polymer, and depletion aggregation is entropically driven in order to minimise bacteria-polymer interactions.

These two proposed mechanisms result in different aggregated structures which are not considered traditional bacterial biofilms. Bridging aggregation forms disordered aggregates, and depletion aggregation resulting in laterally aligned layers of bacteria which can eventually result in a complete phase separation of bacteria and supernatant.[32]

The outcome of the bacteria-polymer interaction depends on the chemical nature of the polymer; positively charged glycopolymer chitosan induces bridging type aggregation, whereas high molecular weight neutral polyethylene glycol (PEG), and more recently vitamin B5 derived polymethacrylate have been shown to induce depletion type aggregation in bacteria. [33,34] Aggregation of bacteria can be induced by a wide range of naturally occurring polymers present at infections sites such as mucin and DNA, and it has been proposed that this aggregation can advantage the bacteria by stimulating the production of stress-response phenotypes which are less susceptible to antibiotics.[33] This example taken from nature demonstrates how

inducing aggregation of bacteria has the potential to change their phenotype, and with this in mind, assessment of these potential off-target effects when designing materials for anti-adhesion therapy should be carefully considered.

i. e. Designing linear polymers to target bacteria

Linear polymers are a class of macromolecular architecture that offer wide scope to examine the structure-activity relationships in biological applications owing to their "simple" and easily tunable chemistry.[23]

For applications requiring multivalence, the most important chemical property of linear polymers, with respect to biological activity, are the functional groups associated with the repeated chain. These can be further broken down into side-chain and main-chain functionality. Recent work carried out by Yan and co-workers investigated the impact of side-chain functionality versus main-chain functionality on the antimicrobial activity (**Figure 3**).[35]

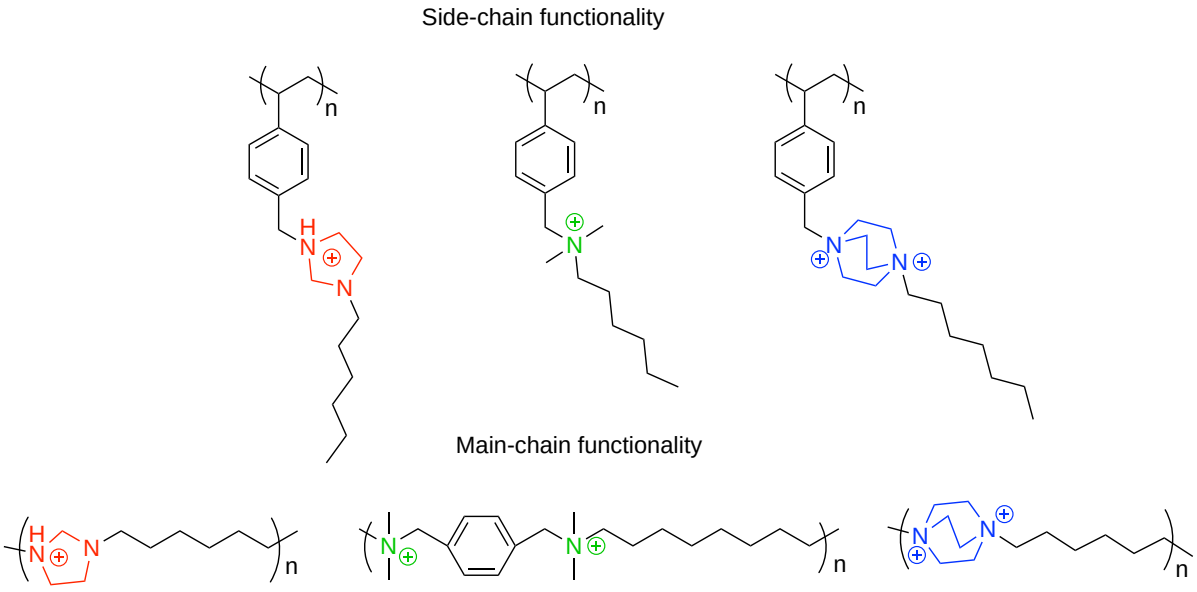

Figure 3. Examples of synthetic polymers with cationic functionality on the side-chain of the polymer or the main-chain of the polymer.[35]

The authors reported that while all polymers tested were more active against bacteria compared to their corresponding monomers, main chain functionality provided slightly higher antimicrobial activity than side-chain functionality.[35] It should be noted that polymer molecular mass was not consistent between the polymers tested.

In order for a polymer to exhibit antimicrobial activity, which will not be discussed in detail here, polymers are generally synthesised to possess positively charged groups which are strongly attracted to the negatively charged phospholipids present in bacterial cell walls.[36] The non-specific electrostatic interaction aided by hydrophobic moieties on the polymer can result in the disruption of the bacterial cell wall, eventually leading to cell death,[37] although recently there have been suggestions that these interactions may be more specific than simple electrostatics.[38]

Cationic linear polymers have also been researched for their application as bacterial sequestrants, by a mechanism of electrostatic attraction between polymer and bacteria similarly to that of antimicrobial polymers, but without conferring toxicity to the bacteria.

In this respect, the location of the positive charge on the polymer chain may be less critical for polymers designed to interact with bacteria in a non-specific manner. However in order to mediate specific receptor binding, as described earlier, ability of multivalent ligands displayed on a polymer to fit into binding pocket of a receptor is key to their activity, and as such, the majority of research into polymers for receptor binding focuses on the chemical functionality of the side-chain.[23]

It is well established that bacterial adhesion to the host cell is predominantly mediated through recognition and binding to the glycocalyx, a layer of highly heterogenous glycoconjugates which can include polysaccharides, glycolipids and glycoproteins which are expressed on the cell surface.[39] As previously discussed, this

initial adhesion step is critical for the bacteria to successfully colonise and cause disease to the host whilst being able to withstand the body's own mechanical and immunological clearance mechanisms.[11] The bacterial receptors which bind to carbohydrates in the glycocalyx are called lectins, a class of proteins that bind to but do not have enzymatic activity on carbohydrate containing ligands.[40] In fact, it has been suggested that the glycocalyx may serve as a barcode, enabling bacteria to distinguish between suitable and unsuitable binding sites *via* specific lectin binding interactions.[41] With this in mind, a common strategy is the synthesis of polymers displaying sugars on the side-chain, therefore offering a potential route to synthetic glycocalyx mimics designed to competitively bind bacterial lectins in a specific manner and inhibit the adhesion to biotic or abiotic surfaces.[42]

Current research into targeting and binding bacteria focuses on polymers containing cationic groups, targeting the negatively charged cell wall, and also polymers containing carbohydrates (glycopolymers) to target and bind to bacterial lectins (**Figure 4**).

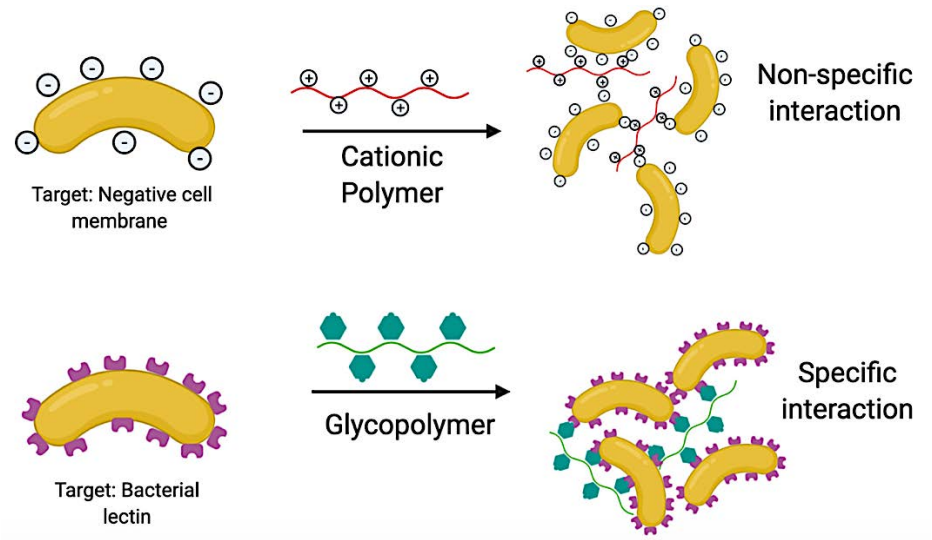

Figure 4. Approaches taken in the design of polymers to aggregate bacteria.

While certain polymer chemistries have been well explored, as will be discussed later, predicting the contribution that a particular property makes to the overall observable activity, and hence determining the mechanism of action from first principles remains difficult for macromolecules.[43] A common design goal for targeting bacterial adhesion is increasing the activity and selectivity towards a pathogen, while remaining innocuous to the host. Probing the relationship between structure and activity in these materials has become a vital element to furthering research in this area. In particular, it is often challenging to simultaneously probe how different chemistries effect a range of different biological properties. progress in this area has been slow, due to the technical difficulties in screening large libraries of polymers efficiently under standardised chemical and biological conditions, in order to better assess the structure-activity relationship of these macromolecules.

More work needs to be carried out to determine the influence of chemical and physical factors involved with polymer-mediated bacterial aggregation, to improve specificity and activity. This will be best achieved through evaluation of structure-activity relationships using large libraries of polymers with modulated properties.

One of the challenges that faces polymer chemistry is reproducibility and uncertainty over the absolute chemistry. “Normalising” the biological effect to differences in the absolute polymer chemistry is difficult even with advanced controlled polymerisation techniques and some degree of uncertainty will still remain. For this reason, polymer scaffolds which are able to undergo a wide range of side group modifications after polymerisation are attractive ways of removing the uncertainty arising from variations in polymer structure and allowing access to a wide range of potential polymer functional groups. The strength of this strategy lies in the ability to

conduct high-throughput screening, akin to drug discovery methodologies, which may uncover ideal multivalent chemistries to target bacterial adhesion.

i. f. Polymer scaffolds for biological high-throughput screening

There is a great deal of interest in designing scaffolds to access a library of polymers with different functionalities all originating from the same parent polymer.[43] The synthesis of polymer scaffolds facilitates high-throughput screening approaches, towards addressing the uncertainty associated with evaluating the activity of polymeric materials in biology (**Figure 5**).[44]

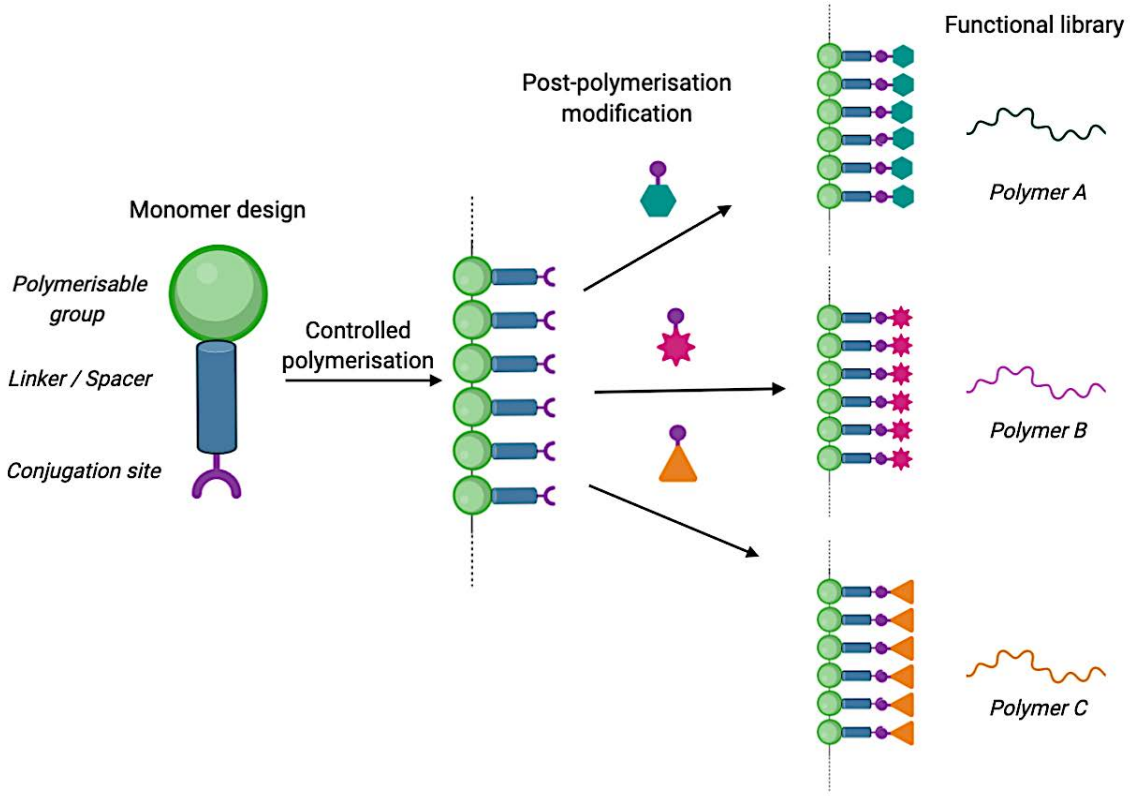

Figure 5. Description of the route taken in the synthesis of a polymer scaffold, and subsequent post-polymerisation modification towards the preparation of a library of functional polymers.

A range of possible polymerisation methods are available to the polymer chemist in order synthesise polymers capable of undergoing further post-

polymerisation modification, but there are some “design goals” which should be considered.

To begin with, the chemical group capable of undergoing post-polymerisation modification should not interfere with the ability of the monomer to be polymerised, which may require the use of protecting groups.[45] Ligands should react with the polymer scaffold through easily-accessible functional groups; complicated synthetic routes to install the required functionality for the conjugation reaction reduces the efficiency of the scaffold for high-throughput screening applications. Ideally, ligands of interest for the screening application would be commercially available without the need for further purification or modification. Functional polymers which are designed to be used for biological applications *in situ* should be soluble or compatible with aqueous media. The use of toxic additives such as catalysts should be minimised where possible, to reduce the impact that impurities, not removed by purification, may have in biology. In addition, complicated purification steps may reduce the efficiency of the screening system and also remove certain polymer molecular weights in a non-reproducible manner (for example dialysis or filtration). Finally, the conjugation reaction should be highly efficient and reproducible with the conjugates stable at physiological pH and concentration.

These design goals align with the concept of “click-chemistry” a phrase first coined by Sharpless in 2001[46] to describe and characterise a broad group of “spring loaded” chemical reactions which are; “*modular, wide in scope, give very high yields, generate only inoffensive by-products that can be removed by non-chromatographic methods, and be stereospecific*”.[46] More recently, updated guidelines on “click” reactions, specifically tailored to the application of polymer modification were outlined in 2011, which proposed that click reactions must proceed with fast time scales, result

in high yields with equimolar concentrations of reagents, and that purification (if required) must be able to be carried out on a large scale.[47]

The principles of click-chemistry, which focus on the discovery of new properties, rather than new compounds have been incredibly influential in the field of polymer science, in particular post-polymerisation modification of polymer scaffolds.[48] However, post-polymerisation modification strategies often require time-consuming purification steps before biological testing can be carried out. This can limit the efficiency of polymer scaffolds as a tool for high-throughput screening of large libraries of polymer functionalities with potential therapeutic properties.

Following the principles of click-chemistry set out by Sharpless, the ability to evaluate the activity of polymer chemistries *in situ* without the need to purify has the potential to greatly streamline combinatorial approaches towards the discovery of new therapeutic compounds.[49] The major barriers to *in situ* screening of polymers are purification steps and solvent. But, by carefully choosing the chemistry by which to modulate the polymer it is possible to satisfy these requirements.

ii. Important conjugation reactions for post-polymerisation modification

ii. a. Copper(I)-catalysed azide-alkyne cycloaddition

By far the most famous “click” chemistry reaction is the copper-catalysed azide-alkyne cycloaddition (CuAAC),” as described by Sharpless.[46] The “spring loaded” reaction between azide and alkyne functional group catalysed by Cu(I) was reported in 2001 by Meldal and Sharpless independently,[50,51] and proceeds to quantitative yields *via* the formation of a 1,2,3-triazole without the generation of by-products (**Figure 6**).

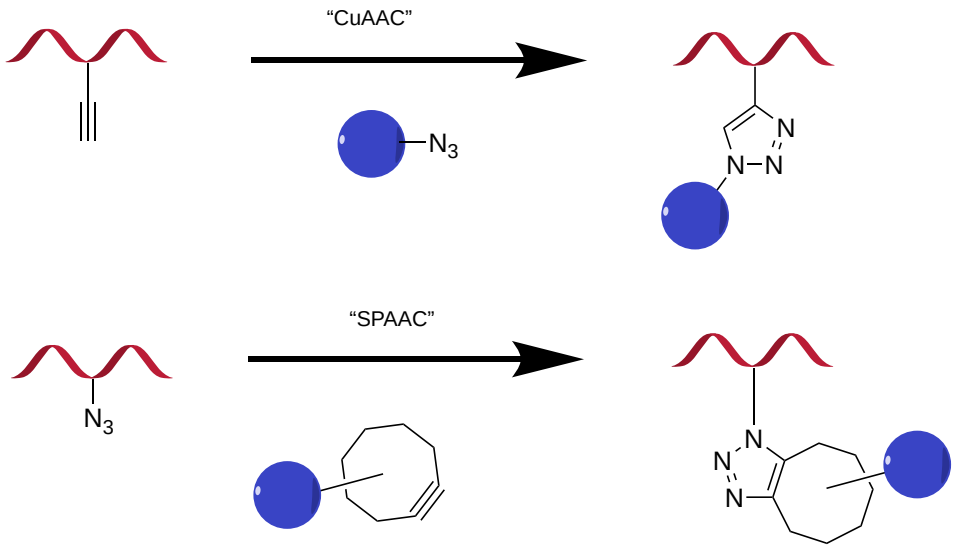

Figure 6. Copper(I)-catalysed azide-alkyne cycloaddition reaction (CuAAC) *via* the formation of a 1,2,3-triazole**,** and copper free strain promoted azide-alkyne cycloaddition (SPAAC).

CuAAc can be applied to conjugate different chemical groups in wide range of solvents under mild condition, and thus has been applied to countless modifications of nanomaterials, including polymers.[52] CuAAC has been particularly well established in the synthesis of glycopolymers,[53-55] whereby sugars containing an azide functional group were "clicked" onto an alkyne containing polymer scaffold. It is also possible to "click" alkyne containing ligands onto polymer scaffolds displaying aizde groups, *via* direct polymerisation of azide-containing monomers.[56] A limitation of this method is the use of copper ions, which are known to be toxic and, in some cases, limit this strategy for bioorthogonal reactions (chemical reactions that can occur inside a biological system).[57] To address these issues, Bertozzi and co-workers reported a copper-free cycloaddition reaction by exploiting a strained alkyne system (SPAAC – strain promoted azide-alkyne cycloaddition) (**Figure 6**).[58] The drawback of this approach is the low solubility in aqueous media, and the cost of producing the required ligands (compared with CuAAC).[59]

ii. b. Thiol – X

Thiol-X is a broad term to describe any thiol-based conjugation reaction, including the widely used thiol-ene reaction by the addition of a thiol to an alkene. These modifications are highly efficient and can be applied to a wide range of commercially available functional thiols. Thiol-ene reactions, for example, satisfy the requirements for "click-chemistry" and can offer advantages over CuAAC, on account of their readily available starting materials and lack of required catalytic Cu(I).[60] Thiol-X reactions were reported for the modification of polymers in notable work carried out by Hoyle,[61] which has led to a large "toolbox" of possible thiol-X reactions for post polymerisation modification (**Figure 7**).

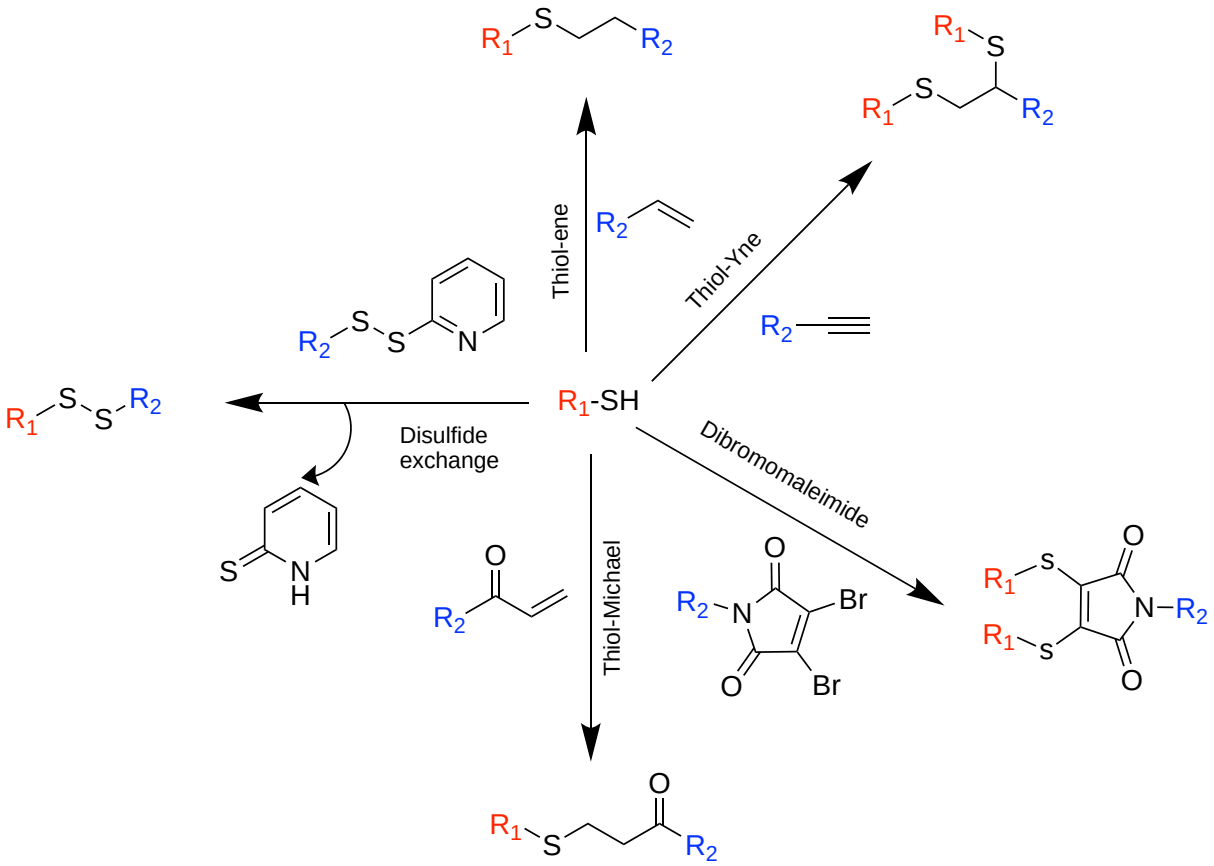

Figure 7. Notable thiol-X reactions involved with polymer modification.[48]

Thiol-X reactions are particularly well researched for modification of polymer end-groups prepared by reversible addition-fragmentation chain transfer (RAFT)

polymerisation,[60,62] and have been employed in the installation of fluorescent probes.[63,64] One of the major considerations is the reactivity of the thiol and the alkene under traditional radical polymerisation. This remains a challenge that can only be overcome if the vinyl group on the monomer designed to undergo polymerisation has a significantly different reactivity to the alkene designed for subsequent modification with thiols. Thiol-X modifications therefore, are often used in tandem to install subsequent functionality after an initial post-polymerisation modification, for example; side-chain modification of a synthetic polymer with a peptide,[65] and the selective end group modification of glycopolymers with maleimide modified biotin.[66]

ii. c. Activated esters

The amide bond is one of the most fundamental chemical bonds found in nature, and probably best known as nature's preferred method of linking amino acids to form peptides. Amide bonds have good stability towards acidic, basic, oxidising and reducing conditions, but the formation of these bonds, *via* the condensation of an amine and a carboxylic acid, requires forcing conditions such as heat, and the addition of a catalyst. In the case of activated esters, the energy required to form the amide bond is significantly lowered *via* the incorporation of a leaving group and thus makes this chemistry more compatible with post-polymerisation modification. The two most popular activated esters, N-hydroxysuccinimide (NHS) esters and Pentafluorophenyl (PFP) esters, offer leaving groups which are readily soluble in water, and in the case of PFP esters, offer the ability to monitor the post-polymerisation modification reaction by ^{19}F NMR (**Figure 8**).[48,67]

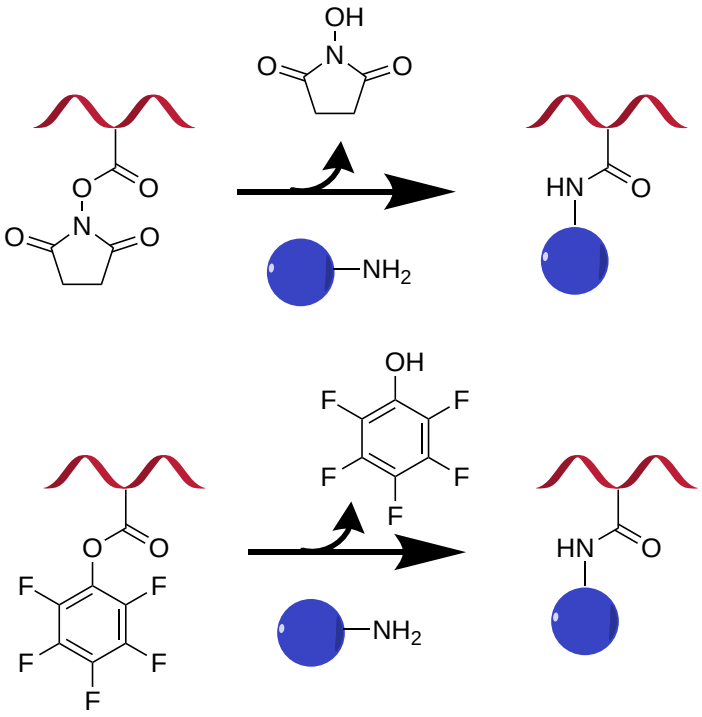

Figure 8. Common polymer modification reactions *via* NHS esters (top) and PFP esters (bottom).

Polymers which containing PFP ester side chains have been used to install alkyne functionality onto the polymer backbone, followed by CuAAC in a two-step post-polymerisation modification process for the synthesis of glycopolymers designed to bind bacterial toxins,[53] or in a single step with the addition of glucosamine or galactosamine.[66] One of the key limiting factors of using PFP esters for post-polymerisation modification is that, while the resulting material may be stable and soluble in aqueous media, the PFP polymer is liable to hydrolyse and therefore, the modification reaction is generally carried out in the water miscible solvent e.g. DMF and 1 eq. TFA. This requirement limits the use of this method for in-situ biological screening as purification steps would be required.

Less reactive than PFP esters, but highly versatile, NHS-esters are one of the first examples of post-polymerisation modification. Notably, Whitesides and co-workers employed poly NHS esters to prepare a library of sialic acid containing

polymers *via* post-polymerisation modification to identify inhibitors for the influenza infection.[68] On the downside, NHS esters are susceptible to ring opening side reactions with amines, instead of the desired substitution reaction, and also to intramolecular attack between an NHS ester and adjacent methacrylamide, resulting in the formation of a backbone glutarimide.[69]

ii. d. Isocyanates

Isocyanates are less commonly used in polymer side-chain modification, but offer a highly efficient synthetic for polymer modification and are compatible to react with a variety of nucleophiles; amines without the need for forcing conditions, alcohols with the addition of Sn(II) and thiols under basic conditions (**Figure 9**).

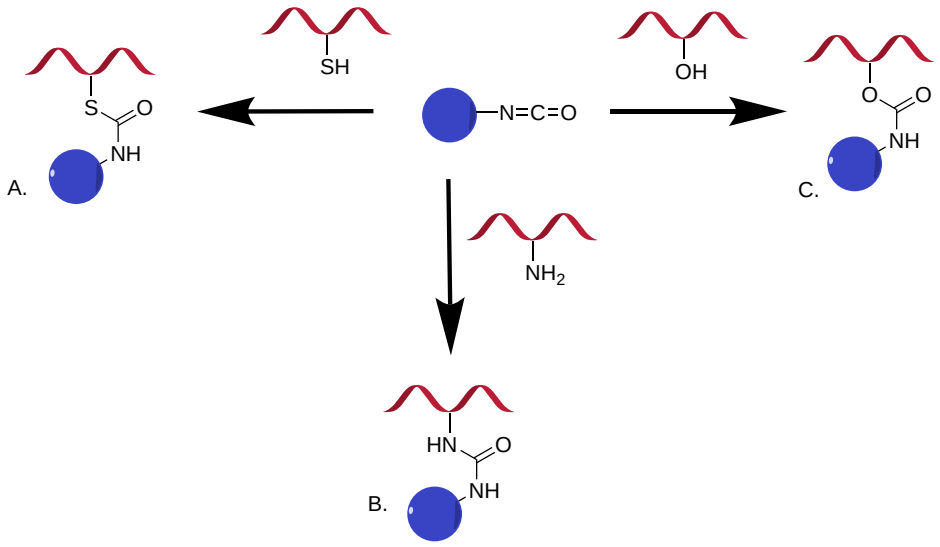

Figure 9. Examples of polymer modification reactions *via* isocyanate containing ligands resulting in the formation of A) thiourethane, B) urea and C) urethane derivatives.

Although isocyanate-containing polymers can be difficult to store due to their sensitivity to moisture,[48] direct polymerisation of isocyanate monomers is an appealing strategy to access readily available ligands for post-polymerisation modification. Polymerisation of isocyanate-containing monomers has been reported by McCormick,

but was found to be more challenging to control, resulting in lower conversions and broad dispersity in the polymer molecular mass, attributed to loss of the RAFT agent and/or side reactions during the polymerisation process. Some improvement was achieved however through optimising the choice of RAFT agent (to contain a tertiary amine rather than carboxylic acid) and the use of low polymerisation temperatures (**Scheme 1**).[70]

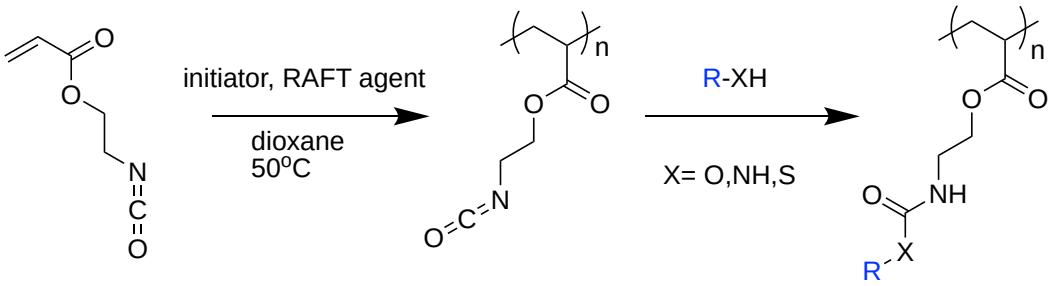

Scheme 1. Direct RAFT polymerisation of isocyanates reported by McCormick.[70]

To overcome these polymerisation challenges, "blocking" of the reactive isocyanate group is favored in order to maintain the side-chain fidelity.[45] McCormick and co-workers demonstrated in follow-up work that polymerisation with monomers containing isocyanates blocked with imidazole, dimethylpyrazole and triazole not only offered a route to highly controlled polymerisation, but allowed for temperature-dependent selective modification of the polymer backbone.[71] Modification of polymers with isocyanate containing ligands can also be achieved, although this strategy can limit the choice of ligand.[72]

ii. e. Ring opening

Ring opening reactions, such as the frequently used epoxide ring opening, are thermodynamically driven by the release of ring strain. Three-membered rings are under significant strain, and therefore undergo highly efficient reactions with a wide range of nucleophiles (**Figure 10**).[73]

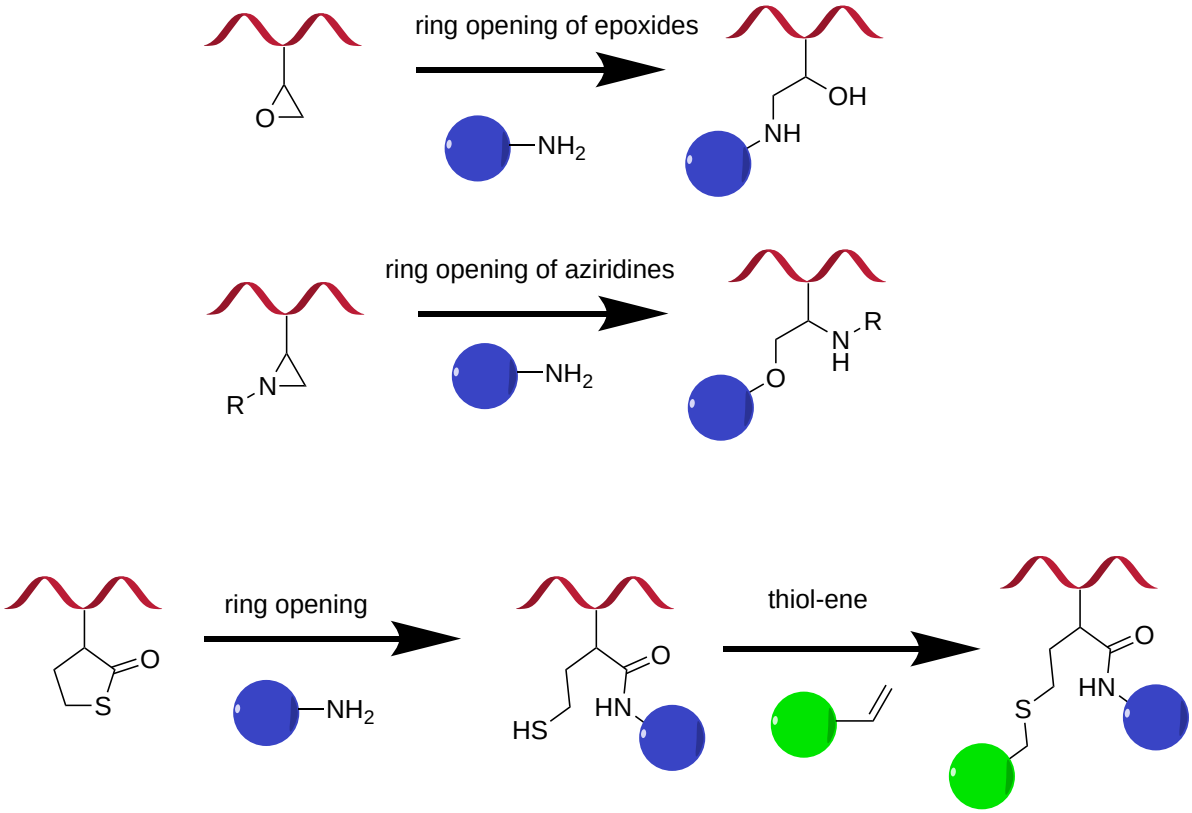

Figure 10. Post-polymerisation modifications involving nucleophilic epoxide and aziridine ring opening. Bottom; example of a tandem post-polymerisation modification involving ring opening and subsequent thiol-ene reactions.

Aziridines are a nitrogen containing analogue of epoxides and have lower reactivities due to the less electron-negative nitrogen atom. However, the interest in these functional groups as building blocks for polymer scaffolds lies in ability to substitute the nitrogen with further chemical groups which can broaden the scope for modification of the scaffold.[74] It should be noted that unsubstituted aziridines are not able to be controlled *via* RAFT or atom transfer radical polymerisation (ATRP) controlled polymerisation techniques due to interactions between the nitrogen and the chain transfer agent (CTA).

Ring opening of thiolactones allows for successive thiol-ene functionalisation in a one pot synthesis, which can be particularly useful for introducing controlled hetero-functionality into the polymer scaffold. Garcia-Verdugo and co-workers described the

synthesis of poly(acrylamide-homocysteine thiolactone) as a polymer scaffold capable of undergoing sequential post-polymerisation modifications.[75] Epoxide ring opening with amines has also been employed in the synthesis of hetero-functionalised glycopolymers for bacterial aggregation.[76]

ii. f. Oximes, Hydrazones and Imines

Amines, hydroxylamines, hydrazines and hydrazides can undergo highly efficient "click" reactions *via* condensation with aldehydes and ketones, with the only by-product being water.[77] A key advantage of this method is the vast array of commercially available aldehyde containing molecules which can undergo conjugation (**Figure 11**).

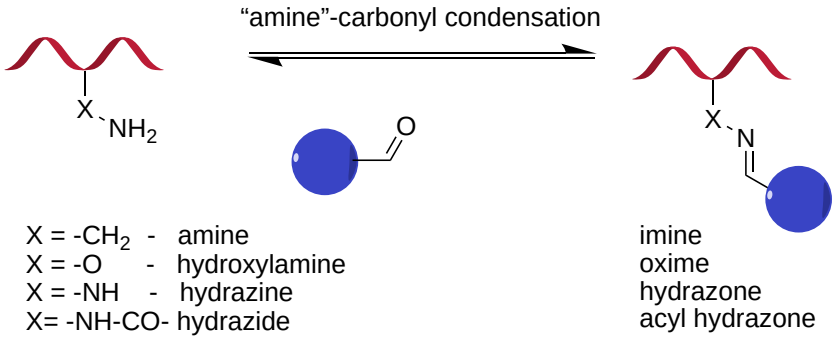

Figure 11. Examples of conjugation reaction with "amines" and aldehydes to form either imines, oximes, hydrazones or acyl hydrazones.

The reaction of amines and carbonyls requires more forcing conditions compared with that of hydroxylamines, hydrazines and hydrazides owing to their lower nucleophilicity, and therefore the majority of this class of conjugation reaction focuses on the formation of oximes and hydrazones (including acyl hydrazones). The increased nucleophilicity and therefore reactivity of hydroxylamines and hydrazides compared to that of amines originates from the α-effect whereby the orbital containing lone pairs of electrons on a hetero atom (O in the case of hydroxylamines, N in the case of hydrazides) overlaps with the lone-pair-containing orbital of the nucleophilic N,

resulting in overlap and increase the HOMO of the nucleophile, rendering it more nucleophilic. The inductive effect of the hetero atom also dictates the hydrolytic stability of the resulting bond, which proceeds *via* the protonation of the nitrogen. Reversibility of the hydrazone or oxime bond is a key consideration when considering these linkages in post-polymerisation modification.[78] Oximes are more stable than hydrazones and acyl hydrazones due to the higher electronegativity of the oxygen hetero atom (χ_o =3.5), compared with N in hydrazones (χ_N =3.0). Hydrazides are often employed for conjugation reactions instead of hydrazines due to the increased stability of the acyl hydrazone bond, which is rationalised as a result of increased resonant forms possible in the distribution of the electron density (**Scheme 2**).

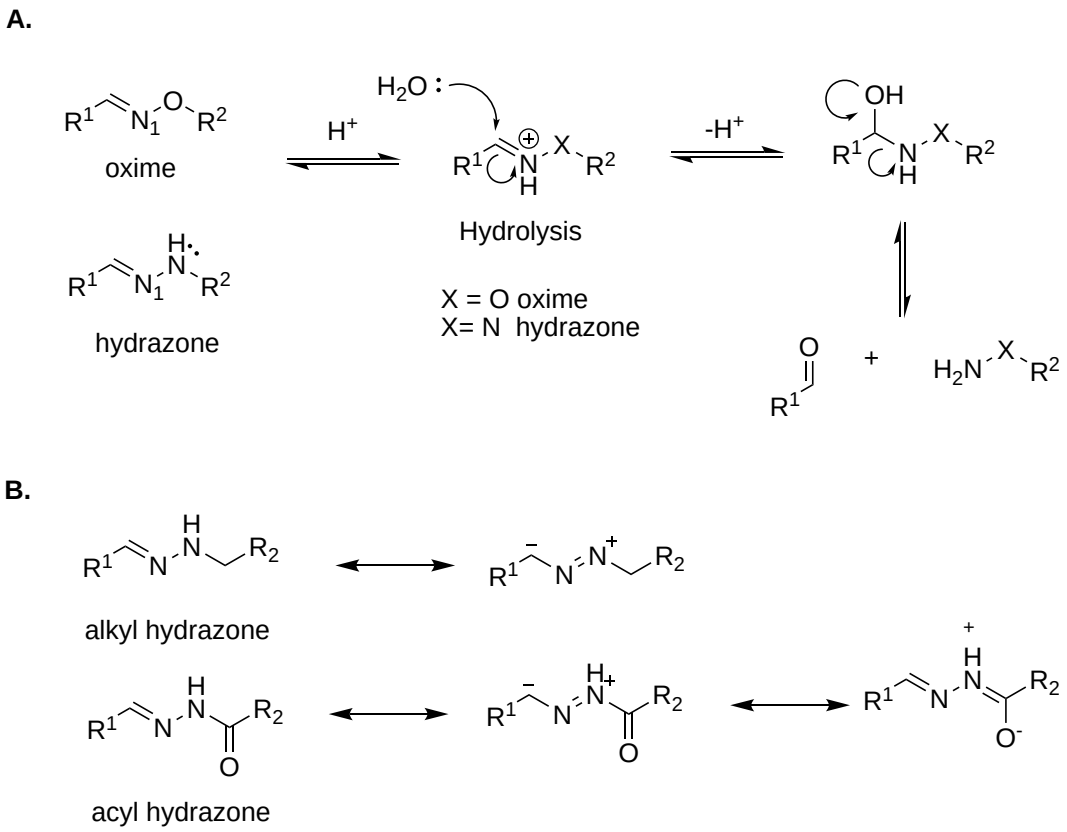

Scheme 2. A) Differences in stability of oximes and hydrazones due to the susceptibility of the N_1 atom to be protonated. B) Major resonance forms of alkyl and acyl hydrazones.

Oxime and hydrazone formation is a commonly employed bioconjugation technique due to its compatibility with aqueous media and mild reaction conditions. It is often described as being bioorthogonal due to the small size and inert nature of aldehydes and ketone functional groups at physiological pH.[79] In this context, hydrazide-functionalised polymers are considered potentially useful scaffolds for combinatorial approaches to drug discovery and fulfil the requirements mentioned earlier for *in situ* screening.[49]

When applied to post-polymerisation modification, polymers can be modified in water at physiological pH and used *in situ* without the need for further purification.[80] It should be noted that the small molecule aldehydes can be completely consumed by employing this technique. Bertozzi demonstrated that poly(acryloyl hydrazide) could be prepared by activated-ester post-polymerisation modification of acetoxime acrylate with the addition of hydrazine.[81] Poly(acryloyl hydrazone) was able to react with unmodified reducing sugars such as mannose, glucose and galactose resulting in near quantitative ligation efficiencies and good stability at physiological pH.[81] A similar synthesis route was taken by Ojha and co-workers,[82] who prepared poly(acryloyl hydrazide) by modification of poly(methyl acrylate) with hydrazine. More recently, a synthetic route to prepare poly(acryloyl hydrazide) by direct polymerisation of a boc-protected hydrazide monomer was reported.[83] This route avoided the use of excess toxic hydrazine during synthesis, and poly(acryloyl hydrazide) could be prepared by simple deprotection in acid. The dynamic nature of the acyl hydrazide linkage has led to its use in pH responsive polymer drug delivery systems,[84] and templating of carbohydrate-functionalised polymers with lectins,[85] further demonstrating the versatility of this conjugation strategy.

ii. g. Post-polymerisation modification toolbox: summary

A vast toolbox of chemical reactions is available to the polymer chemist to efficiently modify a polymer scaffold. The choice of the chemistry is strongly dictated by the application for which the polymer is designed. Originally, post-polymerisation modification was (and still is) a way of accessing polymer functionalities which were not polymerisable from their corresponding monomers. In this regard, the modification should be quantitative, the bond stable, and the linker chemistry such that it does not impact on the overall functionality of the material. Post-polymerisation modification is now being increasingly employed for biological, combinatorial, and *in situ* applications, and therefore demands a greater need for water soluble precursors and conjugates, as well as non-toxic efficient modification methods. In this regard polymer scaffolds have become an attractive platform for high throughput screening of structure-activity relationships. In particular, poly(hydrazide) scaffolds undergo highly efficient and biocompatible “click-chemistry” modification with commercially available aldehydes allowing for *in situ* screening.

iii. *V. cholerae*: A relevant pathogenic target for anti-adhesion therapy

When designing materials to interfere with or sequester bacteria, or any microorganisms for that matter, it is necessary to consider the way that the material will interact with the organism in a physical and chemical sense, but also to predict how the microorganism will respond to this interaction.

Bacteria are highly adapted to surviving in environmental niches by regulating specific genes in response to external cues. Studying the interaction between bacteria and materials designed to target bacterial adhesion can help design new and “better” materials for the application, but could also offer a means of studying less well

understood bacterial regulatory pathways. In this respect, an understanding of certain regulatory pathways and "natural" responses in *V. cholerae* is necessary to interpret the activity of the polymer.

V. cholerae, is a motile Gram-negative pathogen responsible for the disease cholera, associated with watery diarrhea and dehydration, which, if left untreated can result in hypotonic shock and death.[86] Worldwide 1.3 – 4.0 million people contract cholera each year resulting in 21,000-143,000 deaths (World Health Organisation 2018). Outbreaks of cholera are generally restricted to countries where significant numbers of people are without access to clean water and good sanitation. The disease is spread orally *via* hyper-infective *V. cholerae* present in stools of the infected persons if allowed to enter the water system.[87] Where cholera is endemic, outbreaks follow a seasonal pattern which is thought to be linked to changes in water temperature as well as blooms of plankton, and chitin rain, both of which *V. cholerae* adhere to and use as a sole carbon source.[88] The need to find new methods to control this pathogen is currently of high importance since a significant outbreak of cholera is currently ongoing in Yemen and is responsible for what has been described by the UN as the "biggest humanitarian crisis in the world".[89] As sea levels rise and we experience more frequent extreme weather events, these outbreaks, caused by bacterial contamination of water, are expected to become more common,[90] and potentially even more serious with the rise of antimicrobial resistance.

Evaluation of how best to target *V. cholerae* adhesion with polymers requires an understanding of how these bacteria detect and adhere to surfaces, and at what point this leads to pathogenicity. The key processes in the *V. cholerae* virulence program are: adhesion, toxin production, biofilm formation and finally, dispersal (**Figure 12**).[91,92]

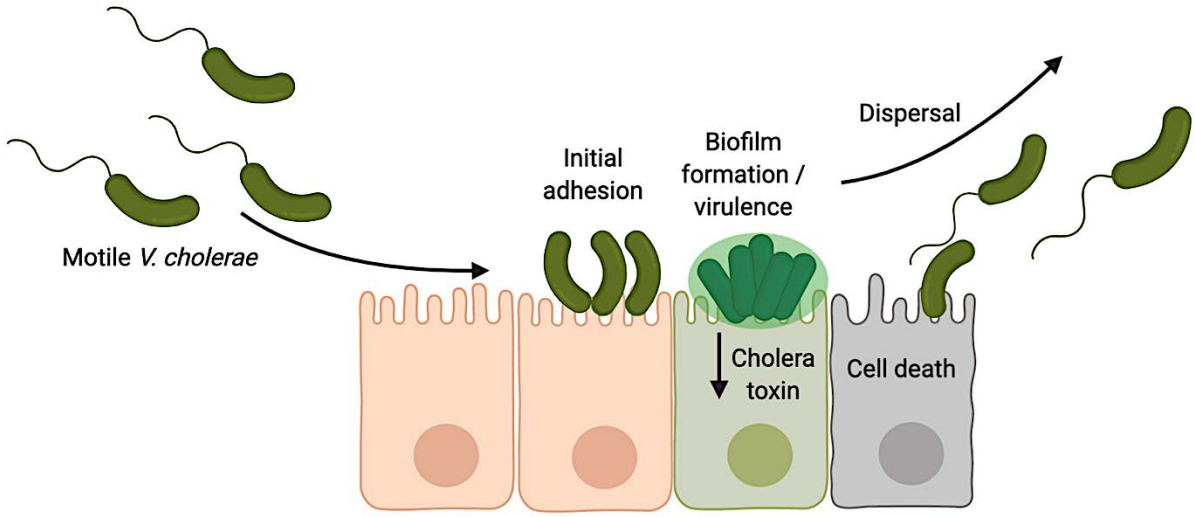

Figure 12. *V. cholerae* stages of infection: Motile *V. cholerae* bind the cell surface initially *via* non-specific interactions, followed by strong and specific adhesion resulting in microcolony formation, biofilm formation and virulence. At a critical population triggered by QS, *V. cholerae* disperse from biofilms in order to re-infect the host.

iii. a. Targeting V. cholerae surface adhesion mechanisms with polymers.

Since the observation that *E. coli* adhesion to epithelium cells could be inhibited by targeting type-1 pilus mannose-binding protein (FimH) with mannose-containing glycosides,[93] there has been widespread research into the FimH lectin as a promising anti-adhesion target for new therapeutics.[94] However, less research has been conducted into targeting lectins associated with *V. cholerae* adhesion.

V. cholerae have a number of appendages which are employed in the initial attachment to surfaces, and these may serve as potential targets for anti-adhesion polymers. The most commonly studied appendage is the type IV pili which can be visualised as tiny hairs protruding from the bacterial cell surface. Type IV pili are generally much longer than the *V. cholerae* cell (7 microns vs 1.3 microns) but less than 10 nm in diameter, which explains their significant attachment and sensing capabilities and their inability to be visualised using optical microscopy.[95] *V. cholerae* adhesins such as type IV pili are believed to possess lectin functionality in order to bind

to sugars and therefore offer a promising target for anti-adhesion therapy with glycopolymers.[96] *V. cholerae* use a combination of a type IV pili, MSHA (mannose sensitive haemagglutinin), and their polar flagellum synergistically to "scan" a surface *via* chemo and mechanosensing.[97] Utada and co-workers demonstrated through tracking and modelling the movements on *V. cholerae,* that orbiting bacteria, characterised by repetitive tight circular motions, were associated with irreversible attachment to the surface and microcolony formation. On the other hand, *V. cholerae* lacking the genes to produce flagella and MSHA were not able to form orbiting motions and had significantly decreased biofilm formation (**Figure 13**).[98]

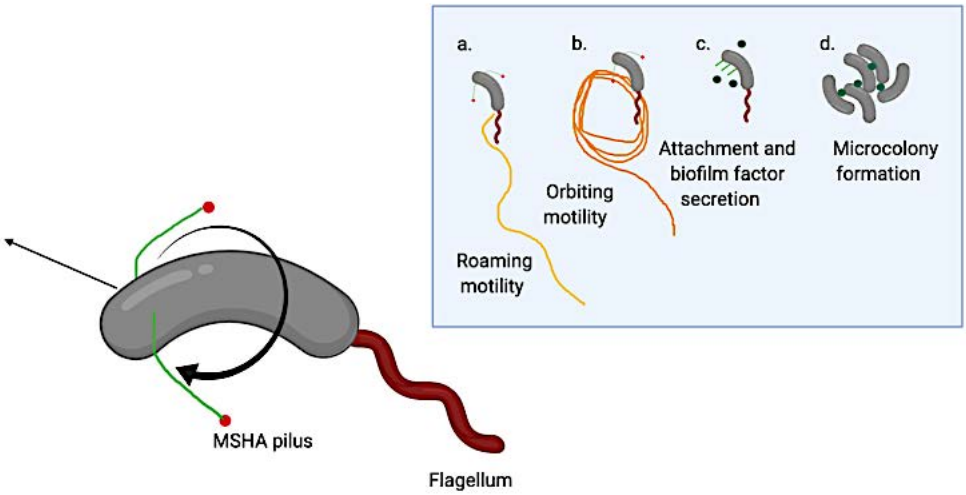

Figure 13. *V. cholerae* use MSHA pilus and polar flagellum synergistically to scan surfaces for suitable adhesion sites. Stronger interactions with the pilus and flagellum result in orbiting motility, initial attachment and finally, microcolony formation. The MSHA pilus is believed to possess lectin functionality at its tip (red dot) in order to bind carbohydrates.

The cause of bacterial attraction to a surface and a switch to orbiting motility is thought to be due to hydrodynamic forces,[99] and drag forces experienced by the polar flagella.[100] By orbiting in this way, *V. cholerae* spend more time over portions of the surface that interact more strongly with the MSHA pili, and eventually form strong and

specific attachments *via* other adhesins, for example, the toxin co-regulated pilus (TCP) and chitin regulated pilus (ChiRP).[98]

Targeting MSHA with mannose containing polymers is an attractive means of targeting and sequestering *V. cholerae via* multivalent binding between the MSHA lectin and mannose side chains in the polymer which may reduce the bacteria's ability to adhere to surfaces. In support of this statement, inhibition of orbiting motility and surface attachment was achieved by addition of a non-metabolisable mannose derivative, which corroborates the idea that MSHA binds mannosides,[101] and this can interfere with *V. cholerae's* ability to further bind surfaces. The selectivity for mannose over other glycans is not well understood, and indeed the name of the MSHA pilus originates from the observation that *V. cholerae* agglutinate red blood cells and this agglutination can be inhibited/reduced on addition of mannose. Early work on purification of the MSHA lectin from *V. cholerae* O1 strain reported a high affinity for both D-mannose and D-glucose.[102]

More recent and detailed work on the MSHA pilus of closely related *Vibrio parahaemolyticus* employed a high-throughput glycan binding assay to identify the target glycan of MSHA. Glycans displaying highest activity towards binding compared with the MSHA mutant, contained terminal fucose, galactose and GalNAc, but interestingly not mannose,[103] unlike the understood mannose binding MSHA of *V. cholerae.* Intriguingly, MSHA biosynthesis has been reported to be repressed during infection, which is thought to protect the bacteria from agglutination by the host's mannose-displaying immunoglobulins and prevents *V. cholerae* from attaching to the surface of epithelial cells.[104] Reports such as these are important for the rational design of mannose-containing anti-adhesion polymers and could account for any observed differences in activity *ex vivo* and *in vivo*.

The chitin-regulated pilus (ChiRP) and chitin-binding proteins (CBP) are important adhesins involved with surface colonisation of *V. cholerae* to chitinous surfaces, e.g. the shells of plankton, in their natural marine environment, where attachment and metabolism of this polysaccharide is vital for their survival.[105,106] Adhesion to GlcNAc, the carbohydrate monomer of chitosan, has been shown to be specific for certain *Vibrios* and can inhibit their adhesion to chitin.[107] A GlcNAc-binding protein GbpA which is secreted by *V. cholerae* has been shown to be crucial in binding chitin, but also human epithelial cells, it is not clear if this protein can bind sugars other than GlcNAc.[108] GlcNAc containing polymers evidently have potential to target *V. cholerae* adhesion, and given the importance of chitin which naturally mediates this, it is unsurprising that antimicrobial polymers containing chitosan have been developed to target a range of microorganisms including *V. cholerae.*[109,110]

The toxin co-regulated pilus (TCP) is a IV pili used by *V. cholerae* to colonise the intestine and is a major virulence factor.[111] Conversely to MSHA and ChiRP, TCP filaments contain glycine-rich portions and serve to hold bacterial cells together in a microcolony during the deployment of the cholera toxin. TCP also behaves as a receptor for cholera toxin phage, which can infect non-pathogenic *vibrios* and provide the required genes to start producing the cholera toxin.[112] More recently it has been demonstrated that TCP mediates the attachment of *V. cholerae* to Caco-2 cells and areas of the small intestine villi in an infant mouse model.[113] It was reported that *V. cholerae* mutants lacking the genes to produce TCP were not able to form microcolonies and as such, were cleared from the intestine in less than 24 hours. The specific role of TCP in cell attachment was probed by electron microscopy which revealed that the initial attachment of *V. cholerae* to epithelial cells *in vivo* was in fact independent of TCP, and rather that TCP plays a crucial role as a colonisation factor.[113]

As a result it may be challenging to specifically target the TCP by multivalent glycopolymers to inhibit adhesion.

iii. b. Summary: targeting V. cholerae adhesion mechanisms with polymers

V. cholerae adhere to surfaces *via* a number of mechanisms, many of which have been discussed here, and is believed to involve the binding of sugars, most notably *via* the mannose sensitive pilus (MSHA), chitin binding pilus or membrane proteins, although this is not well understood. Interestingly, in the case of MSHA, despite an accepted affinity for mannose, the specificity for a particular glycan has not been well established in *V. cholerae,* whereas fucose, galactose and GalNAc were recently found to have high specificity to the MSHA lectin of *V. parahaemolyticus.*[103] Interestingly, MSHA has been shown to be important for attachment of *V. cholerae* to chitin beads suggesting that MSHA may not have specific lectin activity towards mannose.[88] Although clearly mannose and GalNAc both have the potential to act as ligands to inhibit *V. cholerae* adhesion *via* the described adhesion mechanisms, there may also be merit to screening polymers containing a wide range of different sugars and mixtures thereof, in order to establish the most efficient glycan for sequestering *V. cholerae* in this way.

iii. c. V. cholerae gene regulation in response to polymer-mediated aggregation

After initial attachment of the *V. cholerae* cell to a surface, regulation of key virulence and biofilm genes occur. This is associated with a phenotypic switch from a motile to a sessile state of the bacteria.[114] Polymers that sequester bacteria have been proposed as potential means to artificially control bacterial phenotypes, and by doing so, control pathogenicity.[115,116] The regulatory network in *V. cholerae* is complex (and not fully understood) and beyond the scope of this introduction. However, a general

understanding of key processes in *V. cholerae* is important for interpreting the way that bacteria will respond to polymer-mediated aggregation.

To simplify this model, focus will be drawn to the impact quorum sensing has on different bacterial responses (**Figure 14**). In particular, regulation of biofilm formation and virulence, can be modulated in a quorum sensing (inter-bacterial communication) dependent manner by polymers.[116,117] This is rationalised as being due to the artificially high concentration of confined bacteria within aggregates, and therefore, an increased concentration of quorum sensing molecules (autoinducers).[118] Other environmental stimuli that influence virulence and biofilm formation include nutrient availability, chitin di- and oligosaccharides and nitric oxide,[91] and It has been suggested that the environment of the gut (for example temperature and pH) may be a direct cue for the production of virulence factors in *V. cholerae*.[87] A much more comprehensive review of the various inputs and regulatory pathways in *V. cholerae* surface colonisation has been published by Dang and Lovell.[91]

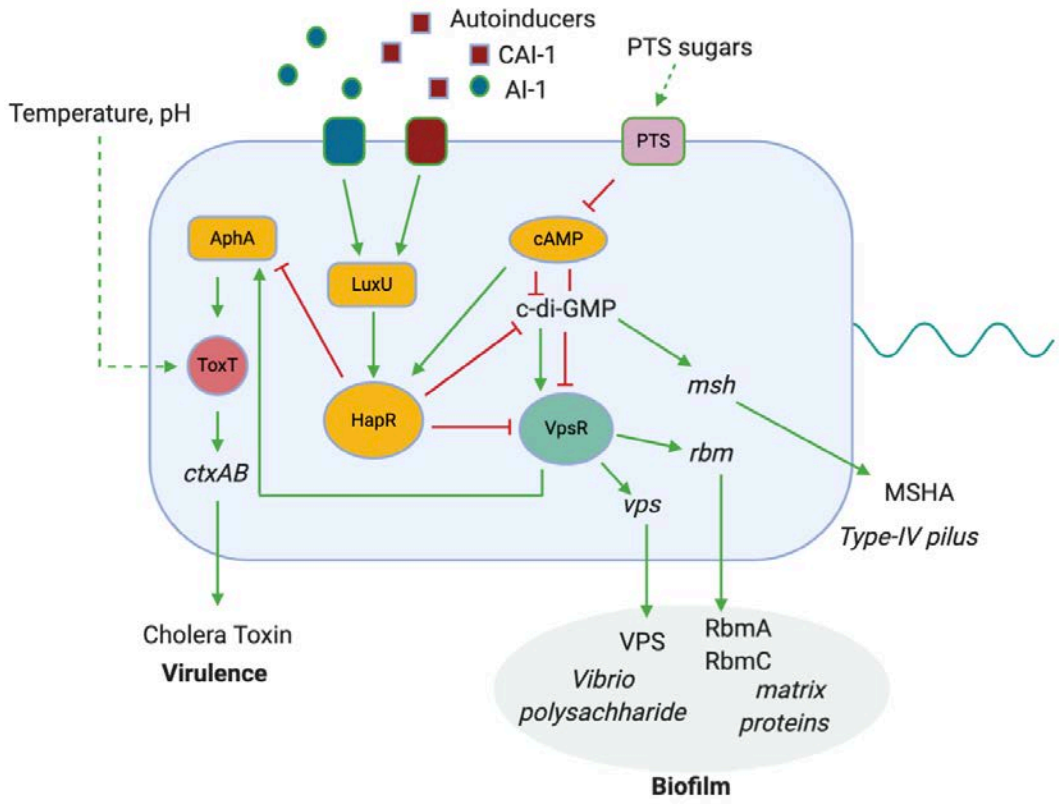

Figure 14. Simplified regulatory pathways in *V. cholerae*. Green arrows describe positive regulation, and red arrows describe suppression of the pathway. At high autoinducer (QS molecule) concentration (red squares and green circles), HapR is expressed and represses *vpsR* transcription, a regulator of biofilm factors. HapR also represses *aphA,* a regulator involved in the expression of virulence factors such as the Cholera toxin. At low cell density, *hapR* is downregulated and thus does not repress the synthesis of biofilm and virulence factors.[87,91,119] Biofilm formation can be triggered (or suppressed) as a result of carbohydrate availability using the Phosphoenopyruvate Phosphotransferase System (PTS). PTS sugars (for example, mannose, glucose) transported by the PTS can increase biofilm formation in *V. cholerae via* repression of cAMP, although this process is not yet fully understood.[91]

A well-studied pathway which governs both the production of virulence factors and the production of biofilm is the quorum-sensing (QS) pathway, which can be simply described as a system for bacterial cell-to-cell communication.[120] At low bacterial cell density, *V. cholerae* regulates its genes in a way that benefits the individual bacteria, while at high cell density genes are regulated to benefit the bacterial community. Information about cell density is imparted to the bacteria by means of small signaling molecules which are released and detected by the bacteria, known as autoinducers.[120]

The autoinducer concentration and thus the relative density of bacterial cells can be deduced. Key regulators HapR and AphA are either activated or deactivated depending on cell density. At low cell density, *aphA* is expressed and *hapR* is downregulated. AphA leads to the expression of genes which encode virulence factors and biofilm and colonisation factors are not suppressed.[87] At high cell density HapR is expressed and represses the production of biofilm and virulence genes (**Figure 14**).[119] Low cell density represents a motile state for *V. cholerae* seeking to colonise and infect the host. When cell density reaches a certain level, it is beneficial for *V. cholerae* to dissipate from a biofilm-associated community in order to infect a new host.[92]

As discussed earlier, Perez-Soto and co-workers recently demonstrated that aggregation of *V. cholerae* by cationic polymers caused an enhancement in QS,[115] which led to a decrease in virulence as predicted (**Figure 14**). However, a significant upregulation of biofilm related genes and increase in the formation of biofilm was also observed which cannot be explained simply through the quorum sensing pathway. The upregulation of biofilm production in polymer-mediated bacterial clusters therefore demonstrated the potential for polymers employed in this way to engineer combinations of useful bacterial phenotypes.

iv. Linear polymers to aggregate bacteria, current state-of-the-art.

Next, current efforts towards aggregating bacteria with linear polymers will be discussed, the design of which largely focuses on targeting specific lectins with glycopolymers, or targeting the negatively charged outer membrane with cationic polymers (**Table 2**).

Table 2. Linear polymers discussed in this section

Polymer class	Synthesis method	Functional groups	Target	Determination of activity	Ref.
Cationic	FRP	Primary and tertiary amine	*V. cholerae*	Microscopy Gene expression Bacterial attachment	115
Cationic	RAFT	Dopamine, tertiary amine	*V. harveyi*	Microscopy Bioluminescence	134
Glycopolymer	RAFT	Glucose	*V. harveyi*	Microscopy	134
Cationic	RAFT	Dopamine, tertiary amine	*S. aureus* *V. harveyi* *E. coli* *P. aeruginosa*	Microscopy Particle sizing LIVE/DEAD staining	156
Cationic/ Zwitterionic	Templating / ATRP	Tertiary amine, Zwitteronic sulphobetaine	*E. coli* *P. aeruginosa*	Microscopy Particle sizing Turbidity Redox potential	140
Cationic	RAFT	Dopamine, tertiary amine	*V. harveyi*	Microscopy Bioluminescence Particle sizing	118
Cationic	FRP	Primary amine, Tertiary amine	*V. cholerae*	Microscopy Bioluminescence Gene expression	116
Cationic	FRP	Quaternary amine	*S. aureus* biofilm	Microscopy Biofilm staining (CV)	138
Cationic	FRP	Primary amine	*E. coli* *V. harveyi*	Microscopy Bioluminescence	117
Glycopolymer	FRP	Glucose, N-isopropylacrylamide	*E. coli*	Microscopy, thermo-responsive aggregation	149
Glycopolymer	RAFT	Mannose	*E. coli*	Particle sizing Microscopy Residual adhesion	151
Cationic / Zwitteronic	RAFT copolymerisation	Tertiary amine, Zwitteronic sulphobetaine	*S. mutans*	Microscopy Particle sizing	55
Glycopolymer	ATRP	Mannose Galactose	*S. mutans*	Microscopy Particle sizing	55
Glycopolymer	Templating / ATRP	Glucose	*E. coli*	Microscopy cell infection strain discrimination	147
Glycopolymer	Pd catalysed ROMP	Mannose Galactose	*E. coli*	Microscopy ConA binding	152
Cationic polymer	Pd catalysed polymerisation	Quaternary amine	*E. coli* *B. subtilis* *C. albicans (fungus)*	Microscopy Species discrimination	136
Cationic polymer	RAFT	Quaternary amine	*P. aeruginosa* Biofilm	CV Microscopy Turbidity	137
Cationic glycopolymer	RAFT copolymerisation	Mannose Quaternary amine	*E. coli*	Con A binding, Cell adhesion	76

		Ethanol amine Taurine			
Glycopolymer	RAFT	Glucose or / and mannose	*E. coli*	ConA Clustering, microscopy	153
Glycopolymer	Self-assembly	Glucose or / and Mannose	*E. coli*	ConA Clustering Microscopy	154
Chitosan	Natural polymer	Primary amine	*E. coli*	Growth curves, *Top10* QS reporter strain (flu), microscopy	128

iv. a. Cationic polymers

Cationic polymers are designed to interact or be attracted to the negatively charged bacterial cell *via* non-specific interactions. Cationic polymers have been extensively researched as antimicrobials, and the mechanism of action is believed to proceed *via* an initial attachment of the polymer to the bacterial cell wall, followed by insertion and/or disruption of the bacterial membrane *via* hydrophobic interactions with the polymer.[121,35] Structure-activity relationships of these materials have been extensively researched, revealing the importance of balancing both charge and hydrophobicity of the polymer for optimal activity.[122] Increasing the cationic portion of the polymer decreases the toxicity towards bacteria and can increase the agglutination of red blood cells, while increasing hydrophobicity can result in poor solubility and high toxicity to red blood cells.[38] It was observed however, that polymers containing predominantly cationic groups at sub-inhibitory concentrations resulted in rapid aggregation of bacterial cells into clusters. This phenomenon was quickly identified as a possible route to control bacterial colonisation by inhibiting bacterial adhesion in a way that minimizes evolutionary pressure on the bacteria.[11]

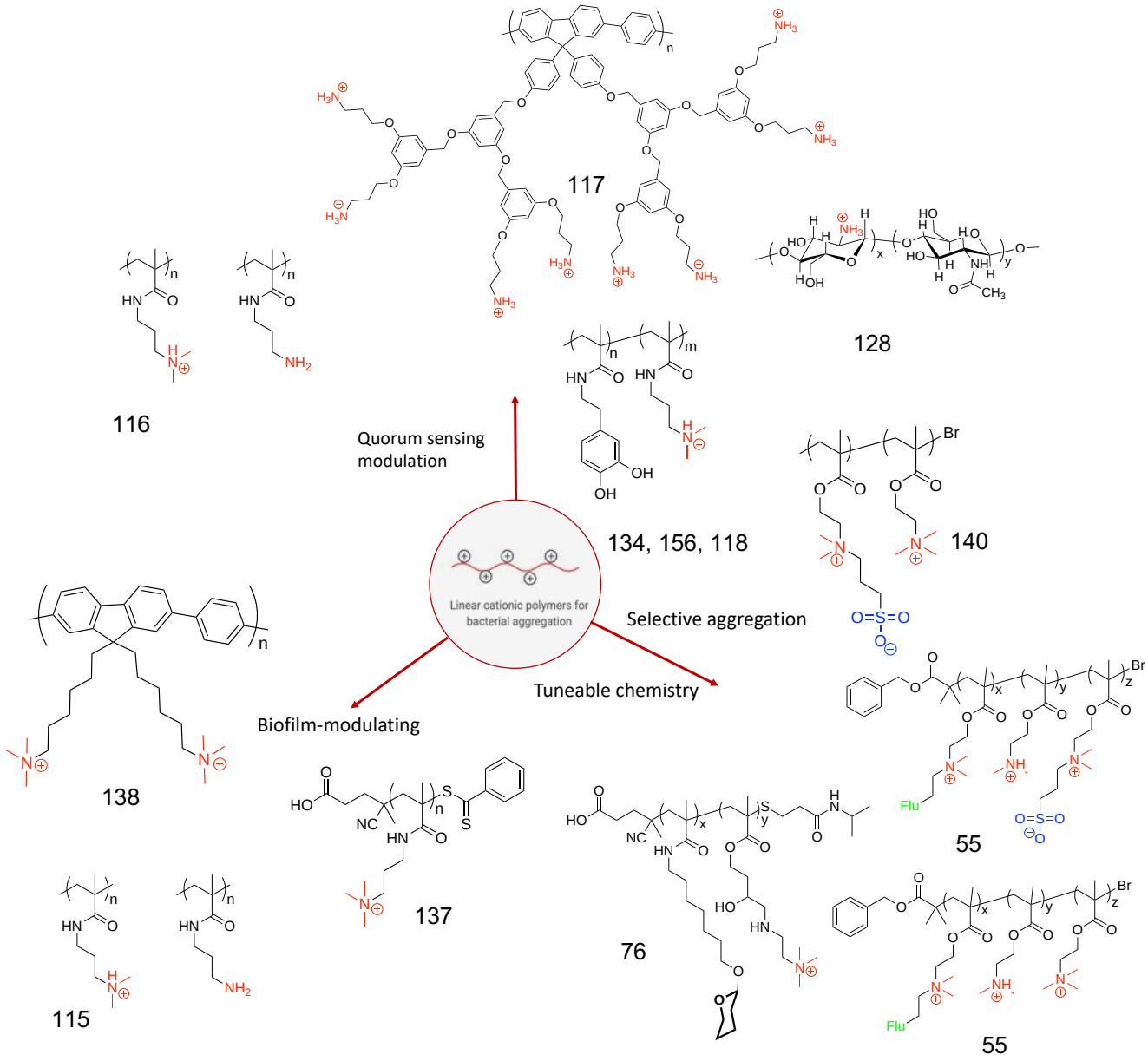

Figure 15. Cationic polymers discussed in this section which demonstrate bacterial aggregation. Numbers indicate the corresponding reference. "Flu" denotes a fluorescent coumarin dye.

iv. b. Cationic polymers for anti-adhesion

Sequestering bacteria with sub-lethal concentrations of polymers has been proposed as a method of protecting cells against bacterial adhesion as a way of reducing infection and disease (**Figure 16**),[11] However, there have been limited literature examples of cationic polymers for this application in solution, with the majority

of anti-adhesion polymers focusing on reducing the adhesion to abiotic surfaces by repelling bacteria.[123]

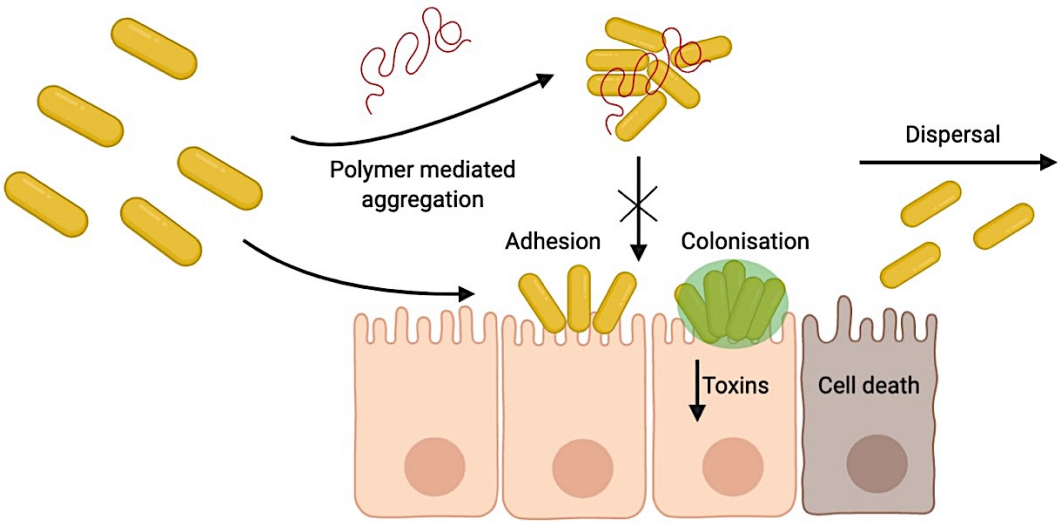

Figure 16. Potential therapeutic effect of polymers as bacterial anti-adhesives.

The ability of the tertiary and primary displaying cationic methacrylamide polymers to competitively bind to, and reduce the adhesion of *V. cholerae* to Caco-2 cell lines was assessed by Perez-Soto and co-workers.[115] Colony forming units (CFUs) from washed Caco-2 cells (a model cell line for the small intestine), revealed the number of attached bacteria was significantly reduced in the presence of both tertiary and primary amine containing polymers. Overall however, the tertiary amine polymers displayed significantly higher activity. The overall protective effects towards the epithelial cells were assessed *via* a lactate dehydrogenase (LDH) assay which confirmed that the primary amine containing polymer, pAPMAm**,** was most effective at a concentration of 0.05 mg ml^{-1}. At higher concentrations however, pAPMAm displayed increasing levels of cytotoxicity towards Caco-2 cells. Levels of cholera toxin activity towards Caco-2 cells were measured by cyclic adenosine monophosphate (cAMP) activity, where elevated cAMP is synonymous with production of the cholera toxin.

Lower levels of cAMP for polymer incubated samples agreed with the previously discussed finding that these polymers can suppress cholera toxin gene expression. Initial *in vivo* studies also indicated that these polymers reduce the accumulation of green fluorescent protein (GFP) expressing *V. cholerae* in the intestinal tract of zebrafish.[115] For polymers designed for *in vivo* therapeutic application, cytotoxicity of the polymer towards host cells (including hemolysis) is inevitably a key consideration. In a particular study by Thoma *et al.* a primary amine bearing methacrylamide was found to be antimicrobial towards *S. aureus in vivo* but displayed significant cytotoxicity to HEp-2 cells at the minimum inhibitory concentration (MIC) of the polymer. However, cytotoxicity was found to be partially overcome by employing polymers with lower degree of polymerisation (DP).[124]

iv. c. Chitosan: cationic linear polymers found in nature

Chitosan is a linear cationic glycopolymer based on a backbone of repeating N-acetyl-D-glucosamine (GlcNAc) and randomly distributed deacetylated D-glucosamine, found and derived from the chitinous shells of crustaceans.[125] Chitosan has attracted attention from researchers due to its antimicrobial properties,[126] as well as the observation that the marine bacteria *V. cholerae* can be commonly found adhered to the chitinous surfaces of shellfish.[88] Cationic glycopolymers have been synthesised by modification of chitosan to incorporate quaternary amines and guanidinium functional groups along the backbone to increase both solubility and antimicrobial activity against *E. coli* and *S. aureus.*[110,127] Chitosan has also been shown to induce clustering of *E. coli,* which was found to be dependent on the degree of acetylation (DA) on the carbohydrate backbone,[31] while more recently Qin and co-workers demonstrated that chitosan could aggregate *E. coli* at non-toxic doses, and

could suppress quorum sensing (inter-bacterial communication). Interestingly, increasing the polymer concentration resulted in an attenuation of the aggregation ability and also of the quorum sensing suppression.[128]

iv. d. Off-target effects: the biological outcome of bacterial aggregation by cationic polymers

Given that naturally occurring cationic polymers can interfere with bacterial regulatory pathways, such as quorum sensing, and that polymer-driven aggregation in nature can drive changes in bacterial phenotype,[33] current research into the aggregation activity of cationic polymers has focused on addressing how bacteria respond to their aggregated state, and whether, through complex regulatory pathways, certain bacterial responses are triggered which could lead to useful applications. To this end, the bacterial responses studied has focused primarily on biofilm formation, which can be easily measured,[129] is associated with persistent infection,[130] and can be a hallmark for environmental responses.[92,114] A secondary focus has been to address whether quorum sensing (the way in which bacteria sense their relative population by the release and detection of small molecules autoinducers),[131] is affected by bacterial clustering, which not only controls biofilm formation in bacteria,[132] but can also control gene regulation involved with virulence and competence (**Figure 17**).[131]

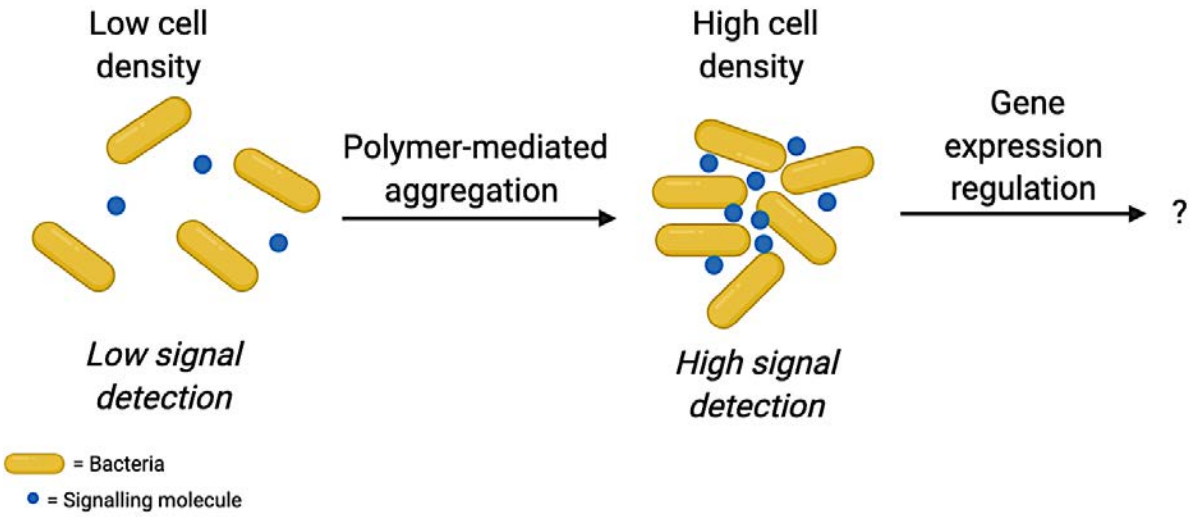

Figure 17. Proposed mechanism by which bacterial aggregation by polymers results in the accumulation of signalling molecules within the cluster, leading to enhanced quorum sensing which controls the regulation of bacterial genes.

iv. e. Impact on quorum sensing of bacteria

Physically confining individual bacteria has been shown to increase quorum sensing owing to the decreased diffusion of signalling molecules.[133] With this in mind, work carried out by Xue and co-workers identified that clustering bacteria in this way provided an opportunity to cluster and interfere with quorum sensing molecules which were expected to be at higher concentrations within confined clusters of bacteria.[134] By co-polymerising a di-methyl amino terminating acrylamide monomer designed to target the bacterial membrane, and a dopamine-containing acrylamide monomer designed to quench boron containing quorum sensing molecule AI-2, a polymer with dual functionality was synthesised. The copolymer was shown to not only cluster bacteria at a concentration of 0.25 mg ml^{-1}, but was able to interfere with the normal patterns of quorum sensing. The authors noted that they suspected that both cell clustering, and QS molecule quenching may impact the quorum sensing regulation.[134] This observation that quorum sensing in bacteria can be affected by dual action cationic polymers was continued by Lui and co-workers who employed the same

copolymer alongside a homopolymer of dimethylamino methacrylamide, pDMAPMa and evaluated the ability to predict aggregation effects and quorum sensing effects using computer modelling. The cationic homopolymer significantly increased the onset of quorum sensing in *V. harveyi* and the effect of positive charge was dominant in the dual action polymer with poor reduction in quorum sensing observed compared to a model quorum sensing quenching molecule. It was concluded therefore, that clustering *via* cationic polymers increases the onset of quorum sensing and that these materials may not be suitable for quorum sensing reduction applications.[118] However, enhancement in quorum sensing has also been shown to trigger useful changes in bacterial phenotypes. For example, Perez-Soto and co-workers demonstrated that for *V. cholerae*, upregulation of quorum sensing induced by bacterial aggregation with cationic polymers was co-regulated with the downregulation of virulence gene expression, but an increase in biofilm production.[116] An enhancement of quorum sensing by polymers in *E. coli* was also reported by Zhang and co-workers who synthesised cationic conjugated polymers displaying dendronized primary amine groups to aggregate the bacteria. The authors noted that the cationic polymers prolonged the time that quorum signalling molecules were being produced, and rationalised that the increase in production of the signalling molecules could also impact planktonic, non-adhered bacteria at low cell density. The authors also found that bacteria treated in this way produced roughly 50% more biofilm, and displayed a higher tolerance to antibiotics.[117]

iv. f. Impact on biofilm production

The potential of surface-bound cationic polymers to adhere and trigger biofilm formation was revealed by Pernagallo and co-workers,[135] who employed a high-

throughput microarray assay to asses a number of polymers for their affinities towards *Salmonella enterica* serovar Typhimurium (*S*. Typhimurium*)* and *E. coli.* In the case of polymers that were most efficient at binding bacteria, including cationic acrylates containing imidazolium groups, early stages of biofilm formation in the form of microcolonies could be detected.[135] However, for polymers in solution, the picture is less clear, with similar cationic polymers reported to both enhance, and reduce the production of biofilm upon clustering bacteria (**Figure 18**).

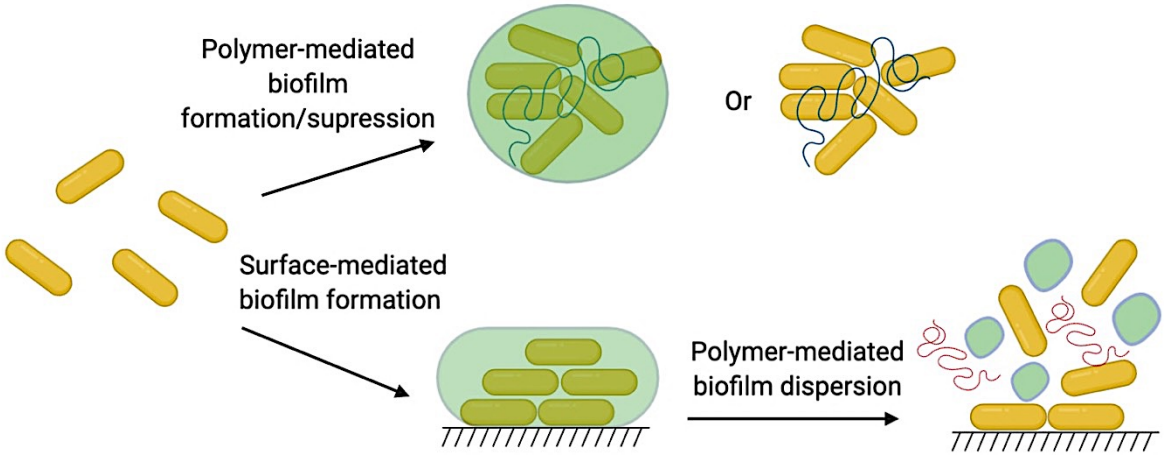

Figure 18. Proposed mechanisms by which polymers may interfere with or enhance biofilm formation.

Cationic polymers that cause aggregation of bacteria have been reported to upregulate biofilm formation in the cases of *E. coli* and *V. cholerae*,[116,136] and reduce biofilm in the case of *Pseudomonas aeruginosa*,[137] and *S. aureus.*[138] The mechanism of this reduction was rationalised by Foster and *et al.* as inhibition of *P. aeruginosa* adhesion to surfaces,[137] while the general rationale for an increase is due to a change in biofilm gene expression triggered by altered quorum sensing signalling.[116,132] These findings initially suggest that different species of bacteria respond differently to this class of material. However due to the variability in polymer chemistry and experimental conditions employed it is hard to draw solid conclusions. In this respect, small

differences in the toxicity of the polymers towards bacteria could have large impacts on the production of biofilm for example, as a defence mechanism in response to stress. [139] To fully assess whether these findings are as a result of differences in the polymer chemistry, differences in the bacterial species or differences in experimental conditions, it would be beneficial to compare how each of these materials behave towards all four species of bacteria under identical biological conditions. This is one example of how non-standardised methods and materials lead to uncertainty over the mechanism of the observed biological activity.

iv. g. Combinational approaches: Improving activity and specificity

Aside from off-target effects, another concerted effort in the area of cationic polymers for bacterial sequestration has been focused on modulating the chemistry on the polymer side chains to increase specificity and activity towards a particular species of bacteria. Work has been recently carried out by Magennis *et al.* using a copolymer system based on methacrylamide, whereby portions of the polymer containing a tertiary amine monomer and zwitterionic sulfobetaine monomer could be modulated by varying molar ratios during synthesis. The selectivity for binding the Gram-positive oral pathogen *S. mutans* over Gram-negative *E. coli* was found to be increased with increasing proportions of the zwitterionic component, and significantly, when the polymer consisted of 100% zwitterionic side chains, bacterial binding was exclusive to *S. mutans* in mixed cultures. The aforementioned study highlights the strength of systematically modulating one aspect of the polymer chemistry while observing the biological effect, demonstrating crucially that, by choosing the right chemistry, charged polymers can display selectivity towards a particular bacterial species.[55]

A recent dynamic approach involves the direct polymerisation of monomers "templated" to a target, thus generating a polymer possessing the optimal complimentary chemistry for that target (**Figure 19**).

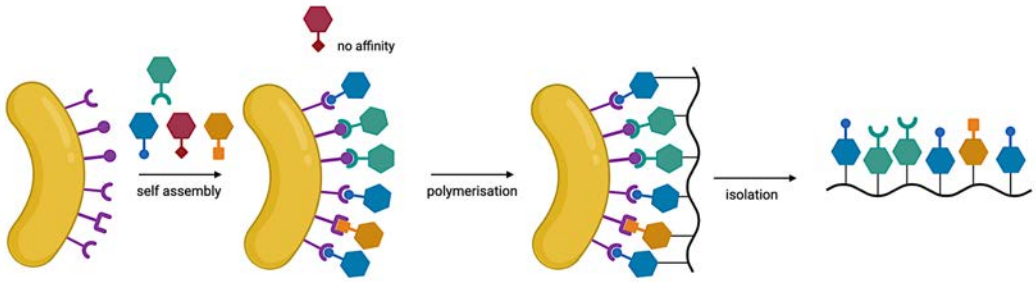

Figure 19. Generating polymers with optimal affinity to a bacterial target by templating.

This supramolecular polymerisation technique, known as templating, has been applied in the application of binding and aggregating bacteria selectively, and has the potential to be used in microbial detection. Work carried out by Magennis and co-workers demonstrated that synthesising "bacteria-instructed" polymers afforded selective aggregation of bacterial strains and species. To achieve bacteria-instructed polymer synthesis, *P. aeruginosa* and *E. coli* were separately incubated with quaternary amine and sulfobetaine methacrylate monomers, whereby the monomers were allowed to interact with the microbial surface and assemble into an "ideal" conformation.[140] Harnessing the reducing properties of the bacterial to generate Cu(I) species, ATRP style polymerisation proceeded from the surface-associated monomers. The group postulated that monomers on the surface of the bacteria would polymerise first and generate polymers with high affinity for that particular bacteria. Polymers synthesised in this way were isolated by washing bacterial cells with water and sodium chloride, before purifying by dialysis and recovering by lyophilisation. Templated polymers were then compared to the corresponding polymers synthesised

in the absence of bacteria and found that not only inter-species discrimination could be achieved but also inter-strain discrimination between clinical isolates and lab strains. This method highlights the potential for bacterial selectivity with cationic polymers but also offers a promising pathway towards simple detection methods for bacteria.[140]

iv. h. Aggregation of bacteria by glycopolymers

Bacterial aggregation by glycopolymers is believed to be driven by multivalent carbohydrate-protein interactions between the carbohydrate side-chain on the polymer and bacterial lectins.[96] Given the specificity of these binding interactions, which may be influenced by the sequence of displayed glycans,[141] synthetic strategies have focussed on controlling or defining the sequence of the glycopolymer side-chain *via* orthogonal reactions,[53,81,142] controlled polymerisations such as iterative type polymerisations, [143-145] and templating methods.[85,146,147]

The synthesis of glycopolymers to directly bind bacteria has focused on modulating the nature and location of the carbohydrate displayed on the polymer chain in order to increase complimentary binding to specific bacterial receptors (**Figure 20**).[148]

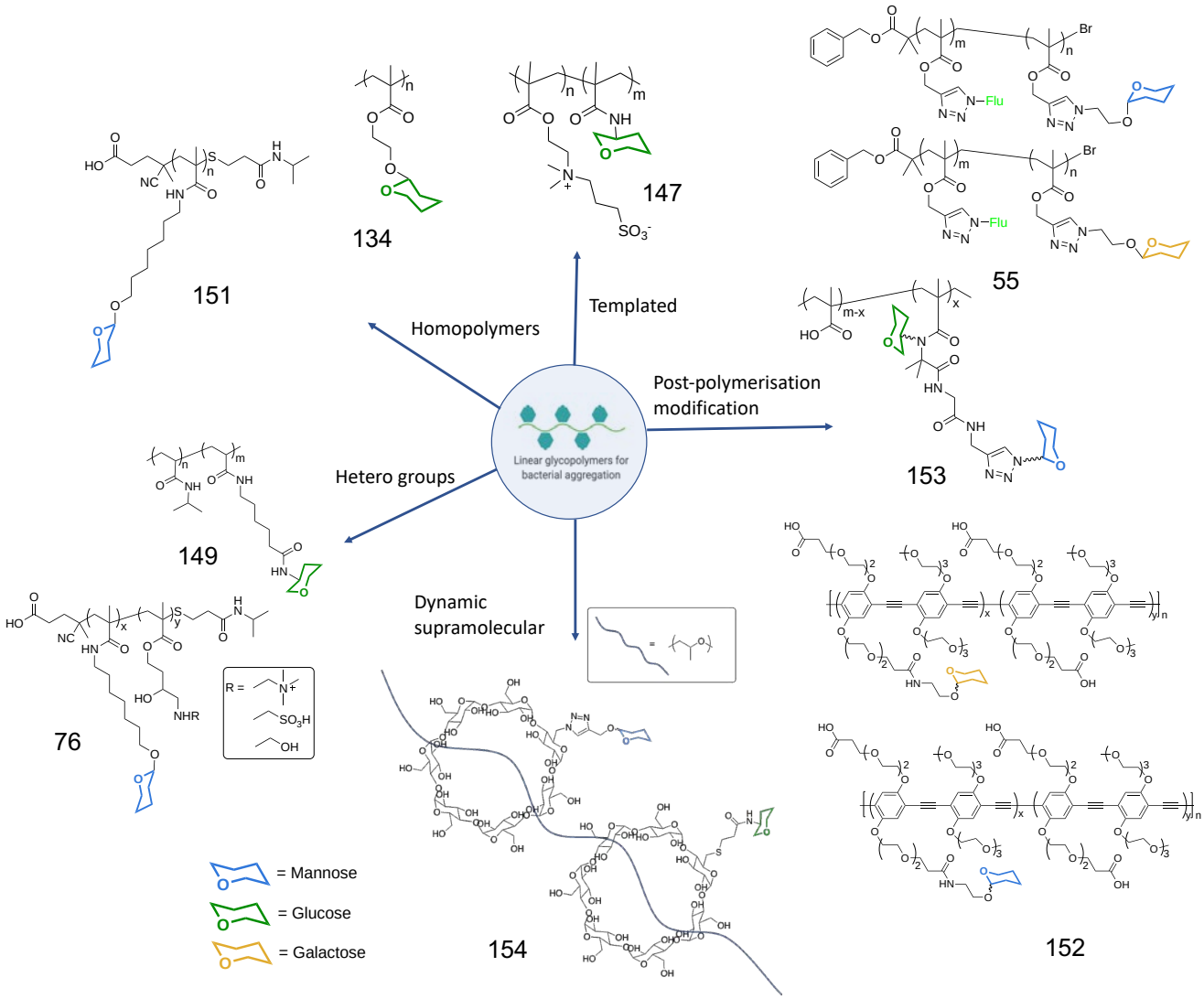

Figure 20. Glycopolymers discussed in this section which demonstrate direct bacterial aggregation. Numbers indicate the corresponding reference.

iv. i. Homo-glycopolymers

Glucose-displaying glycopolymers have been prepared from poly(2-glucosyloxyethyl methacrylate) p(GEMA) *via* RAFT and demonstrated to be effective at aggregating *E. coli,* which is known to bind glucose *via* the lectin FimH.[134] Bacterial aggregation could be controlled thermo-responsively by copolymerisation with a N-Isopropylacrylamide (NIPAM) containing monomer, yielding polymers that can "shield" the sugar from the bacteria in a temperature dependent manner by altering the tertiary structure of the polymer.[149] Adding increasing amounts of free glucose into the system

was reported to reduce and then completely inhibit this binding effect, suggesting that there was competition for the FimH binding sites. Sucrose, which does not bind as strongly to FimH in *E. coli,* was not able to reduce the size of the clusters formed.[149] This work demonstrated that linear glycopolymers can induce and control aggregation of *E. coli* rationalised as being due to specific protein- carbohydrate interactions.

In similar work, Yan and co-workers synthesised a methacrylate polymer displaying mannose on the side-chain with two different linker lengths, again designed to target the FimH lectin but with a stronger reported binding affinity compared with glucose (K_d = 2.3 μM) vs (K_d = 9.24 mM.[150]) The authors observed aggregation of *E. coli* upon exposure to 1-3 μM polymer concentration without antimicrobial activity and also explored the activity towards the FimH protein *ex vivo* by DLS measurement of glycopolymer-FimH complexes. The results of this provided evidence that a single glycopolymer could bind to multiple FimH proteins. Interestingly, star-shaped versions of the linear glycopolymer were assessed and found to have lower activity compared with linear glycopolymers, and more substantial was the discovery that the linker between the sugar and the polymer backbone was important for binding, with the longer linker and greater degrees of polymerisation (DPs) displaying higher activity with respect to suppressing bacterial adhesion to T84 cells.[151] The potential for this compound to reduce adhesion to host colon cells was examined by residual adhesion of *E. coli* to T84 epithelial cells. T84 cells were chosen here as a cell line to model the colon epithelium and are known to contain a key glycoprotein involved with attachment of *E. coli* in Crohn's disease patients. Polymer ligands were found to have a stronger inhibitory effect than their monovalent counterparts, in agreement with the principles of the cluster glycoside effect. The adhesion study was carried out by preincubating cells with glycopolymers prior to the addition of bacteria and also incubating the cells

with bacteria prior to adding the polymers. Then adhesion inhibition and ability of the glycopolymer to disrupt pre-adhered *E. coli* from the cell surface could be evaluated. The authors found that the most active glycopolymer reduced bacterial adhesion in both pre- and post-incubation studies by 45% and 47% respectively compared to non-treated conditions. *Ex vivo* studies were also carried out using a colonic loop model which revealed that a concentration of 3.4 μmol (with respect to the mannose component of the polymer) resulted in a 61% decrease in *E. coli* adhering to the colonic mucosa. The authors reported that increased DP was beneficial for the anti-adhesive activity, and that 3-arm and 8-arm stars constructed from the same linear displayed, on average, lower overall anti-adhesion activity. Also noted was that the length of the linker separating the glycan and the polymer backbone is important and, in this case, glycopolymers with short linkers were not able to inhibit adhesion.[151] Gouin and co-workers built on this work in a later study by copolymerising the most efficient monomer employed in the previous study with a monomer capable of undergoing post-polymerisation modification by epoxide ring opening. To this end, three scaffolds with different glycan/epoxide order were prepared and each underwent post polymerisation modification with either taurine, ethanolamine or (2-aminoethyl)trimethylammonium chloride (quaternary amine) resulting in a library of 27 compounds which were screened for ability to inhibit *E. coli* adherence to T84 cells. The authors acknowledged that these polymers exhibited some bacteriostatic activity, but this was not considered significant to the anti-adhesion assays. The results of this study, which investigated polymers containing both sugars and cationic groups, revealed very similar anti-adhesion activities for the most active hetero-glycopolymer compared to the most active homo-glycopolymer in the previously described work. The authors concluded that there was no clear correlation between the density or order of the glycan and the

nature of the hetero group on the polymer,[76] which suggests that presence of the mannose group in this case is the dominating contribution to the anti-adhesive effect compared to cationic groups.

iv. j. Different sugars, different specificity

In an earlier study, Disney and co-workers reported the synthesis of a fluorescent conjugated polymer comprising a poly(*p*-phenylene ethynylene) scaffold which could undergo post-polymerisation modification *via* carboxylic acid polymer groups and amine derivatised sugars to install mannosides and galactosides. An average loading of 25% sugars onto the polymer was achieved in this way, by means of a phenol sulfuric acid test. The prepared glycopolymers were tested for their ability to bind lectin ConA, as well as cluster *E. coli*, the first time such a study had been undertaken. The advantage of this approach was the formation of visible fluorescent clusters of bacteria without the need to further stain the bacteria or fluorescently label the polymer. The work confirmed that unbound mannose was not able to aggregate bacteria and that mannose- rather than galactose-displaying glycopolymers aggregated *E. coli* and could bind to ConA respectively, which is consistent with an aggregation mechanism of mannose specific multivalent binding. Importantly, it was shown that at concentrations of 10 μM or above of unbound mannose, bacterial aggregation was significantly decreased, indicating that the free sugar may bind to, and saturate bacterial lectins at these concentrations.[152]

Another approach taken by Magennis and co-workers saw fluorescently-labelled homo-glycopolymers of mannose and galactose prepared by CuAAC assessed with respect to their binding activity towards *S. mutans* and *E. coli*. Fluorescent microscopy determined that clustering *via* interaction with the mannose

polymer was favoured by *E. coli* while *S. mutans* displayed a greater affinity for the galactose polymer.[55] However, in this study, polymer efficacy was determined only by relative levels of fluorescence quantified from fluorescent images, and therefore heavily reliant on the polymer labelling strategy. The results were consistent with previous research reporting that *S. mutans* binds galactose residues specifically, and demonstrated the potential to differentiate between bacterial species by displaying different sugars on the polymer.[55]

In a similar approach by Xue and co-workers, a polymer scaffold was employed in the preparation of both homo- and hetero-glycopolymers by 2-stage post polymerisation modification.[153] In this study three glycopolymers were explored; two homopolymers of glucose or mannose and one polymer containing a mixture of both mannose and glucose. Post-polymerisation modification proceeded by the installation of either a glucose or mannose residue *via* a Ugi reaction, followed by a second modification of either glucose or mannose by CuAAc. It is important to note that in the first stage of the post polymerisation modification, 45% sugar loading with respect to glucose was observed, but the second stage this conversion was not calculated. The binding efficiencies of these polymers to lectins was tested with ConA, which demonstrated that, while the mannose homo-glycopolymer bound more strongly than the glucose homo-glycopolymer, the polymer containing both glycans showed significantly greater activity than either. This discovery was rationalised as a synergistic effect of hetero-glycopolymers known as the "heteroglycocluster effect".[148] With respect to binding *E. coli,* modest levels of aggregation were reported, however greater levels of aggregation were observed for the glycopolymer containing both mannose and glucose residues.[153]

iv. k. Dynamic approaches to glycopolymers

In a recent dynamic approach taken by Chen and co-workers, mannose and glucose were grafted onto cyclodextrin *via* thiol-ene and copper-catalysed azide-alkyne cycloaddition (CuAAc) click chemistry, and self-assembled on a poly propyleneglycol chain resulting in a polyrotaxane.[154] In this way, sugars tethered to the supramolecular polymer have increased degrees of freedom to access ligand orientations that best compliment bacterial receptors. Mannose and glucose homo-glycopolymers and hetero-glycopolymers were prepared and evaluated with respect to binding activity of ConA, and *E. coli.* In agreement with the "heteroglycocluster effect", polymers containing both glucose and mannose displayed the greatest activity towards bacterial aggregation and ConA binding, while the mannose homo-glycopolymer displayed greater activity than the glucose homo-glycopolymer.[154]

Templating polymers for bacterial aggregation has recently been reported for the preparation of glycopolymers,[147] in an effort to generate polymers with the ability to discriminate between different strains of the same bacteria. As discussed previously, templating cationic polymers towards strain-selective aggregation of bacteria has been reported,[140] and there are examples in the literature of glycopolymer synthesis based on templating bacterial lectins such as ConA. [85,146] However, until recently, templating glycopolymers has not been attempted for bacterial aggregation. Lou and co-workers designed a templating system employing a mannose containing monomer and an amphiphilic non-binding monomer to act as a spacer. Monomers previously incubated with *E. coli* were polymerised *via* bacteria mediated ATRP, and the resulting "templated" polymer was compared to a non-templated counterpart from the solution phase rather than the bacterial surface. It was noted that glycopolymers isolated from surface templating of bacteria resulted in a higher overall sugar content to those

isolated in the solution phase (50% vs 30%). Clustering of *E. coli* was assessed by microscopy for both the templated and untemplated glycopolymers, as well as homopolymers of each of the monomers. The templated polymer resulted in the greatest aggregation of *E. coli* by visual assessment, greater than the mannose homopolymer, suggesting that a greater density of the glycan does not always result in greater affinity. The templated polymer also displayed significant selectivity towards the templating strain in separate and mixed aggregation experiments employing a second *E. coli* strain as a control, whereas the mannose homopolymer displayed similar levels of aggregation for both strains. The potential therapeutic use for templated glycopolymers was demonstrated by their superior ability to supress *E. coli* adhesion to endothelial (blood vessel) cells.[147] These results support the hypothesis that glycan conformation can be complimentary to that of the binding sites of the bacteria, and might offer a route towards specific therapies.

iv. I. Linear polymers to aggregate bacteria: summary

Both cationic polymers and glycopolymers administered in sub-inhibitory concentrations have been shown to cause aggregation of bacteria. The mechanism of aggregation is generally accepted to be different for both classes of polymers, but both are attributed to multivalent bridging type aggregation; cationic polymers are predicted to interact with the negatively charged phospholipid-rich outer membrane *via* electrostatic interactions, while glycopolymers are designed to interact with bacteria lectins. Conclusions cannot be drawn about differences in the morphology of the aggregation driven by glyco- or cationic polymers, only that the aggregates, in all cases appear to agree with a bridging mode of aggregation, and thus are driven by multivalent interactions.

The antimicrobial effects of cationic polymers are well documented,[155] and are driven by a combination of positively charged groups and hydrophobic groups which disrupt bacterial membranes. For this reason, it is important when assessing biological activity to distinguish between bacteriostatic and bactericidal effects, both of which may result in the aggregation of bacteria. Employing sub-inhibitory concentrations to achieve the desired therapeutic effect not only reduces evolutionary pressure which could lead to resistant strains, but also reduces the likelihood that these materials will cause cytotoxicity to host cells. Conversely, glycopolymers (and glycol-nanomaterials) are considered more biocompatible than cationic polymers and therefore research into their application as a non-toxic sequestrant or inhibitor rather than an antimicrobial is more well established.

The aggregation of bacteria by polymeric materials can result in off-target effects as a result of bacteria responding to adhesion. These are often overlooked, especially in the case of glycopolymer research. Bacteria are highly adaptable and can withstand environmental changes by responding to environmental cues. As previously discussed, one of the ways bacteria perceive their surroundings is by quorum sensing. Detection of quorum sensing molecules by bacteria in response to population density triggers gene regulation responsible for toxin and biofilm regulation.[120] Work with cationic polymers and quorum sensing quenchers suggests clustering results in an overall enhancement of quorum sensing phenotypes,[117,118] while a quorum sensing molecule quencher can result in an oscillating pattern of quorum sensing expression and repression.[134] Changes in gene expression and biofilm formation *via* incubation with polymers have been attributed to gene regulation by quorum sensing, and clustering by cationic polymers can also trigger an increase in biofilm formation.[115,116,156] However, other studies have demonstrated that biofilm formation is

reduced or dispersed after treatment with cationic polymers.[137,138] It is not clear from the current research if lectin specific aggregation by glycopolymers results in attenuation of quorum sensing and biofilm formation, although main-chain glycopolymers containing cationic side-groups, analogous to chitosans, have been shown to have anti-biofilm properties *in vitro*.[157]

While there is some preliminary evidence that cationic polymers can reduce the virulence of *V. cholerae*,[116] there are studies which suggest that bacterial aggregates may be less susceptible to antibiotics.[33,117] Clearly, when designing these materials as antiadhesives, it is important to assess a range of relevant off-target effects and their possible implications.

With respect to cationic polymers, the impact that molecular weight of the polymer has on the binding activity is not clear. However, in the application of antimicrobials, longer cationic polymers have been reported to be less efficient at killing bacteria *via* membrane penetration,[122,158] whereas longer glycopolymers have been found to display greater binding than shorter linear glycopolymers in one study.[151] With regards to the tertiary structure, linear polymers have been shown to possess a greater binding affinity to lectins compared to star-shaped polymers.[151] Conversely, cationic dendrimers have been shown to exhibit greater clustering ability than their linear counterparts.[24]

The specific requirements of the cationic side group have not been probed but modulation of the cationic and zwitterionic portion of a cationic polymer has been reported for bacterial discrimination.[55,140]

With respect to glycopolymers, the nature of the sugar has been shown to be highly important for bacterial aggregation, and consistent with a receptor-binding mechanism of action. Multiple studies have outlined the benefits of heterogeneity when

designing glycopolymers, with combinations of strongly binding sugars such as mannose, and weakly binding sugars such as glucose displaying a higher level of binding compared to corresponding homo-glycopolymers. This observation may in part be also linked to the density of strongly bound glycans on the polymer chain, with one study into binding ConA suggesting that a lower density of the glycan component of the polymer can increase lectin binding affinity, possibly as a result of steric crowding.[53] However, higher densities are expected to increase binding with respect to statistical binding modes.[23] Lastly, there is strong evidence that a longer linking group separating the glycan and the polymer backbone benefits binding to bacterial receptors.[53,151] This may be accounted for by an increase in the degrees of freedom afforded to the glycan to allow better access to the lectin binding pocket.

iv. m. Conclusions

Adhesion to surfaces is a critical step for the success of pathogenic bacteria, and targeting and interfering with this step offers a potential route to control pathogenic bacteria, without inducing evolutionary pressure which drives antibiotic resistance. Materials that contain multivalent groups able to crosslink and aggregate bacteria through specific interactions are ideal for this purpose and take advantage of the "cluster-glycoside effect". In this regard, linear polymers are targeted as ideal nanomaterials capable of highly efficient bridging interactions with bacteria resulting in polymer engineered artificial microbial communities.

Current research discussed here, includes examples of both sugar containing polymers designed to target bacterial lectins, and cationic polymers, designed to interact non-specifically with the negatively charged bacterial cell membrane. By sequestering bacteria in this way, Polymers are positioned as an anti-adhesion

therapeutics, but also as a way to control pathogenicity through aggregation driven phenotypic changes.

A clear picture of structural and chemical requirements of these polymers for optimal activity and specificity is lacking. One of the greatest challenges in polymer science is controlling heterogeneity of the synthetic polymer so that the true nature of the structure-activity relationship can be deduced. Controlled radical polymerisation techniques such as RAFT polymerisation, have seen significant improvements in the control and predictability of molecular weight distributions, and an extensive choice of post-polymerisation conjugation strategies has allowed significantly greater scope to probe different polymer chemistries deriving from functional scaffolds. These polymerisation tools combined offer the potential for *in situ* and high-throughput screening of new polymer chemistries for many applications in nanomedicine, including bacterial anti-adhesion therapy.

Glycopolymers and cationic polymers show a huge potential for *ex vivo* anti-adhesion applications, such as wound dressings and oral treatments, but are currently unlikely to be a “silver bullet” for treating infections in a similar way to traditional antibiotics. This is due to a lack of absolute specificity towards a bacterial target. For example, in the same process whereby glycopolymers bind bacterial lectins and have been shown to cause agglutination of bacterial cells, they may bind host lectins and result in undesired agglutination for example, in blood cells. Furthermore, inhibition of carbohydrate-protein interactions *in vivo* is likely to have negative but unknown consequences to the host.[141] That being said, with advances in control over the polymer side-chain chemistry, alongside sequence-controlled,[143] and sequence-defined,[144] glycopolymers as well as bacterial instructed templating techniques,[85,140] it

is conceivable that polymers could one day target and cluster bacteria in a species-specific manner by the rational discovery of new polymer functionalities.

v. Objectives

This thesis represents an exploratory and multidisciplinary approach to optimising and evaluating the use of poly(acryloyl hydrazide) as a platform to screen rationally designed and unexplored polymer chemistries in the application of sequestering and modulating the physiology of *V. cholerae.*

In particular we will explore the use of cationic functional groups such as aromatic amines, which have not yet been reported in the application of sequestering bacteria (Chapter 2), and a small library of glycopolymers containing distinct side-chain carbohydrate functionality which have yet to be synthesised or tested in our labs (Chapter 3). Poly(acryloyl hydrazide) allows access to both cationic and glycopolymers such that the synthesis, application and the biological responses of each class of functional polymer will be compared under standardised conditions (Chapters 2 and 3).

Outside of the direct application of sequestering *V. cholerae*, increasing the versatility of the scaffold will be explored. Specifically, optimisation of the RAFT polymerisation of poly(acryloyl hydrazide) in order to access controlled polymerisations at higher DPs (Chapter 1), and additionally, to install and quantify new -group functionality on the polymer for subsequent control over fluorescent labelling with commercially available fluorescent dyes (Chapter 4).

vi. References

1 N. Rosenblatt-Farrell, *Environ. Health Perspect.*, 2009, 117, A244–50.

2 A. Khondker, A. K. Dhaliwal, S. Saem, A. Mahmood, C. Fradin, J. Moran-Mirabal and M. C. Rheinstädter, *Communications Biology*, 2019, 1–11.

3 K.-F. Kong, L. Schneper and K. Mathee, *APMIS*, **118**, 1–36.

4 G. Kapoor, S. Saigal and A. Elongavan, *J Anaesthesiol Clin Pharmacol*, 2017, **33**, 300–6.

5 Antibacterial agents in clinical development: an analysis of the antibacterial clinical development pipeline, including tuberculosis. Geneva: World Health Organization; 2017 (WHO/EMP/IAU/2017.12). Licence: CC BY-NC-SA 3.0 IGO.

6 Barber, S. (2017) Antimicrobial resistance. House of Commons Library Briefing Paper no. 8141. London: House of Commons Library.

7 The PLOS Medicine Editors, *PLoS Med*, 2016, **13**, e1002130–3.

8 R. C. Allen, R. Popat, S. P. Diggle and S. P. Brown, *Nature Reviews Microbiology*, 2014, **12**, 300–308.

9 O. Fleitas Martínez, M. H. Cardoso, S. M. Ribeiro and O. L. Franco, *Front. Cell. Infect. Microbiol.*, 2019, **9**, 808–24.

10 S. Alizon, A. Hurford, N. Mideo and M. van Baalen, *Journal of Evolutionary Biology*, 2008, **22**, 245–259.

11 A. M. Krachler and K. Orth, *Virulence*, 2014, **4**, 284–294.

12 B. N. Anderson, A. M. Ding, L. M. Nilsson, K. Kusuma, V. Tchesnokova, V. Vogel, E. V. Sokurenko and W. E. Thomas, *Journal of Bacteriology*, 2007, **189**, 1794–1802.

13 D. Rana and T. Matsuura, *Chemical Reviews*, 2010, **110**, 2448–2471.

14 D. Campoccia, L. Montanaro and C. R. Arciola, *Biomaterials*, 2013, **34**, 8533–8554.

15 J. S. Pinkner, H. Remaut, F. Buelens, E. Miller, V. Aberg, N. Pemberton, M. Hedenström, A. Larsson, P. Seed, G. Waksman, S. J. Hultgren and F. Almqvist, *Proc. Natl. Acad. Sci. U.S.A.*, 2006, **103**, 17897–17902.

16 E. Chorell, J. S. Pinkner, C. Bengtsson, T. S.-L. Banchelin, S. Edvinsson, A. Linusson, S. J. Hultgren and F. Almqvist, *Bioorganic & Medicinal Chemistry*, 2012, **20**, 3128–3142.

17 J. E. Klinth, J. S. Pinkner, S. J. Hultgren, F. Almqvist, B. E. Uhlin and O. Axner, *Eur Biophys J*, 2012, **41**, 285–295.

18 M. Hartmann and T. K. Lindhorst, *Eur. J. Org. Chem.*, 2011, **2011**, 3583–3609.

19 A. Bernardi, J. Jiménez-Barbero, A. Casnati, C. De Castro, T. Darbre, F. Fieschi, J. Finne, H. Funken, K.-E. Jaeger, M. Lahmann, T. K. Lindhorst, M. Marradi, P. Messner, A. Molinaro, P. V. Murphy, C. Nativi, S. Oscarson, S. Penadés, F. Peri, R. J. Pieters, O. Renaudet, J.-L. Reymond, B. Richichi, J. Rojo, F. Sansone, C. Schäffer, W. B. Turnbull, T. Velasco-Torrijos, S. Vidal, S. Vincent, T. Wennekes, H. Zuilhof and A. Imberty, *Chem. Soc. Rev.*, 2013, **42**, 4709–4727.

20 S. Ghosh, K. Chakraborty, T. Nagaraja, S. Basak, H. Koley, S. Dutta, U. Mitra and S. Das, *Proc. Natl. Acad. Sci. U.S.A.*, 2011, **108**, 3348–3353.

21 H. W. Moon and T. O. Bunn, *Vaccine*, 1993, **11**, 213–220.

22 N. Sharon and I. Ofek, *Glycoconjugate Journal*, 2000, **17**, 659–664.

23 J. E. Gestwicki, C. W. Cairo, L. E. Strong, K. A. Oetjen and L. L. Kiessling, *J. Am. Chem. Soc.*, 2002, **124**, 14922–14933.

24 E. Leire, S. P. Amaral, I. Louzao, K. Winzer, C. Alexander, E. Fernandez-Megia and F. Fernandez-Trillo, *Biomater. Sci.*, 2016, **4**, 998–1006.

25 M. A. Mintzer, E. L. Dane, G. A. O'Toole and M. W. Grinstaff, *Mol. Pharmaceutics*, 2012, **9**, 342–354.

26 M. Hartmann, P. Betz, Y. Sun, S. N. Gorb, T. K. Lindhorst and A. Krueger, *Chemistry*, 2012, **18**, 6485–6492.

27 K. Abstiens, M. Gregoritza and A. M. Goepferich, *ACS Appl. Mater. Interfaces*, 2018, **11**, 1311–1320.

28 M. Mammen, S.-K. Choi and G. M. Whitesides, *Angewandte Chemie International Edition*, 1998, **37**, 2754–2794.

29 L. L. Kiessling and N. L. Pohl, *Chem. Biol.*, 1996, **3**, 71–77.

30 J. J. Lundquist and E. J. Toone, *Chemical Reviews*, 2002, **102**, 555–578.

31 S. P. Strand, K. M. Vårum and K. Østgaard, *Colloids and Surfaces B: Biointerfaces*, 2003, **27**, 71–81.

32 J. Schwarz-Linek, G. Dorken, A. Winkler, L. G. Wilson, N. T. Pham, C. E. French, T. Schilling and W. C. K. Poon, *Europhys. Lett.*, 2010, **89**, 68003–7.

33 P. R. Secor, L. A. Michaels, A. Ratjen, L. K. Jennings and P. K. Singh, *Proc. Natl. Acad. Sci. U.S.A.*, 2018, **115**, 10780–10785.

34 N. Nazeer and M. Ahmed, *European Polymer Journal*, 2019, **119**, 148–154.

35 J. Guo, J. Qin, Y. Ren, B. Wang, H. Cui, Y. Ding, H. Mao and F. Yan, *Polym. Chem.*, 2018, **9**, 4611–4616.

36 M. R. Yeaman and N. Y. Yount, *Pharmacol Rev*, 2003, **55**, 27–55.

37 L. C. Paslay, B. A. Abel, T. D. Brown, V. Koul, V. Choudhary, C. L. McCormick and S. E. Morgan, *Biomacromolecules*, 2012, **13**, 2472–2482.

38 C. Ergene, K. Yasuhara and E. F. Palermo, *Polym. Chem.*, 2018, **9**, 2407–2427.

39 D. H. Stones and A. M. Krachler, *Biochemical Society Transactions*, 2016, **44**, 1571–1580.

40 H.-J. Gabius, S. André, J. Jiménez-Barbero, A. Romero and D. Solís, *Trends in Biochemical Sciences*, 2011, **36**, 298–313.

41 T. K. Lindhorst, in *Glycopolymer Code*, eds. C. R. Becer and L. Hartmann, Royal Society of Chemistry, Cambridge, 2015, pp. 1–16.

42 N. Sharon, *Biochimica et Biophysica Acta (BBA) - General Subjects*, 2006, **1760**, 527–537.

43 E. P. Magennis, A. L. Hook, M. C. Davies, C. Alexander, P. Williams and M. R. Alexander, *Acta Biomaterialia*, 2016, **34**, 84–92.

44 M. A. van Dongen, C. A. Dougherty and M. M. Banaszak Holl, *Biomacromolecules*, 2014, **15**, 3215–3234.

45 S. Bode, M. Enke, H. Görls, S. Hoeppener, R. Weberskirch, M. D. Hager and U. S. Schubert, *Polym. Chem.*, 2014, **5**, 2574.

46 H. C. Kolb, M. G. Finn and K. B. Sharpless, *Angew. Chem. Int. Ed. Engl.*, 2001, **40**, 2004–2021.

47 C. Barner-Kowollik, F. E. Du Prez, P. Espeel, C. J. Hawker, T. Junkers, H. Schlaad and W. Van Camp, *Angewandte Chemie International Edition*, 2010, **50**, 60–62.

48 E. Blasco, M. B. Sims, A. S. Goldmann, B. S. Sumerlin and C. Barner-Kowollik, *Macromolecules*, 2017, **50**, 5215–5252.

49 Y. Zhong, B. J. Zeberl, X. Wang and J. Luo, *Acta Biomaterialia*, 2018, **73**, 21–37.

50 C. W. Tornøe, C. Christensen and M. Meldal, *J. Org. Chem.*, 2002, **67**, 3057–3064.

51 V. V. Rostovtsev, L. G. Green, V. V. Fokin and K. B. Sharpless, *Angewandte Chemie International Edition*, 2002, **41**, 2596–2599.

52 P. L. Golas and K. Matyjaszewski, *Chem. Soc. Rev.*, 2010, **39**, 1338–1354.

53 S.-J. Richards, M. W. Jones, M. Hunaban, D. M. Haddleton and M. I. Gibson, *Angewandte Chemie International Edition*, 2012, **51**, 7812–7816.

54 D. Ponader, F. Wojcik, F. Beceren-Braun, J. Dernedde and L. Hartmann, *Biomacromolecules*, 2012, **13**, 1845–1852.

55 E. P. Magennis, N. Francini, F. Mastrotto, R. Catania, M. Redhead, F. Fernandez-Trillo, D. Bradshaw, D. Churchley, K. Winzer, C. Alexander and G. Mantovani, *PLoS ONE*, 2017, **12**, e0180087.

56 B. S. Sumerlin, N. V. Tsarevsky, G. Louche, R. Y. Lee and K. Matyjaszewski, *Macromolecules*, 2005, **38**, 7540–7545.

57 E. M. Sletten and C. R. Bertozzi, *Angewandte Chemie International Edition*, 2009, **48**, 6974–6998.

58 N. J. Agard, J. A. Prescher and C. R. Bertozzi, *J. Am. Chem. Soc.*, 2004, **126**, 15046–15047.

59 C. J. Pickens, S. N. Johnson, M. M. Pressnall, M. A. Leon and C. J. Berkland, *Bioconjugate Chem.*, 2018, **29**, 686–701.

60 H. Willcock and R. K. O'Reilly, *Polym. Chem.*, 2010, **1**, 149–157.

61 C. E. Hoyle, A. B. Lowe and C. N. Bowman, *Chem. Soc. Rev.*, 2010, **39**, 1355–34.

62 P. J. Roth, C. Boyer, A. B. Lowe and T. P. Davis, *Macromol. Rapid Commun.*, 2011, **32**, 1123–1143.

63 C. W. Scales, A. J. Convertine and C. L. McCormick, *Biomacromolecules*, 2006, **7**, 1389–1392.

64 M. P. Robin, M. W. Jones, D. M. Haddleton and R. K. O'Reilly, *ACS Macro Lett.*, 2011, **1**, 222–226.

65 N. K. Singha, M. I. Gibson, B. P. Koiry, M. Danial and H.-A. Klok, *Biomacromolecules*, 2011, **12**, 2908–2913.

66 C. Boyer and T. P. Davis, *Chem. Commun.*, 2009, **119**, 6029–3.

67 M. I. Gibson, E. Fröhlich and H.-A. Klok, *J. Polym. Sci. A Polym. Chem.*, 2009, **47**, 4332–4345.

68 M. Mammen, G. Dahmann and G. M. Whitesides, *J. Med. Chem.*, 1995, **38**, 4179–4190.

69 S. R. A. Devenish, J. B. Hill, J. W. Blunt, J. C. Morris and M. H. G. Munro, *Tetrahedron Letters*, 2006, **47**, 2875–2878.

70 J. D. Flores, J. Shin, C. E. Hoyle and C. L. McCormick, *Polym. Chem.*, 2010, **1**, 213–220.

71 E. A. Hoff, B. A. Abel, C. A. Tretbar, C. L. McCormick and D. L. Patton, *Macromolecules*, 2016, **49**, 554–563.

72 F. Biedermann, E. A. Appel, J. del Barrio, T. Gruendling, C. Barner-Kowollik and O. A. Scherman, *Macromolecules*, 2011, **44**, 4828–4835.

73 A. K. Yudin, Aziridines and Epoxides in Organic Synthesis, 2006.

74 H.-J. Jang, J. T. Lee and H. J. Yoon, *Polym. Chem.*, 2015, **6**, 3387–3391.

75 S. Montolio, O. Zagorodko, R. Porcar, M. Isabel Burguete, S. V. Luis, H. Tenhu and E. García-Verdugo, *Polym. Chem.*, 2017, **8**, 4789–4797.

76 X. Yan, A. Sivignon, N. Barnich, S. G. Gouin, J. Bouckaert, E. Fleury and J. Bernard, *Polym. Chem.*, 2016, **7**, 2674–2683.

77 D. K. Kölmel and E. T. Kool, *Chemical Reviews*, 2017, **117**, 10358–10376.

78 J. Kalia and R. T. Raines, *Angewandte Chemie International Edition*, 2008, **47**, 7523–7526.

79 R. K. V. Lim and Q. Lin, *Chem. Commun.*, 2010, **46**, 1589–29.

80 J. M. Priegue, D. N. Crisan, J. Martínez-Costas, J. R. Granja, F. Fernandez-Trillo and J. Montenegro, *Angewandte Chemie International Edition*, 2016, **55**, 7492–7495.

81 K. Godula and C. R. Bertozzi, *J. Am. Chem. Soc.*, 2010, **132**, 9963–9965.

82 A. Kumar, R. R. Ujjwal, A. Mittal, A. Bansal and U. Ojha, *ACS Appl. Mater. Interfaces*, 2014, **6**, 1855–1865.

83 D. N. Crisan, O. Creese, R. Ball, J. L. Brioso, B. Martyn, J. Montenegro and F. Fernandez-Trillo, *Polym. Chem.*, 2017, **8**, 4576–4584.

84 A. K. Pearce, B. E. Rolfe, P. J. Russell, B. W. C. Tse, A. K. Whittaker, A. V. Fuchs and K. J. Thurecht, *Polym. Chem.*, 2014, **5**, 6932–6942.

85 C. S. Mahon, M. A. Fascione, C. Sakonsinsiri, T. E. McAllister, W. Bruce Turnbull and D. A. Fulton, *Org. Biomol. Chem.*, 2015, **13**, 2756–2761.

86 R. C. Charles and E. T. Ryan, *Current Opinion in Infectious Diseases*, 2011, **24**, 472–477.

87 A. J. Silva and J. A. Benitez, *PLoS Negl Trop Dis*, 2016, **10**, e0004330.

88 K. L. Meibom, X. B. Li, A. T. Nielsen, C.-Y. Wu, S. Roseman and G. K. Schoolnik, *Proc Natl Acad Sci USA*, 2004, **101**, 2524–2529.

89 F. Federspiel and M. Ali, *BMC Public Health*, 2018, **18**, 626.

90 M. A. Shannon, P. W. Bohn, M. Elimelech, J. G. Georgiadis, B. J. Mariñas and A. M. Mayes, *Nature*, 2008, **452**, 301–310.

91 H. Dang and C. R. Lovell, *Microbiol. Mol. Biol. Rev.*, 2015, **80**, 91–138.

92 J. K. Teschler, D. Zamorano-Sánchez, A. S. Utada, C. J. A. Warner, G. C. L. Wong, R. G. Linington and F. H. Yildiz, *Nature Reviews Microbiology*, 2015, **13**, 255–268.

93 N. Firon, S. Ashkenazi, D. Mirelman, I. Ofek and N. Sharon, *Infect. Immun.*, 1987, **55**, 472–476.

94 M. M. Sauer, R. P. Jakob, J. Eras, S. Baday, D. Eriş, G. Navarra, S. Bernèche, B. Ernst, T. Maier and R. Glockshuber, *Nature Communications*, 2016, **7**, 190–13.

95 J. Li, M. S. Lim, S. Li, M. Brock, M. E. Pique, V. L. Woods Jr. and L. Craig, *Structure*, 2008, **16**, 137–148.

96 S. R. S. Ting, G. Chen, M. H. Stenzel. *Polym. Chem.,* 2010*,* **1**, 1392-1412.

97 A. K. Harapanahalli, J. A. Younes, E. Allan, H. C. van der Mei and H. J. Busscher, *PLoS Pathog*, 2015, **11**, e1005057.

98 A. S. Utada, R. R. Bennett, J. C. N. Fong, M. L. Gibiansky, F. H. Yildiz, R. Golestanian and G. C. L. Wong, *Nature Communications*, 2014, **5**, 44.

99 A. P. Berke, L. Turner, H. C. Berg and E. Lauga, *Phys. Rev. Lett.*, 2008, **101**, 23–4.

100 S. Kojima, K. Yamamoto, I. Kawagishi and M. Homma, *Journal of Bacteriology*, 1999, **181**, 1927–1930.

101 G. Jonson, J. Holmgren and A.-M. Svennerholm, *Microbial Pathogenesis*, 1991, **11**, 433–441.

102 D. Sasmal, B. Guhathakurta, A. N. Ghosh, C. R. Pal and A. Datta, *FEMS Immunology & Medical Microbiology*, 1999, **23**, 221–227.

103 N. O'Boyle, B. Houeix, M. Kilcoyne, L. Joshi and A. Boyd, *International Journal of Medical Microbiology*, 2013, **303**, 563–573.

104 A. Hsiao, Z. Liu, A. Joelsson and J. Zhu, *Proc Natl Acad Sci USA*, 2006, **103**, 14542–14547.

105 N. Keyhani, *Biochimica et Biophysica Acta (BBA) - General Subjects*, 1999, **1473**, 108–122.

106 R. Tarsi and C. Pruzzo, *Appl. Environ. Microbiol.*, 1999, **65**, 1348–1351.

107 L. Vezzulli, E. Pezzati, B. Repetto, M. Stauder, G. Giusto and C. Pruzzo, *Lett Appl Microbiol*, 2007, **46**, 119-125.

108 T. J. Kirn, B. A. Jude and R. K. Taylor, *Nature*, 2005, **438**, 863–866.

109 R. C. Goy, D. de Britto and O. B. G. Assis, *Polímeros*, 2009, **19**, 241–247.

110 P. Sahariah, V. S. Gaware, R. Lieder and S. Jónsdóttir, *Marine Drugs*, 2014, **12**, 4635–4658.

111 C. Muanprasat and V. Chatsudthipong, *Future Medicinal Chemistry*, 2013, **5**, 781–798.

112 M. K. Waldor and J. J. Mekalanos, *Science*, 1996, **272**, 1910–1914.

113 S. J. Krebs and R. K. Taylor, *Journal of Bacteriology*, 2011, **193**, 5260–5270.

114 W. M. Dunne, *Clinical Microbiology Reviews*, 2002, **15**, 155–166.

115 N. Perez-Soto, L. Moule, D. N. Crisan, I. Insua, L. M. Taylor-Smith, K. Voelz, F. Fernandez-Trillo and A. M. Krachler, *Chem. Sci.*, 2017, **8**, 5291–5298.

116 N. Perez-Soto, O. Creese, F. Fernandez-Trillo and A. M. Krachler, *ACS Chem. Biol.*, 2018, **13**, 3021–3029.

117 P. Zhang, H. Lu, H. Chen, J. Zhang, L. Liu, F. Lv and S. Wang, *Anal. Chem.*, 2016, **88**, 2985–2988.

118 L. T. Lui, X. Xue, C. Sui, A. Brown, D. I. Pritchard, N. Halliday, K. Winzer, S. M. Howdle, F. Fernandez-Trillo, N. Krasnogor and C. Alexander, *Nature Chemistry*, 2013, **5**, 1058–1065.

119 M. Jemielita, N. S. Wingreen and B. L. Bassler, *eLife*, 2018, **7**, e1002210–25.

120 B. L. Bassler, *Current Opinion in Microbiology*, 1999, **2**, 582–587.

121 Y. Yang, Z. Cai, Z. Huang, X. Tang and X. Zhang, *Polym J*, 2017, **50**, 33–44.

122 K. Kuroda, G. A. Caputo and W. F. DeGrado, *Chem. Eur. J.*, 2008, **15**, 1123–1133.

123 E. Lih, S. H. Oh, Y. K. Joung, J. H. Lee and D. K. Han, *Progress in Polymer Science*, 2015, **44**, 28–61.

124 L. M. Thoma, B. R. Boles and K. Kuroda, *Biomacromolecules*, 2014, **15**, 2933–2943.

125 C. K. S. Pillai, W. Paul and C. P. Sharma, *Progress in Polymer Science*, 2009, **34**, 641–678.

126 E. I. Rabea, M. E. T. Badawy, C. V. Stevens, G. Smagghe and W. Steurbaut, *Biomacromolecules*, 2003, **4**, 1457–1465.

127 P. Sahariah, B. M. Óskarsson, M. Á. Hjálmarsdóttir and M. Másson, *Carbohydrate Polymers*, 2015, **127**, 407–417.

128 X. Qin, J. Emich and F. Goycoolea, *Biomolecules*, 2018, **8**, 87–14.

129 G. A. O'Toole, *JoVE*, 2011, 1–2.

130 J. W. Costerton, P. S. Stewart and E. P. Greenberg, *Science*, 1999, **284**, 1318–1322.

131 M. B. Miller and B. L. Bassler, *Annu. Rev. Microbiol.*, 2001, **55**, 165–199.

132 C. M. Waters, W. Lu, J. D. Rabinowitz and B. L. Bassler, *Journal of Bacteriology*, 2008, **190**, 2527–2536.

133 E. C. Carnes, D. M. Lopez, N. P. Donegan, A. Cheung, H. Gresham, G. S. Timmins and C. J. Brinker, *Nat Chem Biol*, 2009, **6**, 41–45.

134 X. Xue, G. Pasparakis, N. Halliday, K. Winzer, S. M. Howdle, C. J. Cramphorn, N. R. Cameron, P. M. Gardner, B. G. Davis, F. Fernandez-Trillo and C. Alexander, *Angewandte Chemie International Edition*, 2011, **50**, 9852–9856.

135 S. Pernagallo, M. Wu, M. P. Gallagher and M. Bradley, *J. Mater. Chem.*, 2011, **21**, 96–101.

136 H. Yuan, Z. Liu, L. Liu, F. Lv, Y. Wang and S. Wang, *Adv. Mater.*, 2014, **26**, 4333–4338.

137 L. L. Foster, S.-I. Yusa and K. Kuroda, *Antibiotics*, 2019, **8**, 61–16.

138 P. Zhang, S. Li, H. Chen, X. Wang, L. Liu, F. Lv and S. Wang, *ACS Appl. Mater. Interfaces*, 2017, **9**, 16933–16938.

139 K. Jefferson, *FEMS Microbiology Letters*, 2004, **236**, 163–173.

140 E. P. Magennis, F. Fernandez-Trillo, C. Sui, S. G. Spain, D. J. Bradshaw, D. Churchley, G. Mantovani, K. Winzer and C. Alexander, *Nat Mater*, 2014, **13**, 748–755.

141 T. K. Lindhorst, in *Glycopolymer Code*, eds. C. R. Becer and L. Hartmann, Royal Society of Chemistry, Cambridge, 2015, pp. 1–16.

142 B. Martyn, C. I. Biggs and M. I. Gibson, *J. Polym. Sci. A Polym. Chem.*, 2018, **57**, 40–47.

143 C. Gerke, M. F. Ebbesen, D. Jansen, S. Boden, T. Freichel and L. Hartmann, *Biomacromolecules*, 2017, **18**, 787–796.

144 D. Ponader, F. Wojcik, F. Beceren-Braun, J. Dernedde and L. Hartmann, *Biomacromolecules*, 2012, **13**, 1845–1852.

145 Q. Zhang, A. Anastasaki, G.-Z. Li, A. J. Haddleton, P. Wilson and D. M. Haddleton, *Polym. Chem.*, 2014, **5**, 3876–3883.

146 N. Nagahori and S. Nishimura, *Biomacromolecules*, 2001, **2**, 22–24.

147 Y. Luo, Y. Gu, R. Feng, J. Brash, A. M. Eissa, D. M. Haddleton, G. Chen and H. Chen, *Chem. Sci.*, 2019, **10**, 5251–5257.

148 J. L. Jiménez Blanco, C. Ortiz Mellet and J. M. García Fernández, *Chem. Soc. Rev.*, 2013, **42**, 4518–4531.

149 G. Pasparakis, A. Cockayne and C. Alexander, *J. Am. Chem. Soc.*, 2007, **129**, 11014–11015.

150 J. Bouckaert, J. Berglund, M. Schembri, E. De Genst, L. Cools, M. Wuhrer, C.-S. Hung, J. Pinkner, R. Slättegård, A. Zavialov, D. Choudhury, S. Langermann, S. J. Hultgren, L. Wyns, P. Klemm, S. Oscarson, S. D. Knight and H. De Greve, *Molecular Microbiology*, 2004, **55**, 441–455.

151 X. Yan, A. Sivignon, N. Yamakawa, A. Crepet, C. Travelet, R. Borsali, T. Dumych, Z. Li, R. Bilyy, D. Deniaud, E. Fleury, N. Barnich, A. Darfeuille-Michaud, S. G. Gouin, J. Bouckaert and J. Bernard, *Biomacromolecules*, 2015, **16**, 1827–1836.

152 M. D. Disney, J. Zheng, T. M. Swager and P. H. Seeberger, *J. Am. Chem. Soc.*, 2004, **126**, 13343–13346.

153 L. Xue, X. Xiong, K. Chen, Y. Luan, G. Chen and H. Chen, *Polym. Chem.*, 2016, **7**, 4263–4271.

154 X. Hu, J. Gao, Y. Luo, T. Wei, Y. Dong, G. Chen and H. Chen, *Macromol. Rapid Commun.*, 2017, **38**, 1700434–8.

155 F. Siedenbiedel and J. C. Tiller, *Polymers*, 2012, **4**, 46–71.

156 I. Louzao, C. Sui, K. Winzer, F. Fernandez-Trillo and C. Alexander, *European Journal of Pharmaceutics and Biopharmaceutics*, 2015, **95**, 47–62.

157 V. P. Narayanaswamy, A. P. Duncan, J. J. LiPuma, W. P. Wiesmann, S. M. Baker and S. M. Townsend, *Antimicrob Agents Chemother*, 2019, **63**, 144–11.

158 K. Lienkamp, K.-N. Kumar, A. Som, K. Nüsslein and G. N. Tew, *Chem. Eur. J.*, 2009, **15**, 11710–11714.

Chapter 1

Poly(boc-acryloyl hydrazide): the importance of temperature and RAFT degradation on its preparation

O. Creese, P. Adoni, G. Su, A. Romanyuk and P. Fernández-Trillo, *Polym. Chem.*, 2019, **124**, 14922–7.

Preface to chapter

There are now a number of well-established controlled radical polymerisation (CRP) techniques to exert control over traditional radical chain growth polymerisation. Two of the most studied are atom transfer radical polymerisation (ATRP), and reversable addition-fragmentation chain transfer (RAFT) polymerisation. The general principles behind CRP involves the inclusions of an additional chemical agent into the polymerisation that provides an alternative chemical pathway to radical addition, and thus equilibrium, between active and dormant chains.[1]

RAFT polymerisation, first reported by Moad, Rizzardo and Thang in 1998,[2] has become increasingly popular as a polymerisation technique, a reflection on its compatibility with a wide range of monomers, ease of application, low dispersities ($Đ_M$) and end group fidelity allowing for further chain extension or end group modification.[3] A RAFT agent takes the general form of Z(SR)C=S where Z and R substituents can be modified to tune the reactivity of the RAFT agent to match that of the monomer. The mechanism (**Scheme 3**) initially follows that of traditional radical addition polymerisation from generation of radicals (Step 1.) and addition of monomers to form a short polymer chain ($P_n^{\cdot}$) (Step 2.). At this point radicals add to the RAFT agent and addition-fragmentation equilibrium is set up (Step 3.). Upon fragmentation, the $R^{\cdot}$ group proceeds to reinitiate dormant chains (Step 4.). This fragmentation is followed by the main addition-fragmentation equilibrium between propagating radicals and "deactivated" dormant chains associated with the RAFT agent (Step 5.), effectively "passing" the radical between propagating chains. In general, for a controlled polymerisation by RAFT, the propagation rate should be lower than the deactivation

rate so that fewer than one monomer is added per cycle. In this way, all polymer chains should grow at similar rates to a similar degree of polymerisation (DP). However, if the poly-RAFT-adduct is too stable, and thus equilibrium is shifted away from fragmentation, very little propagation with occur and result in a retardation of the polymerisation.[3]

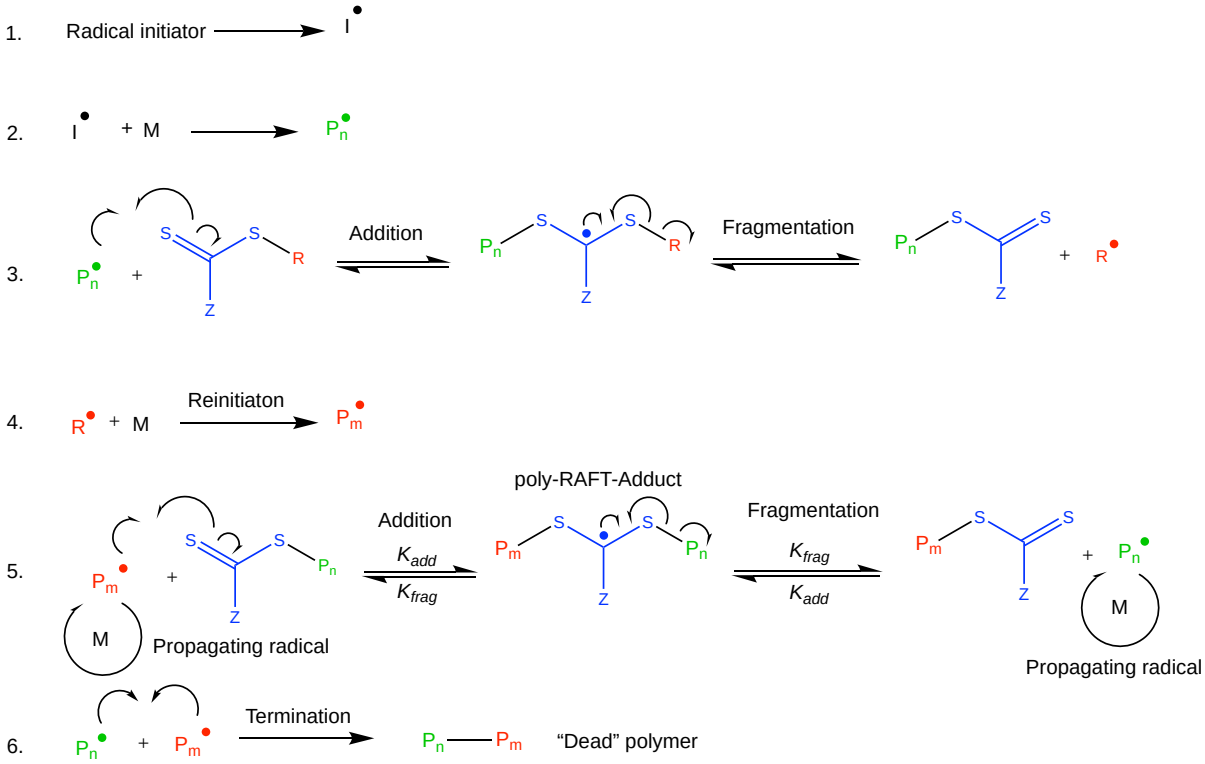

Scheme 3. General mechanism of RAFT polymerisation detailing the steps outlined above.

The requirement for a successful polymerisation by RAFT is to employ a RAFT agent containing Z and R groups best compatible with the monomer to afford favourable equilibrium. In an ideal RAFT polymerisation, the resulting polymers containing RAFT end-groups are ”living”, and can be chain-extended *via* the addition of further monomer.[4] Degradation or loss of the RAFT agent can thus lead to termination reactions (Step 6.) resulting in “dead” polymer chains, characteristic of an uncontrolled polymerisation process and resulting in broad ($Đ_M$) and low conversions.[5,6] Degradation of the RAFT agent has been reported in the

polymerisation of acrylamides,[5] and something we had observed in the preparation of poly(Boc-acryloyl hydrazide) (**boc-P$_x$**).[7] This chapter describes our efforts towards minimising degradation of the RAFT agent, and as such, affording improved control over the polymerisation of **boc-P$_x$** which was reported in the following publication.

The work presented here outlines improved control of poly(acryloyl hydrazide), the polymer predominantly employed throughout this thesis, which is important when evaluating polymer structure-activity relationships in biological systems in order to negate observable differences in activity arising from differences in the polymer structure.

References

1 S. Perrier, *Macromolecules*, 2017, **50**, 7433–7447.

2 J. Chiefari, Y. K. B. Chong, F. Ercole, J. Krstina, J. Jeffery, T. P. T. Le, R. T. A. Mayadunne, G. F. Meijs, C. L. Moad, G. Moad, E. Rizzardo and S. H. Thang, *Macromolecules*, 1998, **31**, 5559–5562.

3 G. Moad, E. Rizzardo and S. H. Thang, *Aust. J. Chem.*, 2012, **65**, 985–92.

4 L. Martin, G. Gody and S. Perrier, *Polym. Chem.*, 2015, **6**, 4875–4886.

5 B. A. Abel and C. L. McCormick, *Macromolecules*, 2016, **49**, 465–474.

6 J. D. Flores, J. Shin, C. E. Hoyle and C. L. McCormick, *Polym. Chem.*, 2010, **1**, 213–220.

7 D. N. Crisan, O. Creese, R. Ball, J. L. Brioso, B. Martyn, J. Montenegro and F. Fernandez-Trillo, *Polym. Chem.*, 2017, **8**, 4576–4584.

Declaration

All experiments presented in this chapter were designed by the author and Paco Fernandez-Trillo unless stated. All data presented in this chapter was independently analysed by the author and Paco Fernandez-Trillo and Andrey Romanyuk.

All polymerisations reported in the paper were analysed using GPC by the author to determine M_n M_w and $Đ_m$ and all NMR and conversion calculations were run by the author, unless specified below. Baseline correction of GPC traces were performed by Andrey Romanyuk.

Experimental Contributions in this chapter:

Pavan Adoni (University of Birmingham) carried out synthesis and characterisation steps towards the synthesis of small molecule analogue of a DP= 1 of N'-(*tert*-butoxycarbonyl)acryloyl hydrazide, (data presented in Scheme S1, Figure S3, Figure S5), chain extension of "living" and "dead" poly(boc-acryloyl hydrazide), (data presented in figure S6, S7 and S8), and polymerisation kinetics for conditions: DP150 100^{o}C, DP50 80^{o}C and DP100 65^{o}C.

Andrey Romanyuk (University of Birmingham) carried out baseline correction of GPC data prior to final analysis and publication.

Guanglong Su carried out monomer synthesis of N′-(tert-butoxycarbonyl)acryloyl hydrazide (**1**), and performed some of the initial kinetic experiments.

All co-authors contributed actively to discussions during the work and were involved with the proof reading of the final manuscript.

Correction to Figure 1

Figure 1 from the original manuscript has been modified by replacement of the segmental line regression for M_n vs ρ plot with simple linear regression. The former being misleading as to the polymerisation progression past t(dead). The correction does not impact the conclusions of the work and the figure caption is unchanged from the original.

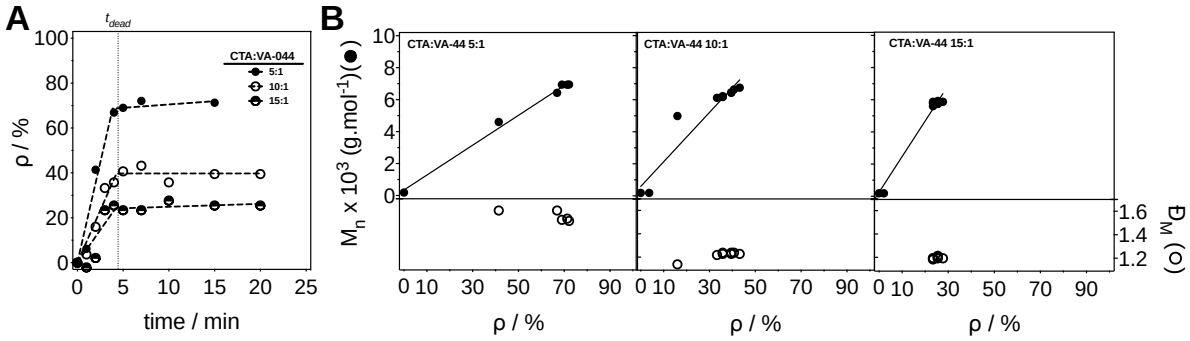

Figure 1. A) Plot of conversion (ρ) vs. time and B) measured number average molecular mass (M_n) vs. conversion (●) and dispersity in molecular mass ($Đ_M$) vs conversion (◯), for polymerisations of N'-(tert-butoxycarbonyl)acryloyl hydrazide (1) performed with different CTA:VA-044 ratios. Conditions: [M]=0.9M, [M]/[CTA]=50/1. M_n and $Đ_M$ calculated by GPC using 0.05 M LiBr in dimethylformamide (DMF) at 60 º C.

Polymer Chemistry

PAPER

View Article Online
View Journal

Cite this: DOI: 10.1039/c9py01222b

Poly(Boc-acryloyl hydrazide): the importance of temperature and RAFT agent degradation on its preparation†

Oliver Creese, Pavan Adoni, Guanlong Su, Andrey Romanyuk and Paco Fernandez-Trillo *

Received 13th August 2019,
Accepted 2nd October 2019

DOI: 10.1039/c9py01222b

rsc.li/polymers

Poly(acryloyl hydrazide) is a versatile polymer scaffold readily functionalised through post-polymerisation modification with aldehydes to yield polymers for biological applications. However, its polymerisation is affected by nucleophilic degradation of the RAFT agent that leads to early termination, an issue often overlooked in the polymerisation of primary acrylamides. Here we report the effect of temperature on the RAFT polymerisation of *N*′-(*tert*-butoxycarbonyl)acryloyl hydrazide (**1**) and demonstrate that by carefully selecting this polymerisation temperature, a balance between rate of polymerisation and rate of degradation of the RAFT agent can be achieved. This way greater control over the polymerisation process is achieved, allowing the synthesis of Boc-protected poly(acryloyl hydrazide) with higher degrees of polymerisation (DP) than those obtained previously, while still maintaining low dispersities ($Đ_M$).

Introduction

Synthetic polymers are increasingly becoming an attractive means of interfacing biological systems *via* multivalent binding, displaying activities orders of magnitude higher than those of their monovalent components.[1–5] Thus, polymers are now widely researched for biomedical applications including as antimicrobials,[6,7] as drug and gene delivery vehicles,[2,8] as biological sensors,[9,10] or as "smart" biomaterials with anti-fouling properties.[11] Highly functional polymers developed for specific applications generally involve the use of functional monomers which either already possess the final desired functionality, or have the capability of undergoing post-polymerisation modification to introduce the desired functionality. This latter approach can greatly broaden the scope of chemical functionalities used. Post-polymerisation modification has normally relied on click chemistries,[12] and has now been greatly expanded through the use of oxime[13] and hydrazone chemistry,[14,15] reductive amination,[16] and epoxide ring opening.[17]

A common limitation when developing synthetic polymers for biomedical applications is the need to screen large libraries of compounds which is costly and time consuming. In this regard, poly(acryloyl hydrazide) has been recently reported as a versatile platform for the synthesis and screening of polymers for biomedical applications.[14,18–20] Functional polymers are obtained by simple incubation of poly(acryloyl hydrazide) with functional aldehydes, both under aqueous or organic conditions,[14] and this polymer has now been applied to the development of glycan arrays,[18] pH sensitive drug-delivery,[21] and nucleic acid delivery.[20,22,23] In our laboratories poly(acryloyl hydrazide) was prepared from Boc-protected precursor **Boc-P$_x$** (Scheme 1) following deprotection with TFA.[14] Reversible addition–fragmentation chain-transfer (RAFT) polymerisation of *N*′-(*tert*-butoxycarbonyl) acryloyl hydrazide (**1**) resulted in a small library of polymers. However, control over the polymerisation was lost with increasing conversion and degree of polymerisation, possibly as a result of degradation of the RAFT agent through intramolecular nucleophilic attack. This degradation has been reported in the RAFT polymerisation of other acrylamide derivatives,[24,25] including closely related methacryloyl hydrazide,[26] with better control reported when the polymerisation is carried out at low temperatures.[25,27] This side-reaction is often overlooked in the polymerisation of primary and secondary acryl- and methacrylamides, and makes synthesising highly functional polymers from this type of monomers inherently challenging.[28] The need for greater control over these materials is more significant when looking to understand better the nature of the structure–activity relationship throughout post-polymerisation modification and biological screening.

Here, we report the effect of temperature and the decomposition rate of the initiator on the polymerisation of *N*′-(*tert*-butoxycarbonyl)acryloyl hydrazide (**1**), as a route to optimise the preparation of poly(acryloyl hydrazide). Polymerisations

School of Chemistry, and Institute of Microbiology and Infection, University of Birmingham, Edgbaston, B15 2TT Birmingham, UK.
E-mail: f.fernandez-trillo@bham.ac.uk

†Electronic supplementary information (ESI) available. See DOI: 10.1039/c9py01222b

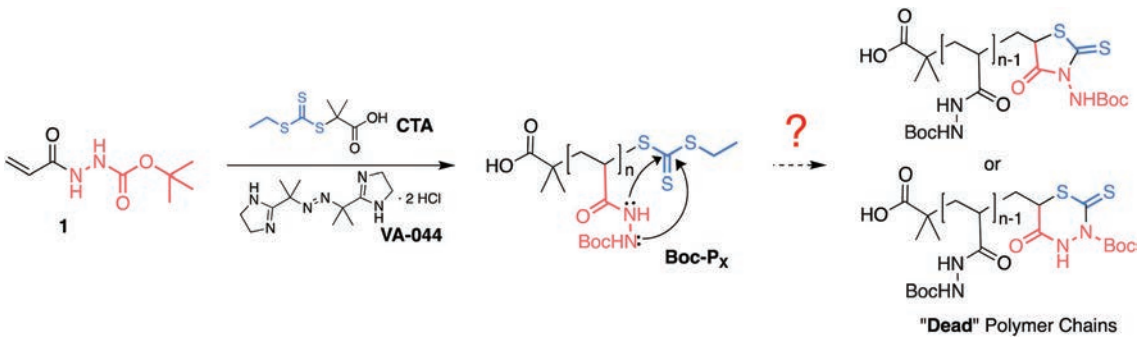

Scheme 1 RAFT polymerisation of *N*′-(*tert*-butoxycarbonyl)acryloyl hydrazide (**1**) and potential degradation by-products.

were carried out using 2,2′-azobis[2-(2-imidazolin-2-yl) propane]dihydrochloride (**VA-044**) as a low temperature initiator, so that the rate of generation of radicals could be readily modified as a function of temperature. Our results suggest that while increasing the temperature increases the polymerisation rate, it also speeds up RAFT degradation and thus, loss of control. Conditions have been identified for which the polymerisation "outperforms" this side reaction and polymers with good control over molecular mass and dispersities ($Đ_M$) can be obtained. More importantly, these conditions allowed us to prepare **Boc-P$_x$** with higher degrees of polymerisation and lower $Đ_M$, not accessible with our previous conditions.[14] This improved control over the polymerisation of Boc-protected poly(acryloyl hydrazide) will be of value when DP and $Đ_M$ may underpin future applications.

Experimental section

Materials

2-((Ethylthio)carbonothioyl)thio-2-methylpropanoic acid (**CTA**)[29] and *N*′-(*tert*-butoxycarbonyl)acryloyl hydrazide (**1**)[14,20] were synthesised according to protocols described in the literature. 2,2′-Azobis[2-(2-imidazolin-2-yl)propane] dihydrochloride (**VA-044**) was purchased from Fluorochem and used without further purification. All other chemicals were purchased from Sigma-Aldrich®, Fisher Scientific®, VWR® or Acros®, and used without further purification. All solvents were Reagent grade or above, purchased from Sigma-Aldrich®, Fisher Scientific® or VWR®, and used without further purification. Polymethylmethacrylate standards were purchased from Agilent®.

Characterisation

Nuclear Magnetic Resonance (NMR) spectra were recorded on either a Bruker Avance III 300 MHz or a Bruker Avance III 400 MHz spectrometer. Chemical shifts are reported in ppm (units) referenced to the following solvent signals: dimethylsulfoxide (DMSO)-d_6 H 2.50. Gel Permeation Chromatography (GPC) was performed with a Shimadzu Prominence LC-20A fitted with a Thermo Fisher Refractomax 521 Detector and a SPD20A UV-vis Detector. Poly(*N*′-(*tert*-butoxycarbonyl)acryloyl hydrazide) (**Boc-P$_x$**) was analysed using 0.05 M LiBr in dimethylformamide (DMF) at 60 °C as the eluent, and a flow rate of 1 mL min^{-1}. The instrument was fitted with a Polymer Labs PolarGel guard column (50 × 7.5 mm, 5 μm) followed by two PLGel PL1110-6540 columns (300 × 7.5 mm, 5 μm). Molecular masses were calculated based on a standard calibration method using polymethylmethacrylate standards.

RAFT polymerisation of *N*′-(*tert*-butoxycarbonyl)acryloyl hydrazide (1)

In a typical kinetic experiment 2,2′-azobis[2-(2-imidazolin-2-yl) propane]dihydrochloride (**VA-044**) (11.7 mg, 0.036 mmol), 2-ethylthiocarbonothioylthio-2-methylpropanoic-acid (**CTA**) (40.3 mg, 0.18 mmol) and *N*′-(*tert*-butoxycarbonyl)acryloyl hydrazide (**1**) (1.666 g, 8.950 mmol) were dissolved in DMSO (10.0 mL) and a 100 μL sample was taken at this stage to calculate conversion (ρ). The solution vessel was sealed with a septum, securely fastened with electrical tape to maintain the seal, and degassed by bubbling with argon for 25 minutes. Using a cannula, 1 mL of the solution was transferred to sealed glass vials containing stirrer bars, each degassed for 5 minutes. Vials were then left to react at a pre-set temperature (30–150 °C) for the required amount of time. The reaction was stopped by allowing the tube to cool using a water bath and exposing it to air. 100 μL aliquots of each timepoint were taken at this stage to calculate conversion (ρ) and for GPC analysis. NMR and GPC analysis of each timepoint was carried out from the crude mixture. The natural logarithm of the inverse of the fractional concentration of monomer – $\ln(M_0/M_t)$ – was plotted against time, and the data fitted using GraphPad Prism version 6.0 for Mac Os X, GraphPad Software, La Jolla California USA, http://www.graphpad.com. The in-built segmental line regression was used to fit the data to two intersecting lines. This model was used to identify when a change in the polymerisation kinetics was observed (t_{dead}).

Results and discussion

As reported, our initial efforts to optimise the polymerisation of Boc-protected acryloyl hydrazide **1** focused on reducing the temperature of the polymerisation.[14] RAFT polymerisation of

acrylamides and methacrylamides often suffers from cleavage of the RAFT agent through intramolecular addition–elimination of the weakly nucleophilic amides to the trithiocarbonate group (Scheme 1).[25] Under our previously reported conditions for the polymerisation of **1**, a change in the rate of polymerisation was observed with increasing conversion (Fig. S1A†) which we associated with this degradation of the terminal trithiocarbonate in the growing chain. It has been proposed that reducing the polymerisation temperature would significantly reduce the rate of this side reaction.[25] Thus, optimisation of the polymerisation was at that time carried out under the same conditions but using initiators with different 10 hours half-life decomposition temperatures (t_{10}) (Fig. S1†). This way, the rate of formation of radicals was kept as similar as possible for all polymerisations while reducing the temperatures to 50 °C (**V-65**) or 44 °C (**VA-044**). Despite the use of lower temperatures, in all cases, a change in the kinetics of the polymerisation was observed, although this change was not as obvious for the polymerisations performed at 44 °C (Fig. S1A,† right). To identify when this change in rate of polymerisation was occurring, the natural logarithm of the inverse of the fractional concentration of monomer – $\ln(M_0/M_t)$ – was plotted against time, and the data fitted to a segmental line regression. This function fits the data to two different lines, before and after a breakpoint. In our case, we termed the breakpoint t_{dead} because we think that after this point, side reactions have a predominant effect on the kinetics of the polymerisation resulting in an increasing number of dead polymer chains. This change in kinetics was reflected on the relatively high dispersity in molecular mass ($Đ_M$ = 1.38–1.95) obtained for the polymers prepared under these conditions.[14] Overall, no clear benefit from reducing the temperature was observed, with a t_{dead} of approximately 4 and 4.5 hours for polymerisations at 50 °C and 70 °C respectively. Interestingly, t_{dead} for the polymerisation performed at 44 °C was observed at approximately 2.5 h, which would suggest degradation was occurring faster at this temperature. This was not expected and may suggest that other mechanisms beyond the simple degradation of the RAFT agent may be at play. For instance, polymerisation decay can also be caused by diminishing initiator efficiency at high monomer conversions, which has been observed for some azo-initiators.[30,31] However, this factor normally becomes significant at much higher conversions than the ones we reported.

Attempts to perform the polymerisation at an even lower temperature (30 °C) using **VA-044** as the source of radicals resulted in a very long induction period followed by a short period of linear increase of the fractional concentration of monomer until a change in kinetics was again evident (Fig. S2†). The maximum conversion in this case was 50% – $\ln(M_0/M_t)$ = 0.83, worse than that observed for the polymerisations performed at higher temperatures.

In order to determine if degradation of the RAFT agent was indeed possible at low temperatures, we attempted to synthesise a small molecule analogue which mimicked an n = 1 polymer (Scheme S1†). To this end, 2-bromopropionic acid (**2**) was reacted with *tert*-butyl carbazate, and the resulting bromine derivative **3** reacted under standard conditions for the formation of the RAFT agent. ^{1}H NMR analysis of this reaction revealed a very complex mixture, where only traces of something that could resemble trithiocarbonate **4** could be identified (Fig. S4†). This observation was in line with our previous results, and suggested that hydrazide containing trithiocarbonates such as **4** were very amenable to intramolecular nucleophilic attack. Attempts to isolate this trithiocarbonate **4** were unsuccessful, with the main isolated product of this reaction being tentatively assigned to a mixture of the 5- and 6-membered rings in a 6 : 4 ratio (Fig. S5†).

Seeing how lowering the temperature had no beneficial effect on the kinetics of the polymerisation of **1**, and a change in kinetics was still observed, we decided to explore the use of "Ultra-Fast" polymerisation conditions in an attempt to outrun the side reaction.[32–34] Our hypothesis was that by using a low temperature initiator such as **VA-044** at a significantly higher temperature (*e.g.* 100 °C) than the reported t_{10} (44 °C), an increase in the concentration of radicals in solution would be achieved. This way, the concentration of propagating radicals would be higher with a greater number of chains growing at the same time, resulting in the synthesis of polymers with better control over the molecular mass and $Đ_M$. This methodology is particularly suitable for fast-propagating monomers such as acrylamides, and since the rate of polymerisation is directly proportional to the concentration of these propagating radicals (and the monomer concentration, $R_p = k_p[M][P^\bullet]$), we postulated that running the polymerisation under these conditions could outperform the side reaction observed under standard RAFT polymerisation conditions. In a first attempt, the polymerisation conditions previously reported by us for the polymerisation of **1** (Fig. S1†)[14] were modified so that the initiator used was **VA-044** and the polymerisation temperature was 100 °C. A shorter polymer was targeted this time and, as expected, the polymerisation was very fast, reaching up to 70% conversion in less than five minutes (Fig. 1A, **CTA : VA-044** 5 : 1 ●). The change in reaction rate could not be suppressed and was again evident, with a t_{dead} of approximately 4.5 min. Before t_{dead}, the polymerisation retained the features of a controlled polymerisation, with the molecular mass of the polymer directly proportional to the conversion and, comparable dispersities (Fig. 1B, left) to those observed with our previous conditions.[14]

These results were promising and we therefore explored decreasing the concentration of initiator in our polymerisations, in an attempt to suppress termination, increase the number of chains growing from the RAFT agent and thus optimising the dispersities. However, while dispersities were decreased, reducing the concentration of initiator in these polymerisations resulted in slower reactions, with no effect observed in t_{dead} (Fig. 1A). As a result, the maximum conversion obtained when the **CTA : VA-044** ratio was increased to 10 : 1 or 15 : 1 (40% and 24% conversion respectively) was lower than in the previous case (70%).

We decided next to run the polymerisations at 150 °C, in an attempt to further increase the concentration of radicals

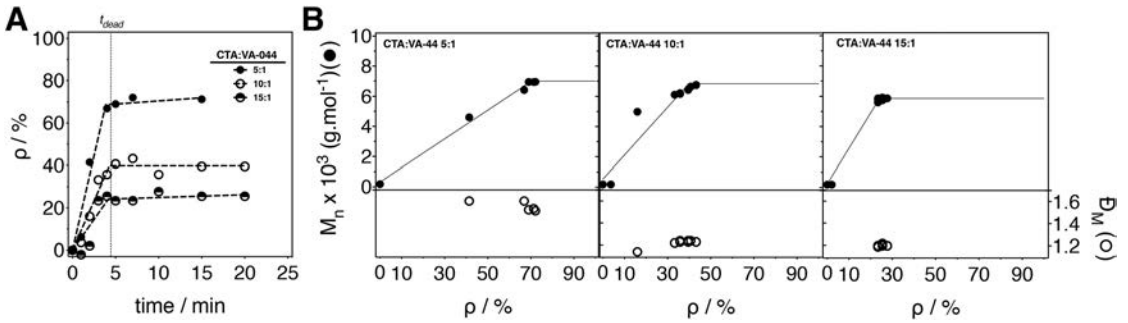

Fig. 1 (A) Plot of conversion (ρ) *vs.* time and (B) measured number average molecular mass (M_n) *vs.* conversion (●) and dispersity in molecular mass ($Đ_M$) *vs.* conversion (○), for polymerisations of *N*′-(*tert*-butoxycarbonyl)acryloyl hydrazide (**1**) performed with different **CTA** : **VA-044** ratios. Conditions: [M] = 0.9 M, [M]/[**CTA**] = 50/1. M_n and $Đ_M$ calculated by GPC using 0.05 M LiBr in dimethylformamide (DMF) at 60 °C.

during early stages of polymerisation, and thus the rate of propagation. However, these conditions not only resulted in lower conversions (Fig. S9†) but a colour change of the reaction mixture from yellow to dark brown, suggesting that thermal decomposition of the trithiocarbonate group was ocurring.[35] Thermal decomposition of the RAFT agent was confirmed *via* ^{1}H NMR where signals consistent with the β-elimination of the trithiocarbonate could be observed (Fig. S10†).[35,36]

Having identified conditions to run the polymerisation of **1** at 100 °C, which resulted in similar conversions and dispersities to those previously reported, we decided to explore the use of these conditions to prepare polymers of higher DP (Fig. 2), which were harder to control using our previously reported method.[14] Three different DPs were targeted (*i.e.* [**1**]/[**CTA**] = 50, 100 and 150), by maintaining the concentration of **1** and reducing the amount of RAFT agent and initiator used. As

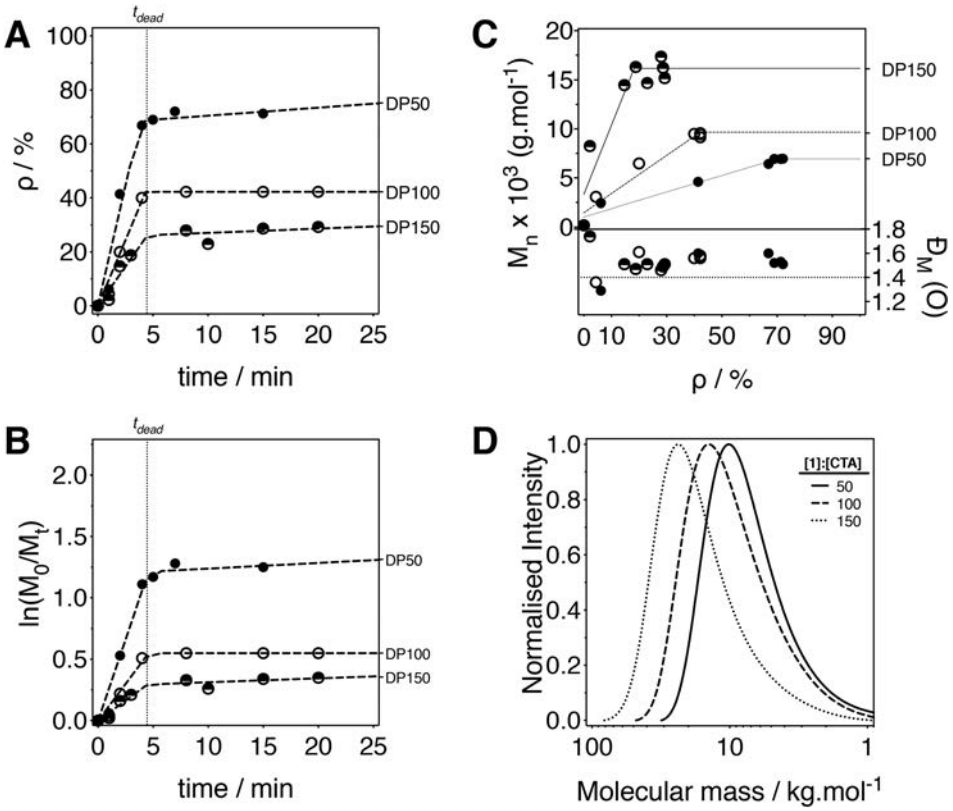

Fig. 2 (A) Plot of conversion (ρ) *vs.* time, (B) fractional concentration of monomer ln(M_0/M_t) *vs.* time, and (C) measured number average molecular mass (M_n) *vs.* conversion (ρ) (top) and dispersity in molecular mass ($Đ_M$) *vs.* conversion (ρ) (bottom), for polymerisations of *N*′-(*tert*-butoxycarbonyl) acryloyl hydrazide (**1**) performed at 100 °C with different **1** : **CTA** ratios. (D) GPC chromatograms of the resulting polymers at the highest conversion obtained. Conditions: [M] = 0.9 M, [**CTA**]/[**VA-044**] = 5/1. M_n and $Đ_M$ calculated by GPC using 0.05 M LiBr in dimethylformamide (DMF) at 60 °C.

expected, this resulted in slower polymerisations, while t_{dead} still remained at around 4.5 min (Fig. 2A). As a consequence, polymerisations targeting 100 and 150 monomer units only reached low conversions (~40% and 30% respectively). In any case, control over the molecular mass of the polymer was still observed during the first stages of the polymerisation, with the average molecular mass (M_n) increasing linearly with time until the change in polymerisation rate was evident (t_{dead}) (Fig. 2B). A clear shift towards lower retention time was observed in the gel permeation chromatograms when higher DPs were targeted, suggesting that, at least during the initial phase of the reaction, the polymerisation was maintaining features of a controlled radical polymerisation. $Đ_M$ remained similar across the three targeted molecular masses which demonstrates an improvement compared to our previous conditions where $Đ_M$ increased with increasing targeted DP.

At this point, our results suggested that a compromise could be obtained between increasing the rate of propagation by increasing the polymerisation temperature, and delaying t_{dead} by reducing the polymerisation temperature. Therefore, we investigated polymerisations at intermediate temperatures (Fig. 3). While a change in polymerisation rate was still evident for the new temperatures investigated, higher conversions could be achieved for the polymerisation performed at 65 °C (90%) while the next highest conversions at 80 °C and 50 °C were 77% and 80% respectively (Fig. 3B, ●). Temperature had a significant effect on the time at which a change in polymerisation rate was evident (t_{dead}), with this inflection point happening sooner as the temperature was increased (Fig. 3B, ○).

With encouraging results from the polymerisations at 65 °C, we set out to probe the "livingness" of the polymer before and after t_{dead} and thus whether t_{dead} was due to degradation of the RAFT agent. To this end, we isolated and purified two polymerisations of **1**, one that had been stopped at intermediate conversions (ρ = 47%, t = 30 min), before t_{dead} (Fig. S6A†) and one that was stopped at maximum conversion (ρ = 85%, t = 120 min), after t_{dead} (Fig. S6B†). As expected, **Boc-P$_x$** isolated before t_{dead} was able to undergo complete chain extension with further addition of **1** and initiator (Fig. S6A†), thus demonstrating that at intermediate conversions the RAFT agent was still present in significant amounts. GPC analysis of **Boc-P$_x$** isolated after t_{dead} indicated that no chain extension had occurred, instead showing a bimodal distribution of molecular mass and high dispersities (Fig. S6B†) demonstrating that after t_{dead} the RAFT group had been degraded. To probe if the RAFT agent degradation was temperature driven, we isolated and purified a second "living" **Boc-P$_x$** at intermediate conversions (ρ = 52% t = 30 min) (Fig. S7†). This polymer was then heated for 90 minutes under standard polymerisation conditions, but this time without addition of **1** and initiator. We anticipated that heating the polymer this way should result in degradation of the RAFT agent, a hypothesis that was confirmed upon attempting to chain extend this terminated **Boc-P$_x$**. In this case, high dispersities, together with a shoulder at high molecular mass, were observed, indicating that the **Boc-P$_x$** which had been subjected to further heating was "dead" (Fig. S7†). Additional evidence of the RAFT agent degradation was obtained from NMR spectroscopy, where the protons associated with both the R and Z end group of the polymer chain could be observed for the "living" **Boc-P$_x$** whereas "dead" **Boc-P$_x$** showed a loss of the Z group (Fig. S8†).

Seeing how running the polymerisations at 65 °C gave the highest conversions (90%) at t_{dead} of all the conditions evaluated, we decided to target different degrees of polymerisation using these conditions (Fig. 4). As before, targeting higher DPs resulted in slower rates of polymerisation, in particular for DP200 and DP300. While slower rates had a significant effect on the maximum conversion achieved (approx. 90%, 89%, 68% and 55% for DP 50, 100, 200 and 300 respectively), little effect was observed on the t_{dead}, with most polymerisations "stopping" after 1 h (Fig. 4A).

Under these optimised conditions, the polymerisations retained features of a controlled polymerisation, with the molecular mass of the polymers increasing linearly with conversion, narrow dispersities in molar mass (Fig. 4C) and good end group fidelity if isolated before t_{dead}. In all cases, the dispersities obtained were similar or lower to those reported previously.[14] This improvement was particularly the case when targeting DPs of 100 and 200 with dispersities of <1.4 being observed at maximum conversion.

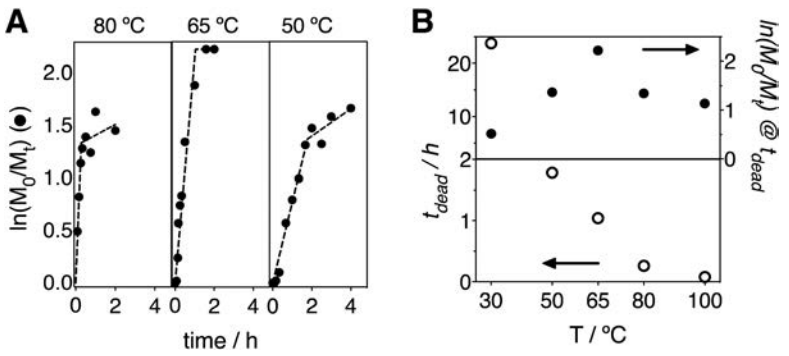

Fig. 3 (A) Plot of fractional concentration of monomer $\ln(M_0/M_t)$ *vs.* time for polymerisations of *N*′-(*tert*-butoxycarbonyl)acryloyl hydrazide (**1**) performed at different temperatures. (B) Effect of temperature on the time at which deviation from linearity for the plot of $\ln[M]_0/[M]_t$ *vs.* time is observed (t_{dead}) (○), and the fractional concentration of monomer $\ln(M_0/M_t)$ at this point (●). Conditions: [M] = 0.9 M, [M]/[**CTA**]/[**VA-044**] = 50/1/0.2.

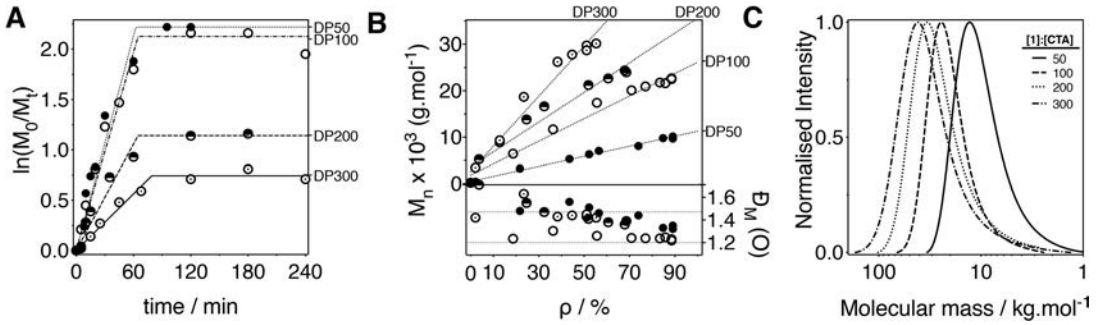

Fig. 4 (A) Plot of fractional concentration of monomer $\ln(M_0/M_t)$ *vs.* time. (B) Measured number average molecular mass (M_n) *vs.* conversion (ρ) (top) and dispersity in molecular mass ($Đ_M$) *vs.* conversion (ρ) (bottom), for polymerisations of *N*′-(*tert*-butoxycarbonyl)acryloyl hydrazide (**1**) performed at 65 °C with different **1** : **CTA** ratios. (C) GPC chromatograms of the resulting polymers at the highest ρ obtained. Conditions: [M] = 0.9 M, [**CTA**]/[**VA-044**] = 5/1. M_n and $Đ_M$ calculated by GPC using 0.05 M LiBr in dimethylformamide (DMF) at 60 °C.

Conclusion

Here we have demonstrated the role of temperature and RAFT agent degradation in the polymerisation of *N*′-(*tert*-butoxycarbonyl)acryloyl hydrazide (**1**). Our results highlight that the polymerisation of this hydrazide monomer **1** *via* RAFT can be severely hampered by the degradation of the chain transfer agent and that, under some circumstances, this degradation cannot be eliminated but rather outperformed if the rate of polymerisation is tuned. We demonstrate that by using a low-temperature initiator such as **VA-044**, optimal polymerisation conditions can be achieved at 65 °C. This way, poly(*N*′-(*tert*-butoxycarbonyl)acryloyl hydrazide)s with high degrees of polymerisation could be obtained while still maintaining low dispersities. We believe that further improvement of the polymerisation could be achieved through the choice of RAFT agents such as pyrazole or quaternised pyridinium dithiocarbamates,[37,38] the use of photopolymerisation,[39] or the use of alternative controlled polymerisation techniques. Our efforts in these directions will be reported in due course.

Author contributions

PFT, OC and PA designed the work. OC, PA, GS and AR performed all the experimental work. OC, AR and PFT analysed the data. OC and PFT wrote the paper, with all other authors contributing to the final version of the manuscript.

Conflicts of interest

There are no conflicts of interest.

Acknowledgements

All authors thank the P. F. T. group for useful discussions. P. F. T. thanks the University of Birmingham for the John Evans Fellowship. O. C. and P. A. thank BBSRC's Midlands Integrative Biosciences Training Partnership MIBTP (BB/M01116X/1) for PhD scholarships and A. R. thanks the European Union's Horizon 2020 Research and Innovation Programme (Marie Sklodowska-Curie Grant Agreement No. 795082).

References

1 J. E. Gestwicki, C. W. Cairo, L. E. Strong, K. A. Oetjen and L. L. Kiessling, *J. Am. Chem. Soc.*, 2002, **124**, 14922–14933.
2 R. Duncan, *Nat. Rev. Drug Discovery*, 2003, **2**, 347–360.
3 C. Zhu, L. Liu, Q. Yang, F. Lv and S. Wang, *Chem. Rev.*, 2012, **112**, 4687–4735.
4 J. Li, F. Yu, Y. Chen and D. Oupický, *J. Controlled Release*, 2015, **219**, 369–382.
5 J. J. Green and J. H. Elisseeff, *Nature*, 2016, **540**, 386–394.
6 A. Muñoz-Bonilla and M. Fernández-García, *Prog. Polym. Sci.*, 2012, **37**, 281–339.
7 E.-R. Kenawy, S. D. Worley and R. Broughton, *Biomacromolecules*, 2007, **8**, 1359–1384.
8 D. W. Pack, A. S. Hoffman, S. Pun and P. S. Stayton, *Nat. Rev. Drug Discovery*, 2005, **4**, 581–593.
9 H. N. Kim, Z. Guo, W. Zhu, J. Yoon and H. Tian, *Chem. Soc. Rev.*, 2011, **40**, 79–93.
10 S.-J. Richards, M. W. Jones, M. Hunaban, D. M. Haddleton and M. I. Gibson, *Angew. Chem., Int. Ed.*, 2012, **51**, 7812–7816.
11 Z. Cao, L. Mi, J. Mendiola, J. R. Ella Menye, L. Zhang, H. Xue and S. Jiang, *Angew. Chem., Int. Ed.*, 2012, **51**, 2602–2605.
12 *Functional Polymers by Post-Polymerization Modification*, ed. P. Théato and H.-A. Klok, Wiley-VCH Verlag GmbH & Co. KGaA, Weinheim, Germany, 2012.
13 J. Collins, Z. Xiao, M. Müllner and L. A. Connal, *Polym. Chem.*, 2016, **7**, 3812–3826.
14 D. N. Crisan, O. Creese, R. Ball, J. L. Brioso, B. Martyn, J. Montenegro and F. Fernandez-Trillo, *Polym. Chem.*, 2017, **1**, 1392–1399.
15 D. K. Kölmel and E. T. Kool, *Chem. Rev.*, 2017, **117**, 10358–10376.

16 E. R. L. Brisson, Z. Xiao, L. Levin, G. V. Franks and L. A. Connal, *Polym. Chem.*, 2016, **7**, 1945–1952.
17 E. M. Muzammil, A. Khan and M. C. Stuparu, *RSC Adv.*, 2017, **7**, 55874–55884.
18 K. Godula and C. R. Bertozzi, *J. Am. Chem. Soc.*, 2010, **132**, 9963–9965.
19 A. Kumar, R. R. Ujjwal, A. Mittal, A. Bansal and U. Ojha, *ACS Appl. Mater. Interfaces*, 2014, **6**, 1855–1865.
20 J. M. Priegue, D. N. Crisan, J. Martínez-Costas, J. R. Granja, F. Fernandez-Trillo and J. Montenegro, *Angew. Chem., Int. Ed.*, 2016, **55**, 7492–7495.
21 A. Kumar, R. R. Ujjwal, A. Mittal, A. Bansal and U. Ojha, *ACS Appl. Mater. Interfaces*, 2014, **6**, 1855–1865.
22 J. M. Priegue, I. Lostalé-Seijo, D. Crisan, J. R. Granja, F. Fernandez-Trillo and J. Montenegro, *Biomacromolecules*, 2018, **19**, 2638–2649.
23 M. Juanes, O. Creese, P. Fernández-Trillo and J. Montenegro, *MedChemComm*, 2019, **526**, 351–357.
24 J. D. Moskowitz, B. A. Abel, C. L. McCormick and J. S. Wiggins, *J. Polym. Sci., Part A: Polym. Chem.*, 2015, **54**, 553–562.
25 B. A. Abel and C. L. McCormick, *Macromolecules*, 2016, **49**, 465–474.
26 E. A. Hoff, B. A. Abel, C. A. Tretbar, C. L. McCormick and D. L. Patton, *Polym. Chem.*, 2017, **8**, 4978–4982.
27 B. A. Chalmers, A. Alzahrani, G. Hawkins and F. Aldabbagh, *J. Polym. Sci., Part A: Polym. Chem.*, 2017, **55**, 2123–2128.
28 S. Perrier, *Macromolecules*, 2017, **50**, 7433–7447.
29 J. Skey and R. K. O'Reilly, *Chem. Commun.*, 2008, **31**, 4183.
30 G. Moad, *Prog. Polym. Sci.*, 2019, **88**, 130–188.
31 Y. Zhou, Z. Zhang, A. Postma and G. Moad, *Polym. Chem.*, 2019, **10**, 3284–3287.
32 G. Gody, T. Maschmeyer, P. B. Zetterlund and S. Perrier, *Nat. Commun.*, 2013, **4**, 2505.
33 G. Gody, T. Maschmeyer, P. B. Zetterlund and S. Perrier, *Macromolecules*, 2014, **47**, 639–649.
34 G. Gody, R. Barbey, M. Danial and S. Perrier, *Polym. Chem.*, 2015, **6**, 1502–1511.
35 Y. Zhou, J. He, C. Li, L. Hong and Y. Yang, *Macromolecules*, 2011, **44**, 8446–8457.
36 T. M. Legge, A. T. Slark and S. Perrier, *J. Polym. Sci., Part A: Polym. Chem.*, 2006, **44**, 6980–6987.
37 J. Gardiner, I. Martinez-Botella, J. Tsanaktsidis and G. Moad, *Polym. Chem.*, 2016, **7**, 481–492.
38 D. J. Keddie, C. Guerrero-Sanchez, G. Moad, E. Rizzardo and S. H. Thang, *Macromolecules*, 2011, **44**, 6738–6745.
39 M. Chen, M. Zhong and J. A. Johnson, *Chem. Rev.*, 2016, **116**, 10167–10211.

Supporting Information

Poly(Boc-acryloyl hydrazide): The importance of temperature and RAFT agent degradation on its preparation

*Oliver Creese, Pavan Adoni, Guanlong Su, Andrey Romanyuk and Paco Fernandez-Trillo**

School of Chemistry, and Institute of Microbiology and Infection, University of Birmingham,

Edgbaston, B15 2TT Birmingham

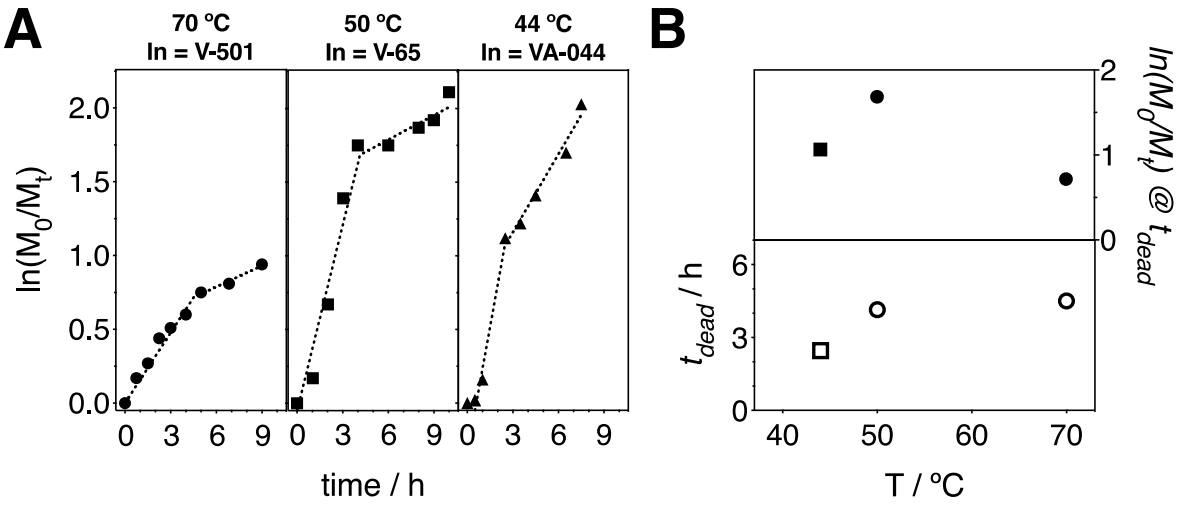

Figure S1. A) Plot of fractional concentration of monomer ln(M_0/M_t) vs time for polymerisations of N'-(tert-butoxycarbonyl)acryloyl hydrazide (**1**) performed at different temperatures. Conditions: [M]=0.9M, [M]/[CTA]/[In]=100/1/0.2. 4,4'-Azobis(4-cyanovaleric acid) (**V-501**) - circles, 2,2'-azobis(2,4-dimethylvaleronitrile) (**V-65**) - squares, and 2,2'-azobis[2-(2-imidazolin-2-yl)propane]dihydrochloride (**VA-044**) - triangles. Adapted with permission from Crisan, D. N.; Creese, O.; Ball, R.; Brioso, J. L.; Martyn, B.; Montenegro, J.; Fernandez-Trillo, F. Polym. Chem. **2017**, 8 (31), 4576–4584 - Published by The Royal Society of Chemistry. B) For polymerisations carried out in S1A, effect of temperature on the time at which deviation from linearity for the plot of ln$[M]_0/[M]_t$ vs time is observed ($\boldsymbol{t}_{dead}$), and the fractional concentration of monomer $ln(M_0/M_t)$ at this point.

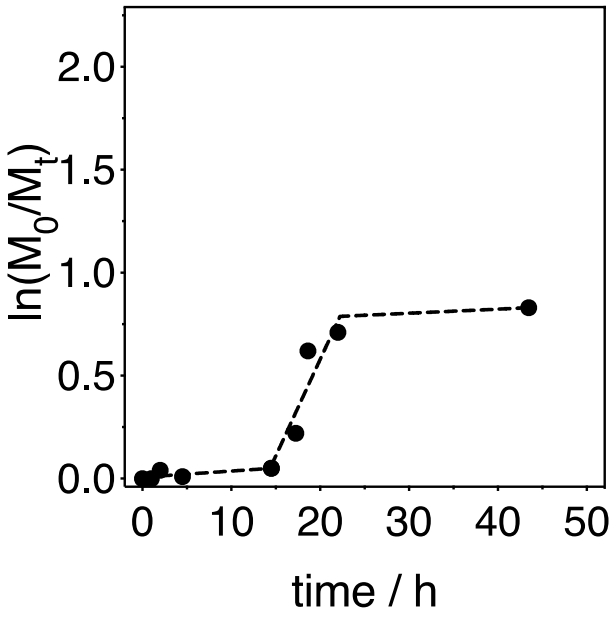

Figure S2. Plot of $ln(M_0/M_t)$ vs time for the polymerisation of N'-(tert-butoxycarbonyl)acryloyl hydrazide (**1**) at 30 ºC. Conditions: [M]=0.9M, [M]/[CTA]/[VA-044]=50/1/0.2.

Small molecule analogue of a DP= 1 of N'-(*tert*-butoxycarbonyl)acryloyl hydrazide (1).

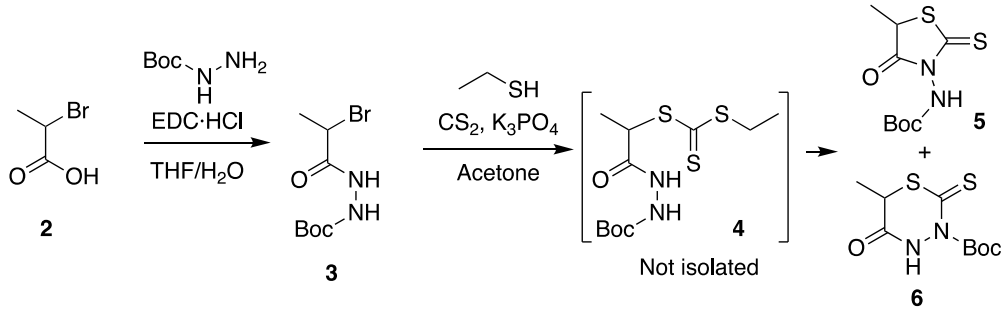

Scheme S1. Attempted route for the synthesis of a DP= 1 analogue of N'-(tert-butoxycarbonyl)acryloyl hydrazide (**1**).

***tert*-butyl 2-(2-bromopropanoyl)hydrazine-1-carboxylate (3):** 2-Bromopropionic acid (**2**) (10 g, 59.9 mmol) and tert-butyl carbazate (6.56 g, 49.6 mmol) were dissolved in a 2:1 mixture of water/THF (180 ml). N-(3-Dimethylaminopropyl)-N′-ethylcarbodiimide hydrochloride (13.3 g, 69.5 mmol) was added in portions to the solution over 15 minutes and the mixture was left stirring for 3h at room temperature. The solution was extracted into EtOAc (3 x 60 ml) and a basic work-up performed with $NaCO_3$ (3 X 60 ml). The organic layer was further washed with water (2 x 60 ml), dried with Na_2SO_4, filtered and the solvent removed under reduced pressure to leave a white solid. This solid was then recrystallised using ethyl acetate to afford white crystalline material which was

washed with ice cold diethyl ether and dried under reduced pressure (8.9 g, 64 %): ^{1}H NMR (300MHz, DMSO-d_6) δ (ppm) 9.9 (s, 1H), 9.0-8.3 (s, 1H), 4.45 (q, 1H), 1.65 (d, 3H), 1.38 (s, 9H).

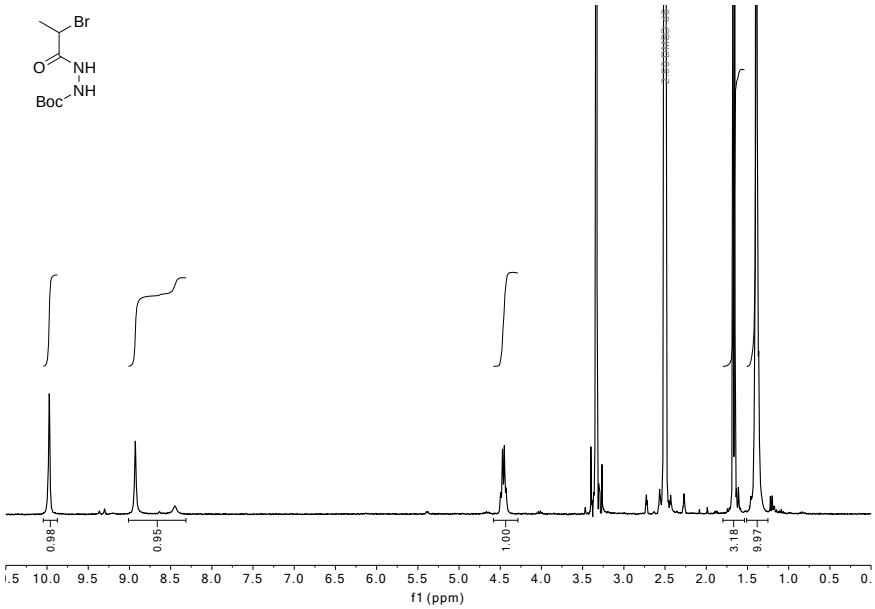

Figure S3. ^{1}H NMR (300 MHz, $CDCl_3$) spectrum of *tert*-butyl 2-(2-bromopropanoyl)hydrazine-1-carboxylate (**3**).

***tert*-butyl 2-(2-(((ethylthio)carbonothioyl)thio)propanoyl)hydrazine-1-carboxylate (4) (not isolated):** Ethanethiol (0.49 ml, 6.59 mmol) was added to a suspension of K_3PO_4 (1.4 g, 6.59 mmol) in acetone (20 ml) and was left stirring at room temperature for 10 minutes. CS_2 (1.09 ml, 6.59 mmol) was then added and the reaction mixture was left for a further 10 minutes. *tert*-butyl 2-(2-bromopropanoyl)hydrazine-1-carboxylate (**1**) (1.6 g, 5.99 mmol) was added in one portion and the mixture left to react for 13 hours. The solvent was then removed under reduced pressure and HCl (100 ml, 1 M) was added to the crude of the reaction. The resulting mixture extracted into DCM (2 x 100 ml). The organic layer was then washed with water (2 x 100 ml) and brine (2 x 100 ml), dried with Na_2SO_4, filtered and the solvent removed under reduced pressure. The resulting orange oil was purified by column chromatography using a 7:3 ratio of diethyl ether and hexane, then dried under reduced pressure to leave a viscous orange liquid (0.12 g, 7 %) which consisted of two compounds, none of which is the title compound. a; ^{1}H NMR (300MHz, $CDCl_3$) δ (ppm) 10.3-9.7 (1H, s, NH), 4.66 (q, 1H), 1.58 (d, 3H), 1.44 (s, 9H) and b; ^{1}H NMR (300MHz, $CDCl_3$) δ (ppm) 10.3-9.7 (1H, s, NH), 4.73 (q, 1H), 1.59 (d, 3H), 1.44 (s, 9H).

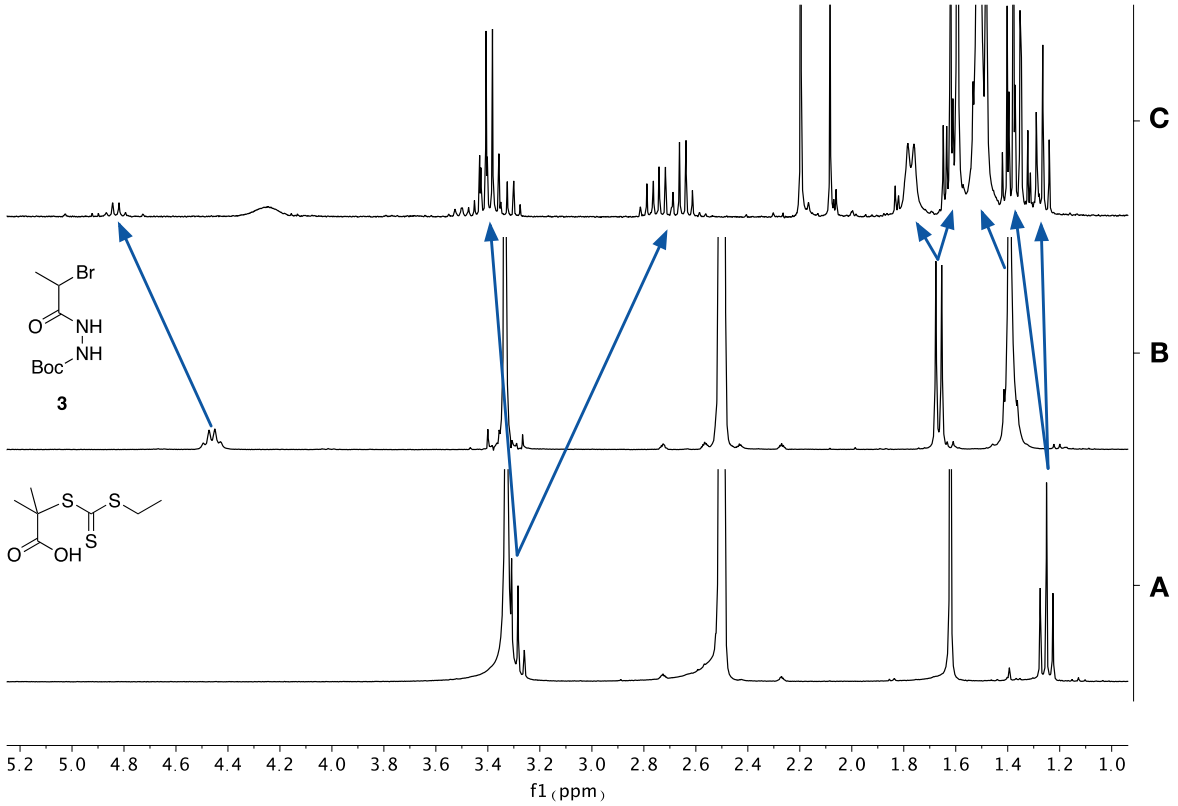

Figure S4. A) ^{1}H NMR (300 MHz, DMSO) spectrum of 2-((ethylthio)carbonothioyl)thio-2-methylpropanoic acid (**CTA**). B) ^{1}H NMR (300 MHz, CDCl3) spectrum of tert-butyl 2-(2-bromopropanoyl)hydrazine-1-carboxylate (**3**). C) ^{1}H NMR (300 MHz, CDCl3) spectrum of the reaction of ethanethiol with carbon disulfide and tert-butyl 2-(2-bromopropanoyl)hydrazine-1-carboxylate (**3**).

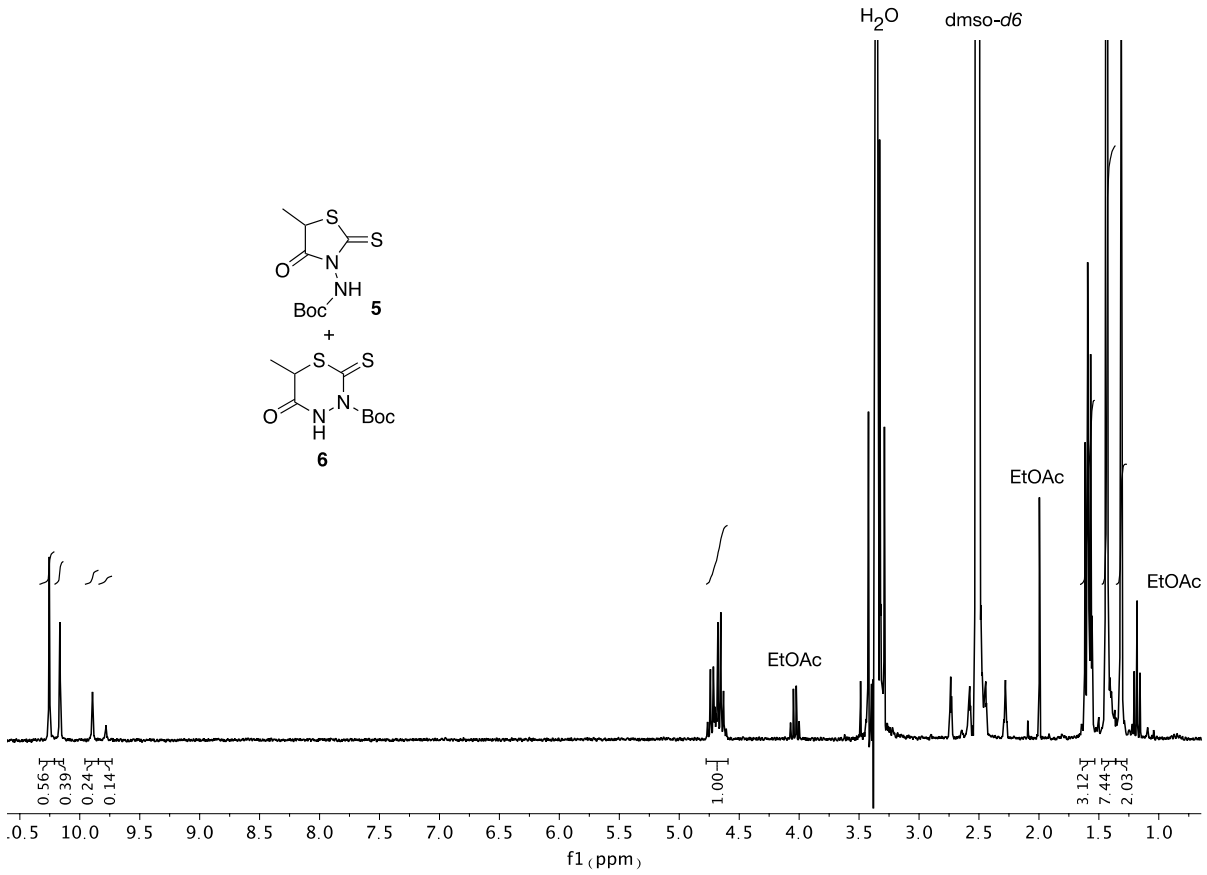

Figure S5. ^{1}H NMR (300 MHz, $CDCl_3$) spectrum of the main fraction isolated following the reaction of ethanethiol with carbon disulfide and *tert*-butyl 2-(2-bromopropanoyl)hydrazine-1-carboxylate (**3**).

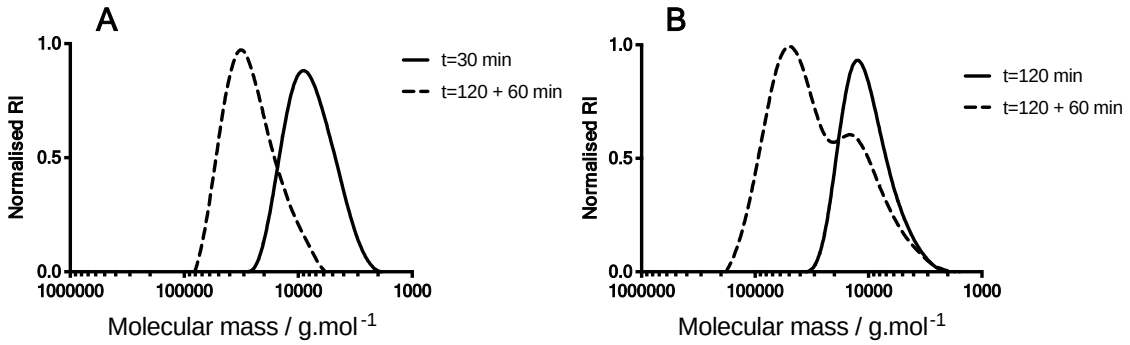

Figure S6. A) GPC traces (DMF LiBr 0.05M) of "living" **Boc-P$_x$** after (t=30 min) and subsequent chain extension with (**1**)(t=30+60 min). B) "dead" **Boc-P$_x$** (t=120 min) and subsequent inability to chain extend with (**1**) (t=120+60 min).

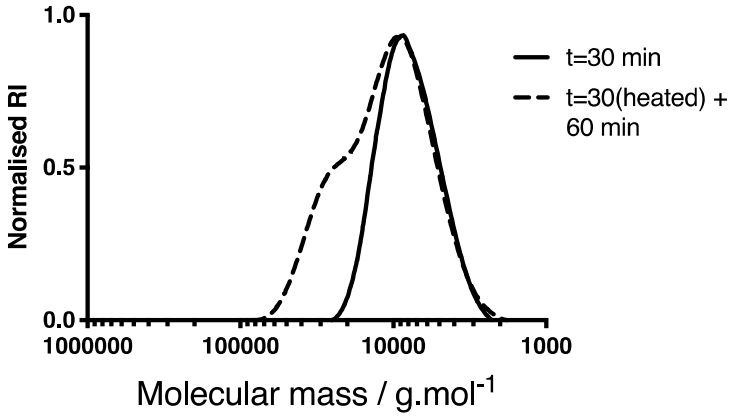

Figure S7. GPC traces (DMF LiBr 0.05M) of isolated "living" **Boc-P$_x$** after (t=30 min) after further heating (60 ºC t=90 min), and subsequent inability to chain extend with (**1**) (t=30+60 min).

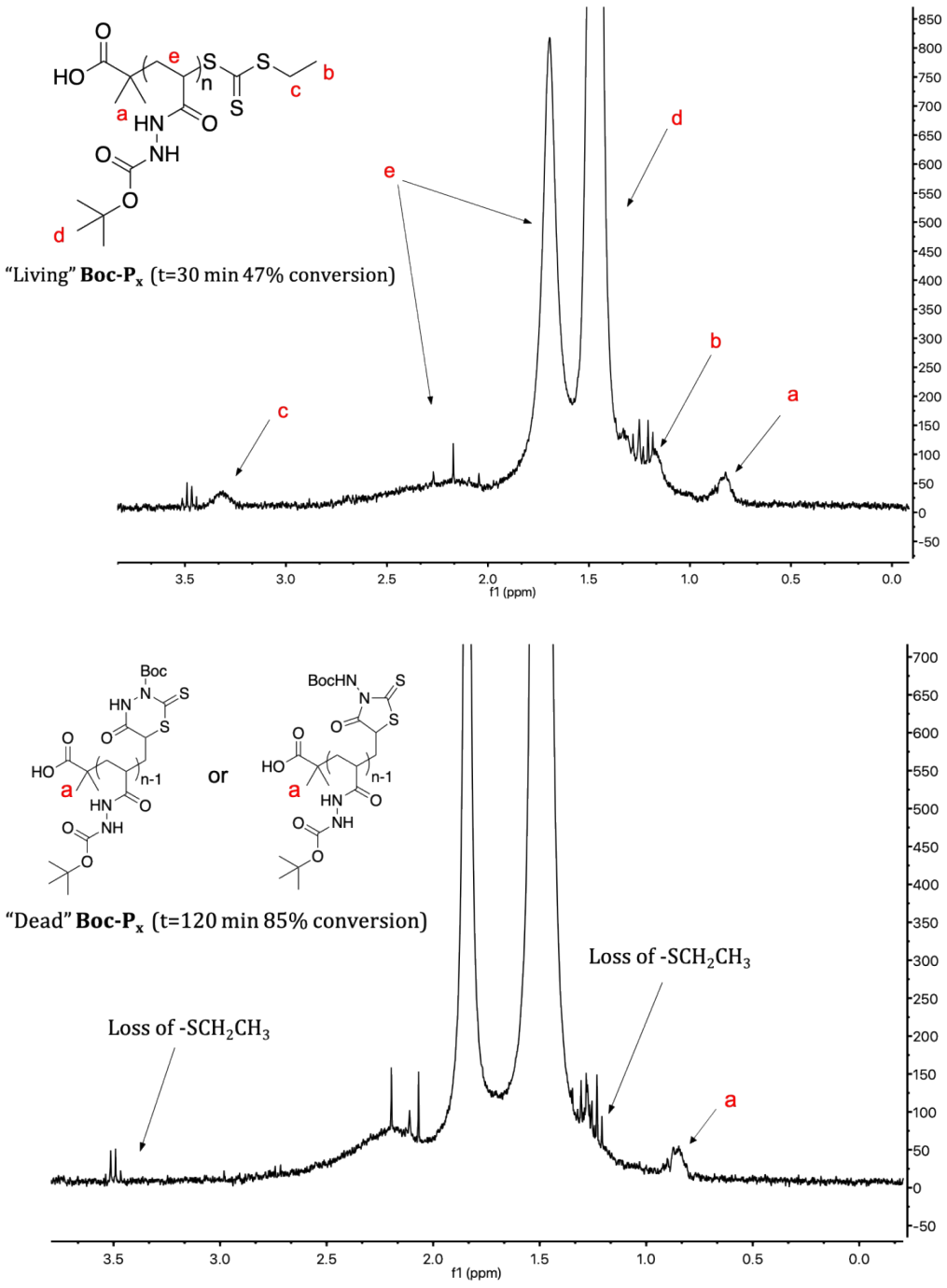

Figure S8. Top: ^{1}H NMR (300 MHz, $CDCl_3$) of "living" **Boc-P$_x$** after polymerisation reaction was stopped after 30 minutes, before full conversion (47%). Bottom: ^{1}H NMR (300 MHz, $CDCl_3$) of "dead" **Boc-P$_x$** after polymerisation for 120 minutes to maximum conversion (85%).

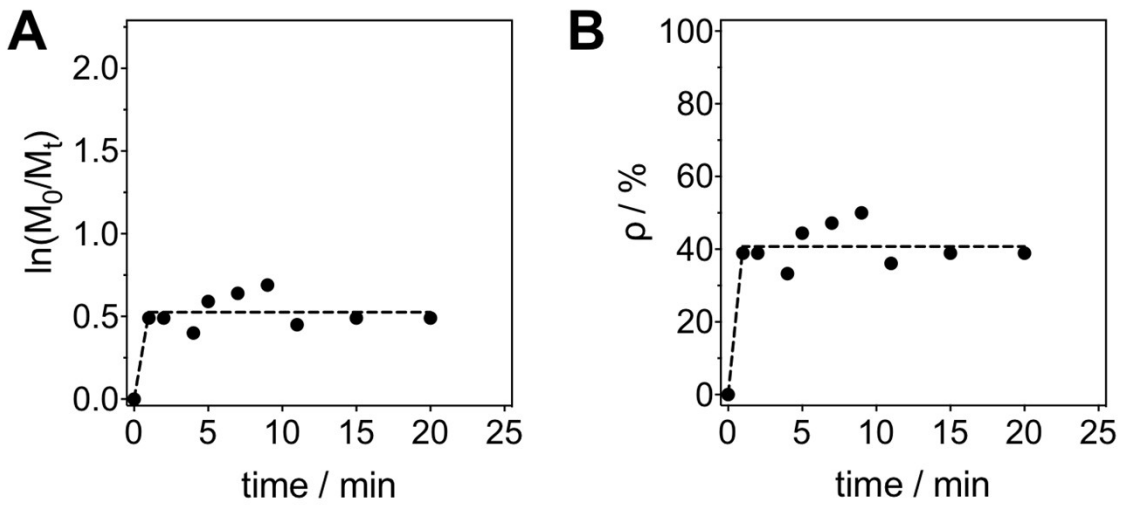

Figure S9. Plot of $ln(M_0/M_t)$ vs time (A) and conversion (ρ) vs time (B) for the polymerisation of N'-(tert-butoxycarbonyl)acryloyl hydrazide (**1**) at 150 ºC. Conditions: [M]=0.9M, [M]/[CTA]/[VA-044]=50/1/0.2.

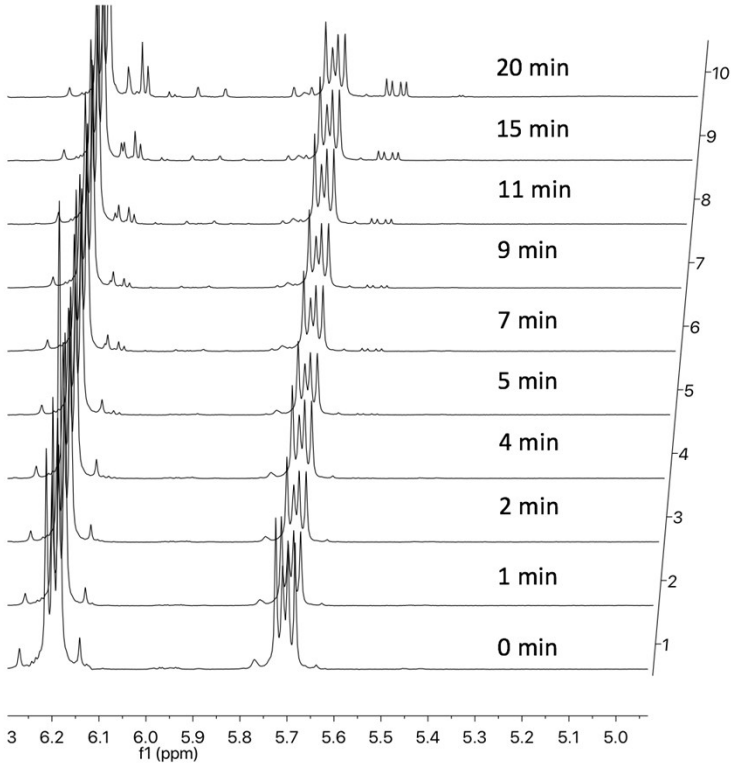

Figure S10. ^1H NMR (300 MHz, $CDCl_3$) spectrum showing vinyl region at varying time points in the polymerisation of N'-(tert-butoxycarbonyl)acryloyl hydrazide (**1**) at 150 ºC. Conditions: [M]=0.9M, [M]/[CTA]/[VA-044]=50/1/0.2. New vinyl protons can be observed from 7 minutes, suggestive of β-elimination products.

Chapter 2

Studies into the synthesis and structure-activity relationship of cationic polymers and their application in sequestering *Vibrio cholerae*

2.1 Background

With increasing rates of resistant bacteria reported for traditional antibiotics, and few new classes of antibiotics in the pipeline,[1] we face the prospect of a "post-antibiotic era",[2] whereby previously simple to treat infections could prove life-threatening. Antimicrobial resistance (AMR) is currently estimated to be responsible for over 700,000 deaths per year globally, and predicted to rise to over 10 million by 2050 overtaking that of both cancer and diabetes combined.[2,3]

In this regard, alternative broad-spectrum approaches to controlling pathogenic bacteria are urgently needed to address AMR. Targeting bacterial virulence in a way that "disarms" the bacteria, rather than kills bacteria, could offer a route to control pathogenic infection without inducing evolutionary pressure which can ultimately lead to resistance.[4-6] A crucial step in the pathogenicity of many bacteria is adhering to surfaces, which is a prerequisite for survival and the ability to cause disease to the host. Targeting bacterial adhesion mechanisms, sometimes described as "anti-adhesion therapy" has been positioned as a promising strategy by which to control bacteria. In this regard polymers have been explored as surface coatings to repel the adhesion of bacteria,[7,8] and in solution as "drug-like" polymers which can induce clustering of bacteria, preventing their adhesion to host cells.[9,10] Cationic polymers have been reported to sequester planktonic bacteria in this way as a result of non-specific multivalent "cross-linking" of negatively charged bacteria and positively charged polymers which is often referred to in this context as bridging aggregation (**Figure 21**).[11]

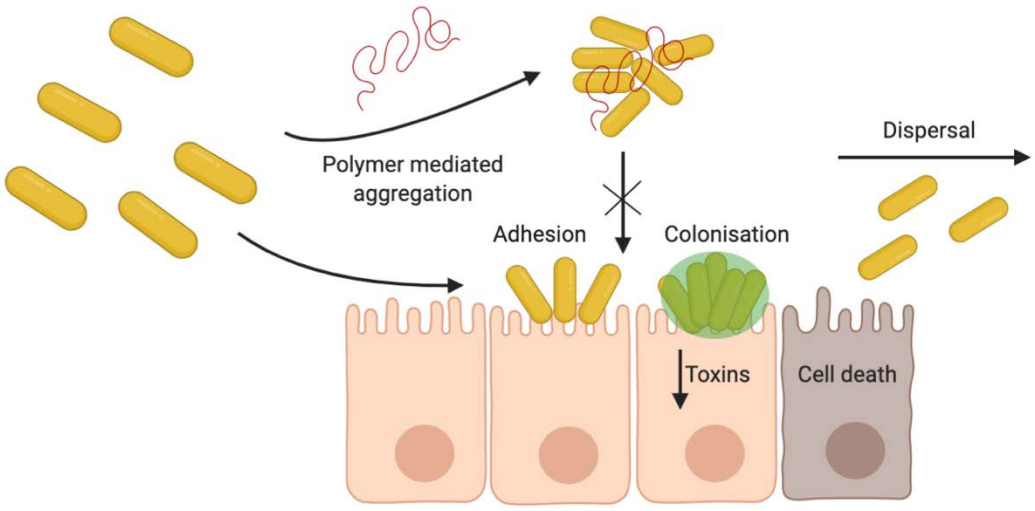

Figure 21. Polymer-mediated aggregation of bacterial cells as an "anti-adhesion therapy" reduces their ability to colonise and cause toxicity to the host.

The general design principles of cationic polymers reported to sequester bacteria are similar to those of more extensively researched cationic antimicrobial polymers (AMP). AMPs generally employ the use of primary, secondary, tertiary or quaternary amines to impart an overall cationic charge on the polymer while hydrophobicity is introduced in order to tune antimicrobial properties,[12,13] although there has been difficulty in translating general design principles when targeting different bacteria.[14,15] The impact of cationic polymer chemistry on the binding of bacteria is less well understood, and cationic portions of synthetic polymers for bacterial clustering have exclusively consisted of primary, tertiary or quaternary amines (**Introduction**). Previous work carried out in our labs determined that tertiary amine containing methacrylate polymers were less toxic to *Vibrio cholerae,* and exhibited similar clustering and anti-adhesion properties to primary amine containing polymers,[9] although methacrylate AMPs synthesised from closely related primary and tertiary amine containing monomers were found to exhibit opposite trends in toxicity towards *Escherichia coli* and *Mycobacterium smegmatis* and different mechanisms of action on the cell membrane.[15] It is not clear if observed differences originate from the nature of

the side-chain or the architecture of the polymer itself. In this regard a better understanding of the structure-activity relationships of these materials is needed. Heterogeneity is a major hurdle in polymer chemistry,[16] especially when designing polymers for biomedical applications. With this in mind, post-polymerisation modification of a polymer scaffold is an attractive means of generating new chemically distinct polymers originating from the same parent polymer so as to negate effects arising from different polymerisations.[17] Further control over the material can be achieved using controlled polymerisation techniques (CRP) to reduce the dispersity in the polymer molecular mass, aiding predictability and reproducibility of these materials as well as allowing access to different degrees of polymerisation (DP). Popular examples of CRP techniques include reversible addition-fragmentation chain transfer (RAFT),[18,19] and atom transfer radical polymerisation (ATRP).[20]

Cationic polymers have been reported as being able to trigger additional bacterial responses as a consequence of aggregation, in particular, biofilm formation,[21,22] or repression,[23,24] where it has been proposed that increased biofilm formation may be a result of increased quorum sensing of bacteria sequestered into clusters (**Figure 22**).[21,22]

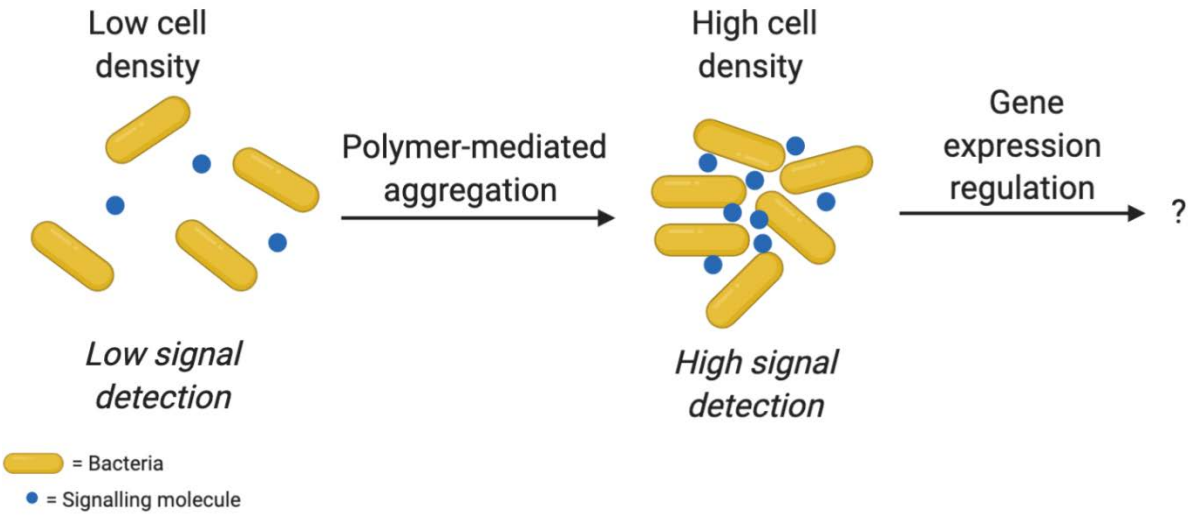

Figure 22. High cell density results in increased concentration and detection rates of quorum sensing molecules which influences how bacteria regulate certain genes.

While enhanced quorum sensing has been reported and linked to an upregulation in biofilm production in both *V. cholerae* and *E. coli* after clustering with cationic polymers, this observation is easily justified in *E. coli*, which upregulate biofilm in response to quorum sensing,[25] although, not easily explained for *V. cholerae* which downregulate biofilm formation in response to quorum sensing.[26] These observations suggest that there may be mechanisms other than quorum sensing triggering bacterial responses. A greater certainty over the polymer chemistry, coupled with high-throughput approaches to screening different polymer chemistries will broaden the understanding of interactions between synthetic cationic polymers and bacteria.

2.2 Objectives

The primary objective of this work was to evaluate the use of poly (acryloyl hydrazide) ($\mathbf{P_x}$) as a scaffold to screen a library of cationic polymers for their activity in sequestering and modulating the physiology of *V. cholerae.* The motivation behind this work was to relate polymer chemistry and biological activity and to explore the side-chain chemical space outside of primary amines, dimethylamines and quaternary

amines. To this end, the versatility of $\mathbf{P_x}$ was exploited so that the degree and nature of the side-chain functionalisation and the degree of polymerisation could be modulated in a controlled and systematic way.

A secondary objective was to critically evaluate the methods used in comparing the activities of polymer on the clustering of bacteria. Heterogeneous growth, as is the case in either clustering or biofilm formation can hamper the interpretation of certain indirect measurements such as optical density and fluorescence during growth curves. Directly observing bacteria *via* optical methods therefore is a valuable means to corroborate the reported data. And further to this, traditional imaging workflows involve the pipetting of samples onto slides and imaging which involves a level of invasiveness and can lead to bias when it comes to evaluation. In this regard investigation into polymer activity will be carried out using time-lapse microscopy under standard assaying conditions in order to better interpret the activity of cationic polymers **P1** and **P2 (Figure 24)** reported in our previous work[9,22], and further novel cationic polymers generated from $\mathbf{P_x}$.

2.3 Results and discussion

2.3.1 Cationic polymers P1 and P2 induce different effects on growth and biofilm formation of V. cholerae

It was previously reported in our labs that cationic polymers poly(N-(3-aminopropyl) methacrylamide (**P1**) and Poly(N-[3-(dimethylamino)propyl] methacrylamide) (**P2**), cause aggregation of *V. cholerae.*[9,22] Aggregation is understood to be driven by multivalent electrostatic interactions between the positively charged polymer and the negatively charged bacterial membrane and has been proposed as a means of inhibiting adhesion of bacteria to surfaces. It has been demonstrated

previously that polymers designed to bind bacteria can offer a protective effect towards host cells against pathogenic infection.[9,10] We reported that *V. cholerae* aggregated after treatment with **P1** and **P2** resulted in an enhancement in quorum sensing due to a local increase in quorum sensing molecules within bacterial aggregates.[22] Quorum sensing downregulates biofilm and virulence factor production in *V. cholerae,*[26,27] to allow dissipation of the bacteria in response to high cell density.[28] However, enhanced quorum sensing driven by **P1** and **P2** resulted in a downregulation of toxin genes but an upregulation of biofilm genes and increase in biofilm formation.[22]

The role side-chain chemistry on these reported effects was not clear, and in order to better understand how bacteria respond after incubation with **P1** and **P2**, time-lapse microscopy was carried out to assess subtle differences in bacterial responses to these polymers, such as abnormal growth dynamics, clustering and biofilm formation. To evaluate this, we imaged *V. cholerae* growth in response to **P1** and **P2** treatment every 30 minutes without shaking, using an oCelloScope high-throughput microplate imager which allowed for continual imaging on multiple samples during incubation without disturbing the sample (**Figure 23**).

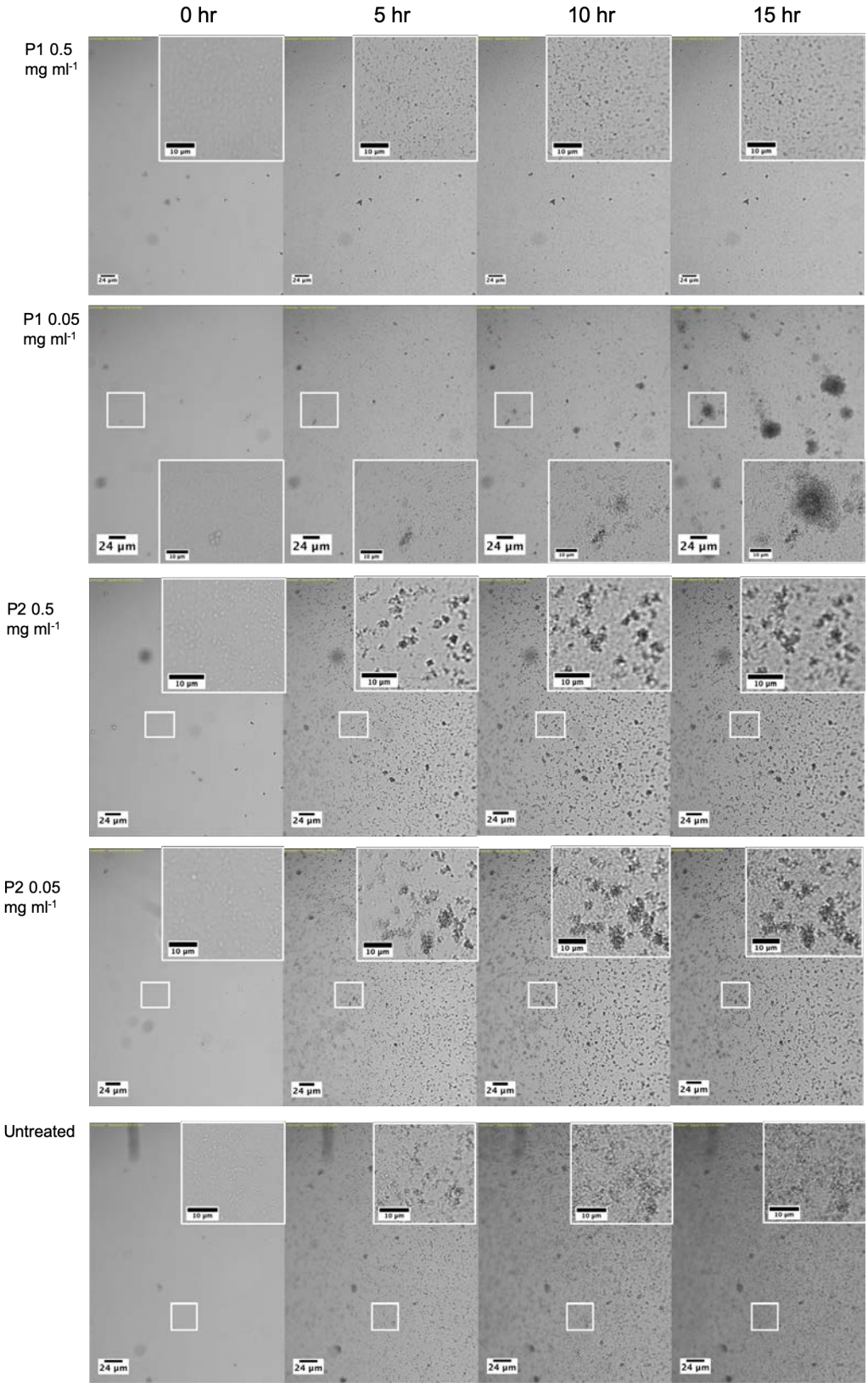

Figure 23. Optical microscope images of *V. cholerae* growth progression in clear DMEM at 37 °C, taken at indicated timepoints with an oCelloScope (4X objective), treated with **P1** or **P2** at 0.5 and 0.05 mg ml^{-1}. Each image represents the bottom of a 96 well plate and samples were recorded in triplicate. Initial OD_{600} was 0.02.

Imaging growth in this way revealed large differences between the effects of both polymers, and we were surprised to observe nucleation of *V. cholerae* biofilm,[29] for samples treated with **P1** at 0.05 mg ml^{-1} not replicated for **P2**. These biofilms which nucleated and grew at identical rates, were present in each of the triplicates tested and further observed in independent experiments. Growth curves based on image contrast during the time-lapse imaging (**Figure 24**) were in agreement with growth curves previously reported,[9] suggesting that **P1** was toxic at 0.5 mg ml^{-1} and **P2** was non-toxic at both concentrations tested. Interestingly biofilm nucleation occurring at around 10 hours, was represented in the growth curve by an initial delay in growth followed by accelerated growth after biofilms had nucleated (**Figure 24**).

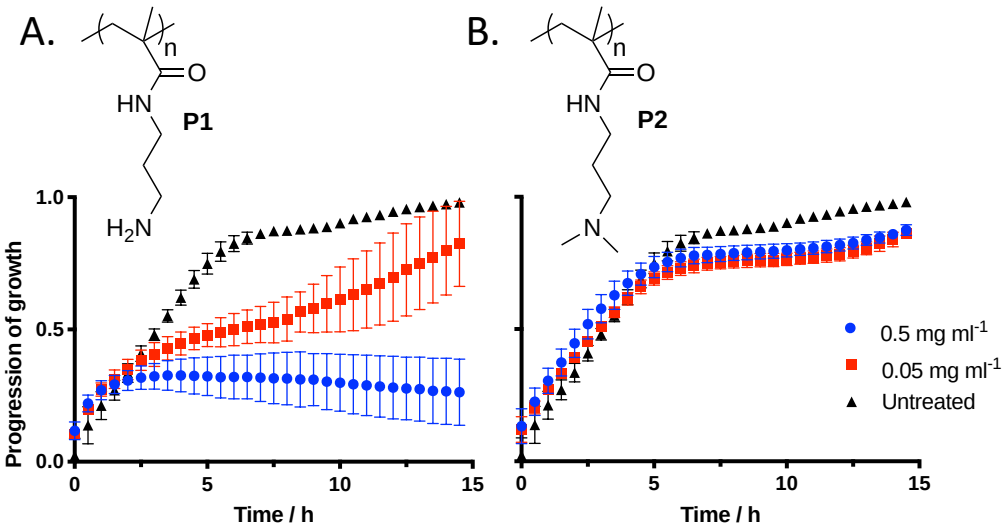

Figure 24. Growth curve estimates for *V. cholerae* incubated at 37 ºC, dispersed in clear DMEM. Estimates cacluated from oCelloScope time lapse imaging data using the in-built software (Biosensesolutions) for A) **P1 and** B) **P2.**

It was rationalized that the nucleation of biofilms by **P1** would not be observable to the same extent while shaking occurred during the incubation process, as in our previously reported work,[22] but could account for the reported bacterial clustering due to partially dispersed microcolonies. On account of these observations, and given **P1** had been previously shown to upregulate the production of key biofilm scaffolding

protein RbmA to a greater degree than **P2,**[22] it was investigated whether this would translate to differences in biofilm accumulation measurable by traditional crystal violet staining, and thus further support our observation that **P1** has a distinct effect on biofilm formation of *V. cholerae* to **P2.** The crystal violet assay, is a simple procedure which can be carried out in 96 well plates as described by O'Toole,[30] whereby after incubation residual attachment of bacterial biofilm components to the sides and bottom of a 96 well plate after washing can be quantified by staining with the triarylmethane dye; crystal violet **(Figure 25)**.

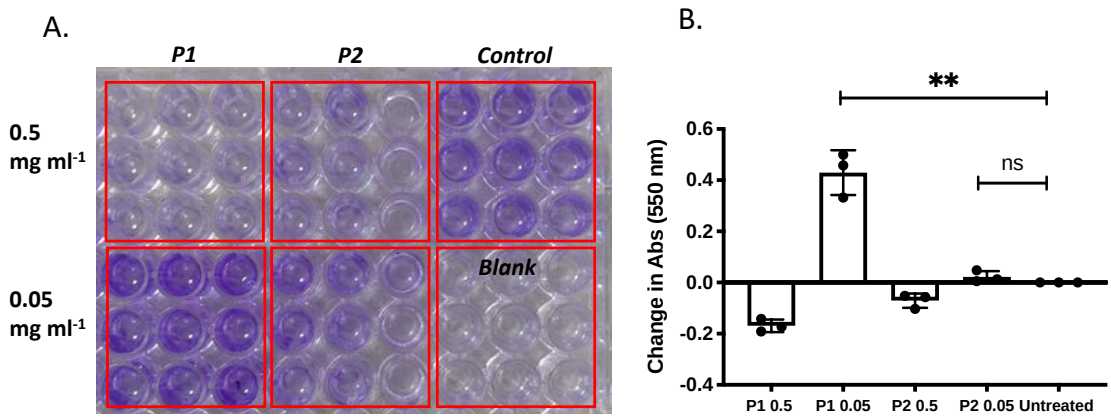

Figure 25. A) Image of crystal violet plate layout, showing polymer-modulated biofilm formation by crystal violet staining, for *V. cholerae* after 24-hour incubation (37 °C, clear DMEM). B) Assessment of biomass production by absorbance at 550 nm for the corresponding wells in A., indicating a significant increase in biomass for *V. cholerae* treated with 0.05 mg ml^{-1}. Each point represents a biological replicate (n=3) as average of 3 technical replicates. Significance was calculated using a student's t test (** P=0.0021).

The results of the assay revealed a significant increase in biofilm formation for *V. cholerae* treated with **P1** at 0.05 mg ml^{-1} which was not replicated for **P2**, correlating well with evidence of biofilm formation by microscopy (**Figure 23**). We suspect that although sequestering of bacteria with **P2** resulted in a reported upregulation of biofilm controlling genes,[22] this aggregation process may also restrict bacterial attachment to the surface of the well resulting in reduced staining by crystal violet. A similar conclusion was made by Kuroda and co-workers who reported a reduction in crystal

violet staining due to clustering of *Pseudomonas aeruginosa* incubated with a quaternary amine derivative of **P2.**[23] Bacterial clustering with tertiary and quaternary amines such as **P2** has been well established**,**[23,32-38] however primary amines are less well researched for this use, and are reported as having higher antimicrobial activities than tertiary and quaternary amines despite possessing a lower overall positive charge.[14] Higher antimicrobial activity for primary amine containing polymer is likely to be due to fact that primary amines interact more strongly with negatively charged phospholipids compared to sterically more hindered tertiary amines.[31] Having considered that small differences in the chemical properties of polymers such as charge, sterics and hydrophobicity of the side-chain can result trigger different bacterial responses as we have seen here for **P1** and **P2,** we decided to investigate the chemical properties of the side-chain by taking a post-polymerisation modification approach, in order to better evaluate structure-activity relationships, and facilitate the discovery of novel polymeric compounds which could sequester and control pathogenic bacteria.

In Chapter 1, we reported the synthesis a highly versatile poly(acryloyl hydrazide) (**P_x**) scaffold,[32,33] by controlled Reversible addition-fragmentation chain transfer (RAFT) polymerisation[18,19] which yielded polymers with improved control over the molecular mass. **P_x** affords access to libraries of new functional polymers with potential biological applications *via* post-polymerisation modification with functional aldehydes (**Scheme 4**).[32]

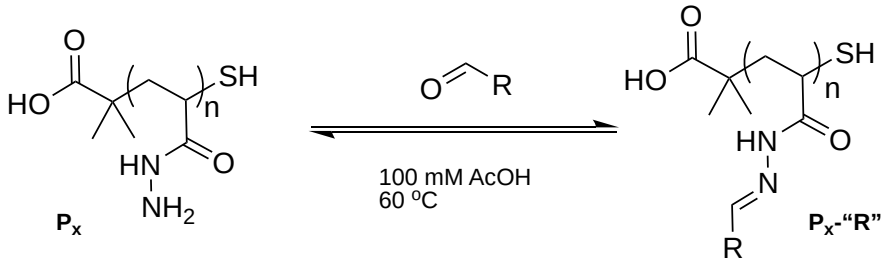

Scheme 4. Synthetic route for polyhydrazide scaffold (**P_x**) and post-polymerisation modification with aldehydes (**P_x-"R"**).

This methodology allowed evaluation into the impact of the side-chain chemistry on bacteria, while negating differences in activity arising from uncertainty over polymer molecular mass and dispersity ($Đ_m$), which is often overlooked and can be especially challenging to control in polymer chemistry where differences in the molecular mass and shape of the molecular mass dispersity ($Đ_m$) impact the materials properties.[34,35]

With this in mind, and before exploring different side-chain chemistries we prepared **P_x** at different molecular masses to investigate the impact on toxicity towards *V. cholerae*. **P_x** targeting DP50 and DP100 *via* RAFT, and **P_x** prepared by free radical polymerisation were analysed by SEC (**Figure 26**).

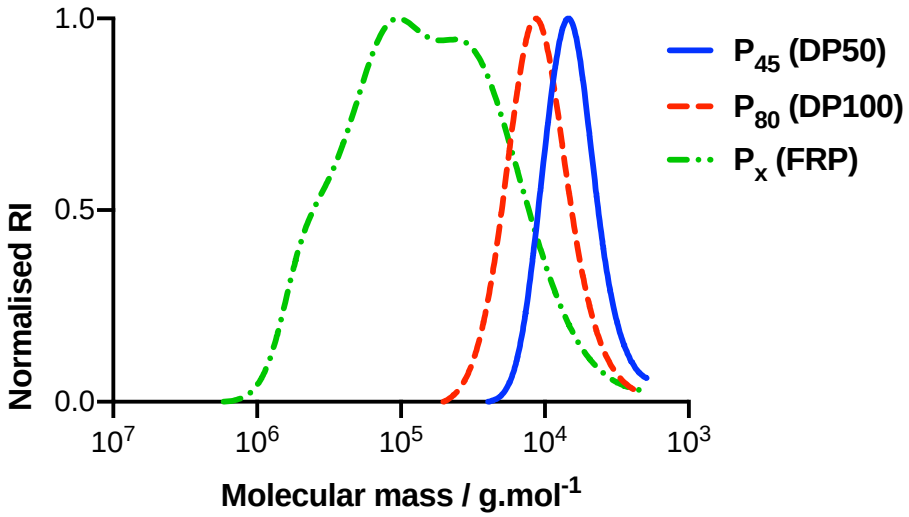

Figure 26. Molecular mass distributions (SEC, Lonza DPBS) for **P_x** targeting DP50, DP100 and prepared by free radical polymerisation (FRP). Values calculated by a standard method with PEG/PEO calibrants.

Table 3. SEC data for $\mathbf{P_x}$ described in **Figure 26**.

Targeted DP	M_p[a] (theo)	M_n[b] (SEC)	$Đ_m$ (SEC)
DP50	4094	6014	1.21
DP100	7104	9509	1.32
N/A (FRP)	N/A	26695	5.6

[a] Polymer molecular weight calculated by monomer conversion ($g.mol^{-1}$); [b] Number average molecular weight was calculated by SEC (Lonza DPBS) using standard calibration methods with PEG/PEO ($g.mol^{-1}$).

Smaller $Đ_m$ was noted for polymers targeting DP50 and DP100 in agreement with our results for optimised polymerisation conditions (**Chapter 1**), and a significantly larger and highly disperse "free radical" polymer (**FRP**), when the RAFT agent was replaced with cysteamine ([**1**][CTA][In] = [100][2][0.4]).

After preparing $\mathbf{P_x}$ at different molecular masses, we assessed the impact molecular mass of the polymer had on the growth of a GFP-producing strain of *V. cholerae* by optical density (OD_{600}) and fluorescence (GFP). GFP was used throughout this work as a proxy of bacterial growth so as to negate uncertainties in OD_{600} due to bacteria clustered by polymers (**Figure 27**).

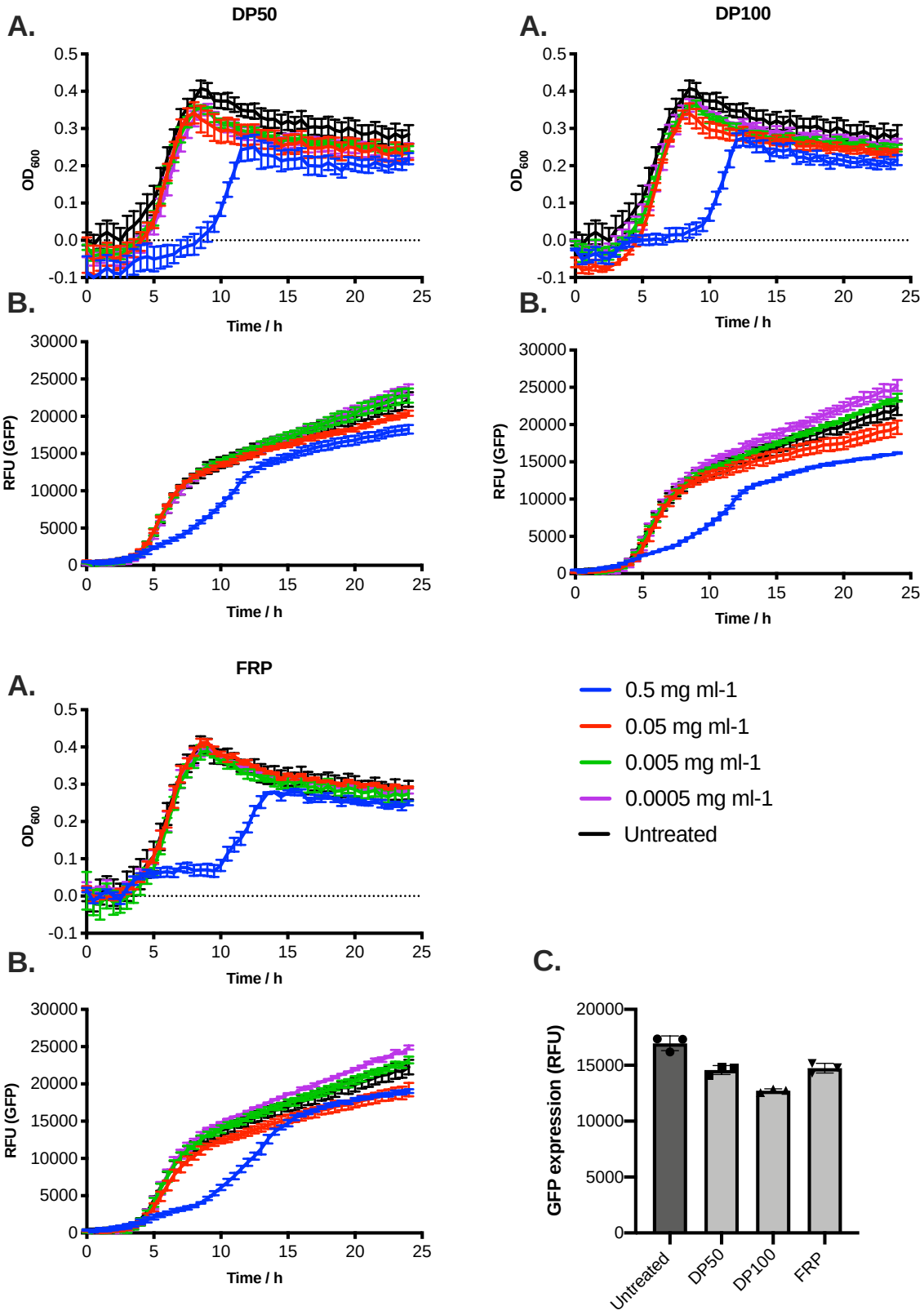

Figure 27. Growth curves for *V. cholerae* incubated at 37 ºC in clear DMEM treated with varying concentrations of $\mathbf{P_x}$ prepared at different targeted molecular masses (DP100, DP50 and FRP). Growth measured by A) OD_{600} and B) fluorescence (GFP) in triplicates (n=1) and C) GFP expression from GFP growth curves at 15 hours.

In all cases $\mathbf{P_x}$ displayed little growth inhibition towards *V. cholerae* except at the highest concentration, 0.5 mg ml^{-1} where growth was delayed prior to 10 hours, but recovered to similar levels after 15 hours. It was proposed that low toxicity may be as a result of the poorly protonated hydrazide group (pKa ~ 4) at physiological pH,[36] which may also account for the observed inability for $\mathbf{P_x}$ to form clusters of bacteria. GFP expression at 15 hours by fluorescence for *V. cholerae* incubated with different molecular mass $\mathbf{P_x}$ (**Figure 27** C) was compared in order to deduce whether the polymer molecular mass influenced toxicity towards the bacteria. However, no evidence was found for a correlation between $\mathbf{P_x}$ molecular mass and bacterial growth (**Figure 27**).

2.3.2 Post-polymerisation modification of poly(acryloyl hydrazide)

Having established that molecular mass of poly(acryloyl hydrazide) ($\mathbf{P_x}$) did not impact the growth of *V. cholerae*, we next set out to investigate how modulating the side-chain chemistry of $\mathbf{P_x}$ would affect its biological properties with the aim being to sequester *V. cholerae*. Hydrazide side chains present in $\mathbf{P_x}$ are very amenable to reactions with aldehydes *via* hydrazide-carbonyl condensation to form acyl hydrazone polymer-aldehyde conjugates, and in this way, we prepared $\mathbf{P_x}$ with different degrees of functional aldehyde loading. Two commercially available hydrophobic aldehydes possessing aromatic amines; Imidazole-4-carbaldehyde (**IMI**) and 2-amino-3-formyl pyridine (**2A3FP**) were chosen to modulate hydrophobicity and protonation of $\mathbf{P_x}$ **(Scheme 5**).

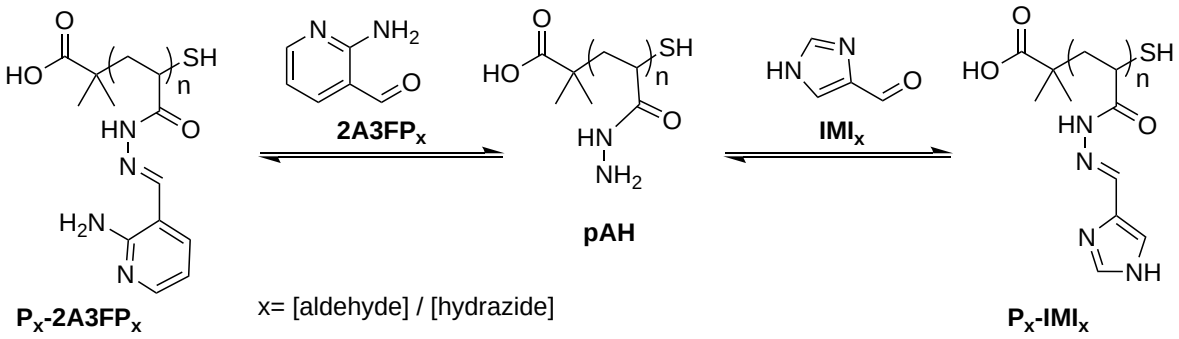

Scheme 5. Synthetic routes taken in the post-polymerisation of $\mathbf{P_x}$ to yield polymers with varying degrees of aromatic amine **IMI** or **2A3FP**.

IMI and **2A3FP** have an estimated pKa of 6.03 and 6.19 respectively which corresponds to intermediate levels of protonation at physiological pH compared to **P1** and **P2** (pKa ~ 8.3 and 7.5 respectively),[31] but significantly more protonated than the hydrazide groups of $\mathbf{P_x}$.[36] The conjugation reactions were carried out by combining stock solutions of a $\mathbf{P_{45}}$ and the aldehyde in 100 mM acetic acid buffer at different ratios (**Table 4**).

Table 4. Representative experimental set up for the preparation of $\mathbf{P_{45}}$**-IMI** and $\mathbf{P_{45}}$**-2A3FP** at different degrees of functionalisation[a] . Detailed experimental conditions for $\mathbf{P_x}$ functionalisation can be found in the appendix.

[aldehyde] / [hydrazide]	$\mathbf{P_x}$[b]	Aldehyde[b]	Buffer[b]	Total[b]
0	300	0	300	600
0.25	300	75	225	600
0.5	300	150	150	600
0.75	300	225	75	600
1.0	300	300	0	600

[a] Concentration for both aldehyde and $\mathbf{P_x}$ stock was 0.12M. [b] Volumes reported in µL.

Post-polymerisation modification was carried out in HPLC vials fitted with micro stirrer bars and heated at 60 °C for 24 hours. The loading efficiency of **IMI** or **2A3FP** onto the polymer was evaluated by proton NMR by monitoring the reduction in the free aldehyde proton region (total = 1H), versus the residual proton signals for **IMI (Figure 28)** or **2A3FP** (**Figure 29**), which were visible as either sharp or broad signals depending on the conjugated or unconjugated state of the aldehyde (**Table 5**).

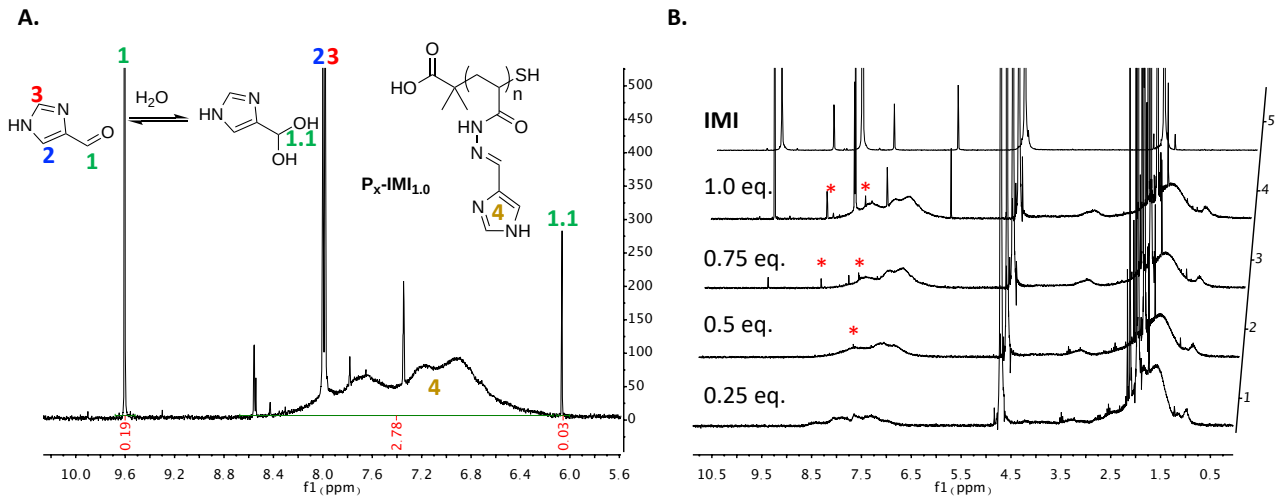

Figure 28. Proton NMR (D_2O) following the reaction of **P_{45}** with **IMI**. A) Expanded aldehyde region showing peaks involved with calculating degree of functionalisation. Peaks labelled **1** and **1.1** represent the aldehyde and the corresponding hydrate respectively. B) Stacked NMR spectrums for the reaction of **P_{45}** with different equivalents of **IMI** after 24 hours and in the absence of **P_{45}** (top) mono and dihydrazone impurities are denoted by *. All samples were incubated in 100 mM AcOH / D_2O.

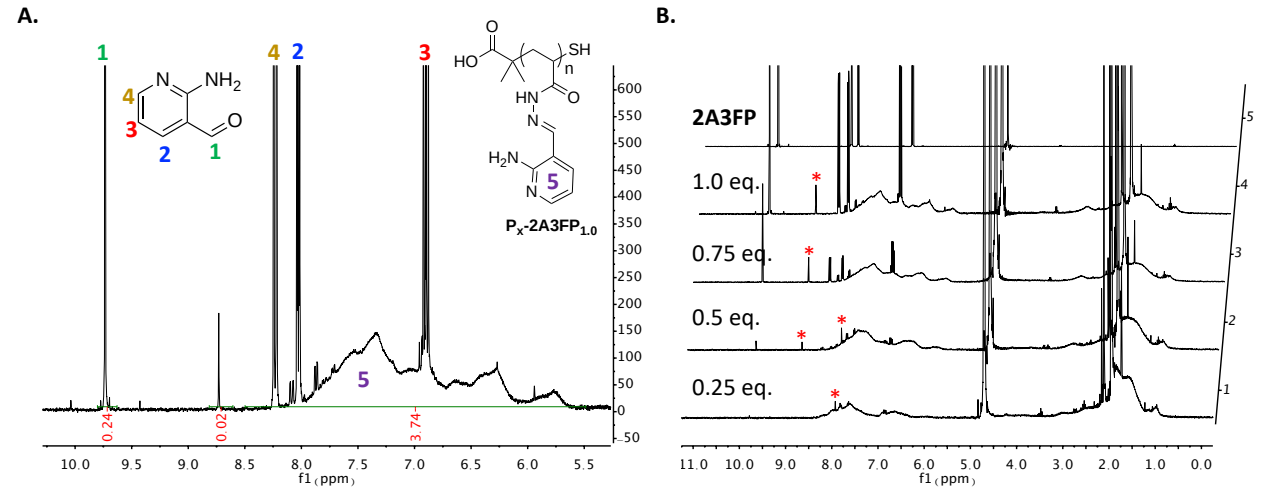

Figure 29. Proton NMR (D_2O) following the reaction of **P_{45}** with **2A3FP**. A) Expanded aldehyde region showing peaks involved with calculating degree of functionalisation. B) Stacked NMR spectrums for the reaction of **P_{45}** with different equivalents of **2A3FP** after 24 hours and in the absence of **P_{45}** (top) mono and dihydrazone impurities are denoted by *. All samples were incubated in 100 mM AcOH / D_2O.

Table 5. Percentage loading in coupling reactions at varying equivalents of the aldehyde. X= [Aldehyde]/[Hydrazide].

Entry	x=0.25	x=0.5	x=0.75	x=1.0
P_{45}-IMI$_x$	25%	50%	74%	77%
P_{45}-2A3FP$_x$	25%	50%	70%	76%

IMI displayed similar loading efficiencies to our previously published results,[32] which was closely replicated for modification with **2A3FP** which has not been previously reported with **P_{45}**. Evidence of a hydrazone cleavage products were visible in the proton NMR for **P_{45}-IMI** and **P_{45}-2A3FP** (highlighted *) (**Figure 28, Figure 29).** At intermediate loading of **P_{45}-2A3FP**, a new sharp peak at 7.92 ppm was visible (**Figure 29**) and was likely due to intramolecular cleavage of the C-N bond on the acyl hydrazone side-chain of the polymer by an adjacent unmodified hydrazide moiety to form a new monohydrazone species as proposed in our previous work.[32]

At higher equivalents of aldehyde, the monohydrazone has been shown to react with free aldehyde to form a dihydrazone species,[32] consistent with the presence of a new, sharp peak that was observed here at 8.73 ppm, visible between 0.5 and 1.0 equivalents of **2A3FP,** and the disappearance of the mono-hydrazide peak between 0.5 and 0.75 equivalents of **2A3FP**. The abundance of dihydrazone species remained largely unchanged between 0.75 and 1.0 equivalents of **2A3FP** which highlighted the involvement of unreacted hydrazide moieties (29.5% and 24% respectively) of **P_{45}** on the formation of the cleavage product. Similar impurities were noted for **P_{45}-IMI** at 7.78-7.80 ppm and 8.55 ppm for the mono and dihydrazone respectively, which had been previously reported in our work,[32] although in this case, the formation of the dihydrazone was not as favorable as compared with **P_{45}-2A3FP** (**Table 6**).

Table 6. Relative abundance of mono and dihydrazone impurities for different [Aldhyde]/[Hydrazide] conjugation conditions, calculated by proton NMR (100 mM AcoH/D_2O).

Entry	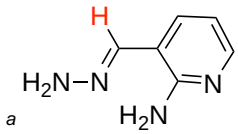 [a]	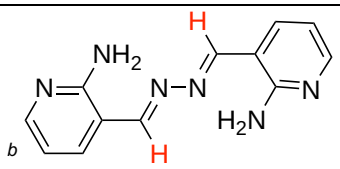 [b]	**2A3FP** consumption (%)	Total impurity (%)
P_{45}-2A3FP$_{0.25}$	100	0	100	0.25
P_{45}-2A3FP$_{0.5}$	34	66	99	0.5
P_{45}-2A3FP$_{0.75}$	4	96	94	0.75
P_{45}-2A3FP$_{1.0}$	0	100	76	0.5

Entry	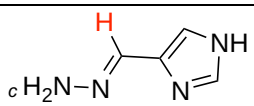 [c]	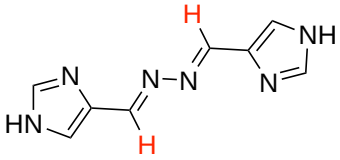 [d]	**IMI** consumption (%)	Total impurity (%)
P_{45}-IMI$_{0.25}$	100	0	100	<0.01
P_{45}-IMI$_{0.5}$	100	0	100	0.3
P_{45}-IMI$_{0.75}$	43	57	99	0.33
P_{45}-IMI$_{1.0}$	54	46	77	0.67

[a] Relative abundance (%) of proposed monohydrazone (7.92 ppm), [b] relative abundance (%) of proposed dihydrazone (8.73 ppm) (%). [c] Relative abundance (%) of proposed monohydrazone (7.78 ppm), [d] relative abundance (%) of proposed dihydrazone (8.55 ppm).

In all cases formation of the proposed hydrazone cleavage impurity was small, accounting for under 1% of the total proton signals, and we were encouraged by the efficient loading to very similar degrees for both aldehydes. With loading of the aldehyde quantified by NMR, next was studied the incorporation of the aldehyde onto the polymer by SEC (100 mM AcOH), in order to corroborate our calculated loading by NMR, and assess possible changes in the overall polymer architecture in response to different degrees of functionalisation which cannot be easily assessed by NMR (**Figure 30**).

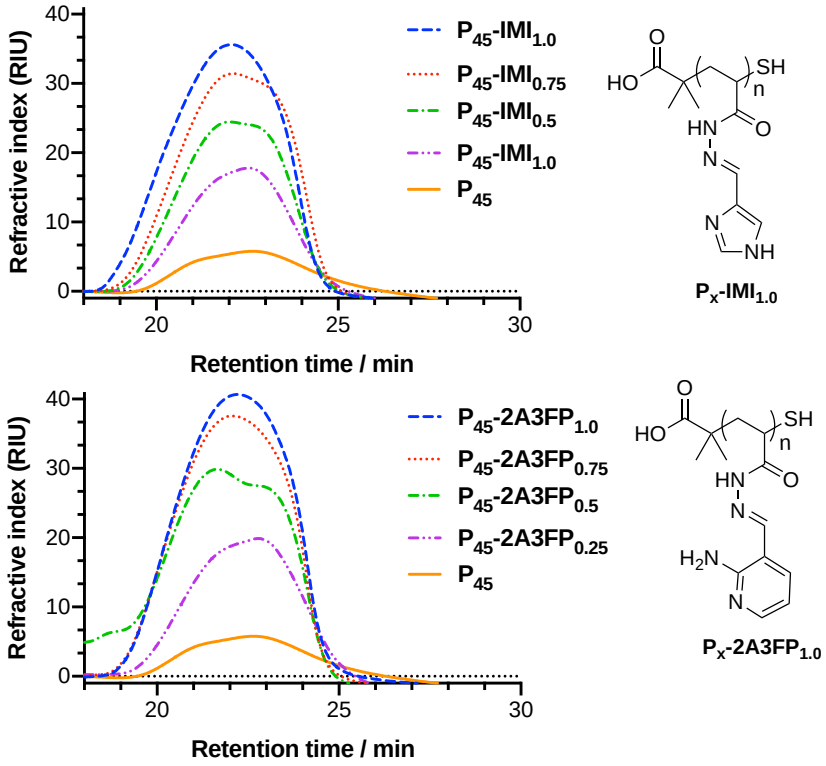

Figure 30. SEC (100 mM AcOH) trace (refractive index) for **P_{45}-IMI$_x$** and **P_{45}-2A3FP$_x$** at varying degrees of targeted functionalisation (x= [Aldehyde]/[Hydrazide]).

Refractive index (RI) increased for the polymer region (20-25 minutes) in the SEC trace, with increasing functionalisation degree (x) for both **P_{45}-IMI$_x$** and **P_{45}-2A3FP$_x$**. We also noted a slight shift in RT for the maximum RI signal towards earlier retention times with increasing x. which, rather than transitioning as a single polymer dispersity as seen in living radical polymerisation,[37] resembled two distinct polymer species at intermediate loading, but a single species at maximum loading. The observation of two distinct polymer distributions was most noticeable for **P_{45}-2A3FP$_{0.5}$** and could indicate different polymer conformations accessible to **P_x** at intermediate loading,[38] uneven distribution of the modification, or structural changes in the polymer.[39]

Having prepared and characterised an array of functional polymers based on the modification of **P_x** with aromatic amines; **IMI and 2A3FP,** we investigated their

activity *in situ*, in order to probe various responses of *V. cholerae* as a function of degree of loading and nature of the aldehyde on the polymer.

2.3.3 Impact of side-chain chemistry on V. cholerae

To determine whether **P_x-IMI$_x$** and **P_x-2A3FP$_x$** imparted different toxic effects towards *V. cholerae,* growth curves for GFP expressing *V. cholerae* treated with **P_{80}-IMI$_{1.0}$** and **P_{80}-2A3FP$_{1.0}$**. Seeing how **P_{80}-IMI$_{1.0}$** and **P_{80}-2A3FP$_{1.0}$** were screened *in situ* without purification, contribution of the buffer (100 mM AcOH) and corresponding free aldehyde was also assessed in each case to account for this (**Figure 31**).

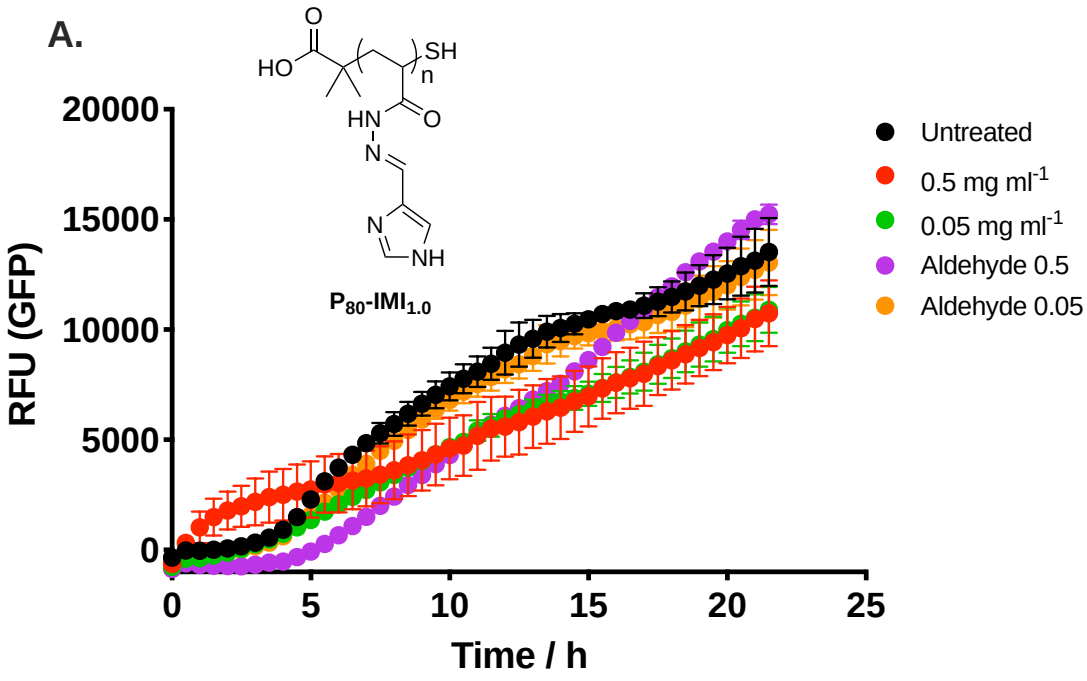

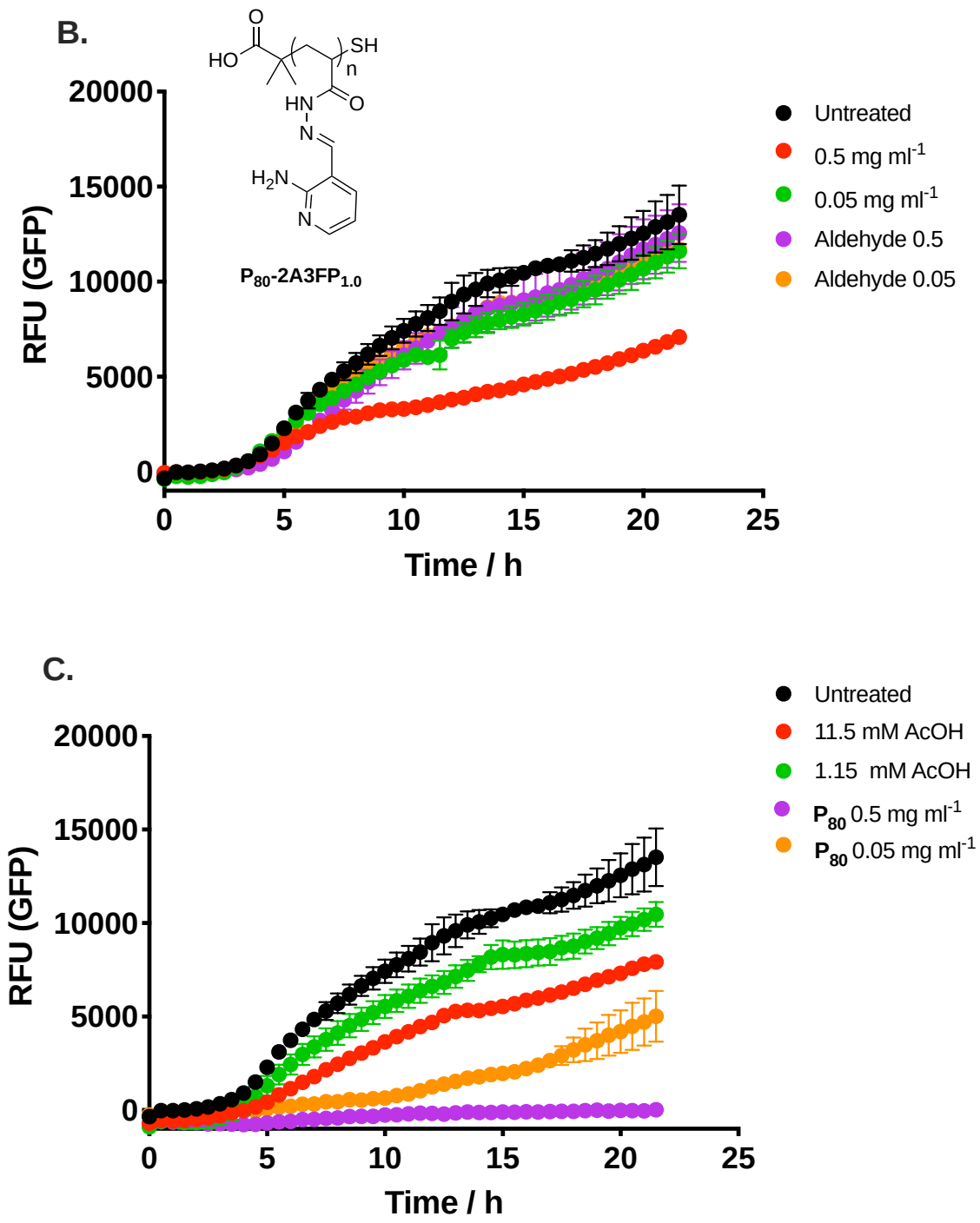

Figure 31. GFP based Growth curves for GFP expressing *V. cholerae* (37 °C, clear DMEM) treated with A), **P_{80}-IMI$_{1.0}$**, and the corresponding concentration of **IMI** (0.56 and 0.056 mg ml^{-1} respectively), B) **P_{80}-2A3FP$_{1.0}$**, and the corresponding concentration of **2A3FP** (0.71 and 0.071 mg ml^{-1} respectively) and C) unmodified polymer scaffold (**P_{80}**) and representative concentrations of AcOH buffer (100 mM) added for concentrations 0.5 mg ml^{-1} and 0.05 mg ml^{-1} conditions.

Growth curves revealed that the acetic acid buffer significantly increased the toxicity of the unmodified scaffold compared to that observed previously for **P_{80}** (**Figure**

27) , likely due to protonation of the hydrazide side-chain groups which is well known to increase the antimicrobial activities of nitrogen containing polymers.[31] The pKa of the hydrazide groups is around 4, compared to the pKa of a primary amine at around 10-11,[36] which helps explain the low toxicity of $\mathbf{P_x}$ in the absence of acidic buffer (**Figure 27**), where it remains almost entirely unprotonated. $\mathbf{P_{80}}$**-2A3FP**$_{\mathbf{1.0}}$ displayed higher levels of toxicity to *V. cholerae* at 0.5 mg ml^{-1} compared to $\mathbf{P_{80}}$**-IMI**$_{\mathbf{1.0}}$ which displayed little difference in toxicity at both 0.5 and 0.05 mg ml^{-1}. Interestingly, no lag phase in the growth of *V. cholerae* treated with 0.5 mg ml^{-1} $\mathbf{P_{80}}$**-IMI**$_{\mathbf{1.0}}$ was observed, instead, an increase in observed fluorescence intensity was apparent at early time points (t < 5h), which we reasoned could be attributed to high-density clusters of fluorescent bacteria rather than dispersed bacteria. *V. cholerae* responded differently to aldehyde controls; **IMI** and **2A3FP,** with **2A3FP** displaying very little change in shape or intensity in the growth curve over the untreated sample, while **IMI** at the higher concentration (0.56 mg ml^{-1}) resulted in a longer lag period in growth, followed by nearly linear growth progression which in this case increased even beyond that of the untreated *V. cholerae* after 20 hours. This interesting behavior may be in part due to **IMI**s analogy to the biologically important amino acid histidine and we were interested to observe further the effect of **IMI**. AcOH buffer was found to have an inhibitory effect on the growth of *V. cholerae,* even at the lowest concentration (representative of the concentration transferred for 0.05 mg ml^{-1} conditions). Owing to the low solubility of **IMI** and **2A3FP** we were unable to increase the concentration of the polymer and the aldehyde or decrease the molarity of the buffer so as to minimize the concentration of AcOH transferred to biological samples.

Since AcOH is understood to exhibit antibacterial properties and had previously been utilised in this regard as a biocide in wound treatment,[40] we explored the use of

alternative buffers for conjugation reaction in an effort to reduce the background toxicity. To this end, we tested the use of Citric acid buffer (pH 2.4) and Phosphate buffer (pH 2.8) which were both found to be suitable alternatives for the synthesis of **P_x-IMI** and **P_x-2A3FP**, however no benefit was found with respect to toxicity over that of AcOH.

Solubility issues were observed at 0.5 mg ml^{-1} for both **P_x-IMI** and **P_x-2A3FP** on addition of the polymer solution (100 mM AcOH) into the assay media (DMEM) resulting in the formation of a mucus-like precipitate(**Figure 32**).

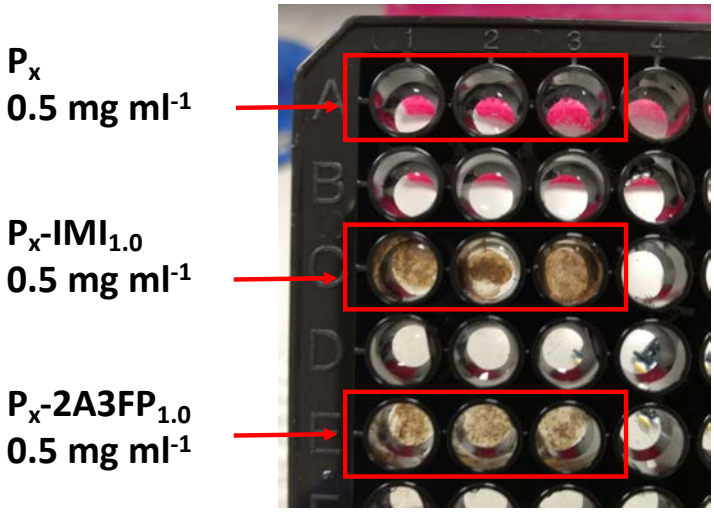

Figure 32. Polymer precipitates formed in DMEM (200 uL) during a growth curve assay.

The appearance of precipitates is likely due to the poor solubility of the conjugate at above pH 3 owing to the increased hydrophobicity on conjugation of the aldehyde. Interestingly the aldehydes on their own were perfectly soluble at both concentrations in DMEM, and both **P_x-IMI** and **P_x-2A3FP** were readily soluble in deionised water probably owing to the absence of any buffering salts. Nevertheless, we reasoned that despite the issues with solubility, which are often overlooked when designing polymer for biological applications, the polymers may still yield interesting and useful properties with respect to sequestering *V. cholerae* and may act in a similar

way to a synthetic mucus which are researched for similar applications, especially with the potential to further modify these materials with glycans.[41]

2.3.4 Impact of degree of functionalisation on V. cholerae

With an understanding of how **IMI** and **2A3FP** modulate the properties of $\mathbf{P_x}$ and the toxicity towards *V. cholerae,* we next assessed how modulating degree of $\mathbf{P_x}$ functionalisation modulated the biological response of *V. cholerae* in order to begin to evaluate the structure-activity relationship. We have seen how different side-chain chemistries of polymers result in different biological outcomes, for example in the case of **P1** and **P2,** and that polymer architecture can also influence the activity.[10] To this end, we synthesised $\mathbf{P_x}$**-IMI**, which we deemed to display more promising biological activity, and targeted different degrees of polymerisation (DP) and degrees of functionalisation (DF), in order assess the impact of each of these properties on *V. cholerae*. $\mathbf{P_x}$ targeting DP50 and DP150 was prepared by RAFT and $\mathbf{P_{FRP}}$ was prepared by FRP and each was functionalised with **IMI** to yield $\mathbf{P_x}$**-IMI**$_x$ with different degrees of functionalisation (**Figure 33**, **Table 7**).

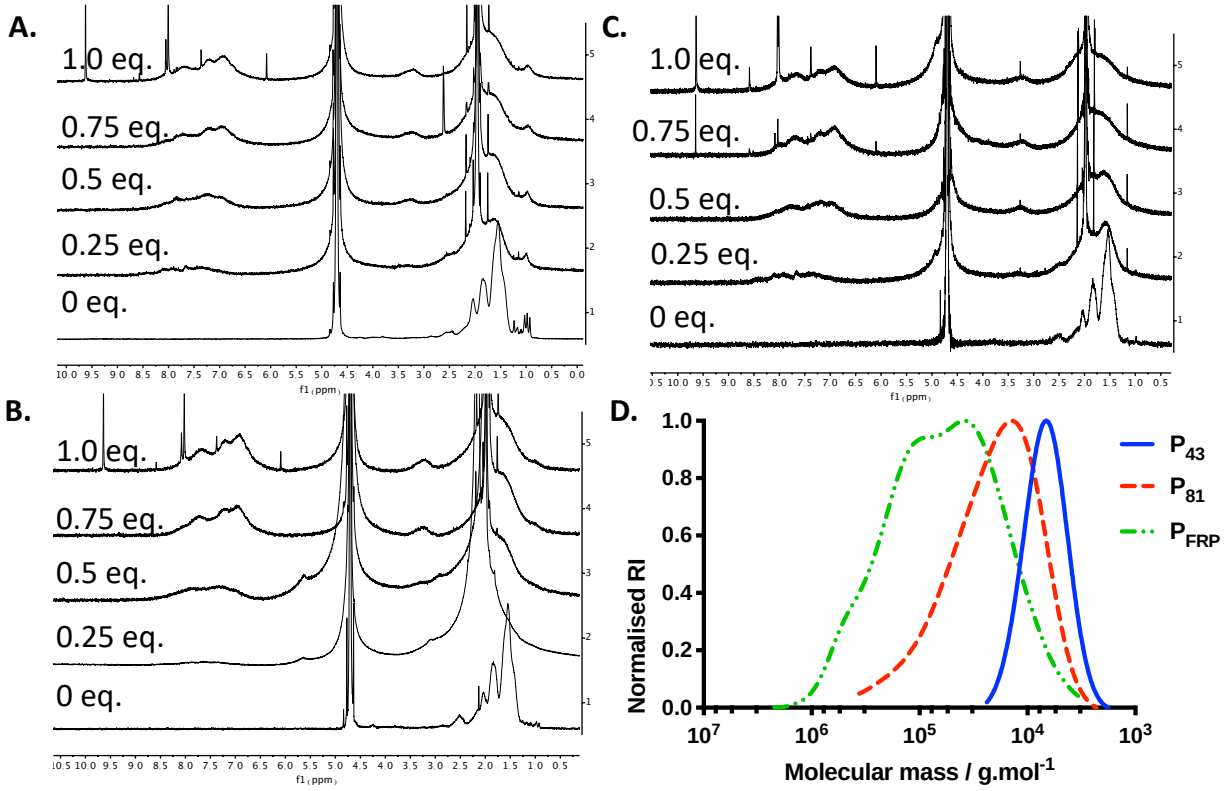

Figure 33. Stacked proton NMRs (D_2O) for A) $\mathbf{P_{43}}$ B) $\mathbf{P_{81}}$ C) $\mathbf{P_{FRP}}$ after incubation with increasing equivalents of **IMI** and D) Molar mass distributions (SEC, Lonza DPBS) for unmodified $\mathbf{P_x}$.

Table 7. SEC and aldehyde functionalisation data for polymers described in **Figure 13**.

	Polymer properties (SEC)			Functionalisation with **IMI** (NMR)			
Entry	Target DP	[a] $M_{n(SEC)}$	$Đ_M$	[b]0.25 eq.	0.5 eq.	0.75 eq.	1.0 eq.
$\mathbf{P_{43}}$	50	6037	1.25	25%	50%	75%	81%
$\mathbf{P_{81}}$	150	11908	2.45	25%	50%	75%	88%
$\mathbf{P_{FRP}}$	N/A	26306	4.31	25%	50%	74%	73%

[a] Number average molecular mass ($g.mol^{-1}$) calculated by SEC (Lonza DPBS) [b]targeted eq. of **IMI** based on [Aldhyde]/[Hydrazide].

To evaluate the impact that molecular mass and degree of functionalization (DF) had on the growth of *V. cholerae*, GFP growth curve data employing $\mathbf{P_x}$ at different molecular masses and DF was compiled across multiple biological replicates. In order to best compare multiple datasets, growth under treated conditions was normalised to

untreated *V. cholerae* for each case in an effort to negate the unavoidable biological variation apparent when carrying out biological growth on different days and from different colonal stocks. Differences between samples were highlighted after 15 hours chosen as representative of the end portion of the stationary phase of the *V. cholerae* growth cycle and therefore representative of maximum growth across all growth curves. Each dataset was further baseline-corrected against the corresponding untreated sample in order to display the results as the mean percentage growth compared with that of the untreated sample (100 % growth). Firstly, as a control, the impact of the free aldehyde (**IMI**) at varying concentrations in AcOH buffer (100 mM), and buffer only, representative of the corresponding polymer conditions was tested (**Figure 34**).

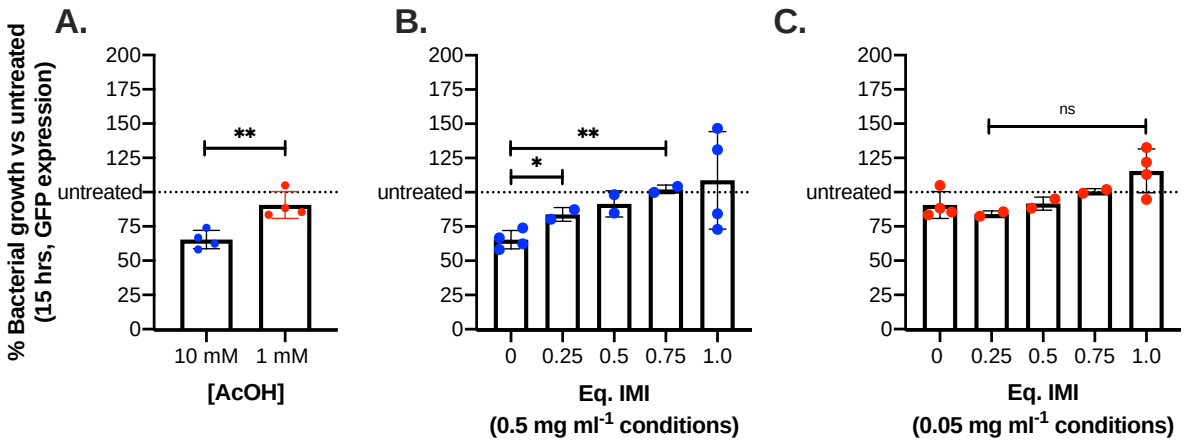

Figure 34. Relative growth of *V. cholerae* (37 °C, clear DMEM), for treated samples after 15 hours incubation. A) Impact of buffer concentration present in 0.5 and 0.05 mg ml^{-1} polymer and aldehyde conditions, and impact of increasing concentration of free aldehyde (**IMI**) representative of B),0.5 mg ml^{-1} C),0.05 mg ml^{-1}polymer conditions at corresponding targeted degrees of functionalisation. Each point represents a biological replicate as a mean of three technical replicates. Significance was calculated using a student's t test (** P = 0.0021, * P= 0.0277).

Acetic acid (AcOH) buffer resulted in a 35% reduction in growth at 10 mM, while a 15 % reduction in growth was observed for 1 mM. Interestingly with increasing portions of **IMI** dissolved in 100 mM acetic acid, corresponding to the concentrations

added to the polymer at different equivalents, a recovery of growth was observed. Recovery on addition of **IMI** was most apparent at higher concentrations of the aldehyde and we rationalized that this could be as a result of the buffering effect of the amine. However, at the highest concentration of **IMI** (**Figure 34**B, 1.0) corresponding to an addition of 0.56 mg ml^{-1} of the aldehyde (1.0 eq.), a large distribution of values was observed, with two independent experiments displaying increased growth over that of the untreated. In order to evaluate the effect of I**MI** on the growth of *V. cholerae*, compared with that of the polymer-**IMI** conjugates**,** *V. cholerae* growth curves with **IMI** treatment at various equivalents, and the corresponding polymer conjugates were compared (**Figure 35**).

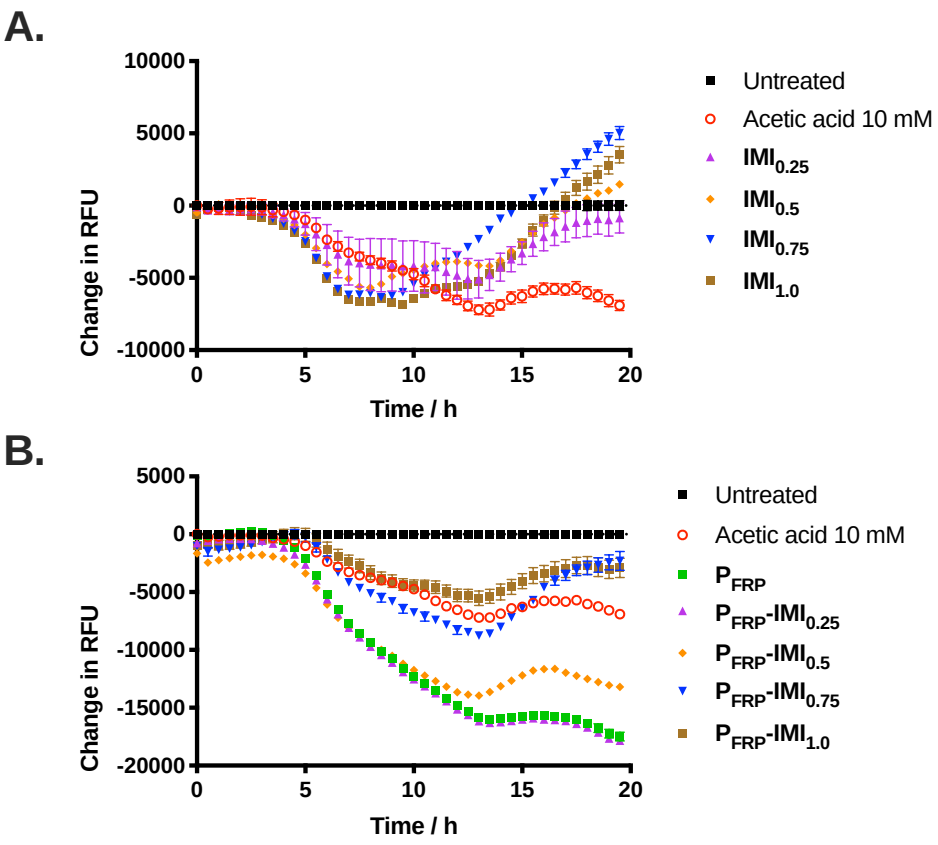

Figure 35. Baselined-subtracted growth curves of *V. cholerae* at 37 °C (GFP) (clear DMEM) for A), **IMI** and B), **P_{FRP}-IMI.** All conditions are representative of 0.5 mg ml^{-1} **P_x-IMI_x** conditions. Growth was recorded in triplicate by fluorescence.

IMI was found to impart a delay in growth compared to untreated bacteria, in a dose dependent manner, but unlike the effect of AcOH, which caused an overall reduction in growth thought the life cycle, *V. cholerae* treated with IMI displayed growth recovery after 10 hours, which, for all but the lowest concentration resulted in an even greater accumulation of bacterial cells compared with the untreated. The aforementioned effect was not reproduced in the corresponding **P_x-IMI** treated samples (Figure 35 B). Based on these observations, it was rationalised that *V. cholerae* may be responding to **IMI** beyond that of the effect of the buffer. In order to study this response in more detail, the experimental conditions in Figure 15 were reproduced but this time bacterial growth was fluorescently imaged every 30 minutes using a JuLI stage plate imager (Cambridge Bioscience) (**Figure 36**).

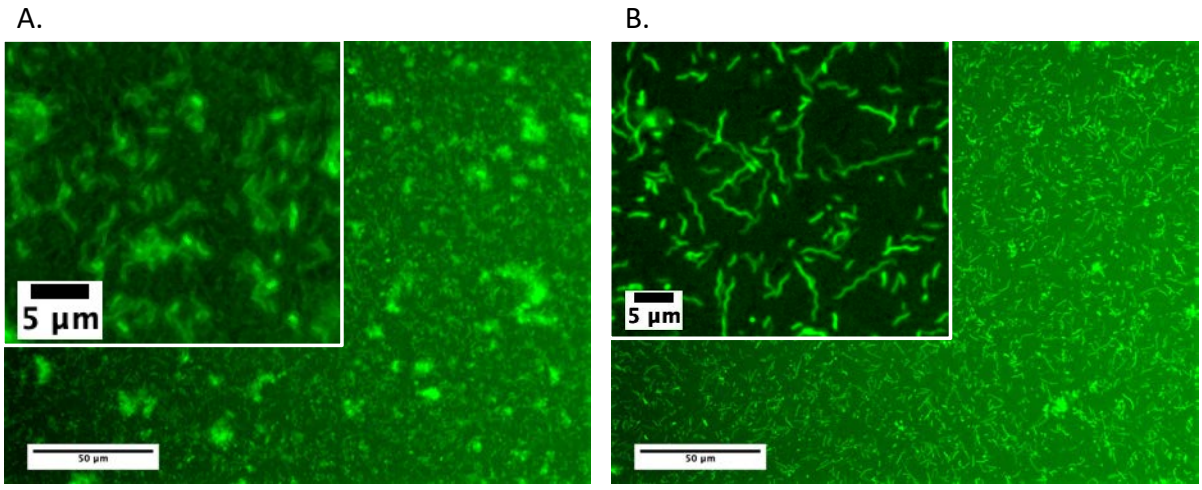

Figure 36. Fluorescent images (JuLi Stage, 60 X objective) of GFP-*V. cholerae* at 5 hours incubation at 37^{o}C (clear DMEM) treated with A) 1 mM AcOH and B) 0.56 mg ml^{-1} **IMI** in AcOH (10 mM).

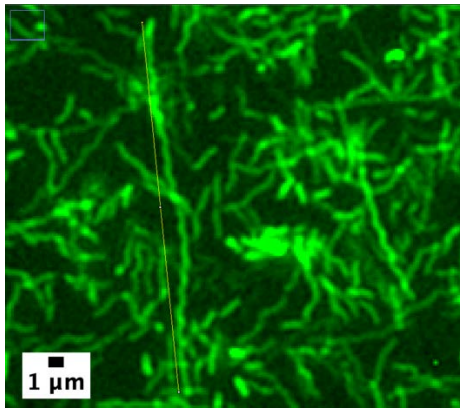

Figure 37. Expanded fluorescent images (JuLi Stage, 60 X objective) of GFP-*V. cholerae* at 13 hours incubation at 37°C. Elongated *V. cholerae* highlighted here was measured at 21 microns in length.

Images revealed that **IMI** induced elongation of the bacterial cells compared to cells treated with AcOH alone, with non-divided bacterial cells found at 21 µm after 13 hours of growth (**Figure 37**). Elongation of *V. cholerae* is known upon treatment with the antibiotic cephalexin, which is employed in research to study the curvature of *V. cholerae*.[42,43] Cephalexin disrupts the bacterial cell wall synthesis as a result of binding irreversibly to membrane bound proteins known as "penicillin binding proteins" which are vital for cell wall synthesis.[44] Recent research into elongation of *V. cholerae* reported a strain (CVD112) which displayed elongation under nutrient-limited conditions which aided adhesion to chitinous surfaces.[45] At this point, the mechanism of **IMI** on the elongation of *V. cholerae* is unknown, however it is plausible that interaction and disruption of the membrane may be involved, as has been reported for histidine rich peptides at acidic pH.[46] or interaction of **IMI** with transmembrane signaling pathway by histidine kinase,[47] as has been shown for imidazole.[48] Furthermore, elongation of *Caulobacter crescentus* has been recently linked to a complex signaling pathway involving histidine kinase.[49]

2.3.5 Effect of polymer molecular mass and degree of functionalisation of toxicity to V. cholerae

Having established the potential activity of **IMI**, we next investigated the effect loading this aldehyde onto the polymer backbone would have on the growth of *V. cholerae* (**Figure 38**).

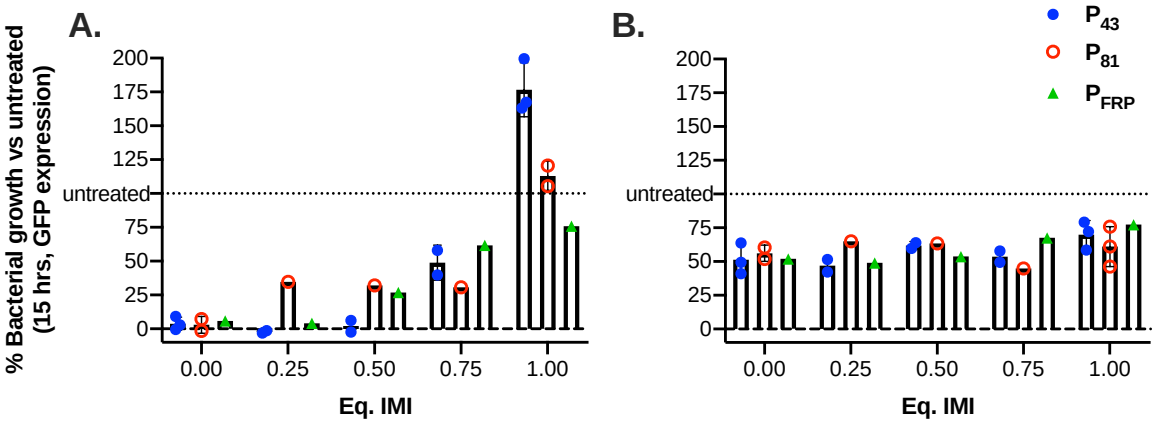

Figure 38. Relative growth of *V. cholerae* in treated samples after 15 hours incubation at 37°C (clear DMEM) for different **P_x-IMI$_x$**. A) Bacteria treated with 0.5 mg ml^{-1} **P_x-IMI$_x$** and B) bacteria treated with 0.05 mg ml^{-1} **P_x-IMI$_x$**. Each point represents a biologcal replicate as a mean of three technical replicates.

The sequential addition of **IMI** onto the polymer scaffold for conditions at 0.5 mg ml^{-1} had a significant impact on the growth of *V. cholerae* with unmodified and 25% loaded polymers, displaying complete inhibition of growth at 15 hours, while there was some, but not statistically significant evidence of lower toxicity at 50% loading. At 75% loading, bacterial growth was restored to around 50%, similar to that of the corresponding AcOH control. In the case of **P_x-IMI$_{1.0}$**, a significant increase in GFP expression was observed, in some cases above that of the untreated condition. Although at higher concentrations of **P_x-IMI** the effect of free **IMI** may be predominating, we reasoned that this could be indicative of non-homogeneous growth due to bacterial clustering.

At concentrations of 0.05 mg ml^{-1} there was no correlation between degree of **IMI** loading and toxicity, and any positive impact on growth would likely be overridden by the impact of AcOH, accounting for roughly 40% reduction in growth after 15 hours in all cases.

Lastly, we assessed if there was a correlation between polymer molecular mass and toxicity as has been reported for some cationic antimicrobial polymers,[50](**Figure 39**).

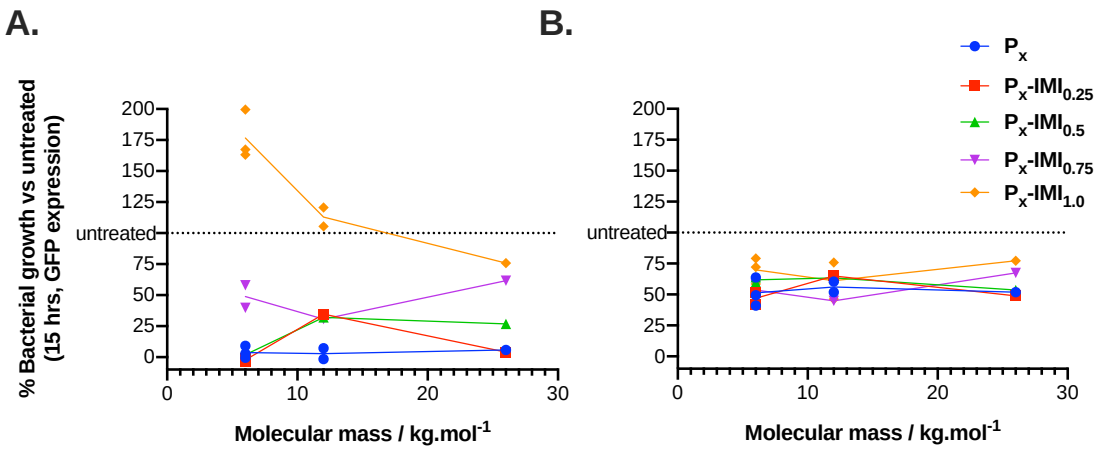

Figure 39. Growth of *V. cholerae* at 15 hours (GFP) in response to different molecular mass of **P_x-IMI** at a concentration of A) 0.5 mg ml^{-1} and B), 0.05 mg ml^{-1} with varying degrees of functionalisation with **IMI.** Each point represents an individual biological replicate as a mean of three technical replicates.

The data was unable to provide evidence of a significant correlation between molecular mass of **P_x-IMI** and the toxicity to *V. cholerae,* although there was a visible trend at the highest loading of IMI. Further biological testing would be required to assess if this trend was statistically significant, and at this point we concluded, similarly to our previous test (**Figure 27**), that **P_x** molecular mass did not influence to a great extent toxicity to *V. cholerae.*

2.3.6 Bacterial capture with P_x-IMI and P_x-2A3FP

Having assessed the influence of polymer properties on toxicity to *V. cholerae,* the ability of these cationic polymers to sequester pathogenic bacteria was tested and possibly cause elongation to the bacterial cell. To this end, growth of *V. cholerae* treated with polymers was followed using time lapse microscopy under identical conditions to those carried out for growth curves described above. In order to best relate observed growth by microscopy to fluorescent growth curves, both growth curves and time-lapse fluorescent microscopy were carried out simultaneously under identical conditions. The importance of this experiment was two-fold; to ascertain, in a non-invasive manner the interaction between the polymer and the bacteria and to identify limitations or considerations that must be made when using spectroscopic methods to better interpret their results.(**Figure 40**, **Figure 41**).

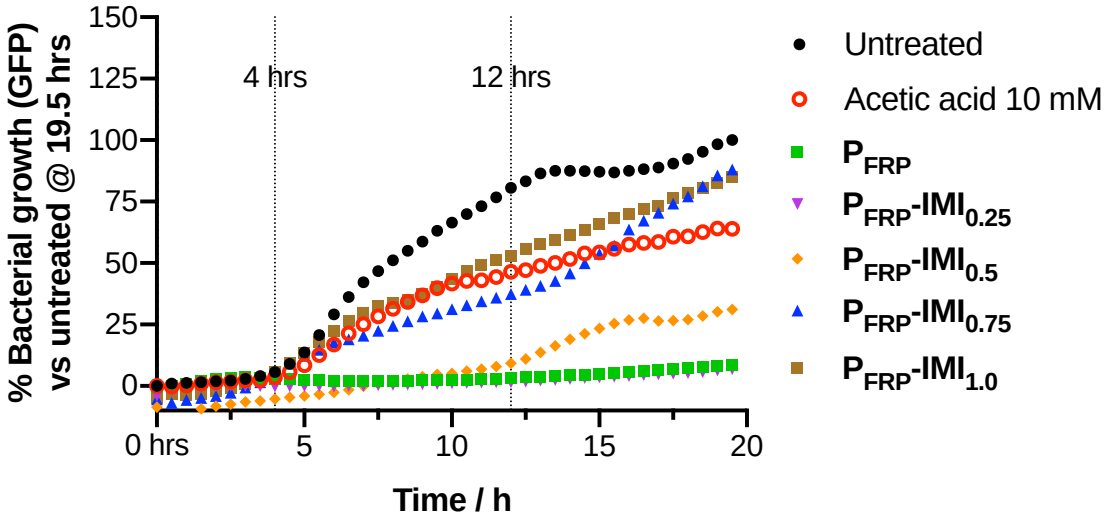

Figure 40. Growth curve (GFP) for *V. cholerae* at 37°C (clear DMEM) with **P_{FRP}-IMI$_x$** (0.5 mg ml^{-1}) at varying degrees of functionalisation with **IMI**. Highlighted times represent those of the corresponding optical images for identical conditions (**Figure 41**).

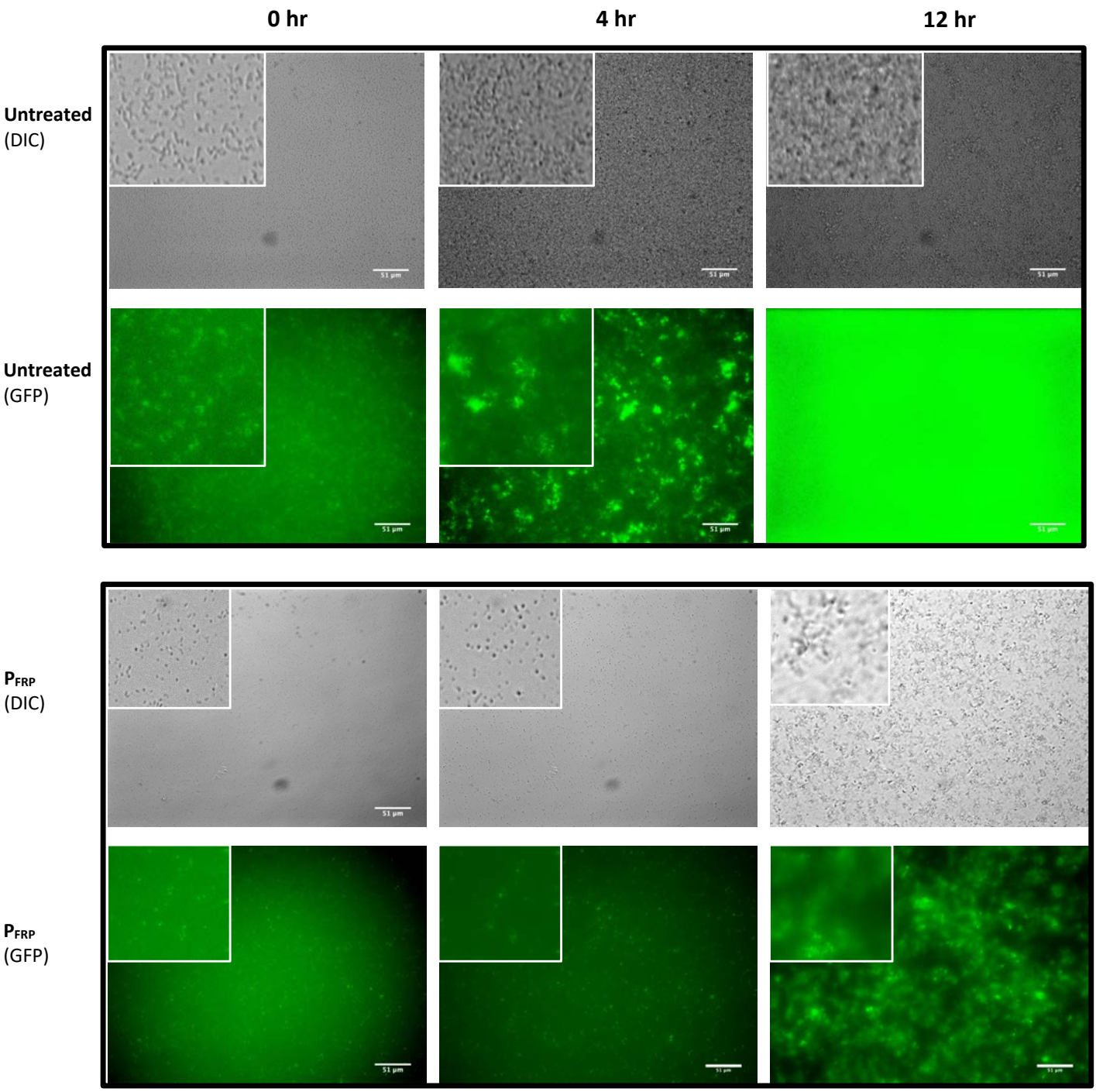
0 hr
4 hr
12 hr
Untreated (DIC)
Untreated (GFP)
P_{FRP} (DIC)
P_{FRP} (GFP)

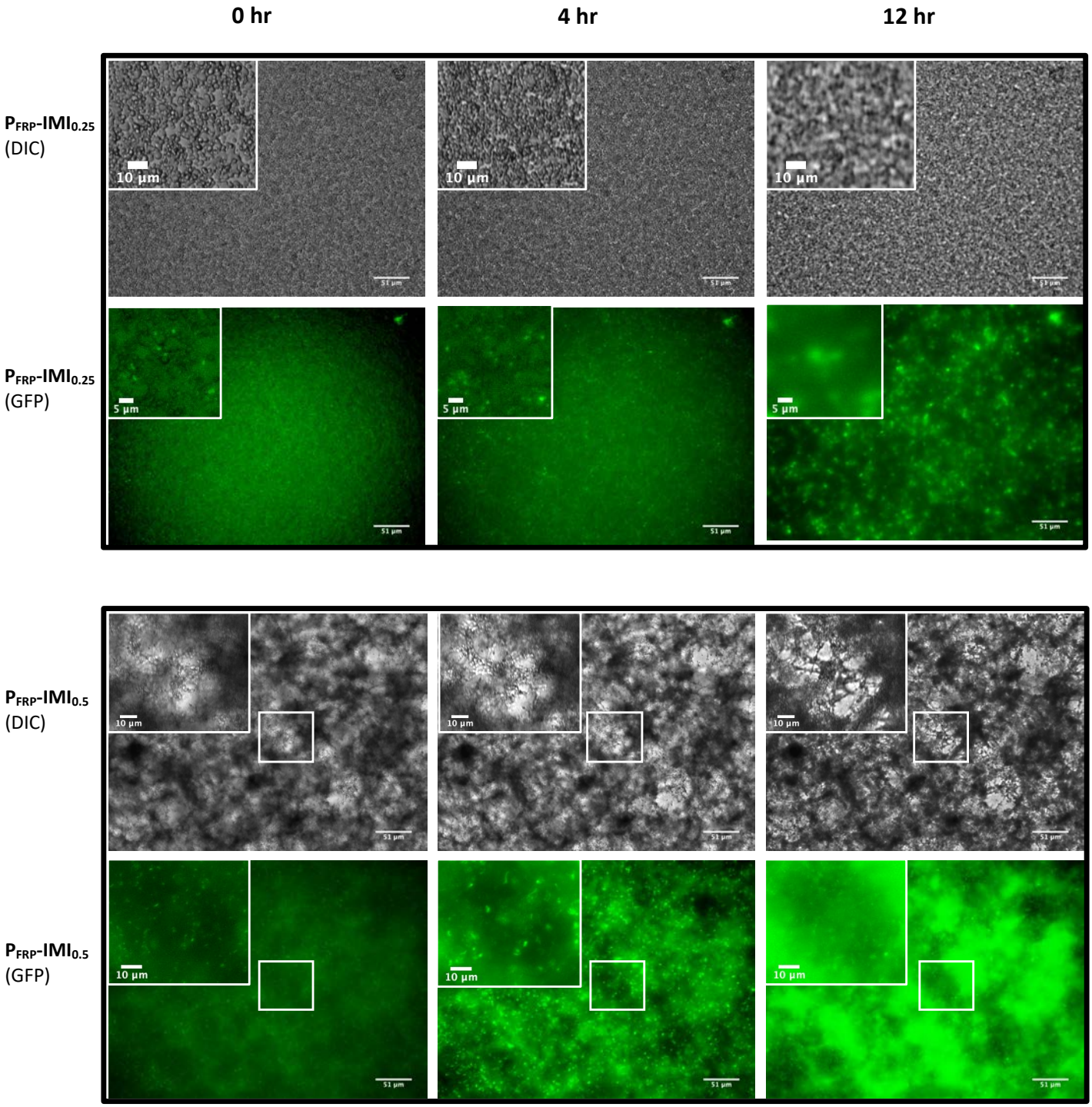
0 hr
4 hr
12 hr
P_{FRP}-$IMI_{0.25}$ (DIC)
P_{FRP}-$IMI_{0.25}$ (GFP)
P_{FRP}-$IMI_{0.5}$ (DIC)
P_{FRP}-$IMI_{0.5}$ (GFP)
10 µm
5 µm

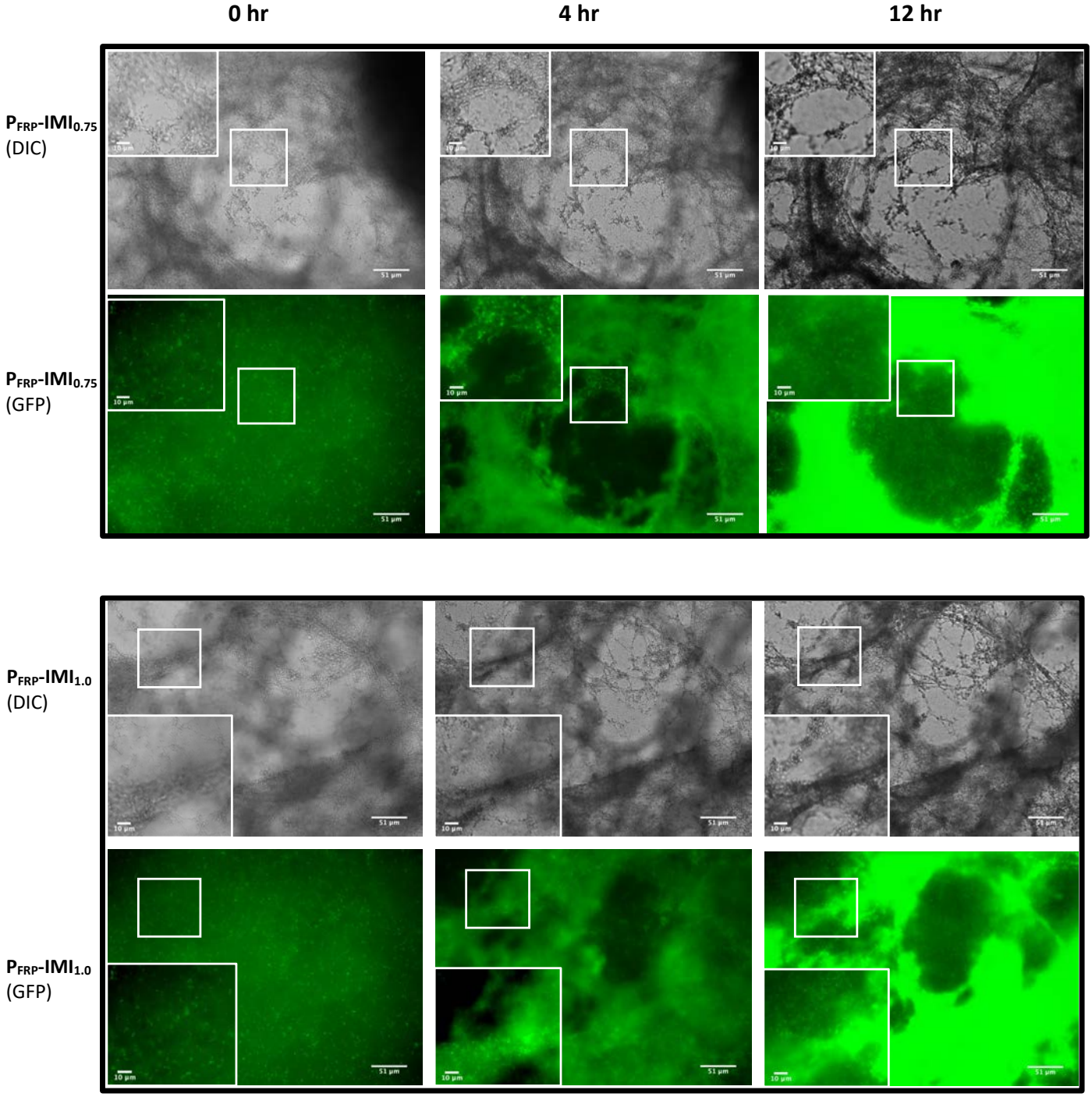

Figure 41. Time-lapse optical microscope images (20 X objective) recorded by fluorescence (GFP) and differential interference contrast (DIC) for the growth progression of *V. cholerae* at 37 °C (clear DMEM) with **P_{FRP}-IMI_x** (0.5 mg ml^{-1}). Conditions were carried out in triplicate and images displayed herein are representative of each replicate. Focal planes represent the bottom of the 96 well plate, Images were taken at fixed positions every 30 minutes and imaging parameters were constant throughout the course of the experiment.

Optical imaging confirmed that **P_{FRP}-IMI$_x$** forms precipitates in the growth media, DMEM, and that appearance of the precipitate was strongly dependent on the degree of loading of imidazole; with small "droplet-like" precipitates visible for **P_{FRP}-IMI$_{0.25}$**, a very fine dispersion of fibers for **P_{FRP}-IMI$_{0.5}$** and fibrous web-like precipitates for both **P_{FRP}-IMI$_{0.75}$** and **P_{FRP}-IMI$_{1.0}$**. Indeed, the appearance of the fibers was very similar for both **P_{FRP}-IMI$_{0.75}$** and **P_{FRP}-IMI$_{1.0}$** which we rationalise as being due to similar levels of **IMI** loading on the polymer. The previously observed sharp increase in *V. cholerae* viability for **P_{FRP}-IMI$_{1.0}$** compared with **P_{FRP}-IMI$_{0.75}$** (**Figure 38**) may be accounted for by the increase in unreacted imidazole-4-carbaldhyde (**IMI**) when targeting 100% functionalisation. We were greatly encouraged to observe *V. cholerae* adhering to the fibers of **P_{FRP}-IMI$_x$** during incubation, and in the case of higher degrees of **IMI** loading, appearing to reduce the background fluorescence associated with non-adhered motile bacteria. Unfortunately, evidence of *V. cholerae* cell elongation with **P_x-IMI$_{1.0}$** was not found.

These results taken together demonstrate how modulating the chemistry on **P_x** modulates its properties, not only affecting the macroscopic appearance of the precipitate, but also the affinity that bacteria have to it. The growth of *V. cholerae* was followed in a similar way, this time in response to **P_x-2A3FP$_{1.0}$** to evaluate if bacterial affinity for the polymer precipitate was comparable to that of **P_{FRP}-IMI$_{1.0}$** (**Figure 42**).

Precipitates of **P_x-2A3FP$_{1.0}$** were less fiber-like compared to precipitates of **P_{FRP}-IMI$_{1.0}$,** and displayed lower levels of bacterial adhesion than for **P_{FRP}-IMI$_{1.0}$**, although this may be accounted for by the greater inhibition of growth at 0.5 mg ml^{-1}(**Figure 31**).

Due to previously observed toxicity towards *V. cholerae* for **P_x-2A3FP$_{1.0}$** at 0.5 mg ml^{-1}, 0.05 mg ml^{-1} conditions of **P_{FRP}-IMI$_{0.75}$** and **P_{80}-2A3FP$_{0.75}$** with *V. cholerae* were also evaluated (**Figure 43**).

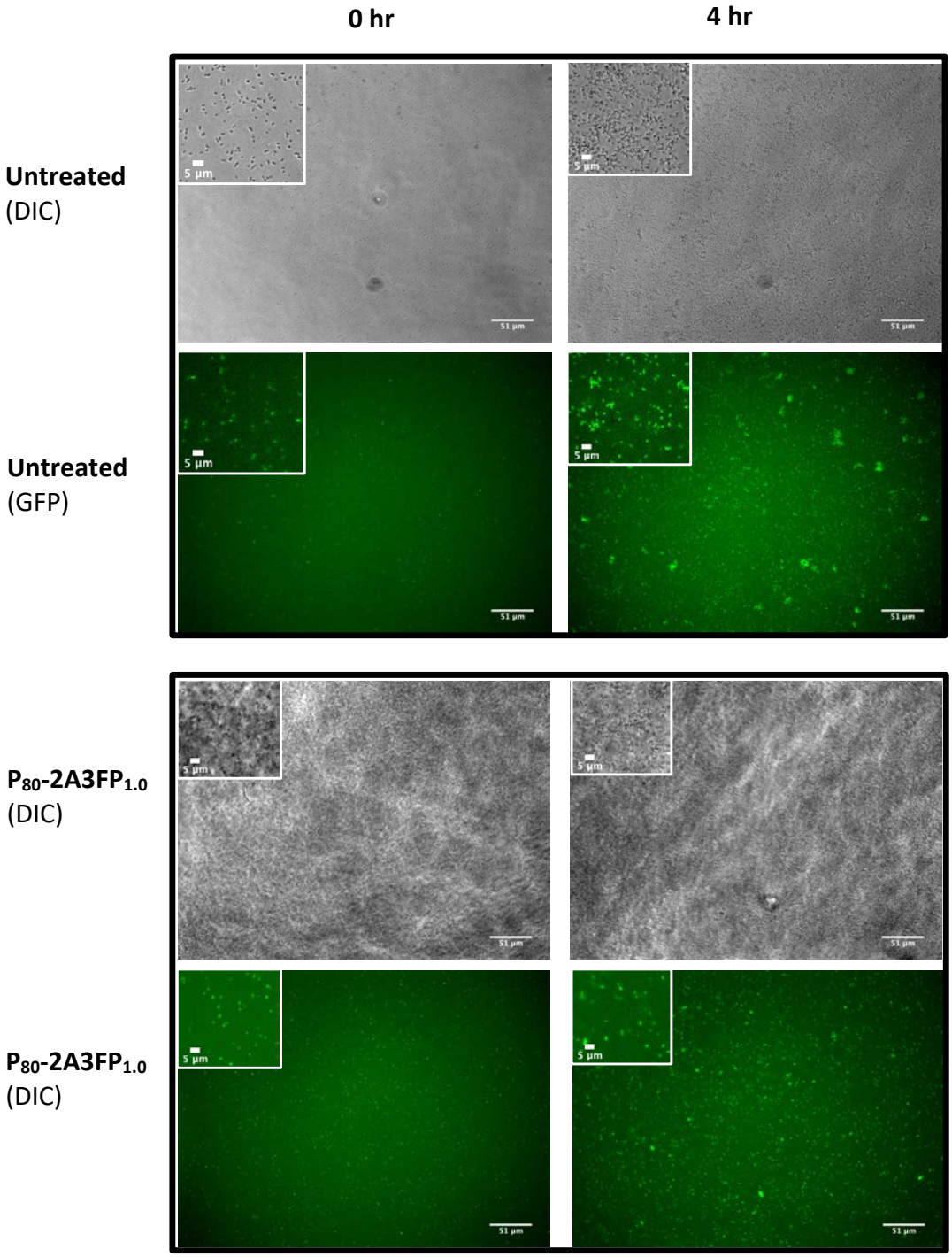

Figure 42. Optical microscope images (20 X objective) recorded by fluorescence (GFP) and differential interference contrast (DIC) for the growth progression of *V. cholerae* at 37 °C in clear DMEM with **P_{80}-2A3FP$_{1.0}$** (0.5 mg ml^{-1}). Conditions were carried out in triplicate and images displayed herein are representative of each replicate. Focal planes represent the bottom of the 96 well plate, imaging parameters were constant for both time points.

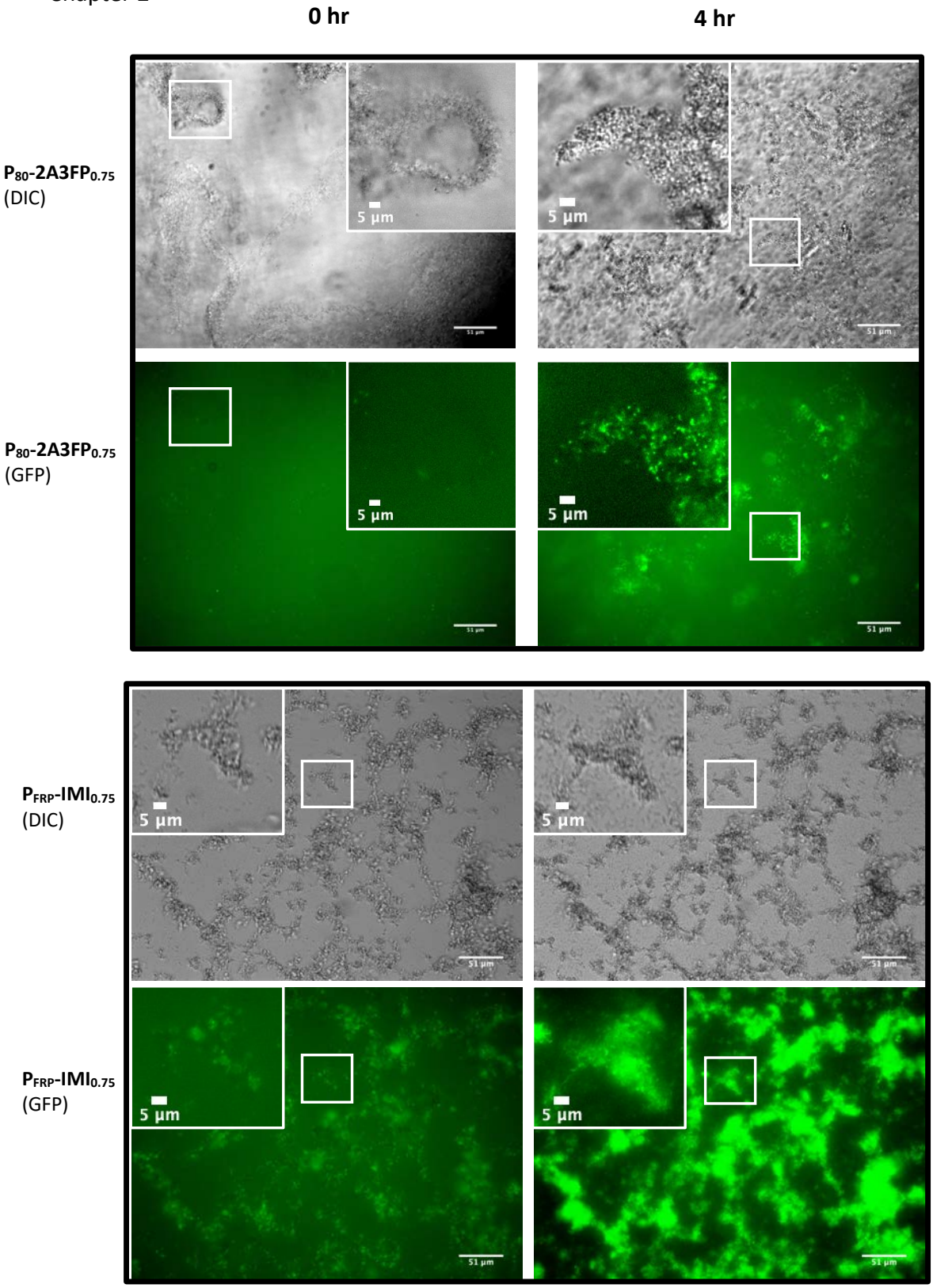

Figure 43. Optical microscope images (20 X objective) recorded by fluorescence (GFP) and differential interference contrast (DIC) for the growth progression of *V. cholerae* at 37 °C in clear DMEM with **P_{80}-2A3FP$_{0.75}$** and **P_{FRP}-IMI$_{0.75}$** (0.05 mg ml^{-1}). Conditions were carried out in triplicate and images displayed herein are representative of each replicate. Focal planes represent the bottom of the 96 well plate, imaging parameters were constant for both time points.

75% polymer modification was targeted as this represented completed consumption of the free aldehyde in both cases. The results confirmed that at sub-inhibitory concentrations *V. cholerae* adhere to **P_{80}-2A3FP$_{0.75}$** precipitates, but to a lesser extent than for **P_{FRP}-IMI$_{0.75}$**, this observation was especially apparent at 0 hours (**Figure 43**) where bacteria were observed adhering to the imidazole-polymer precipitate independently of bacterial growth. However, these results should be treated with caution due to the different sized **P_x** employed. We further assessed whether these materials could sequester and remove motile *V. cholerae* from liquid media, this time using a **P_{45}** in both cases. To this end, a simple flocculation assay (**Figure 44**) was constructed in order to measure changes in turbidity (OD_{600}). Previous studies have demonstrated that on addition of cationic polymers, bacteria flocculate, resulting in an increase in OD_{600} followed by decreased OD_{600} as clusters of bacteria sediment to the bottom of the cuvette.[51,52]

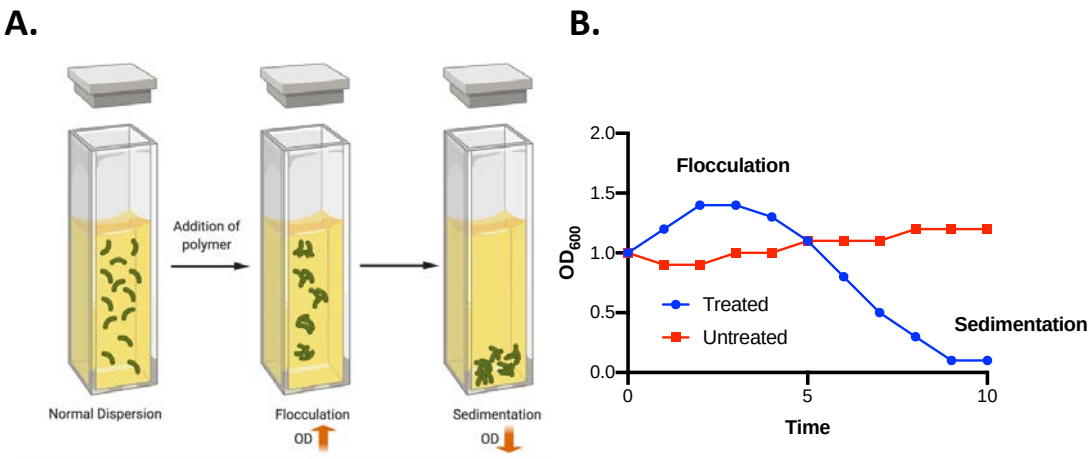

Figure 44. A) Description of a flocculation assay and B) a simulated example of bacterial turbidity after treatment of a polymer which induces bacterial clustering.

P_{45}-IMI$_x$ and **P_{45}-2A3FP$_x$** were added to cuvettes containing *V. cholerae* at initial OD_{600} of 1.0 and concentrations of 0.05 mg ml^{-1} were chosen so as not to impact the growth of *V. cholerae* during the experiment. OD_{600} was measured at varying timepoints at RT without shaking (**Figure 45**, **Figure 46**).

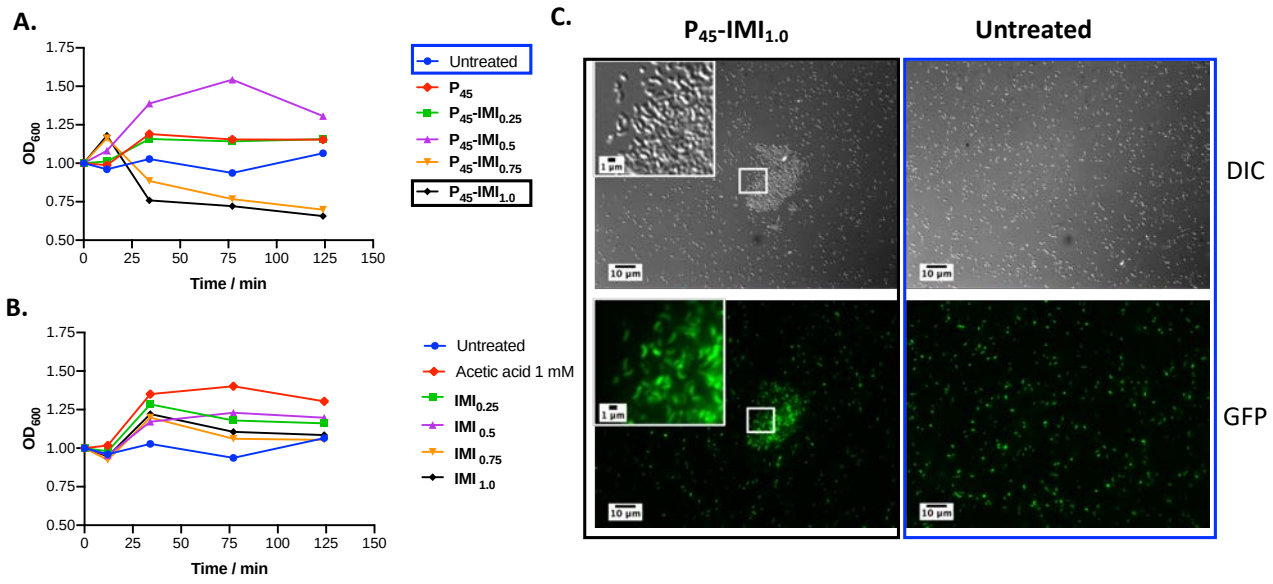

Figure 45. Effect of polymers on turbidity of planktonic *V. cholerae* in response to A), **P_{45}-IMI$_x$** at 0.05 mg ml^{-1} and B), the corresponding buffer and IMI controls. C), Optical images (100 X) of *V. cholerae* sampled from the flocculation assay after 20 minutes incubation, with and without the presence of **P_{45}-IMI$_{1.0}$** (0.05 mg ml^{-1}).

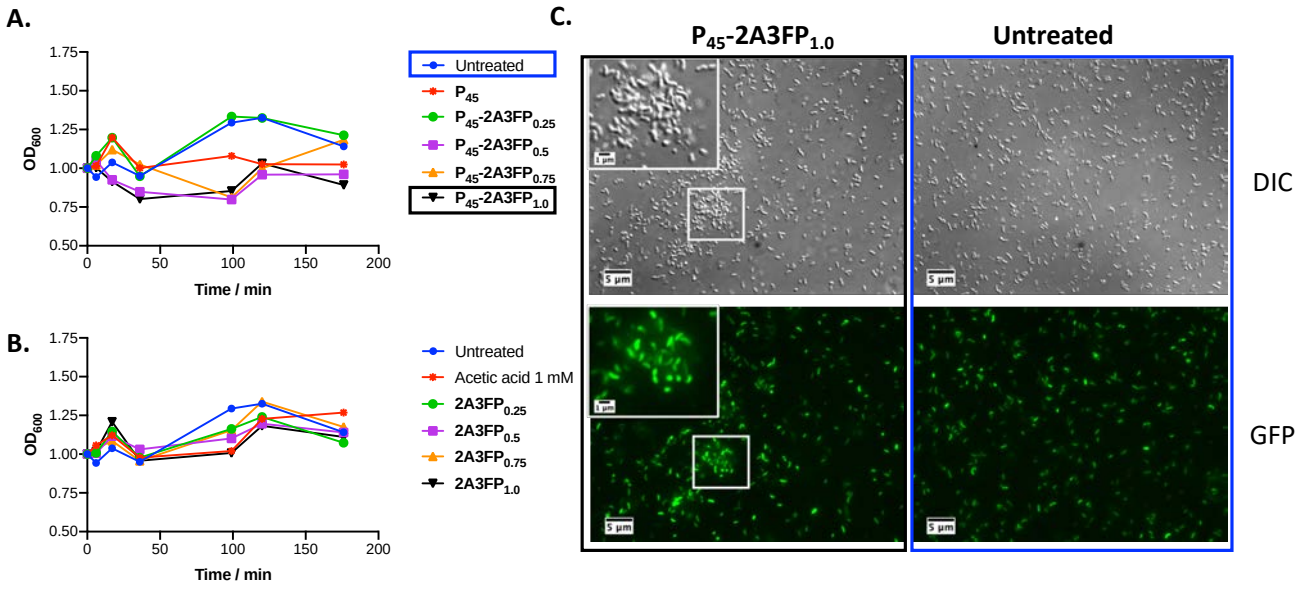

Figure 46. Effect of polymers on turbidity of planktonic *V. cholerae* in response to A) **P_{45}-2A3FP$_x$** at 0.05 mg ml^{-1} and B) the corresponding buffer and IMI controls. C) Optical images (100 X) of *V. cholerae* sampled from the flocculation assay after 20 minutes incubation, with and without the presence of **P_{45}-2A3FP$_{1.0}$** (0.05 mg ml^{-1}).

Upon introduction of the polymer into the bacterial suspension, a very fine precipitate was observed, and after 10 minutes small clusters in samples treated with

P_{45}-IMI$_x$ (x <0.25) were visible to the naked eye throughout the cuvette. In the case of **P_{45}-IMI$_{0.5}$** these clusters remained small and did not sediment during the course of the experiment resulting in high turbidity throughout the experiment. For polymers **P_{45}-IMI$_{0.75}$** and **P_{45}-IMI$_{1.0}$** sedimentation was apparent on visual inspection by reduction in the optical density. **P_{45}-2A3FP$_x$** followed a similar trend to **P_{45}-IMI$_x$** but a lower overall reduction in the turbidity was noted. Microscope images taken after 20 minutes incubation with polymers confirmed clusters of *V. cholerae* were formed, rather than simply polymer precipitates (**Figure 45**C, **Figure 46**C). These results taken together suggest that the polymer precipitate provides a nucleation point for further bacterial aggregation. In light of these encouraging results, we next investigated the impact of polymer concentration on the ability to aggregate and sequester *V. cholerae* (**Figure 47***)*.

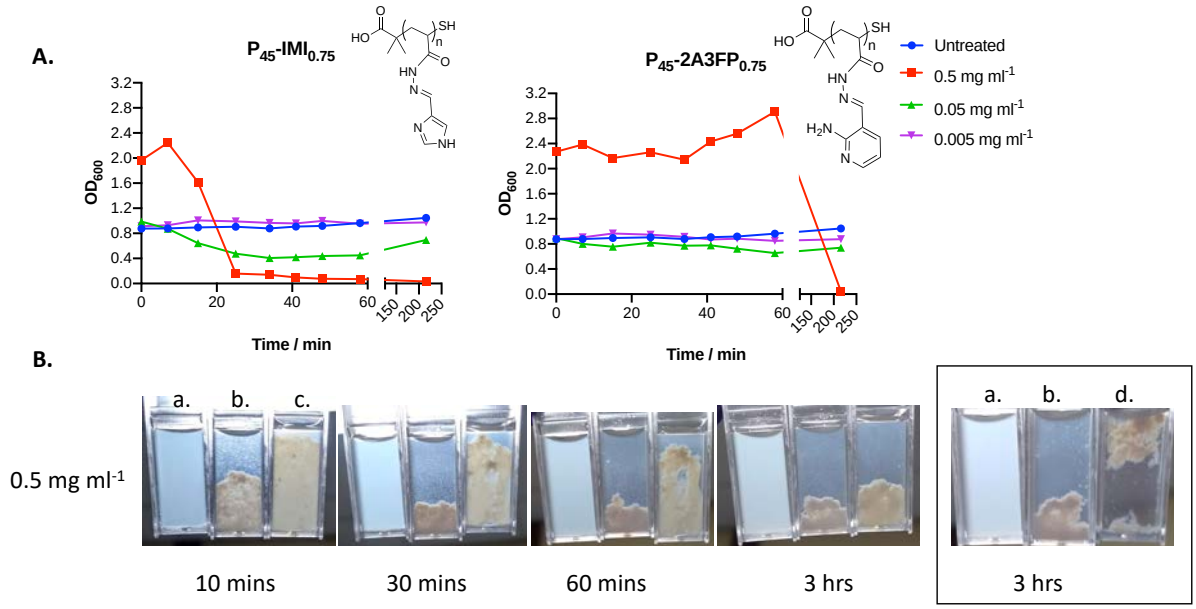

Figure 47. Effect of polymers on turbidity of planktonic *V. cholerae* in response to A) **P_{45}-IMI$_{0.75}$** and B) **P_{45}-2A3FP$_{0.75}$.** C) Corresponding images of *V. cholerae* (OD_{600} = 1.0) dispersed in DMEM at timepoints indicated, a.) without the addition of polymers b.) with addition of **P_{45}-IMI$_{0.75}$** (0.5 mg ml^{-1}) c.) with addition of **P_{45}-IMI$_{0.75}$.** d.) **P_{45}-IMI$_{0.75}$** (0.5 mg ml^{-1}) in DMEM without the addition of *V. cholerae* (t=3 hrs).

Strikingly, 0.5 mg ml^{-1} of **P_{45}-IMI$_{0.75}$** resulted in the rapid formation of a mucus-like precipitate, which visibly reduced the turbidity of the planktonic bacteria after just 10 minutes. After sedimentation of the precipitate a significant drop in the optical density to 0.16 was observed after 25 minutes. Visual inspection of the cuvette confirmed that despite the slower sedimentation time for **P_{45}-2A3FP$_{0.75}$** (0.5 mg ml^{-1}) which obscured OD_{600} measurements until after 3 hours, a higher solution turbidity remained after 30 and 60 minutes (**Figure 47**B). At 0.05 mg ml^{-1} **P_{45}-IMI$_{0.75}$** was able to reduce the optical density to 0.41 after 30 minutes while **P_{45}-2A3FP$_{0.75}$** was not, further supporting our assessment that **P_{45}-IMI$_{0.75}$** displays higher activity with respect to adhering *V. cholerae* regardless of DP.

It was concluded from this study that precipitates of imidazole containing polymer were able to sequester *V. cholerae* remarkably efficiently at a concentration of 0.5 mg ml^{-1} indicating that a strong degree of attraction was occurring between the polymer and the bacteria. Seeing how **P_{45}-IMI$_x$** displayed constantly higher affinity to *V. cholerae,* it was not clear if this effect was driven solely by the cationic charge on the polymer given that **IMI** and **2A3FP** were expected to have similar degrees of protonation under physiological conditions.

2.3.7 Effect of P_x-IMI$_x$ on biofilm formation

Previous work carried out in our labs has demonstrated that the regulation of virulence factors involved with toxin production and biofilm formation is affected in *V. cholerae* upon aggregation with cationic polymer, with toxin related genes being downregulated and biofilm related genes being upregulated.[9] There is strong evidence to support that this regulatory change is a result of an enhancement of quorum sensing in aggregated bacteria.[22]

In order to establish if *V. cholerae* upregulated biofilm in response to adhesion to **P_x-IMI_x** we evaluated the production of biomass using crystal violet staining (**Figure 48**).

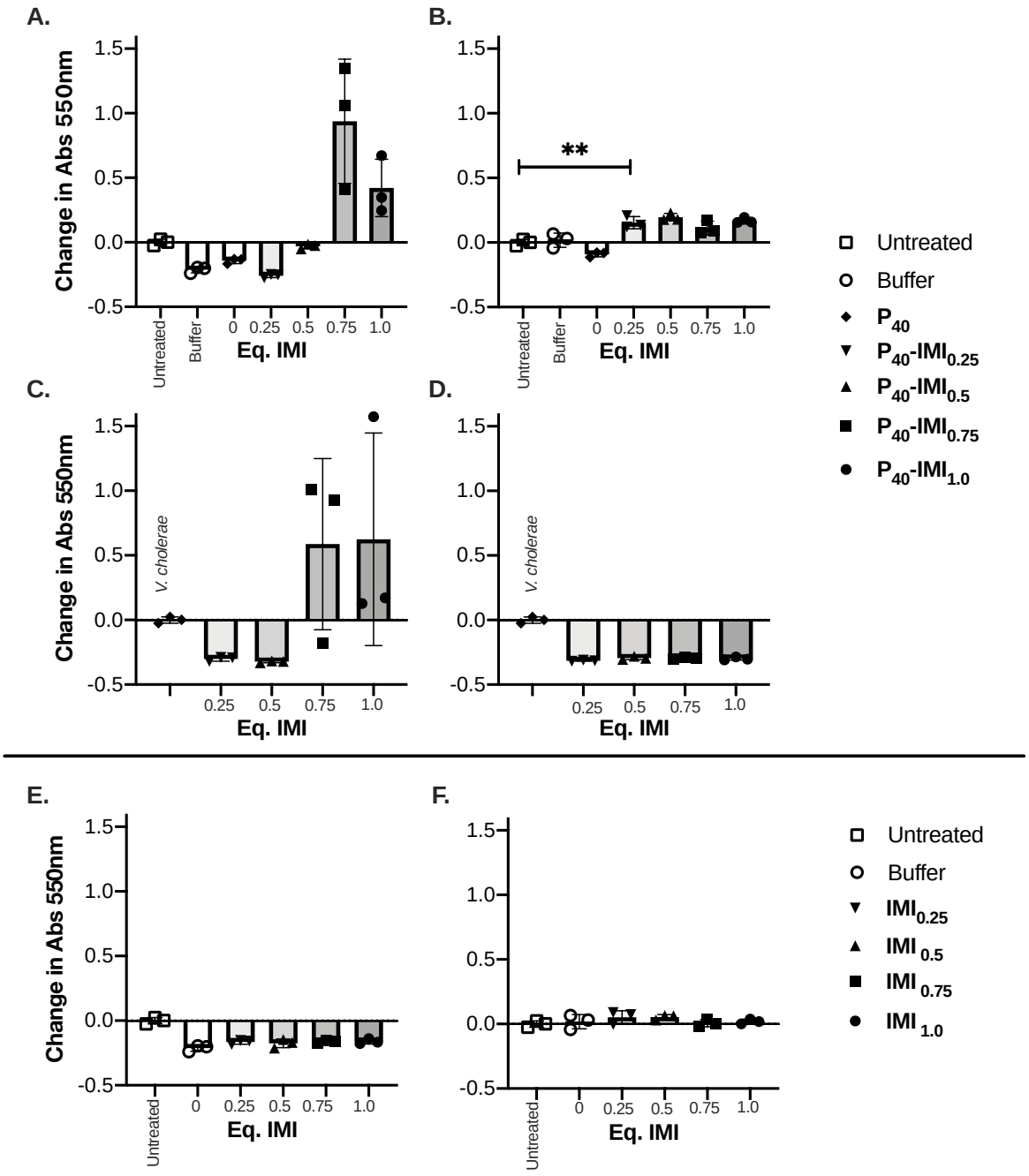

Figure 48. Crystal violet staining of residual biomass (abs 550 nm), indicating levels of biofilm formation for *V. cholerae* with polymers after 20 hours growth in clear DMEM (37 ^{o}C) for conditions at concentrations A) 0.5 mg ml^{-1}, B) 0.05 mg ml^{-1} and C) 0.5 mg ml^{-1} without the addition of bacteria, D) 0.05 mg ml^{-1} without the addition of bacteria, and aldehyde controls at concentrations of E), 0.5 mg ml^{-1} and F), 0.05 mg ml^{-1}. Data was recorded in triplicates and significance indicated (**) was measured using a student's t test represents P = 0.007.

A significant increase in crystal violet staining was noted for *V. cholerae* incubated with polymers modified with 0.75 and 1.0 equivalent of **IMI** at 0.5 mg ml^{-1}(**Figure 48**, A). However, by comparing to corresponding control samples (**Figure 48**, C) without the addition of bacteria, it was determined that the increase was due to residual background staining of **P_{40}-IMI** precipitate within the well**. P_{40}-$IMI_{0.5}$,** induced small clusters of bacteria according to the flocculation assay, but did not produce an insoluble precipitate to the same extent as higher DF polymers. This may help explain the observed reduction in crystal violet staining at 0.5 mg ml^{-1} (**Figure 48**, A) as a result of inhibition of bacterial adhesion to the surface of the well.[23] At lower concentrations all **P_{40}-IMI_x** treated samples displayed a statistically significant increase in crystal violet staining over the untreated condition (**Figure 48**, B), regardless of the loading of DF, the buffer and the polymer backbone treated samples, indicating that changes in biofilm formation could be triggered even at low loading of **IMI**. Comparatively, **IMI** controls (**Figure 48** E,F) displayed no difference in biofilm formation over that of the buffer.

2.3.8 Adhesion to polymers alters V. cholerae gene expression

We had thus far established that *V. cholerae* adhere to cationic polymer **P-IMI_x**, (when $x \geq 0.75$) to the extent that planktonic *V. cholerae* are quickly sequestered and sedimented as a result of the polymer-bacteria interaction. Increased levels of biofilm formation for *V. cholerae* after 20 hours incubation with **P_x-IMI_x** provides initial evidence that physiology of *V. cholerae* may be altered as a result of this binding step.

V. cholerae regulate genes in response to their environment, in particular in response to adhesion characterised by a switch from motile to sessile lifestyle and associated with biofilm production, and in this regard, it was proposed that bacteria

adhered by polymers may undergo a similar change in physiology. In particular, we were interested to investigate changes in regulation of biofilm factors such as the major biofilm regulator VpsR, and biofilm matrix proteins RbmA and RbmC,[53-56] but also the regulation of the cholera toxin (CTX) which is the causative agent of cholera.

To this end reporter strains previously used in our labs, containing promoter regions for the aforementioned genes were chosen so that their expression could be monitored. Reporter strains possessed the pRW50 *oriT* plasmid so that gene expression could be measured by production of the enzyme β-galactosidase and its cleavage of ortho-Nitrophenyl-β-galactoside (ONPG) to yellow o-nitrophenol (Abs 420 nm).[57]

To evaluate whether bacterial adhesion to the imidazole-functionalised polymer trigger adhesion associated phenotypes, reporter strains were incubated with **P_{FRP}-IMI$_{0.75}$** (0.05 mg ml^{-1}) and their transcriptional activity was monitored at various time points. (**Figure 49**).

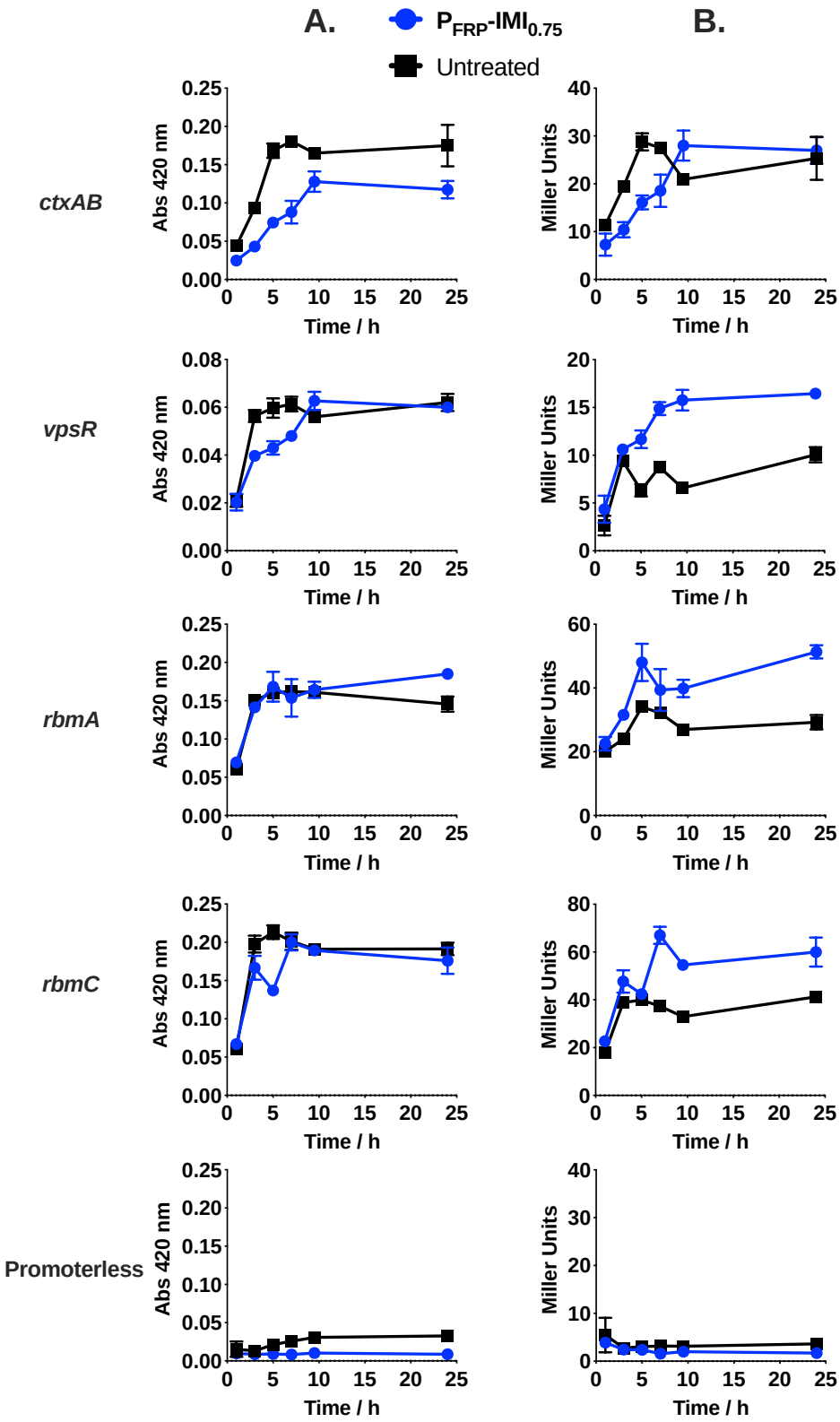

Figure 49. *V. cholerae* A1552 pRW50-*OriT* transcriptional activity (abs 420 nm) for highlighted genes in response to incubation (37 °C clear DMEM) with 0.05 mg ml^{-1} **P_{FRP}-IMI$_{0.75}$** in clear DMEM. A) raw data (blank corrected) and B) growth corrected transcriptional activity based on estimated growth of *V. cholerae* with **P_{FRP}-IMI$_{0.75}$**. Initial OD_{600} of *V. cholerae* was 0.2.

The results suggested *ctxAB* was repressed during early timepoints on incubation with **P_{FRP}-IMI$_{0.75}$**. We rationalised that adhesion to the polymer drives the suppression of the Cholera toxin may be as result of enhanced quorum sensing as pointed to in previous work from our labs,[9,22] and that suppression of this *ctxAB* was most noticeable at early time points due our earlier observation that bacteria exist predominantly in a polymer-adhered state at these time points (**Figure 41**,**Figure 43**). VpsR is the major biofilm regulator in *V. cholerae* and is responsible for the positive regulation of the *Vibrio* polysaccharide (VPS) and is also required for the synthesis of biofilm matrix proteins RbmA and RbmC.[28,53]

Here*, vpsR* was induced by **P_{FRP}-IMI$_{0.75}$**, as was *rbmA* and *rbmC* (although delayed induction was observed for the latter) suggesting that *V. cholerae* were producing more biofilm in response to the polymer. In contrast to the observed suppression of *ctxAB* which largely recovered to levels of the untreated after 10 hours, upregulation of biofilm genes remained elevated throughout the course of the experiment which may suggest that biofilm production is triggered by these polymers rather than strictly dependent on adherence to the polymer. Furthermore, increased biofilm formation on adhesion to polymer cannot be explained solely by quorum sensing, seeing how enhanced QS represses the production of biofilm in *V. cholerae,*[26] and strongly suggests that other regulatory pathways may be involved.

2.4 Conclusions

We have established through the use of time-lapse imaging that cationic polymers **P1** and **P2** induce different responses of *V. cholerae*. Primary amine containing polymer **P1**, was toxic to *V. cholerae* at 0.5 mg ml^{-1} whereas tertiary amine containing polymer **P2** displayed no inhibition of growth at this concentration. Notably

at 0.05 mg ml^{-1}, which was reported to be sub-inhibitory for both polymers towards *V. cholerae*, **P2** induced visible clusters of bacteria whereas *V. cholerae* treated with **P1** produced the visible nucleation of biofilms. This observation was consistent with crystal violet staining of biofilms which suggested a significant increase in biofilm formation for bacteria treated with **P1** over that of **P2**.

Two cationic polymers $\mathbf{P_x\text{-}IMI_x}$ and $\mathbf{P_x\text{-}2A3FP_x}$ were prepared by post-polymerisation modification of polymer scaffold $\mathbf{P_X}$, in order to evaluate *via in situ* screening, the impact of increased hydrophobicity on toxicity and aggregation of *V. cholerae*. We established that the scaffold $\mathbf{P_x}$ was more toxic than **P1** and **P2** towards *V. cholerae* under our reported conditions but that polymer molecular mass did not impact on this toxicity.

It was found that toxicity towards *V. cholerae* was reduced by modifying $\mathbf{P_x}$ with either **IMI** or **2A3FP,** and in the case of **IMI,** was dependent on the degree of loading on the polymer. Polymers targeting higher degrees of modification with aromatic amines became insoluble and resulted in the formation of a mucus like precipitate. *V. cholerae* were observed to adhere quickly to polymer precipitates in the case of $\mathbf{P_{FRP}\text{-}IMI_x}$ and to a lesser extent with $\mathbf{P_x\text{-}2A3FP_x}$. We concluded by use of a flocculation assay that $\mathbf{P_{45}\text{-}IMI_x}$ displayed a greater activity towards sequestering *V. cholerae* than $\mathbf{P_{45}\text{-}2A3FP_x}$ which cannot be explained simply by protonation level of the amines. Notably $\mathbf{P_{45}\text{-}IMI_{0.74}}$ reduced the concentration of planktonic *V. cholerae* in solution from OD_{600} = 1.0 to 0.16 after 25 minutes.

Lastly, $\mathbf{P_x\text{-}IMI_{0.75}}$ induced increased levels of biofilm production in *V. cholerae* while simultaneously suppressing the expression of the cholera toxin, indicating that bacterial adhesion to the polymer results in altered physiology. These conclusions taken together position $\mathbf{P_x\text{-}IMI_{0.75}}$ as a promising means of sequestering *V. cholerae,*

and suppressing its virulence simultaneously, which may have a wide range of potential applications, such as in water treatment or as part of a wound dressing.

2.5 Future work

Further studies should be undertaken to assess the therapeutic value of **P_x-$IMI_{0.75}$**. For example, by establishing whether this polymer offers a protective or cytotoxic effect towards bacterial attachment host cells such as Caco-2 cells, and further, in wound models as a potential topical treatment. The adhesion and sedimentation efficiency observed for **P_x-$IMI_{0.75}$** should be compared with other methods of flocculating bacteria, especially in the application of water treatment to establish the suitability of **P_x-$IMI_{0.75}$** to these applications.

With respect to the synthesis of aldehyde-modified polymer scaffolds, larger arrays of closely related side-chain chemistries and combinations thereof may be explored. In this way, and possibly employing a high-throughput screening type process, a deeper assessment into how the side-chain chemistry imparts different biological activity could be achieved and may lead to a better understanding into the role of hydrophobicity, positive charge and biological antagonists in sequestering and physiology of *V. cholerae.*

Quorum sensing is important for understanding bacterial responses induced by polymer-mediated aggregation and should be evaluated for **P_x-IMI_x** with respect to the reported response induced by **P1** and **P2** outlined in our previous work where a luminescent reporter strain for QS was employed.[22]

Acyl hydrazones are dynamic and susceptible to hydrolysis at low pH. With this in mind, it would be of benefit to assess the fate of hydrazone-linked functional groups after interaction with bacteria to establish if these bonds remain intact, and if not, what

the implications of this are. Along similar lines, dynamic Investigations may be carried out to determine whether acyl hydrazones could serve as a route towards designing “re-writable” chemistries on $\mathbf{P_x}$ so as to achieve biologically-instructed side-chain chemistry which may lead to polymers with higher and more specific affinity to a target.

Finally, with regards to observed differences between cationic polymers **P1** and **P2,** further work should be carried out to establish differences in stress response of *V. cholerae*, and whether stress (for example oxidative stress) can account for increased biofilm production. Furthermore, fluorescently labelled polymers and super resolution confocal microscopy may reveal to what extent **P1** and **P2** interferes with and potentially passes through the bacterial membrane.

2.6 References

1 Antibacterial agents in clinical development: an analysis of the antibacterial clinical development pipeline, including tuberculosis. Geneva: World Health Organization; 2017 (WHO/EMP/IAU/2017.12). Licence: CC BY-NC-SA 3.0 IGO.

2 Barber, S. (2017) Antimicrobial resistance. House of Commons Library Briefing Paper no. 8141. London: House of Commons Library.3 The PLOS Medicine Editors, *PLoS Med*, 2016, **13**, e1002130–3.

4 R. C. Allen, R. Popat, S. P. Diggle and S. P. Brown, *Nature Reviews Microbiology*, 2014, **12**, 300–308.

5 A. E. Clatworthy, E. Pierson and D. T. Hung, *Nat Chem Biol*, 2007, **3**, 541–548.

6 A. M. Krachler and K. Orth, *Virulence*, 2014, **4**, 284–294.

7 E. P. Magennis, A. L. Hook, M. C. Davies, C. Alexander, P. Williams and M. R. Alexander, *Acta Biomaterialia*, 2016, **34**, 84–92.

8 D. Campoccia, L. Montanaro and C. R. Arciola, *Biomaterials*, 2013, **34**, 8533–8554.

9 N. Perez-Soto, L. Moule, D. N. Crisan, I. Insua, L. M. Taylor-Smith, K. Voelz, F. Fernandez-Trillo and A. M. Krachler, *Chem. Sci.*, 2017, **8**, 5291–5298.

10 X. Yan, A. Sivignon, N. Yamakawa, A. Crepet, C. Travelet, R. Borsali, T. Dumych, Z. Li, R. Bilyy, D. Deniaud, E. Fleury, N. Barnich, A. Darfeuille-Michaud, S. G. Gouin, J. Bouckaert and J. Bernard, *Biomacromolecules*, 2015, **16**, 1827–1836.

11 P. R. Secor, L. A. Michaels, A. Ratjen, L. K. Jennings and P. K. Singh, *Proc Natl Acad Sci USA*, 2018, **115**, 10780–10785.

12 C. Ergene, K. Yasuhara and E. F. Palermo, *Polym. Chem.*, 2018, **9**, 2407–2427.

13 K. Kuroda, G. A. Caputo and W. F. DeGrado, *Chem. Eur. J.*, 2008, **15**, 1123–1133.

14 L. C. Paslay, B. A. Abel, T. D. Brown, V. Koul, V. Choudhary, C. L. McCormick and S. E. Morgan, *Biomacromolecules*, 2012, **13**, 2472–2482.

15 D. J. Phillips, J. Harrison, S.-J. Richards, D. E. Mitchell, E. Tichauer, A. T. M. Hubbard, C. Guy, I. Hands-Portman, E. Fullam and M. I. Gibson, *Biomacromolecules*, 2017, **18**, 1592–1599.

16 M. A. van Dongen, C. A. Dougherty and M. M. Banaszak Holl, *Biomacromolecules*, 2014, **15**, 3215–3234.

17 E. Blasco, M. B. Sims, A. S. Goldmann, B. S. Sumerlin and C. Barner-Kowollik, *Macromolecules*, 2017, **50**, 5215–5252.
18 S. Perrier, *Macromolecules*, 2017, **50**, 7433–7447.
19 G. Moad, E. Rizzardo and S. H. Thang, *Aust. J. Chem.*, 2012, **65**, 985–92.
20 V. M. C. Coessens and K. Matyjaszewski, *J. Chem. Educ.*, 2010, **87**, 916–919.
21 P. Zhang, H. Lu, H. Chen, J. Zhang, L. Liu, F. Lv and S. Wang, *Anal. Chem.*, 2016, **88**, 2985–2988.
22 N. Perez-Soto, O. Creese, F. Fernandez-Trillo and A. M. Krachler, *ACS Chem. Biol.*, 2018, **13**, 3021–3029.
23 L. L. Foster, S.-I. Yusa and K. Kuroda, *Antibiotics*, 2019, **8**, 61–16.
24 P. Zhang, S. Li, H. Chen, X. Wang, L. Liu, F. Lv and S. Wang, *ACS Appl. Mater. Interfaces*, 2017, **9**, 16933–16938.
25 A. F. González Barrios, R. Zuo, Y. Hashimoto, L. Yang, W. E. Bentley and T. K. Wood, *Journal of Bacteriology*, 2006, **188**, 305–316.
26 C. M. Waters, W. Lu, J. D. Rabinowitz and B. L. Bassler, *Journal of Bacteriology*, 2008, **190**, 2527–2536.
27 M. Jemielita, N. S. Wingreen and B. L. Bassler, *eLife*, 2018, **7**, e1002210–25.
28 J. K. Teschler, D. Zamorano-Sánchez, A. S. Utada, C. J. A. Warner, G. C. L. Wong, R. G. Linington and F. H. Yildiz, *Nature Reviews Microbiology*, 2015, **13**, 255–268.
29 K. Drescher, J. Dunkel, C. D. Nadell, S. van Teeffelen, I. Grnja, N. S. Wingreen, H. A. Stone and B. L. Bassler, *Proc Natl Acad Sci USA*, 2016, **113**, E2066–E2072.
30 G. A. O'Toole, *JoVE*, 2011, 1–2.
31 E. F. Palermo, D.-K. Lee, A. Ramamoorthy and K. Kuroda, *J. Phys. Chem. B*, 2011, **115**, 366–375.
32 D. N. Crisan, O. Creese, R. Ball, J. L. Brioso, B. Martyn, J. Montenegro and F. Fernandez-Trillo, *Polym. Chem.*, 2017, **8**, 4576–4584.
33 O. Creese, P. Adoni, G. Su, A. Romanyuk and P. Fernández-Trillo, *Polym. Chem.*, 2019, **124**, 14922.
34 D. T. Gentekos, R. J. Sifri and B. P. Fors, *Nature Reviews Materials*, 2019, 1–14.
35 R. Whitfield, N. P. Truong, D. Messmer, K. Parkatzidis, M. Rolland and A. Anastasaki, *Chem. Sci.*, 2019, **10**, 8724–8734.

36 S. Raddatz, *Nucleic Acids Research*, 2002, **30**, 4793–4802.

37 E. A. Hoff, B. A. Abel, C. A. Tretbar, C. L. McCormick and D. L. Patton, *Polym. Chem.*, 2017, **8**, 4978–4982.

38 L. Zhu, M. Zhou, S. Yang and J. Shen, *IJMS*, 2015, **16**, 9078–9096.

39 J. Engelke, J. Brandt, C. Barner-Kowollik and A. Lederer, *Polym. Chem.*, 2019, **10**, 3410–3425.

40 F. D. Halstead, M. Rauf, N. S. Moiemen, A. Bamford, C. M. Wearn, A. P. Fraise, P. A. Lund, B. A. Oppenheim and M. A. Webber, *PLoS ONE*, 2015, **10**, e0136190–15.

41 K. M. Wheeler, G. Cárcamo-Oyarce, B. S. Turner, S. Dellos-Nolan, J. Y. Co, S. Lehoux, R. D. Cummings, D. J. Wozniak and K. Ribbeck, *Nature Microbiology*, 2019, **7**, 3–12.

42 T. M. Bartlett, B. P. Bratton, A. Duvshani, A. Miguel, Y. Sheng, N. R. Martin, J. P. Nguyen, A. Persat, S. M. Desmarais, M. S. VanNieuwenhze, K. C. Huang, J. Zhu, J. W. Shaevitz and Z. Gitai, *Cell*, 2017, **168**, 172–185.e15.

43 H. Konishi, A. Katayama, T. Ito, S. Tanaka and Z. Yoshii, *Journal of Bacteriology*, 1986, **168**, 1476–1478.

44 J. F. Fisher, S. O. Meroueh and S. Mobashery, *Chemical Reviews*, 2005, **105**, 395–424.

45 B. R. Wucher, T. M. Bartlett, M. Hoyos, K. Papenfort, A. Persat and C. D. Nadell, *Proc. Natl. Acad. Sci. U.S.A.*, 2019, **116**, 14216–14221.

46 A. J. Mason, C. Gasnier, A. Kichler, G. Prevost, D. Aunis, M. H. Metz-Boutigue and B. Bechinger, *Antimicrob Agents Chemother*, 2006, **50**, 3305–3311.

47 W.-L. Ng, Y. Wei, L. J. Perez, J. Cong, T. Long, M. Koch, M. F. Semmelhack, N. S. Wingreen and B. L. Bassler, *Proc. Natl. Acad. Sci. U.S.A.*, 2010, **107**, 5575–5580.

48 S. C. Page, R. E. Silversmith, E. J. Collins and R. B. Bourret, *Biochemistry*, 2015, **54**, 7248–7260.

49 K. Heinrich, D. J. Leslie, M. Morlock, S. Bertilsson and K. Jonas, *mBio*, 2019, **10**, 162–17.

50 K. Lienkamp, K.-N. Kumar, A. Som, K. Nüsslein and G. N. Tew, *Chem. Eur. J.*, 2009, **15**, 11710–11714.

51 X. Xue, G. Pasparakis, N. Halliday, K. Winzer, S. M. Howdle, C. J. Cramphorn, N. R. Cameron, P. M. Gardner, B. G. Davis, F. Fernandez-Trillo and C. Alexander, *Angewandte Chemie International Edition*, 2011, **50**, 9852–9856.

52 E. P. Magennis, F. Fernandez-Trillo, C. Sui, S. G. Spain, D. J. Bradshaw, D. Churchley, G. Mantovani, K. Winzer and C. Alexander, *Nat Mater*, 2014, **13**, 748–755.

53 H. Dang and C. R. Lovell, *Microbiol. Mol. Biol. Rev.*, 2015, **80**, 91–138.

54 J. Yan, A. G. Sharo, H. A. Stone, N. S. Wingreen and B. L. Bassler, *Proc. Natl. Acad. Sci. U.S.A.*, 2016, **113**, E5337–E5343.

55 J. Sánchez, G. Medina, T. Buhse, J. Holmgren and G. Soberón-Chavez, *Journal of Bacteriology*, 2004, **186**, 1355–1361.

56 J. C. N. Fong, K. A. Syed, K. E. Klose and F. H. Yildiz, *Microbiology*, 2010, **156**, 2757–2769.

57 K. L. Griffith and R. E. Wolf Jr., *Biochemical and Biophysical Research Communications*, 2002, **290**, 397–402.

Chapter 3

Interaction and recognition of glycopolymers by *Vibrio cholerae*

3.1 Background

Vibrio cholerae is a Gram negative, motile, comma shaped pathogen found in aquatic environments. *V. cholerae* persists in these environments by forming biofilm associated communities on crustaceans, the shells of which mainly comprise of the polysaccharide chitosan. *V. cholerae* is transmitted to humans usually through consumption of contaminated food, or in particular, water. Early stages of colonisation of the host epithelium relies heavily on motility of bacterium and it is believed that *V. cholerae* need to overcome the physical mucus layer in order to colonise the small intestine.[1] Within the host, *V. cholerae* initially detect their surroundings non-specifically *via* chemical interactions and physical forces acting on the flagellum and the pili.[2] In this way *V. cholerae* "loiter" over areas of a surface more suitable for attachment,[3] before adhering more strongly *via* a variety of adhesion factors, in particular protein – carbohydrate interactions. This adhesion step is associated with a switch from a motile to a sessile state and usually involves the formation of biofilm, although this is not well understood *in vivo.*

V. cholerae sense their surroundings not only to identify the mechanochemical environment which can dictate whether the bacterium can adhere to a surface, but also whether to deploy virulence factors.[3] *V. cholerae* have also been shown to sense the presence of sugars as means of a chemical signal to determine the suitability for biofilm growth *via* a Phosphoenolpyruvate Phosphotransferase system (PTS) which was demonstrated to be essential for colonisation.[4]

A main factor in sensing the environment is the mannose sensitive haemagglutinin type IV pilus (MSHA), which in conjunction with the polar flagellar of *V. cholerae* counter rotates the cell body, allows for a "skimming" of the surface.

The MSHA contacts the surface periodically and depending on the strength of the interaction, can generate orbiting motions which then lead to microcolony formation.[2] The importance of this pilus in surface adhesion was demonstrated using *mshA* mutants (lacking genes to produce MSHA), indicating that *V. choleae* deficient in this pilus do not exhibit "orbiting" motility, but also display impaired biofilm formation.[5] The MSHA pilus has also been demonstrated to be critical for adhesion associated cell killing in caco-2 cells, and in the same study It was put forward that MSHA binds most strongly to glycans which feature a terminal or subterminal galactose and terminal or subterminal fucolyations.[6]

We envisage linear polymers containing glycans as ideal compounds for competitive binding to glycan recognition sites on *V. cholerae.* Indeed, the multivalent nature of a glycopolymer has the potential to not only provide a locally high concentration of glycans to an active site on the bacteria, but also present a pathway for bacterial cross-linking and aggregation.[7]

Our previous work has demonstrated that cationic polymers can aggregate and sequester *V. cholerae* at sub-inhibitory concentrations.[8] Polymer-induced bacterial aggregates displayed increased levels of quorum sensing as well as a down regulation of virulence related genes and an upregulation of biofilm related genes.[9]

These results taken together suggest that polymers can trigger a bacterial response which includes modulating gene expression. As such, we set out to assess not only the ability of glycopolymers to bind and aggregate bacteria, but whether *V. cholerae* responds differently to glycopolymers compared with cationic polymers. Furthermore, we were interested to determine whether the choice of sugar on the polymer backbone impacts bacterial responses.

Employing a polyhydrazide scaffold to access glycopolymers directly from unmodified sugars affords a significantly less time consuming and challenging synthetic strategy as opposed to methods requiring prior chemical modification of the sugar; for example, sugar containing monomers,[10] and chemical handles for post-polymerisation modification.[11] Furthermore, glycopolymers prepared in this way can be screened for activity *in situ* to negate uncertainties over contribution of the polymer backbone to biological activity.

3.2 Objectives

The primary objective of this work was to synthesise a library of different sugar-containing polymers derived from a single polymer scaffold. The synthesis and *in situ* screening of glycopolymers prepared from $\mathbf{P_x}$ have not yet been reported in our labs so a focus here was on determining the applicability of this platform for screening glycopolymers *in situ*, thus reaction conditions and stability of the glycoconjugates would need to be accounted for. In this way, cationic polymers and glycopolymers could be directly accessed from the same polymer scaffold so that biological responses could be compared.

Glycopolymers synthesised here were designed to evaluate the activities of polymers displaying mannose, glucose and galactose with respect to aggregating *V. cholerae via* specific carbohydrate-protein interactions. To explore bacterial responses to glycopolymers, growth curves, biofilm formation, optical imaging and gene expression will be assessed in order to determine whether a certain response can be attributed to a particular glycan displayed on the polymer chain.

3.3 Results and discussion

3.3.1 Glycopolymer synthesis and characterisation

It is well documented that reducing sugars can react with hydrazide groups *via* amine-carbonyl condensation.[12,13] reducing sugars exist in a water-catalysed equilibrium between their open form which contains either an aldehyde or ketone functionality and their ring closed pyranose form.[14] Interconversion gives rise to α and β anomers which can be identified in proton NMR and aid characterisation of conjugation products.[13]

The following work was performed on two polymerisations, targeting DP200 and DP50. To this end we synthesised a DP128 and a DP45 $\mathbf{P_x}$ using our optimised RAFT polymerisation conditions described earlier (**Chapter 1**) with a very good dispersity ($Đ_m$ = 1.23 and 1.21) (**Figure 50**).

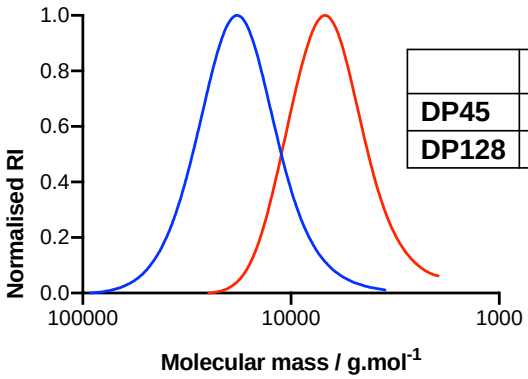

	Mp(theo)	Mn(SEC)	Mw(SEC)	$Đ_M$
DP45	4094	6014	7273	1.21
DP128	11232	15907	19616	1.23

Figure 50. SEC trace (Lonza DPBS) for $\mathbf{P_{128}}$ and $\mathbf{P_{45}}$ described here. M_p, was calculated by monomer conversion, M_n and M_w were calculated by SEC using PEG/PEO standards, reported in $g.mol^{-1}$.

Initially, we attempted to conjugate monosaccharides; D-mannose, D-glucose and D-galactose using our previously reported conditions for aldehyde conjugation, [15] however very low conjugation efficiencies were observed, with 25% loading for mannose, and just 10% loading for glucose and galactose. We concluded that these

conditions were not suitable for loading sugars onto the $\mathbf{P_x}$ scaffold in the same way as described for aldehydes. Instead, focus was drawn to conditions reported by Bertozzi and co-workers for the synthesis of cyclic *N*-glycosides from poly(acryloyl hydrazide).[16] The authors carried out the post-polymerisation modification at reduced pH (5.5) to promote stability of the polymer-sugar conjugate, and employed a significantly higher concentration of both sugar and hydrazide in order to increase the number of ring open species available for conjugation by the hydrazide groups of $\mathbf{P_x}$. In the same study It was reported that this post-polymerisation modification benefited from the addition of an aniline catalyst,[16] a toxic additive that we believed could require removal after reaction, thus impacting on the ability for $\mathbf{P_x}$ to be used *in situ.* Aniline is employed as a catalyst in hydrazone *via* the formation of a Schiff base intermediate, which greatly increases the rate of reaction at lower pH, without disturbing the equilibrium towards the formation of the hydrazone product.[17,18] However, there is a lack of clarity in the literature as to the impact aniline has in catalysing the reaction between reducing sugars and poly hydrazides.

The use of Aniline was undesirable for our screening platform due to its toxicity,[19] and could potentially interfere with the normal growth of *V. cholerae.* Using conditions outlined by Bertozzi, we evaluated the importance of Aniline for the conjugation of D-mannose to $\mathbf{P_x}$ by proton NMR (**Figure 51**).

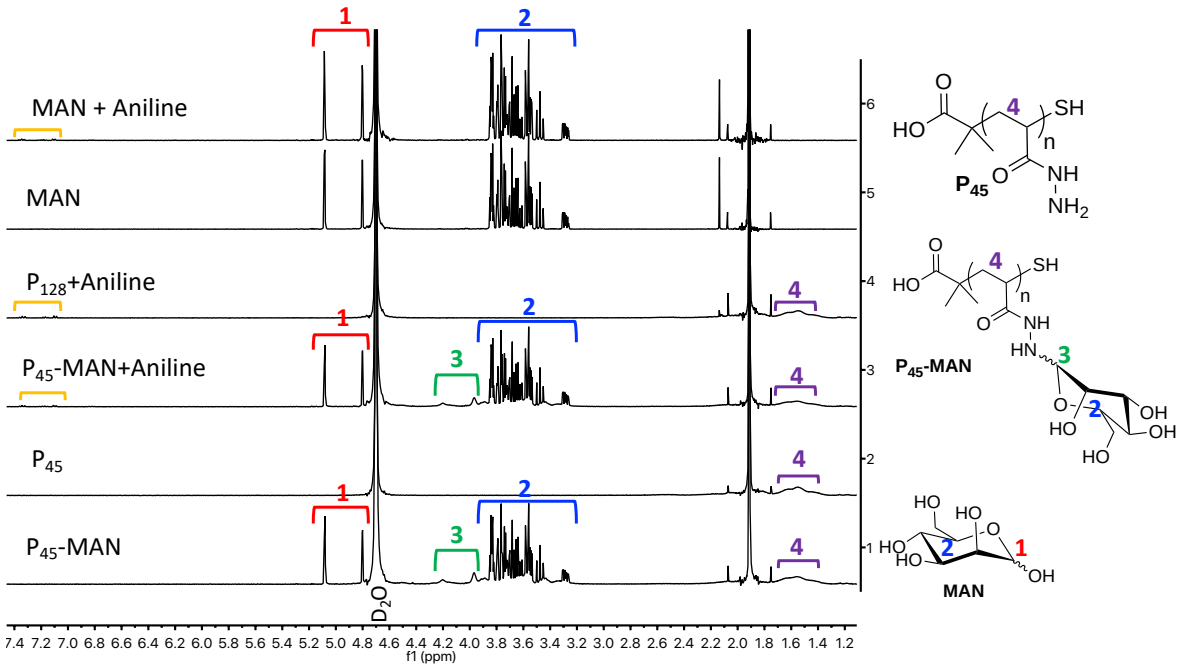

Figure 51. Proton NMR (D_2O) for the conjugation reaction with and without addition of aniline (1mM) between **P_{45}** (0.25 M with respect to the hydrazide group) and 1 eq. D-mannose (MAN) to form the glycoconjugate: **P_{45}-MAN**. Conversion was calculated by reduction of anomeric mannose signals highlighted **1** compared with the proton regions highlighted (**2**,**3**) (total =7H). All samples were incubated for 24 hours at 50ºC in Acetate buffer / D_2O (pH 5.5).

Pleasingly, conjugation efficiencies were unaffected by the presence of aniline and 35% of the sugar was calculated to be conjugated to the polymer backbone in both cases. With this in mind we concluded that at least under these conditions, aniline was not necessary for conjugation.

Next we targeted different sugars and greater degrees of loading on the polymer by increasing the number of equivalents of sugar to hydrazide moiety under different buffering conditions. **P_{128}** was incubated with glucose, galactose and mannose with increasing equivalents (2, 4, 6) of sugar, and different buffers (100 mM acetate pH 5.5 or pyridine pH 6.0) (**Scheme 6**).

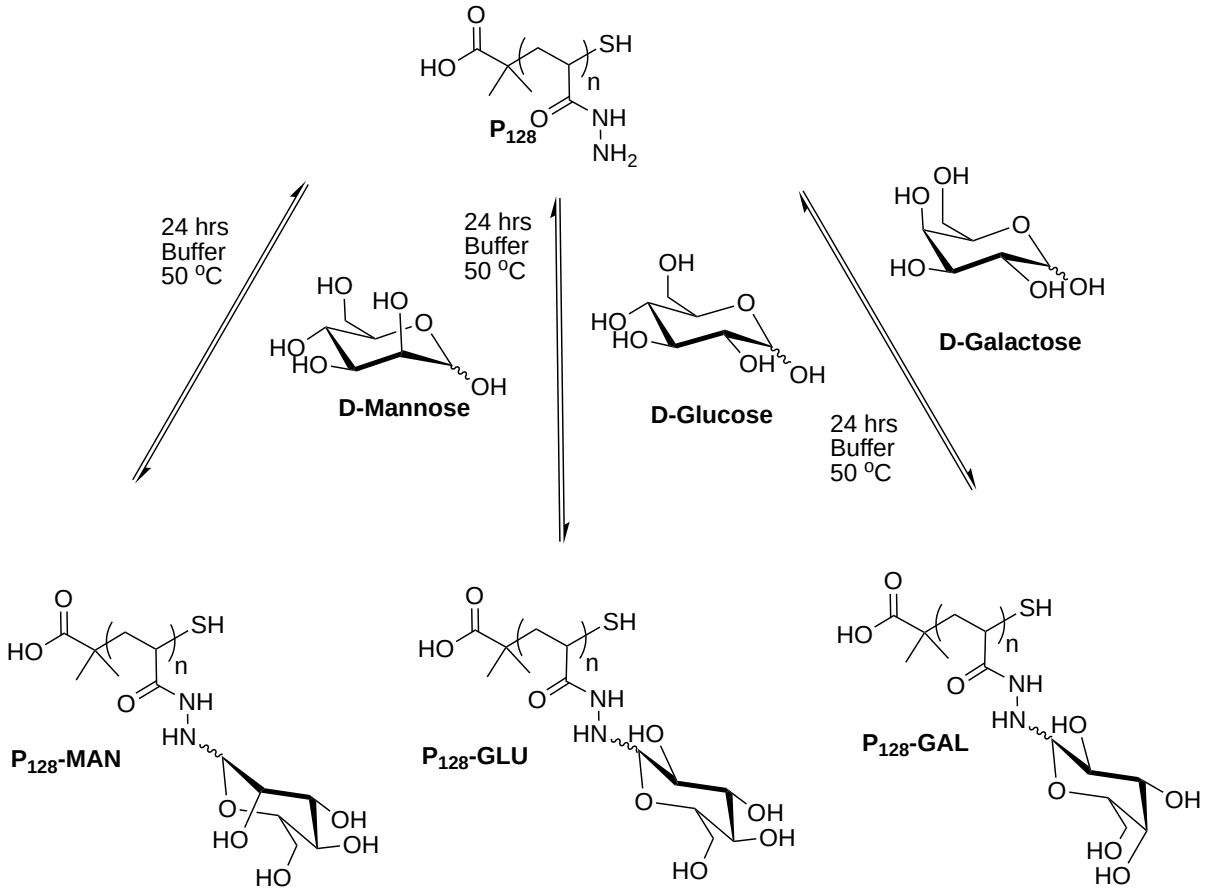

Scheme 6. Proposed synthetic route for the synthesis of glycopolymers.

The efficient chemistry afforded by the acyl hydrazide groups on $\mathbf{P_x}$, allowed for screening of different reaction conditions in parallel within a 96 well plate *via* simple incubation. The reactions described in **Scheme 6** were carried out in D_2O + buffer and incubated in a sealed 96 well plate for 24 hours at 50°C with shaking. For characterization, each sample was diluted in D_2O and analyzed by NMR and GPC.

The conversion of free sugar onto the polymer backbone was calculated by proton NMR for a total of 7 protons on integration of α and β anomeric protons for the free sugar against the region containing the ring protons of the free sugar and the new α and β protons from the glycopolymer which can be observed as distinct broad peaks in the case of $\mathbf{P_{128}}$**-MAN** and $\mathbf{P_{128}}$**-GLU** (**Figure 52**,**Figure 53**,**Figure 54**).

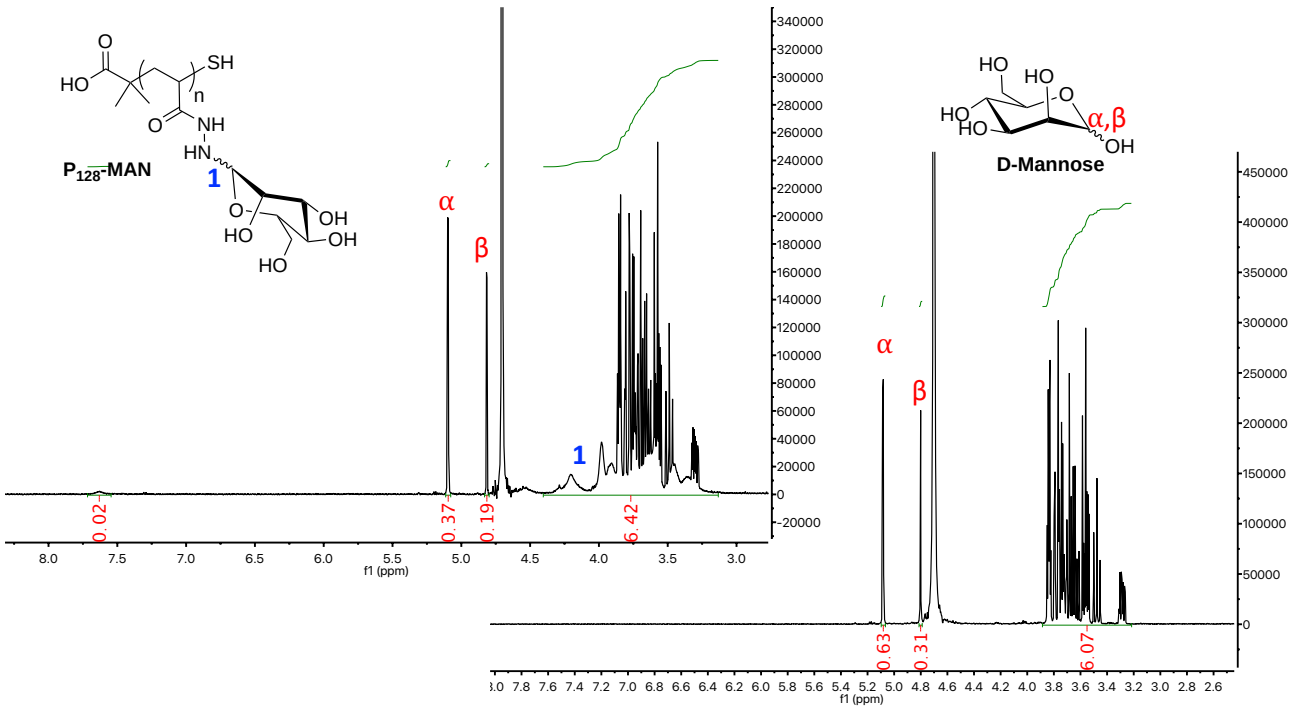

Figure 52. Proton NMR (D_2O) (left) for **P_{128}-MAN** (2.eq. sugar, 88% conversion by integration) and (right) D-mannose prior to addition of **P_{128}.**

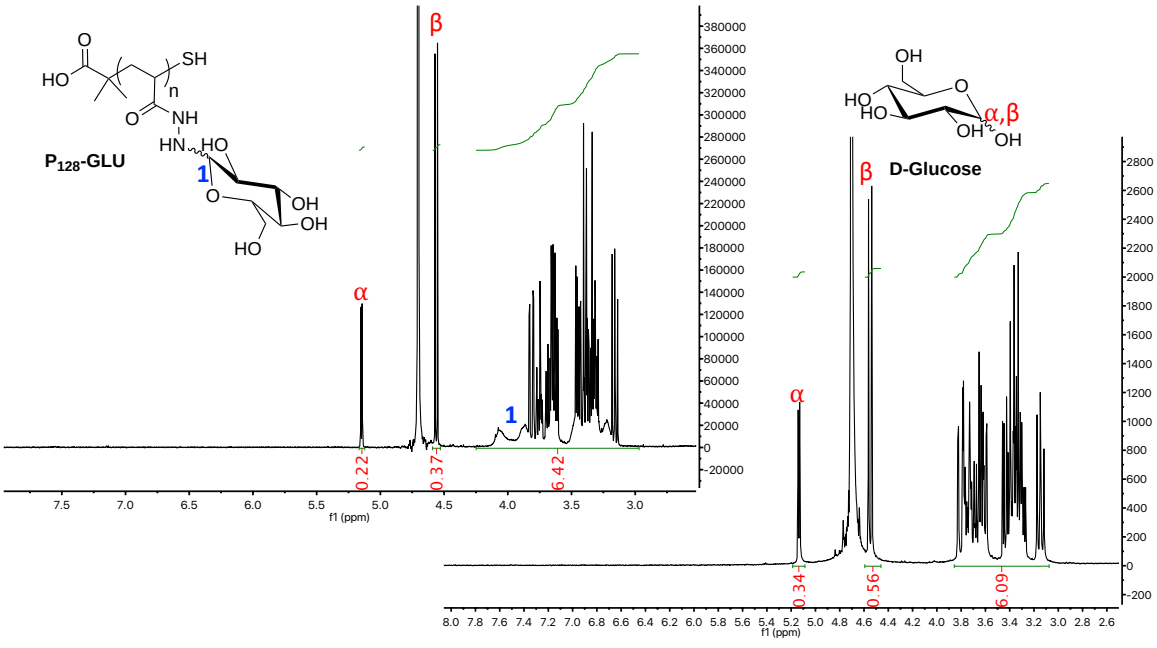

Figure 53. Proton NMR (D_2O) (left) for **P_{128}-GLU** (2.eq. sugar, 84% conversion by integration) and (right) D-glucose prior to addition of **P_{128}.**

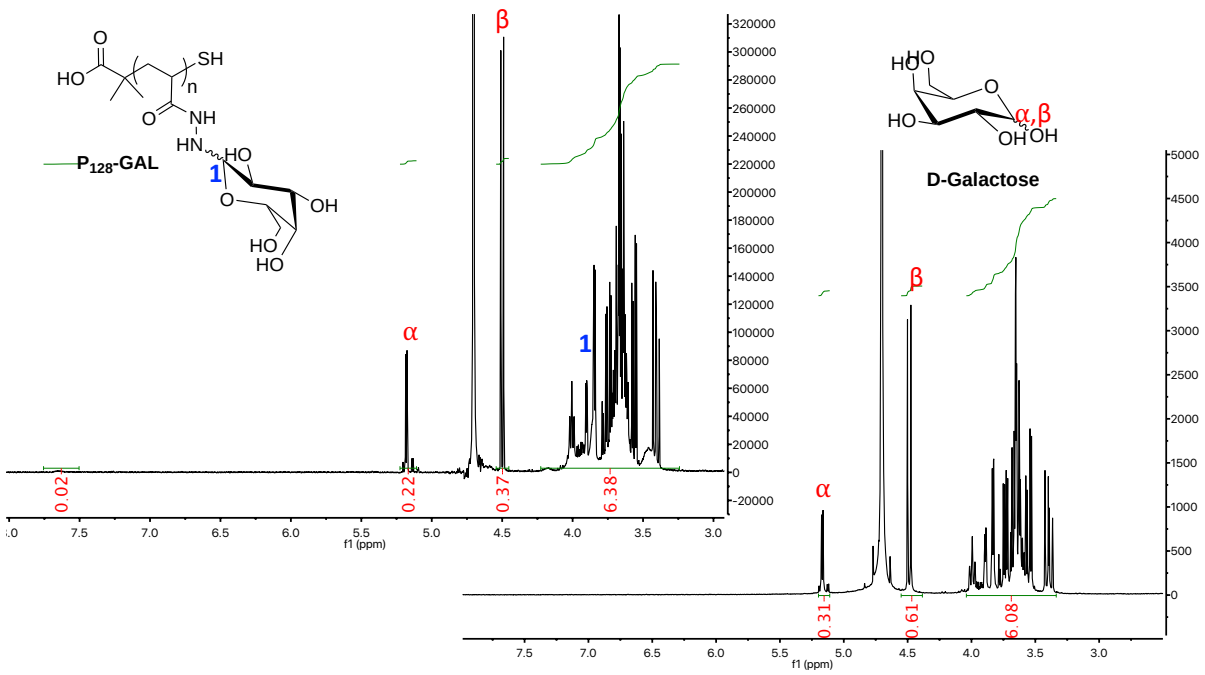

Figure 54. Proton NMR (D_2O) (left) for **P_{128}-GAL** (2.eq. sugar, 80% conversion by integration) and (right) D-galactose prior to addition of **P_{128}.**

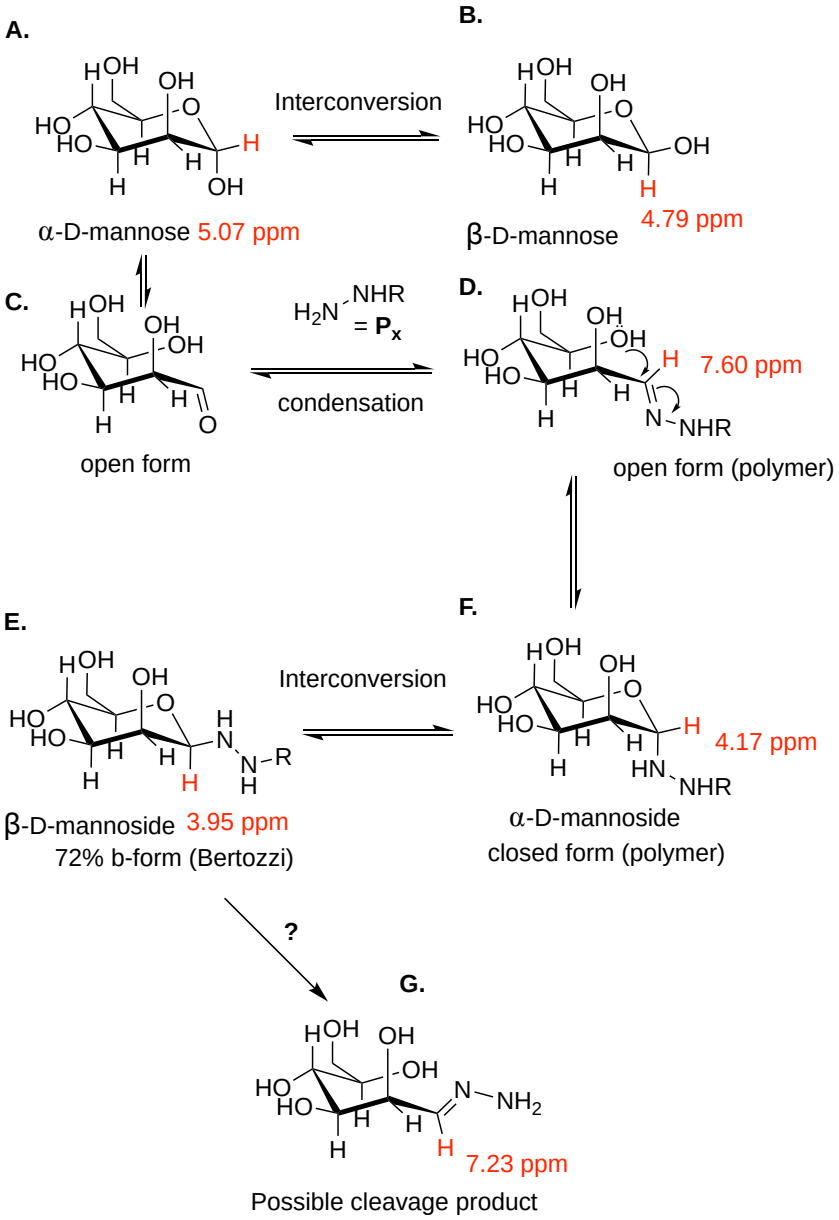

Scheme 7. Reaction pathway for D-mannose with $\mathbf{P_x}$ and possible small molecule cleavage product, highlighting the key proton signals (**Figure 52**) involved with determining conversion of the free sugar onto the polymer backbone.

Distinct α and β proton signals for the free sugar, in the NMR spectrum (**Figure 52-54)** and highlighted in red (**Scheme 7**, A,B) represent the two distinct stereoisomers possible for the cyclic form of the sugar. The ratio of these peaks, (total =1H), indicates the stability of each stereoisomer and is influenced by the anomeric effect which favours the α position, and steric and hydrogen bonding effects which favour the β position.[20] β-glycosides has been reported as the favoured form for *N*-linked

glycoconjugates for poly(acryloyl hydrazide)[16] On glyosidic bond formation with $\mathbf{P_x}$ (**Scheme 7**, D), the resulting conjugate predominantly exists in the ring closed form, (**Scheme 7**, F), as confirmed by new broad α and β proton signals (**Figure 52, $\mathbf{P_{128}}$-MAN,** 4.17, 3.15 ppm), upfield of the corresponding signals for the free sugar (**Figure 52, D-mannose** 5.07, 4.09 ppm). A small broad region at 7.6 ppm(**Figure 52, $\mathbf{P_{128}}$-MAN**) corresponded to the proton adjacent to the acyl hydrazone bond for sugars residing in the open form on the polymer (**Scheme 7**, D),[16] which accounted for roughly 6% of the observed total loading for **$\mathbf{P_{128}}$-MAN** and **$\mathbf{P_{128}}$-GAL** but close to 0% for **$\mathbf{P_{128}}$-GLU** presumably due to added stability of the ring closed form for this glycoconjugate. Interestingly, A sharp doublet signal in the proton NMR with a similar chemical shift to the open form region on the glycopolymer in the proton NMR was observed for all conditions (**Figure 55**).

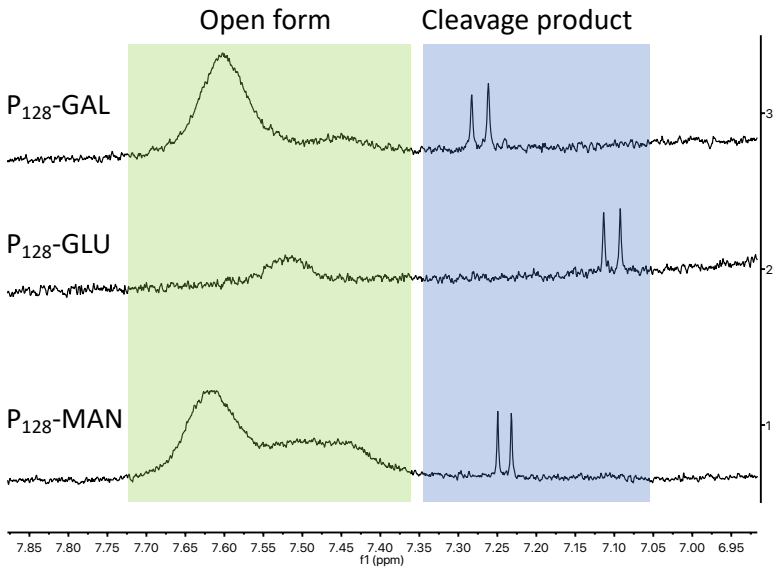

Figure 55. Proton NMR (D_2O) for glycopolymers expanded to show signals associated with the open form glycoconjugate and the possible mono-hydrazone cleavage product.

Work carried out in our labs using $\mathbf{P_x}$ has previously reported the appearance of small sharp signals in the proton NMR when coupling with aldehydes, [15] and in our

work here regarding **P_x-IMI** and **P_x-2A3FP** (**Chapter 2**) consistent with the formation of mono-hydrazones *via* the cleavage of the C-N bond of the **P_x** hydrazone side chains. The mechanism for the formation of this impurity may be as a result of intramolecular nucleophilic attack of an unreacted hydrazide moiety on an adjacent acyl hydrazone conjugate, possibly with the inclusion of a water molecule in a protease-type mechanism.[21] We reasoned that for glycopolymers described in this work, cleavage occurred predominantly *via* the ring-closed form of the glycoconjugate due to similar levels of the impurity being observed for **P_{128}-GLU, P_{128}-MAN** and **P_{128}-GAL** despite a significantly lower abundance of the ring opened form for **P_{128}-GLU.** In any case, this impurity accounted for less than 1% of the total loading and was expected to be more prominent at lower degrees of aldehyde loading.[15]

Loading efficiencies of **P_{128}** with 2. eq. sugars were significantly higher than our observed loading with 1.0 eq. with 84% loading being achieved compared to 35% for **P_{128}-MAN** described previously and we observed that loading could be increased marginally further to quantitative levels with the addition of 4 and 6 eq. (**Table 8**).

Table 8. Loading efficiencies for different sugars with $\mathbf{P_{128}}$ (24 hrs 50 °C).

Sugar	[a] Eq. sugar	[b] Buffer	[c] Loading (%)	[d] Open form (%)	[e] % open form
D-Mannose	2	Acetate	84	0.02	4
	4		92	0.02	6
	6		Quantitative	0.01	6
	2	Pyridine	62	0.01	2
	4		96	0.02	6
	6		96	0.01	6
D-Glucose	2	Acetate	80	0	0
	4		88	0	<1%
	6		86	0	<1%
	2	Pyridine	82	0	0
	4		88	0	<1%
	6		90	0	<1%
D-Galactose	2	Acetate	84	0.02	4
	4		Quantitative	0.03	12
	6		Quantitative	0.01	6
	2	Pyridine	74	0.01	2
	4		84	0.02	8
	6		Quantitative	0.01	6

[a] With respect to hydrazide groups, [b] prepared at 100 mM, [c] calculated by 1H NMR, [d] integral (1H NMR) corresponding to open sugar form on the polymer backbone (total = 7 protons), [e] calculated as a percentage of the total loading on the polymer by 1H NMR.

Having quantified the conversion by NMR, next we evaluated changes in polymer size by SEC before and after loading of the sugar for conditions described in **Table 8** to establish if conjugation with sugars resulted in an increase in polymer molecular mass or impacted the shape and intensity of the refractive index response as was demonstrated for aldehydes in Chapter 2 (**Table 9, Figure 56**).

Table 9. Molecular mass and dispersity ($Đ_M$) for glycopolymers and **P_{128}**, calculated by GPC (Lonza DPBS) using PEG/PEO standards.

Entry	[a]Eq. sugar	[b]Buffer	[c]$M_{p(theo)}$	[d]$M_{n(SEC)}$	[d]$M_{w(SEC)}$	$Đ_M$
P_{128}	0	n/a	11,232	15907	19616	1.23
P_{128}-MAN	2	Acetate	30586	12083	17508	1.45
	4		32429	12035	17403	1.45
	6		36115	12324	17902	1.45
	2	Pyridine	25517	12364	17701	1.43
	4		33350	12273	17903	1.46
	6		33350	12325	17860	1.45
P_{128}-GLU	2	Acetate	29664	11876	17356	1.46
	4		31507	11993	17443	1.45
	6		31046	11855	17328	1.46
	2	Pyridine	30124	12005	17950	1.50
	4		31507	11941	17403	1.46
	6		31968	12004	17650	1.47
P_{128}-GAL	2	Acetate	30585	11757	17231	1.47
	4		36115	9764	15008	1.54
	6		36115	9810	15228	1.55
	2	Pyridine	28281	11597	17234	1.49
	4		30585	9998	15435	1.54
	6		37497	10004	15481	1.55

[a] With respect to hydrazide groups, [b] prepared at 100 mM, [c] calculated by monomer conversion, [d] calculated by SEC (Lonza DPBS).

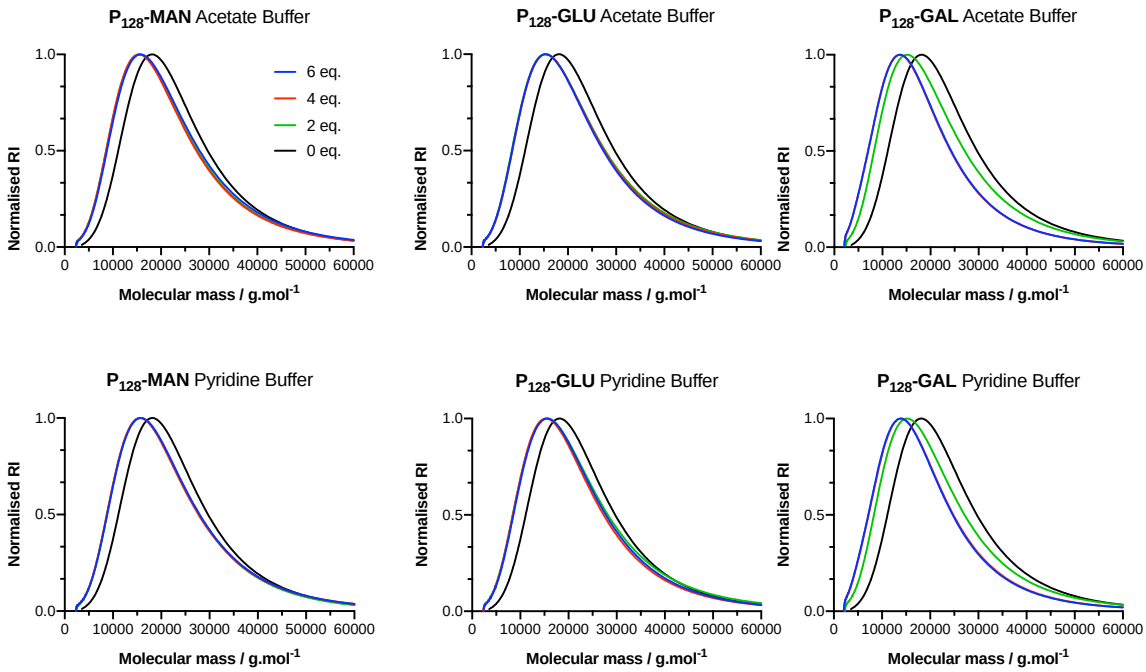

Figure 56. Molecular mass distribution (GPC, Lonza DPBS) for indicated glycopolymers, after reaction with sugars (24 hrs 50 °C) with increasing eq. of sugar and indicated buffers.

Interestingly, glycopolymers displayed broadening of the dispersity $Đ_M$ and longer retention times in the column compared to the corresponding polymer scaffold (**P_x**), resulting in lower experimental molecular mass despite a significantly larger theoretical molecular mass of the glycopolymer. We rationalised that direct comparison of molecular mass between modified and unmodified **P_x** is unfeasible by SEC due to the differences in side-chain chemistry which may affect the hydrodynamic radius of the polymer. A recent review on the matter highlighted that shifts to longer retention times in SEC can indicated the collapse of a linear polymer to a more tightly packed polymer particle which may explain these observations.[22]

Despite this, the observed shift in retention time for the **P_x** treated with sugars provided some further evidence that glycopolymers had been prepared. In particular, a smaller shift in retention time for **P_{128}-GAL** for 2 eq. compared to 4 and 6 eq was in agreement with regard to relative loadings calculated loading by NMR.

3.3.2 Stability of glycopolymers to hydrolysis

Next, the stability of the glycoconjugate was evaluated, this was especially important given the dynamic nature of the acyl hydrazone bond,[23] and the previously discussed possibility of intramolecular cleavage occurring on the polymer backbone (**Figure 55**). To this end loading of each sugar was monitored by proton NMR over a considerable period of time under standard reaction conditions, and after two serial dilutions in the corresponding buffer (**Figure 57**).

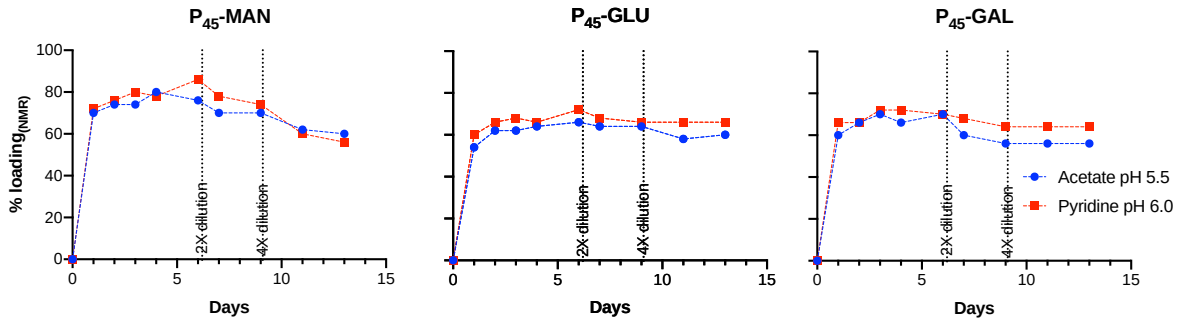

Figure 57. Time-course analysis (proton NMR, D_2O) of sugar loading on glycopolymers (2 eq. sugar) at varying pH and after dilution (2x and 4x as indicated on the graphs). Initial concentration was 0.25 M with respect to the hydrazide side-chain and glycopolymers were stored at RT between timepoints.

After 6 days and prior to dilution, loading was largely unchanged for all glycopolymers, although loading was slightly increase between 24- and 48-hours incubation. After diluting samples by 50% with the same buffer, we noted a small decrease in loading for both **P_{45}-MAN** and **P_{45}-GAL** which appeared to be more prominent at pH 5.5, while **P_{45}-GLU** remained largely unchanged after dilution. After 9 days incubation, samples were diluted buy a further 50%, which resulted a greater reduction in loading was observed for **P_{45}-MAN,** but overall, not a large decrease and after 13 days all glycopolymers displayed similar loadings ~60%. **P_{45}-MAN** displayed the greatest reduction in loading between 2 days and 13 days indicating that *N*-linked Mannose may be more amenable to hydrolysis compared with glucose and galactose.

It should be noted that we observed no increase in signals possibly indicative of a mono-hydrazone cleavage product during the course of the stability experiment.

In summary, stable glycopolymers containing side groups of mannose, glucose and galactose were prepared at high degrees of sugar loading onto the $\mathbf{P_x}$ side chains without the need for catalytic aniline.

3.3.3 Glycopolymer toxicity towards V. cholerae

With confirmation that glycopolymers $\mathbf{P_{128}}$**-MAN**, $\mathbf{P_{128}}$**-GLU** and $\mathbf{P_{128}}$**-GAL** had been successfully prepared to a similarly high degree of loading, we investigated the biological responses of *V. cholerae* to different sugar displaying glycopolymers. Initially we assessed glycopolymers effect on the growth of GFP expressing *V. cholerae* A1552 by monitoring bacterial growth by OD_{600} and fluorescence (GFP) (**Figure 58**, **Figure 59**).

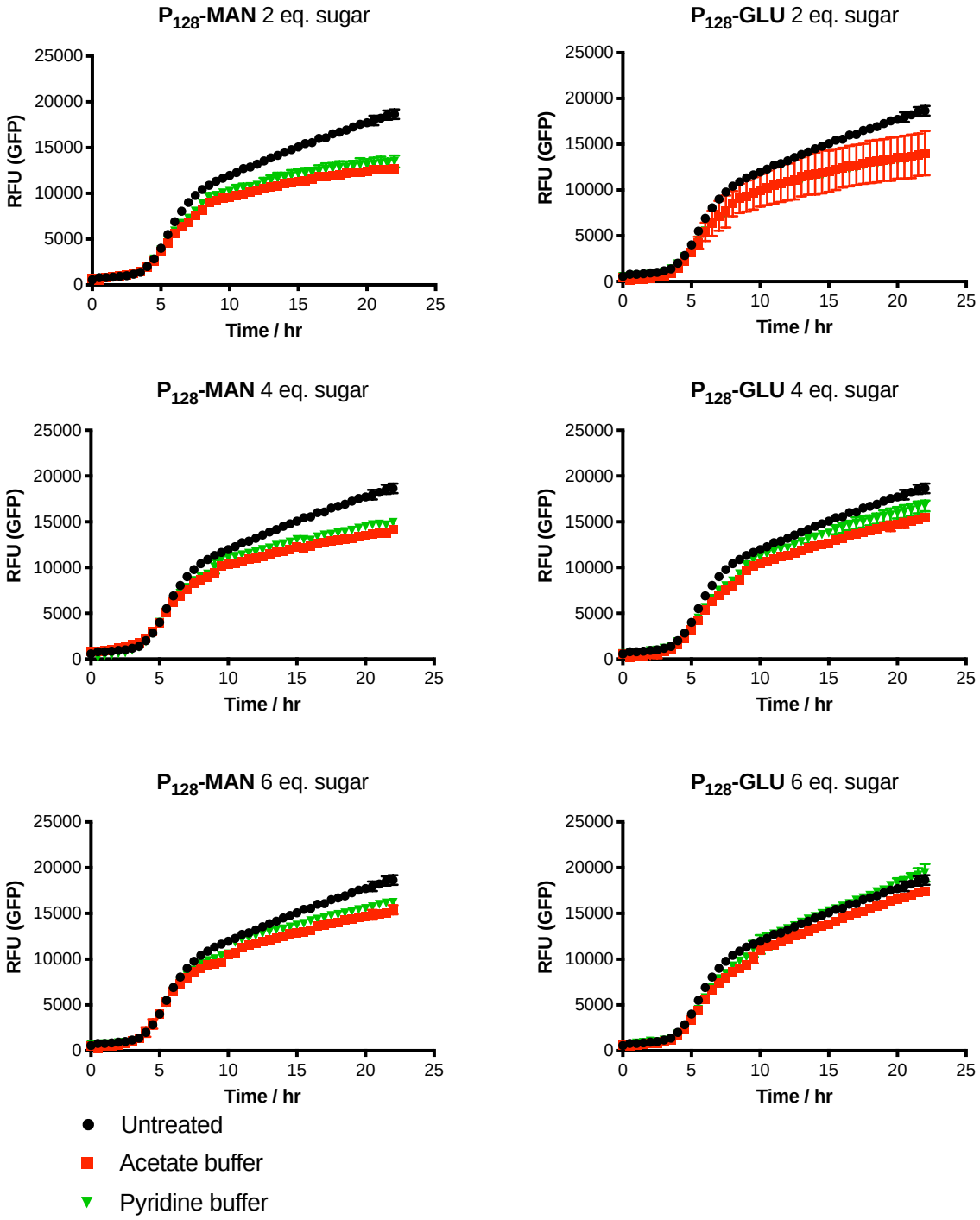
P128-MAN 2 eq. sugar
P128-GLU 2 eq. sugar
P128-MAN 4 eq. sugar
P128-GLU 4 eq. sugar
P128-MAN 6 eq. sugar
P128-GLU 6 eq. sugar
RFU (GFP)
Time / hr
0
5000
10000
15000
20000
25000
0
5
10
15
20
25
Untreated
Acetate buffer
Pyridine buffer

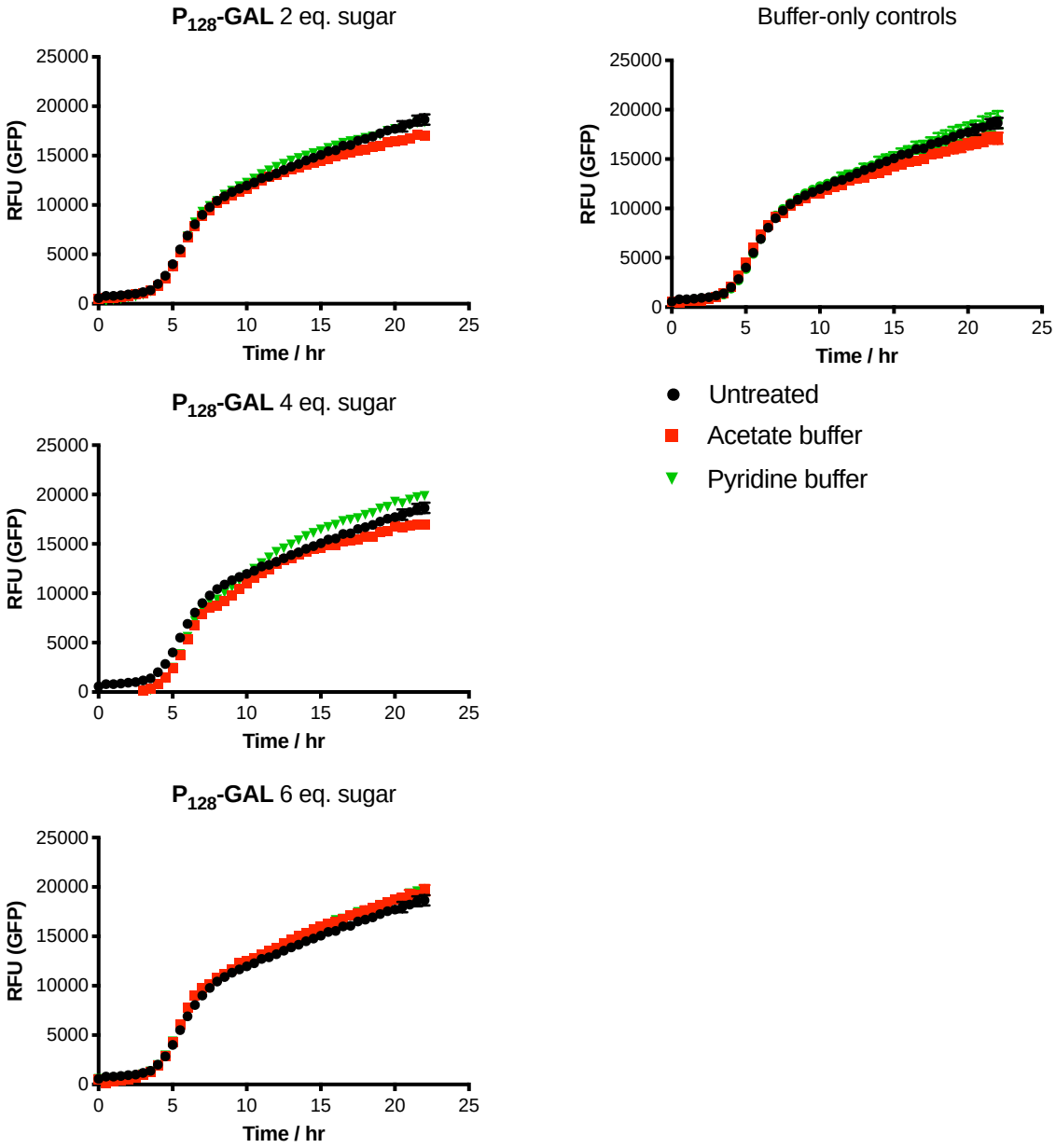

Figure 58. GFP expression as a proxy of bacterial growth for GFP-*V. cholerae* A1552 incubated at 37°C in clear DMEM with 0.05 mg ml^{-1} glycopolymers prepared with different equivalents of the sugar as indicated. Initial OD_{600} = 0.02. Fluorescence was recorded every 30 minutes in the GFP channel.

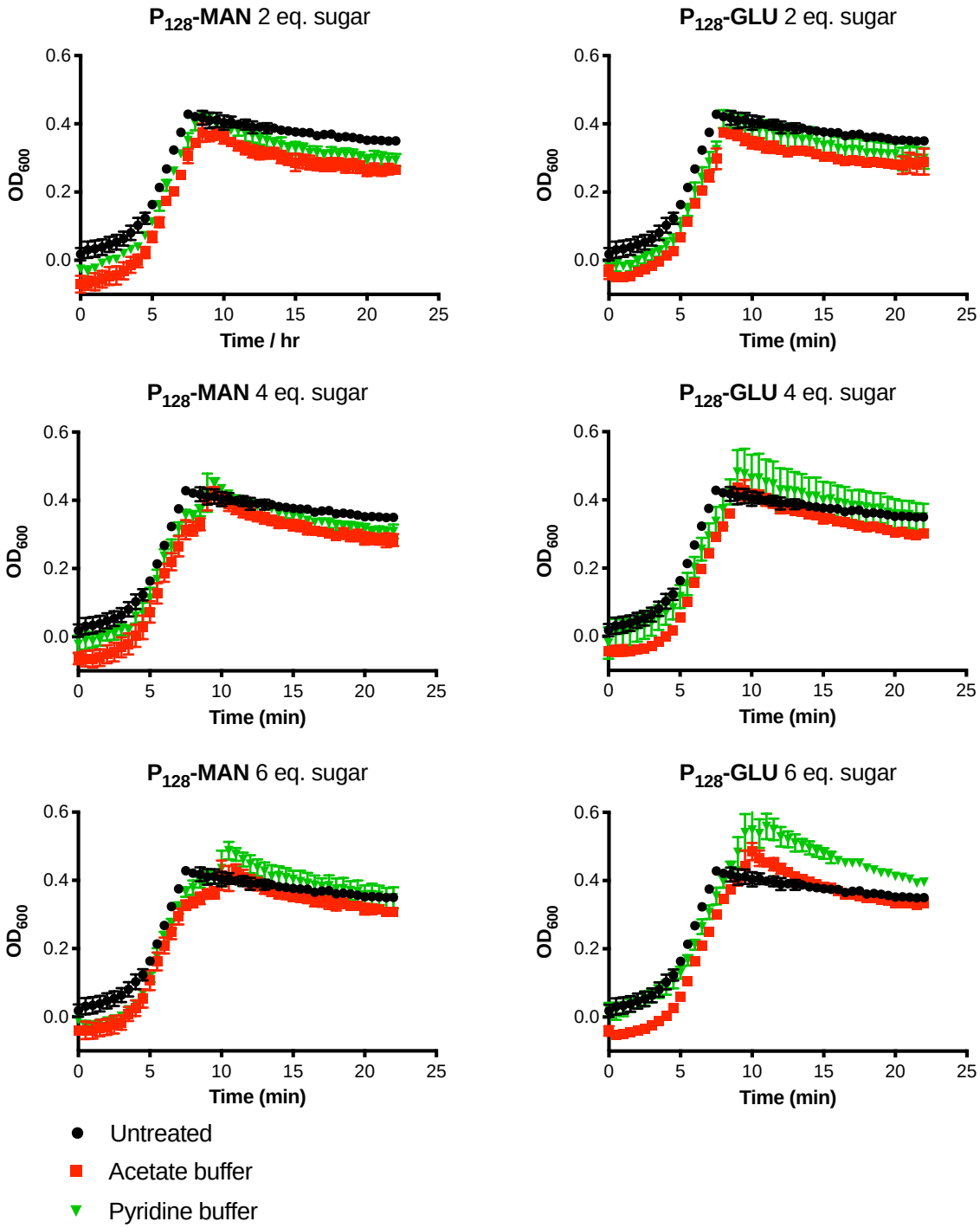
P128-MAN 2 eq. sugar
P128-GLU 2 eq. sugar
P128-MAN 4 eq. sugar
P128-GLU 4 eq. sugar
P128-MAN 6 eq. sugar
P128-GLU 6 eq. sugar
OD600
Time / hr
Time (min)
Untreated
Acetate buffer
Pyridine buffer

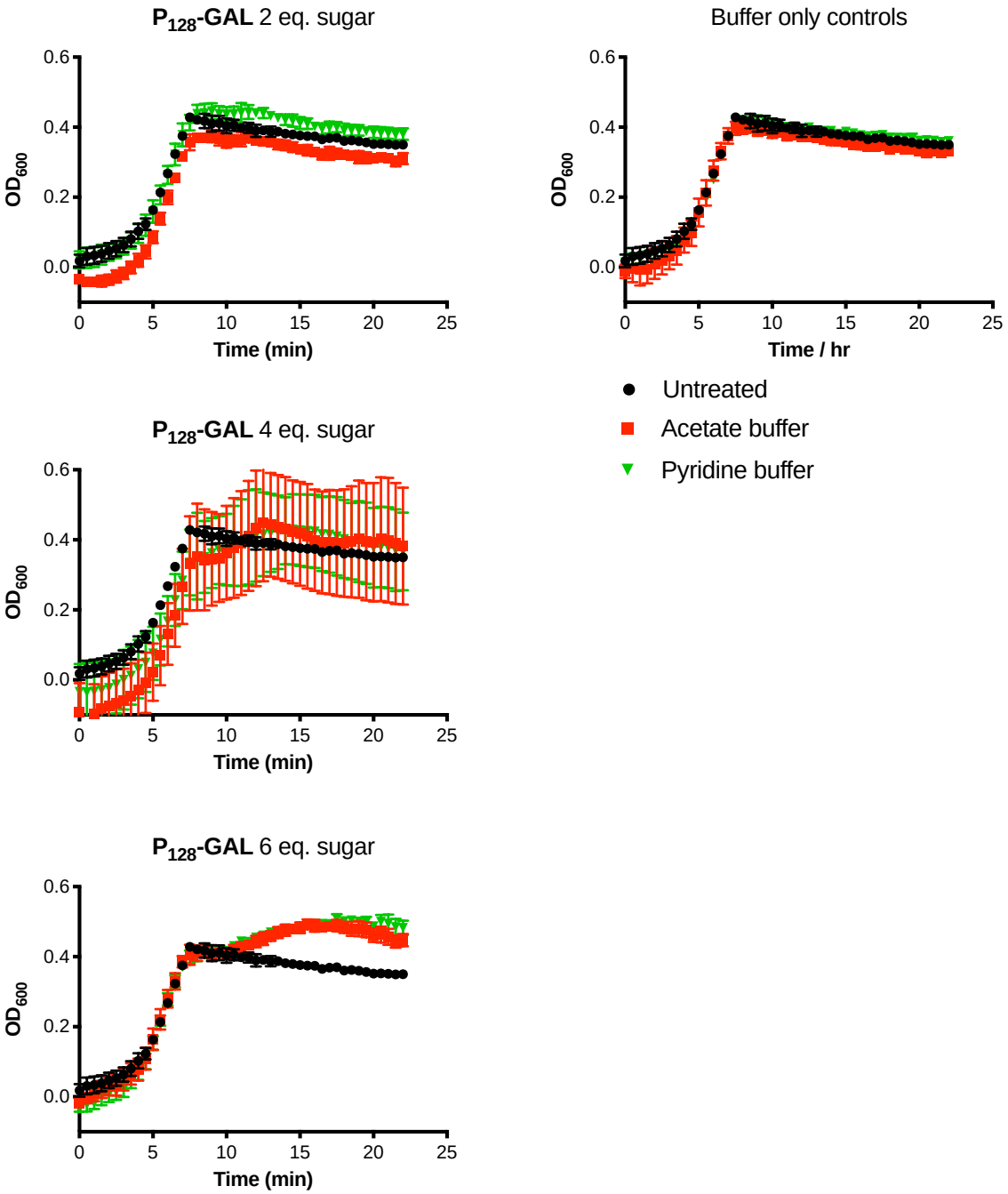

Figure 59. OD_{600} growth curves for GFP-*V. cholerae* A1552 incubated at 37°C in clear DMEM with 0.05 mg ml^{-1} glycopolymers prepared with different equivalents of the sugar as indicated. Initial OD_{600} = 0.02. Optical density (OD_{600}) was recorded every 30 minutes.

A concentration of 0.05 mg ml^{-1} was targeted as representative of the maximum sub-inhibitory concentration of $\mathbf{P_x}$ towards *V. cholerae* (**Chapter 2**) and we observed low overall levels of growth inhibition of *V. cholerae* with glycopolymers tested. **P_{128}-**

MAN displayed relatively higher levels of toxicity towards *V. cholerae*, most noticeable by GFP expression, compared to **P_{128}-GLU** and **P_{128}-GAL** which displayed very little impact on *V. cholerae* growth. OD_{600} (**Figure 59**) displayed good correlation with GFP expression, although observable differences in toxicity were less obvious. Having established that at this concentration, glycopolymers were sub-inhibitory towards *V. cholerae* their ability to bind and sequester bacteria, possibly through sugar specific lectin-carbohydrate interactions was investigated.

Given the high loading of **P_x** with 2 eq. of sugar, we did not pursue further biological studies with glycopolymers prepared with higher excesses (4- or 6 eq.) in order to suppress biological effects such as lectin saturation, arising from an excess of free sugar during *in situ* screening.[24] Acetate buffer (pH 5.5) was also concluded to be the most suitable buffer to perform conjugation reactions with sugars on account of higher overall loading observed for **P_x** with sugars.

3.3.4 Aggregation studies – Turbidity and flocculation

To establish whether glycopolymers induce clustering of *V. cholerae* as reported for cationic polymers in our labs,[8,9] a simple flocculation assay was employed which measures turbidity (OD_{600}) and had been previously described for similar bacterial clustering applications in the literature (**Figure 60**).[25,26]

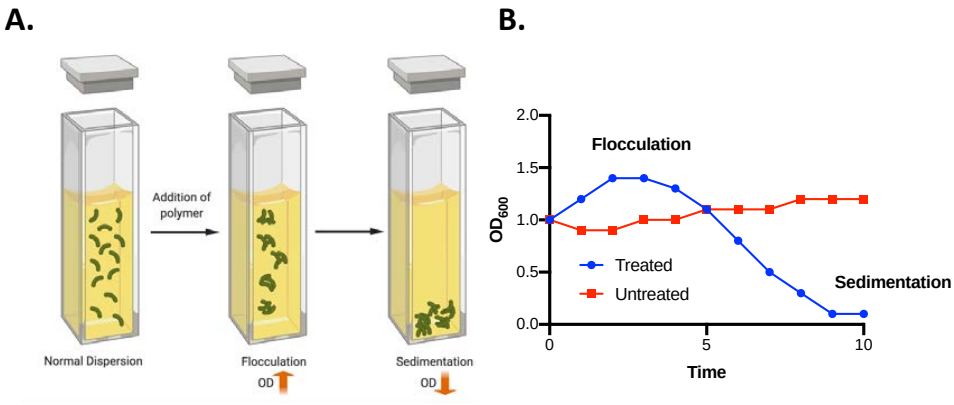

Figure 60. A) Description of a flocculation assay and B) a simulated example of bacterial turbidity after treatment of a polymer which induces bacterial clustering.

V. cholerae were grown overnight in LB, transferred to clear DMEM, adjusted to an initial OD_{600} of 1.0 and treated with glycopolymers and the corresponding free sugar as a control. OD_{600} was measured at timepoints and the cuvettes were left at room temperature without shaking so that the effect of the clustering could be best observed (**Figure 61**).

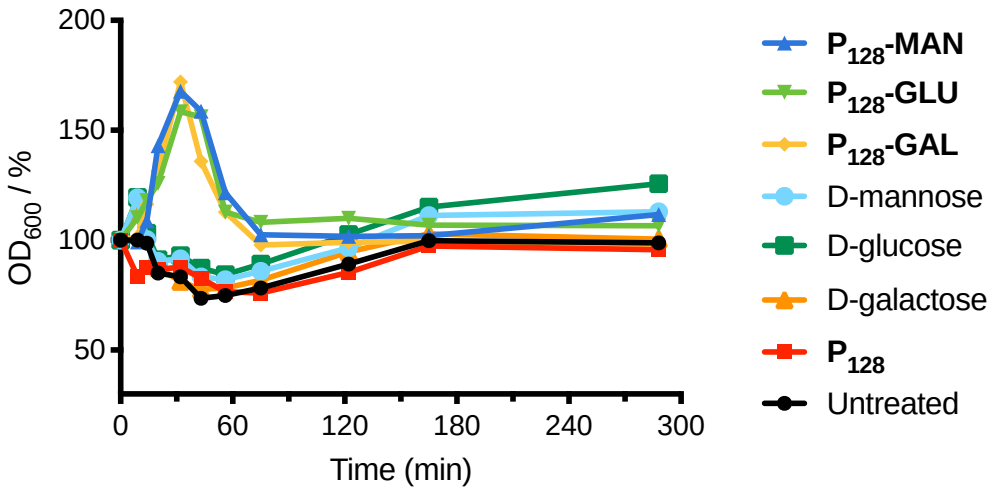

Figure 61. Turbidity of *V. cholerae* dispersed in clear DMEM, after addition of 0.05 mg ml^{-1} glycopolymers as indicated (concentration in respect to **P_{128}**), polymer scaffold (**P_{128}**) or representative concentration of free sugar (0.21 mg ml^{-1}) from a starting OD_{600} = 1.0. All polymer and sugar conditions were dissolved in 100 mM Acetate buffer.

Glycopolymers induced a rapid increase in the turbidity of *V. cholerae* after 20 minutes incubation independently of type of sugar. We had expected that an increase

of turbidity would display some level of specificity to the sugar displayed on the glycopolymer, indicative of bacterial aggregation driven by specific interactions between the sugars on the glycopolymer and bacterial lectins. However, these observations indicated interactions were not specific to the type of sugar and may indicate a more general mechanism of binding or interacting with sugars.

We rationalised that that *V. cholerae* may bind all three glycopolymers to a similar degree seeing how *V. cholerae* adhesion has been associated with galactose,[27] mannose,[28] and glucose.[29] We were encouraged that free sugars did not induce flocculation of bacteria, supporting the hypothesis that the observed increase in turbidity was driven by multivalency and in agreement with the "cluster glycoside effect".[7] $\mathbf{P_x}$ did not induce flocculation of bacteria which was attributed to the low protonation of the hydrazide (pKa ~4.0) under physiological conditions.[30]

Intriguingly, no decrease in the OD_{600} at longer timepoints was observed, suggesting sedimentation was not occurring or occurring at a level not detectable by this system, and certainly, to a much lower extent as was observed for polymers modified with imidazole (**Chapter 2**).

We rationalized that this observation could be due to short-lived interactions between the glycopolymer and the bacteria, either due to the stability of the glyosidic bond or weak polymer-bacteria interactions. In order to evaluate this interaction in more detail *V. cholerae* incubated for 20 minutes with glycopolymers or sugars were imaged by microscopy (**Figure 62**).

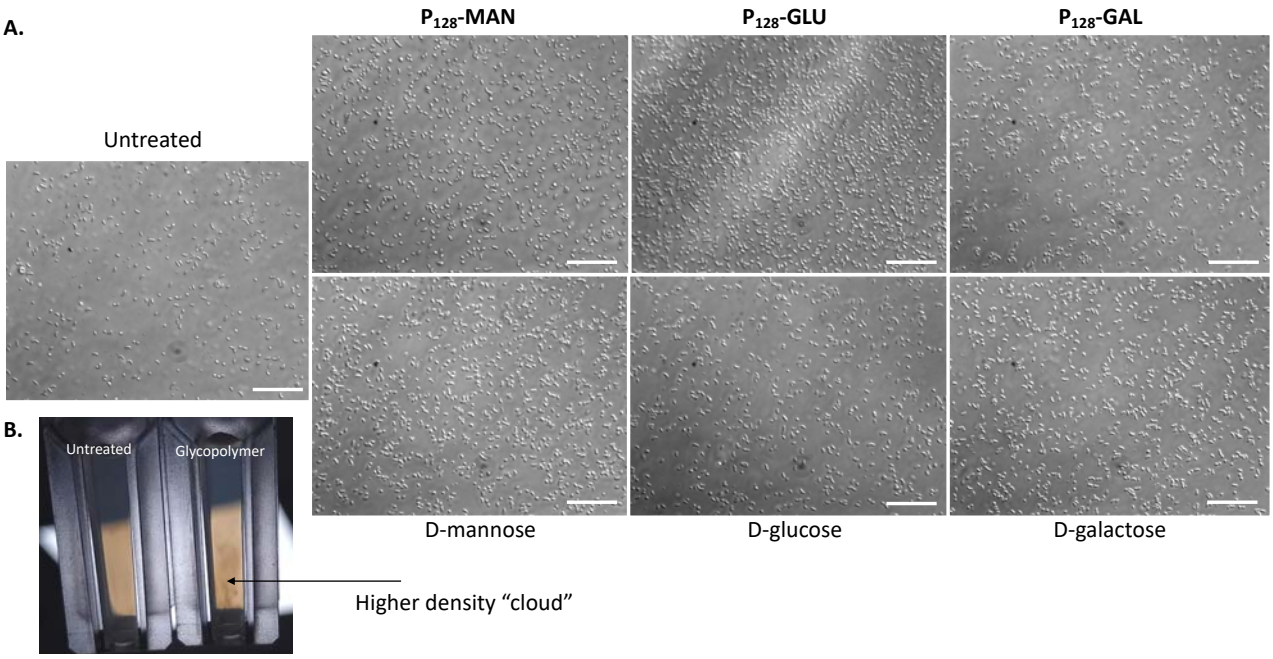

Figure 62. A) Optical microscope images (DIC, 100X objective) for *V. cholerae* after 20 minutes incubation with 0.05 mg ml^{-1} glycopolymers or corresponding free sugar and B) corresponding image of bacterial suspensions showing an area of high density after 20 minutes incubation with glycopolymers. Scale bars represent 10 μm.

Effort was taken to ensure sampling from the same part of the cuvette, which included sampling from an area of higher density visible to the naked eye for glycopolymer treated samples (**Figure 62** B) which we expected would identify the presence of bacterial clusters. However, we found no evidence of clustering, although higher densities of bacteria were observed for both glycopolymers and sugars compared with the untreated sample. It was also not clear what was responsible for area of higher bacterial density which can be observed with the naked eye and in OD_{600} measurements (**Figure 62**, B). However these results taken together with data from the flocculation assay indicate that interactions between *V. cholerae* and glycopolymers do not result in the formation of stable aggregates, indicative of bridging aggregation.[31]

In an attempt to increase the activity of the glycopolymers towards bacterial aggregation, higher concentrations with **P_{128}-MAN** was explored to asses impact on bacterial flocculation and sedimentation (**Figure 63**).

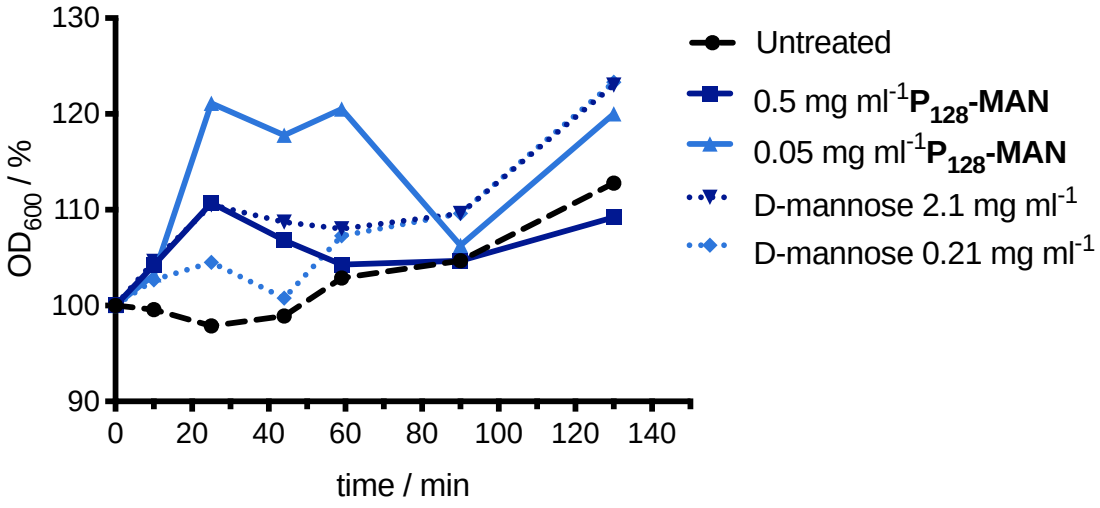

Figure 63. Turbidity of *V. cholerae* dispersed in clear DMEM after addition of mannose glycopolymers **P_{128}-MAN** and D-mannose. Initial OD_{600} = 1.0.

We found that when increasing the concentration of **P_{128}-MAN** to 0.5 mg ml^{-1} the flocculation effect of *V. cholerae* was lost, and we reasoned that this could be due to increased toxicity, given **P_x** was found to display increased toxicity towards *V. cholerae* at this concentration (**Chapter 2**). However, previous studies with cationic polymers demonstrated increased bacterial clustering moving from 0.05 mg ml^{-1} to 0.5 mg ml^{-1} despite increased toxicity.[8] Another possibility is that a higher concentration of unconjugated D-mannose in the more concentrated sample could result in a greater saturation of mannose-binding adhesins on the bacteria (for example MSHA[3]) and competitively inhibit multivalent interactions with the polymer which has been described for other glycopolymers where supplementation of 10 mM D-mannose completely inhibited the binding of *Escherichia coli* to a mannose-displaying glycopolymer.[24]

3.3.5 Biofilm response to glycopolymers

Thus far it had been established that interactions between glycopolymers and *V. cholerae* resulted in a short-lived increase in turbidity, but no evidence of bacterial clustering. These findings suggested that the activity of glycopolymers was distinct to that of $\mathbf{P_x}$ and the free sugars, as well as our previous work with cationic polymers.[8] We therefore considered that despite little evidence of bacterial aggregation, further investigation into other bacterial responses was warranted.

Biofilm production in *V. cholerae* is associated as a response to many different environmental triggers such as adhesion, antibiotics, pH stress and nutrient levels including availability of certain sugars.[3,4,32,33] Cationic polymers have previously been reported to increase biofilm production in aggregated *V. cholerae*,[8] *via* a mechanism which may involve the upregulation of quorum sensing (QS).[9] However since biofilm formation in *V. cholerae* is negatively regulated by QS,[34] alternative regulatory pathways may be responsible, possibly independent of bacterial clustering.

To determine if glycopolymers attenuated the production of biofilm in *V. cholerae,* residual biofilm was measured using crystal violet (CV) assay.[35] Crystal violet staining is a simple and effective tool for detecting by absorbance (550 nm) components of a biofilm which remain adhered to surfaces after mechanical removal of bacterial cells. In the case of *V. cholerae*, the key biofilm components consist of *Vibrio* polysaccharide (VPS), a glycopolymer which is excreted on initial contact with the surface, vital to provide three-dimensional biofilm structure,[36] and scaffolding proteins RbmA, RbmC and Bap1,[37,3] which maintains the structure of the biofilm *via* cell-to-cell and cell-to-VPS binding. We assessed the progression of biofilm formation following 22 hours incubation with glycopolymers prepared in both acetate buffer and pyridine buffer with increasing eq. of sugars (**Figure 64**).

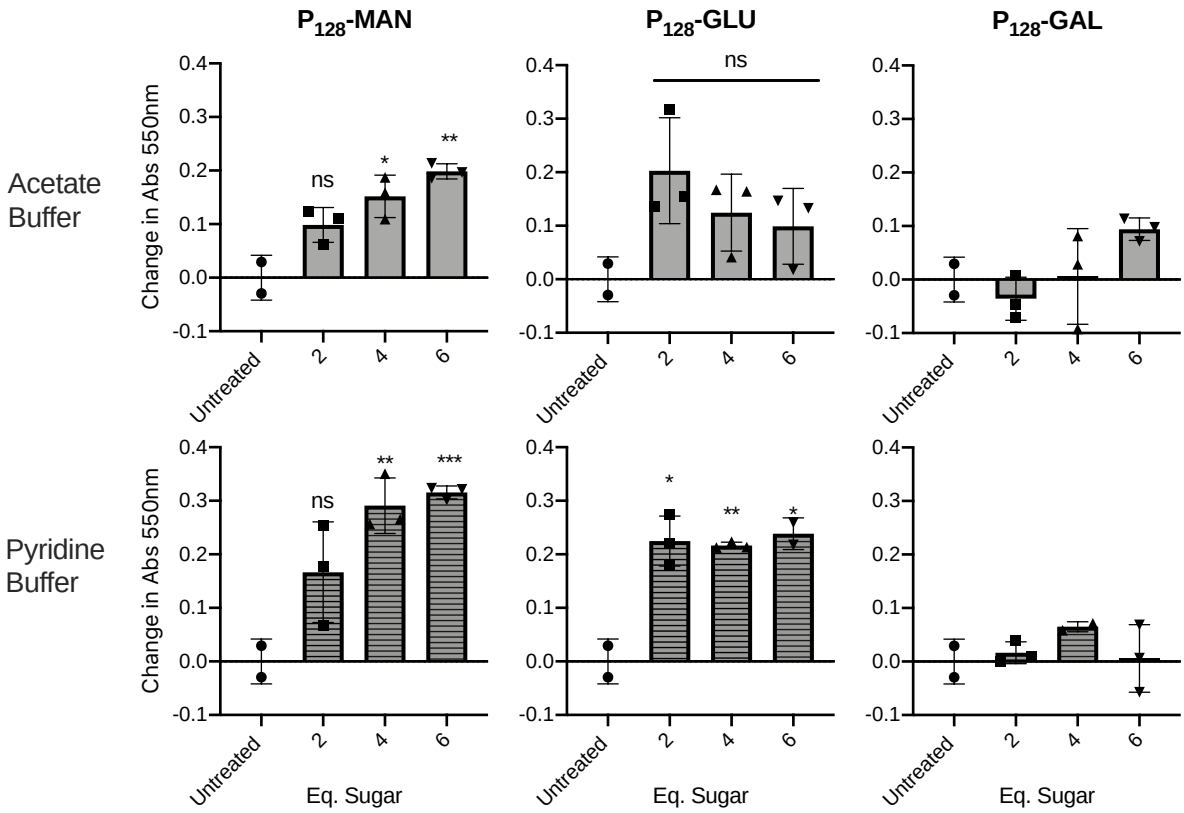

Figure 64. Relative production of biofilm determined by crystal violet staining of residual *V. cholerae* biofilm (Abs 550 nm) after incubation for 22 hours at 37°C with 0.05 mg ml^{-1} glycopolymers prepared in acetate buffer (solid bars) or pyridine buffer (hashed bars). Significance = $P < 0.04$.

Significantly higher levels of crystal violet staining were observed for conditions treated with **P_{128}-MAN** and **P_{128}-GLU** glycopolymers, and increased eq. of mannose appeared to have a positive but not statistically significant impact on biofilm formation. This trend was not as evident for **P_{128}-GLU** and could suggest that free glucose does not have as large an impact as free mannose on the triggering of biofilm. Most notably, **P_{128}-GAL** had a significantly lower impact on biofilm formation and in some cases a reduction over the untreated control sample of *V. cholerae*.

To determine if these observations could be explained by differences in bacterial growth under these conditions at 22 hours, relative GFP expression of *V. cholerae* treated with glycopolymers was plotted as a percentage compared to the untreated bacteria (**Figure 65**).

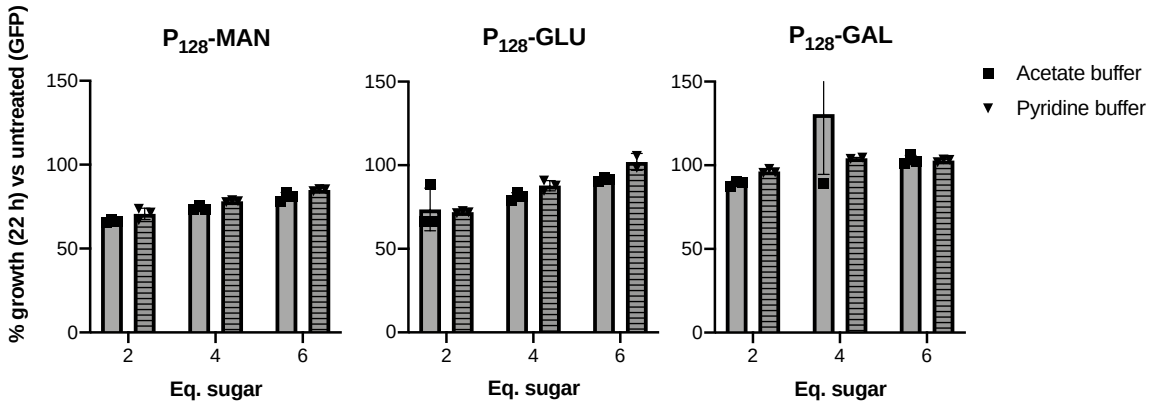

Figure 65. Growth progression (GFP expression) of *V. cholerae* grown in clear DMEM at 22 hours, treated with 0.05 mg ml^{-1} glycopolymers prepared in either acetate buffer (solid bar) or pyridine buffer (dashed bar) as percentage growth of untreated *V. cholerae*.

V. cholerae treated with **P_{128}-MAN** and **P_{128}-GLU** displayed slightly reduced growth and **P_{128}-GAL** displayed almost no change in growth over the untreated sample. On account of this we reasoned that induction of biofilm formation observed for mannose and glucose glycopolymers may be linked to the observation that these glycopolymers also resulted in reduced growth. Under non-inhibitory conditions, growth curves of *V. cholerae* in a planktonic or biofilm associated growth mode have been reported by Bassler and co-workers to be similar,[32] and thus, a reduction in growth and observation of biofilm may indicate a stress or other signaling response.[38]

At this point it was important to rule out possible contributions to crystal violet staining by the glycopolymers themselves (**Figure 66**).

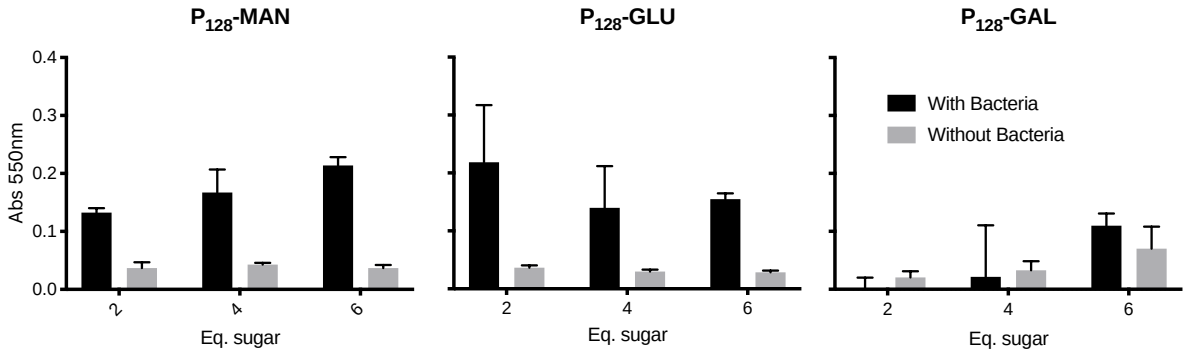

Figure 66. Crystal violet staining for residual biofilm or residual polymers after 22 hours incubation of glycopolymers (0.05 mg ml^{-1}) with and without *V. cholerae*.

Background crystal violet staining with glycopolymers was observed in all cases, and may interfere with reported values in the case of **P_{128}-GAL**, However residual crystal violet staining originating from **P_{128}-MAN** and **P_{128}-GLU** was found to be sufficiently lower than with *V. cholerae* indicating that the increase in staining was indeed due to an increased level of adhesive biofilm factors produced by the bacteria.

Finally, we tested if *V. cholerae* was responding to the glycopolymers on account of unreacted sugar in the polymer samples. A signaling pathway which was previously overlooked, namely, the phosphoenolpyruvate phosphotransferase system (PTS) of *V. cholerae*, acts as an environmental reporter of carbohydrate availability.[4] It has been previously reported by Watnick and co-workers that *V. cholerae* produce biofilm in response to availability of mannose, through PTS signaling, and in the same way, glucose was proposed to repress biofilm formation, most interestingly galactose was not recognised by PTS signaling pathway and did not impact biofilm formation.[39] It should be noted that minimal media with or without supplementation of 0.5 mg ml^{-1} sugars was employed in the aforementioned study, whereas clear DMEM employed in this work is supplemented with 0.584 mg ml^{-1} glucose with additional 0.21 mg ml^{-1} supplementation of sugar on addition of polymer conditions at 0.05 mg ml^{-1}. Crystal violet assays were therefore repeated to include important sugar, polymer scaffold and

buffer controls, to better evaluate contribution to the production in biofilm from all constituents of transferred conditions (**Figure 67**).

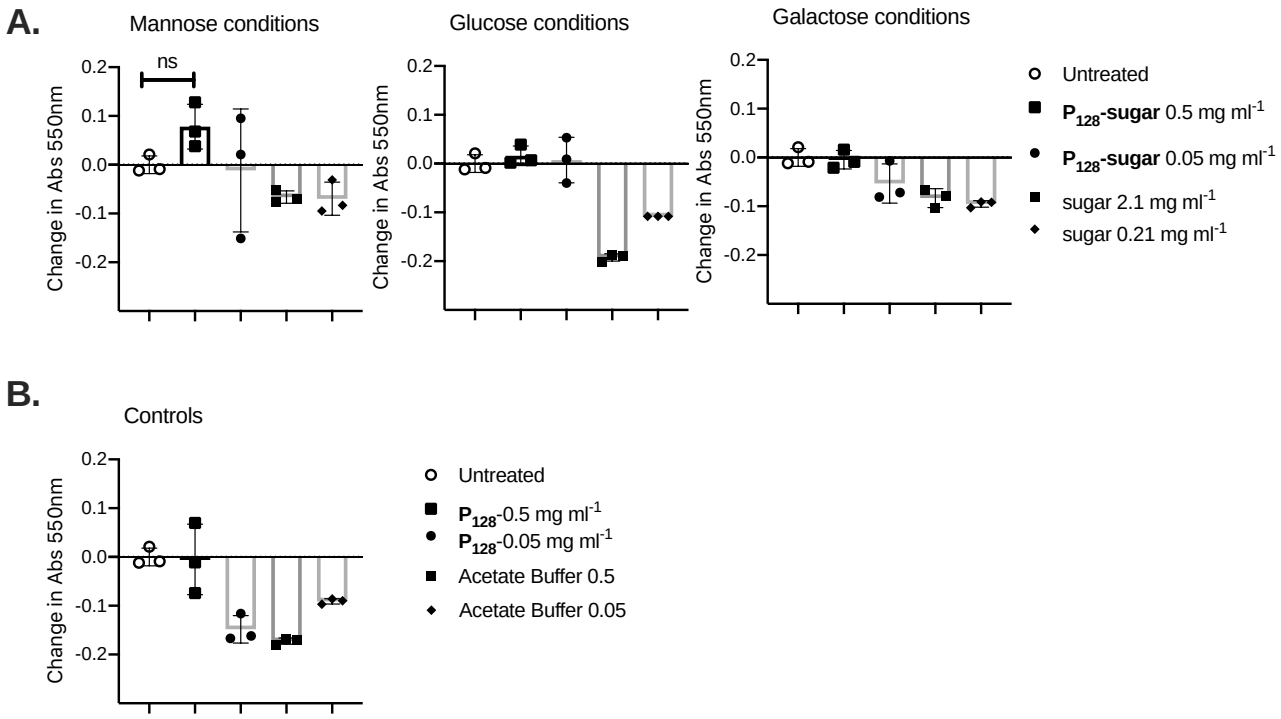

Figure 67. Crystal violet staining for residual biofilm of *V. cholerae* dispersed in clear DMEM incubated for 22 hours at 37 °C with A) glycopolymers prepared in acetate buffer with 2 eq. sugar, and corresponding free sugars and B) polymer scaffold ($\mathbf{P_x}$) and representative concentrations of acetate buffer. Significance was measured using a student's t-test.

The results initially suggested that sugars alone suppressed biofilm in all cases over that of the untreated condition. However, on closer inspection this may have been an effect of the corresponding concentration of acetate buffer, which was also found to negatively impact biofilm formation. Mannose and galactose at 0.5 mg ml^{-1} indicated a recovery of biofilm formation over that of acetate buffer, but glucose displayed suppression in this regard broadly in agreement that glucose suppresses biofilm formation in *V. cholerae* by PTS signaling.[39] Although not statistically significant, but in agreement with our previous results, **P_{128}-MAN** increased the production of biofilm over that of the untreated condition. Increase in biofilm production was especially apparent at 0.5 mg ml^{-1} where the polymer condition displayed increased levels of crystal violet

staining compared to the corresponding mannose, buffer and polymer scaffold controls.

Although more experiments will be required to determine if **P_{128}-MAN** increases biofilm production in *V. cholerae* statistically significantly, it was concluded at this stage that the PTS signaling pathway was likely to be important, and that **P_{128}-MAN** may attenuate this signal possibly through multivalent mannose-specific binding with transmembrane proteins of the PTS system.[4] Further studies would be required to explore this.

3.3.6 Gene expression

Watnick and co-workers demonstrated that genes encoding the PTS are also coregulated with *vps* genes which are involved with the production of biofilm,[40] and with this in mind it was expected that VpsR, the master regulator in the biofilm cascade would be affected if glycopolymers were triggering biofilm formation *via* the PTS system. If this was the case, it was considered that virulence may be attenuated in a similar way to previous observations with cationic polymers (**Chapter 2**).

To this end reporter strains of *V. cholerae* containing promoter regions for *ctxAB*, *vpsR*, *rbmA* and *rbmC* were incubated with glycopolymers, so that expression of the reporter gene could be monitored by production of the enzyme β-galactosidase and its cleavage of ortho-Nitrophenyl-β-galactoside (ONPG) to yellow o-nitrophenol (Abs 420 nm) (**Figure 68**).

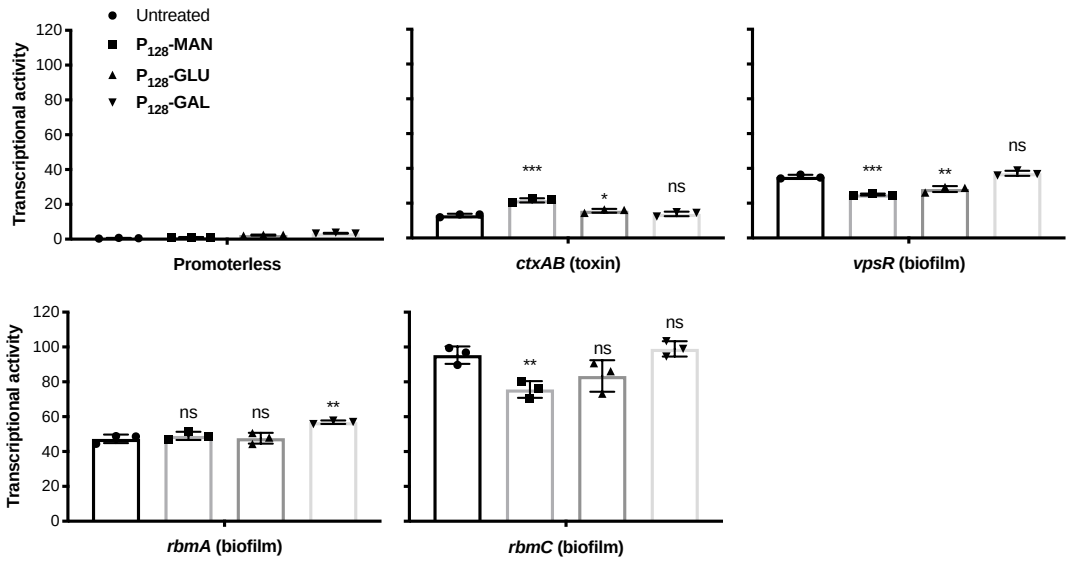

Figure 68. Promoter activities of *ctxAB*- *vpsR*- *rbmA*- *rbmC-lacZ* fusions following incubation at 37 °C with glycopolymers (0.05 mg ml^{-1}) for 5 hours. Significance was calculated using a student's t-test (*=p<0.05).data reported as transcriptional activity (Miller units).

Initially transcriptional activity was evaluated at 5 hours incubation with 0.05 mg ml^{-1} glycopolymers previously shown in this current work to be the time at which maximum transcriptional activity of *ctxAB* is observed in solution (**Chapter 2**). Transcription for these genes indicated that **P_{128}-GAL** had little impact on regulation compared to untreated bacteria, a similar trend to that of biofilm formation and relative growth seen previously. A slight but statistically significant increase in *rbmA* activity after incubation with **P_x-GAL** was observed, notably, RbmA, a scaffolding protein involved with cell-to-cell and cell-to-biofilm adhesion is reported to bind in a specific manner to galactose,[37] and therefore this may indicate a galactose specific response.

Unexpectedly, and contrary to results of crystal violet staining, *vpsR* and *rbmC* was suppressed by both **P_{128}-MAN** and **P_{128}-GLU**, which may have been a result of the chosen time point, despite positive regulation of these genes observed after 5 hours with cationic polymers (**Chapter 3**). Most noticeably, a significant induction of *ctxAB* (CTX) after incubation with **P_{128}-MAN** was observed. We rationalised that

mannose containing glycopolymers may trigger virulence responses in *V. cholerae,* seeing how the mannose binding pilus (MSHA) is linked to transduction of toxin regulation in *V. cholerae.*[41] To investigate further the impact of **P_{128}-MAN** on regulation of the cholera toxin and whether this was a general effect of mannose or specific to the glycopolymer a time course transcriptional assay was conducted (**Figure 69**).

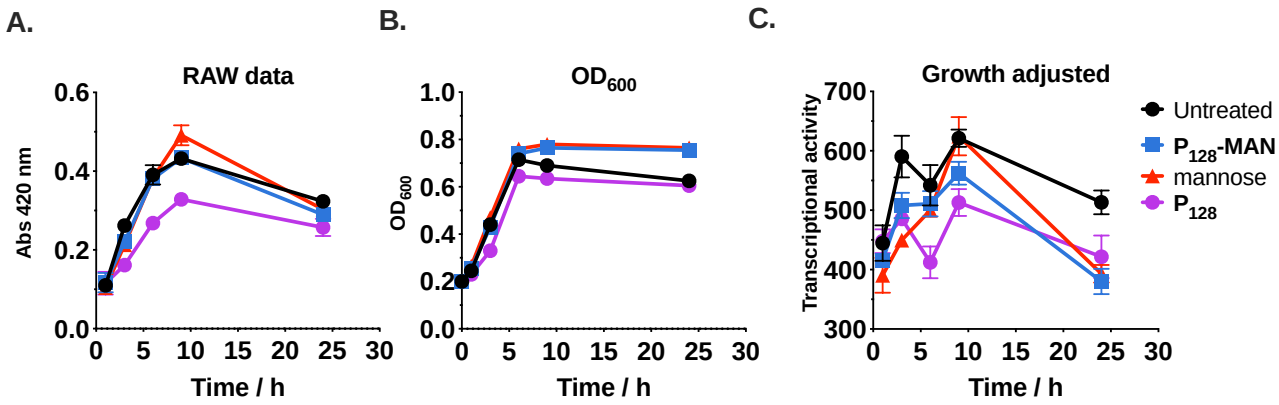

Figure 69. Promoter activities of *ctxAB-lacZ* fusions following incubation at 37 °C with **P_{128}-MAN** (0.05 mg ml^{-1}) at varying time points. A) Raw baseline corrected data Abs 420 nm, B) corresponding OD_{600} of each condition tested, C) growth corrected values (Miller units).

Time course analysis of *ctxAB* expression demonstrated maximum transcription at around 10 hours post incubation, roughly 4 hours after bacterial growth had plateaued according to OD_{600} but in this case there was no evidence that **P_{128}-MAN** could induce production of the cholera toxin. We reasoned that this could be on account of biological variability and that further replicates would need to be conducted to determine if results described in **Figure 68** were reproducible.

3.3.7 Glycoconjugate purification

Seeing how free D-mannose had been shown to decrease the clustering ability of a mannose containing glycopolymer due to saturation of the sugar-binding receptors,[24] it was considered that the free sugar in conditions employed here (due to the *in situ* nature of the screening approach) may be interfering with the activity of the

glycopolymer to a similar extent. To assess the effect of glycopolymer isolation we attempted purification of glycopolymers prepared this time with a **P_{48}** by our usual dialysis method which involved dialysing ~1 mL of a glycopolymer solution (0.25 M with respect to hydrazide groups) against H_2O (5 L) over the course of a week with one water change per day. The resulting mixtures were lyophilized to a white powder and analysed by proton NMR (**Figure 70**).

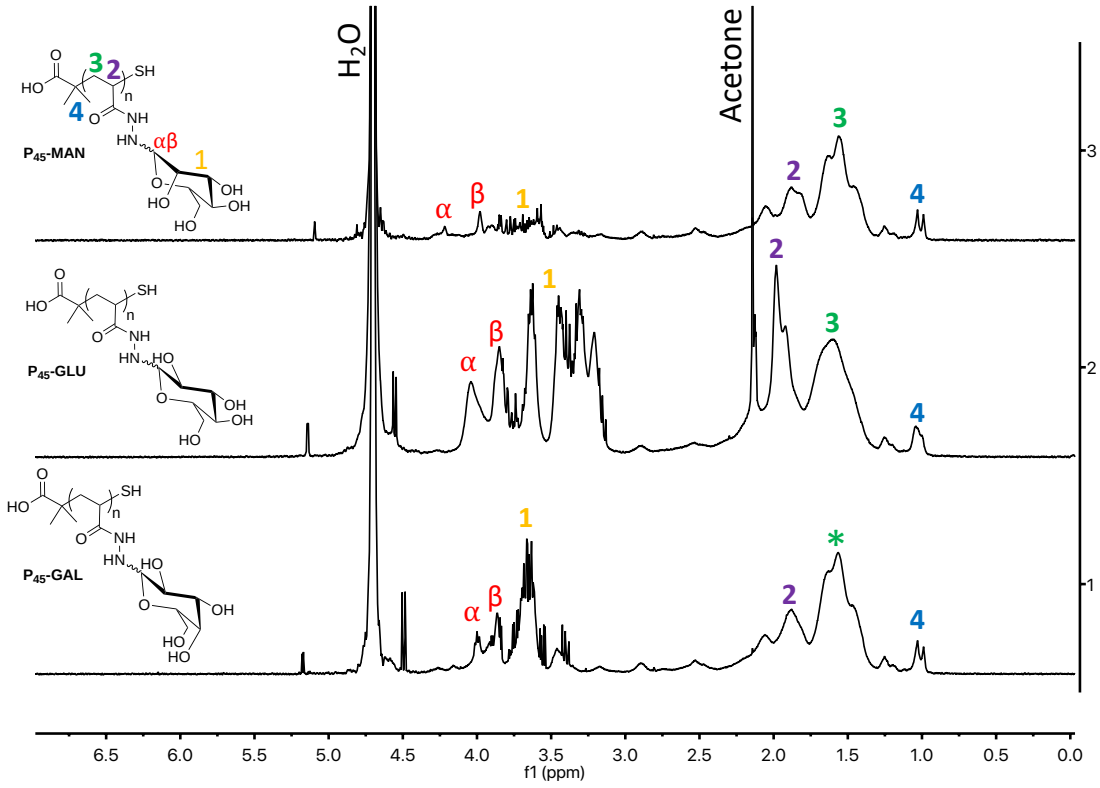

Figure 70. Proton NMR (D_2O) for glycopolymers after dialysis against H_2O (5 L) for one week with one water change per day.

After dialysis loading of sugars on **P_{48}-MAN, P_{48}-GAL** was reduced to just 5%, and 20% respectively indicting that under this degree of dilution, hydrolysis of the glycosidic hydrazone bond was occurring. Interestingly **P_{48}-GLU** retained 55% loading with a loss of just ~5% conjugated glucose. Interestingly, the **P_x** backbone signals were broader for the -CH_2 region but sharper at the -CH region, broadening of the backbone proton signals has been observed also for **P_x-IMI** and **P_x-2A3FP** (**Chapter 3**) and may indicate

altered hydrodynamic radius after post-polymerisation modification, possibly as a result of polymer chain folding or unfolding.[22]

It was rationalised that these differences in levels of hydrolysis of the glycoconjugate are justified by the differences in stability of the closed form of the glycoconjugate sugar, where between 5-10% open form sugars for mannose and galactose conjugates were observed by proton NMR, but only 0-1% for glucose conjugates (**Table 8**) indicative of their greater overall stability. Free sugar in all samples was observed, despite standard dialysis conditions which could indicate further dialysis was required or reflect the dynamic nature of the glyosidic bond. In light of these results, it was concluded that dialysis was not best suited to purifying these materials and instead, purification by SEC could be performed as an alternative.

3.4 Conclusions

The synthesis and characterization of mannose, glucose and galactose glycopolymers *via* post-polymerisation modification of a poly(acryloyl hydrazide) $\mathbf{P_x}$ scaffold has been achieved to universally high degrees of sugar loading under very mild conditions, without the need for catalytic aniline. The suitability of this platform to screen activities using a small library of glycopolymers *in situ* was tested to explore aggregation and physiology of *V. cholerae*. Overall, glycopolymers displayed very low levels of growth inhibition towards *V. cholerae*, but could induce a sharp increase in turbidity in bacterial dispersions after 20 minutes incubation, which is usually associated with the formation of clusters. However, evidence for cluster formation was not found by microscopy indicating that polymer-mediated interactions between bacterial cells may be weak or short-lived. Mannose containing glycopolymers had a pronounced effect on biofilm production, with an increase in biofilm formation observed

in all replicate experiments. Biofilm production was found to be dependent on the type of sugar suggesting that *V. cholerae* was responding to glycopolymers as a result of attenuation of the PTS pathway, which is reported to upregulate biofilm formation in response to mannose availability, and downregulate biofilm formation in response to glucose. Mannose glycopolymers induced increased biofilm production over that of the controls, suggesting that this glycopolymer may interfere with or activate the PTS pathway.

3.5 Future work

Preliminary results suggest that glycopolymers may modulate expression of virulence and biofilm related genes, however further studies are needed to confirm this. In particular the effect of glycopolymers on biofilm gene expression at varying time points should be conducted and may justify the increased biofilm observed in crystal violet after 22 hours.

Work continuing from this study should focus on the purification of these compounds, to evaluate the effect that purified glycopolymers have on clustering, biofilm formation and gene expression. The result of this should determine whether *in situ* screening is appropriate for glycopolymers when competitive binding to the corresponding small molecule may be predicted to mask the activity of the glycopolymer.

On a longer timescale, hydrophobic polymer scaffolds for example $\mathbf{P_x\text{-}IMI_{0.75}}$ (**Chapter 2**) which form mucus-like fibers under physiological conditions, and displayed very high affinity for *V. cholerae*, may be co-functionalised with glycans to prepare a “synthetic mucus” which may result in interesting and potentially useful

physiological changes in bacteria, as was recently reported by Ribbeck and co-workers.[42]

3.6 References

1 Y. A. Millet, D. Alvarez, S. Ringgaard, U. H. von Andrian, B. M. Davis and M. K. Waldor, *PLoS Pathog*, 2014, **10**, e1004405.

2 A. S. Utada, R. R. Bennett, J. C. N. Fong, M. L. Gibiansky, F. H. Yildiz, R. Golestanian and G. C. L. Wong, *Nature Communications*, 2014, **5**, 44.

3 J. K. Teschler, D. Zamorano-Sánchez, A. S. Utada, C. J. A. Warner, G. C. L. Wong, R. G. Linington and F. H. Yildiz, *Nature Reviews Microbiology*, 2015, **13**, 255–268.

4 L. Houot, S. Chang, C. Absalon and P. I. Watnick, *Infect. Immun.*, 2010, **78**, 1482–1494.

5 C. J. Jones, A. Utada, K. R. Davis, W. Thongsomboon, D. Zamorano-Sánchez, V. Banakar, L. Cegelski, G. C. L. Wong and F. H. Yildiz, *PLoS Pathog*, 2015, **11**, e1005068.

6 N. O'Boyle, B. Houeix, M. Kilcoyne, L. Joshi and A. Boyd, *International Journal of Medical Microbiology*, 2013, **303**, 563–573.

7 J. J. Lundquist and E. J. Toone, *Chemical Reviews*, 2002, **102**, 555–578.

8 N. Perez-Soto, L. Moule, D. N. Crisan, I. Insua, L. M. Taylor-Smith, K. Voelz, F. Fernandez-Trillo and A. M. Krachler, *Chem. Sci.*, 2017, **8**, 5291–5298.

9 N. Perez-Soto, O. Creese, F. Fernandez-Trillo and A. M. Krachler, *ACS Chem. Biol.*, 2018, **13**, 3021–3029.

10 S. G. Spain, M. I. Gibson and N. R. Cameron, *J. Polym. Sci. A Polym. Chem.*, 2007, **45**, 2059–2072.

11 V. Ladmiral, G. Mantovani, G. J. Clarkson, S. Cauet, J. L. Irwin and D. M. Haddleton, *J. Am. Chem. Soc.*, 2006, **128**, 4823–4830.

12 S. A. Loskot, J. Zhang and J. M. Langenhan, *J. Org. Chem.*, 2013, **78**, 12189–12193.

13 B. Bendiak, *Carbohydrate Research*, 1997, **304**, 85–90.

14 W. Plazinski, A. Plazinska and M. Drach, *Phys. Chem. Chem. Phys.*, 2015, **17**, 21622–21629.

15 D. N. Crisan, O. Creese, R. Ball, J. L. Brioso, B. Martyn, J. Montenegro and F. Fernandez-Trillo, *Polym. Chem.*, 2017, **8**, 4576–4584.
16 K. Godula and C. R. Bertozzi, *J. Am. Chem. Soc.*, 2010, **132**, 9963–9965.
17 A. Dirksen, S. Dirksen, T. M. Hackeng and P. E. Dawson, *J. Am. Chem. Soc.*, 2006, **128**, 15602–15603.
18 D. K. Kölmel and E. T. Kool, *Chemical Reviews*, 2017, **117**, 10358-10376.
19 J. Pauluhn, *Toxicological Sciences*, 2004, **81**, 198–215.
20 M. U. Roslund, P. Tähtinen, M. Niemitz and R. Sjöholm, *Carbohydrate Research*, 2008, **343**, 101–112.
21 E. Erez, D. Fass and E. Bibi, *Nature*, 2009, **459**, 371–378.
22 J. Engelke, J. Brandt, C. Barner-Kowollik and A. Lederer, *Polym. Chem.*, 2019, **10**, 3410–3425.
23 J. Kalia and R. T. Raines, *Angewandte Chemie International Edition*, 2008, **47**, 7523–7526.
24 M. D. Disney, J. Zheng, T. M. Swager and P. H. Seeberger, *J. Am. Chem. Soc.*, 2004, **126**, 13343–13346.
25 X. Xue, G. Pasparakis, N. Halliday, K. Winzer, S. M. Howdle, C. J. Cramphorn, N. R. Cameron, P. M. Gardner, B. G. Davis, F. Fernandez-Trillo and C. Alexander, *Angewandte Chemie International Edition*, 2011, **50**, 9852–9856.
26 L. L. Foster, S.-I. Yusa and K. Kuroda, *Antibiotics*, 2019, **8**, 61–16.
27 P. Selvaraj, R. Gupta and K. M. Peterson, *SOJ Microbiol Infect Dis*, 2015, **3**, 1–9.
28 G. Jonson, J. Holmgren and A.-M. Svennerholm, *Microbial Pathogenesis*, 1991, **11**, 433–441.
29 D. Sasmal, B. Guhathakurta, A. N. Ghosh, C. R. Pal and A. Datta, *FEMS Immunology & Medical Microbiology*, 1999, **23**, 221–227.
30 S. Raddatz, *Nucleic Acids Research*, 2002, **30**, 4793–4802.
31 P. R. Secor, L. A. Michaels, A. Ratjen, L. K. Jennings and P. K. Singh, *Proc Natl Acad Sci USA*, 2018, **115**, 10780–10785.
32 J. Yan, A. G. Sharo, H. A. Stone, N. S. Wingreen and B. L. Bassler, *Proc. Natl. Acad. Sci. U.S.A.*, 2016, **113**, E5337–E5343.
33 A. Hoštacká, I. Čižnár and M. Štefkovičová, *Folia Microbiol*, 2010, **55**, 75–78.
34 C. M. Waters, W. Lu, J. D. Rabinowitz and B. L. Bassler, *Journal of Bacteriology*, 2008, **190**, 2527–2536.

35 G. A. O'Toole, *JoVE*, 2011, 1–2.

36 J. C. N. Fong, K. A. Syed, K. E. Klose and F. H. Yildiz, *Microbiology*, 2010, **156**, 2757–2769.

37 M. Maestre-Reyna, W.-J. Wu and A. H. J. Wang, *PLoS ONE*, 2013, **8**, e82458–10.

38 A. J. Silva and J. A. Benitez, *PLoS Negl Trop Dis*, 2016, **10**, e0004330.

39 L. Houot and P. I. Watnick, *Journal of Bacteriology*, 2007, **190**, 311–320.

40 S. Moorthy and P. I. Watnick, *Molecular Microbiology*, 2005, **57**, 1623–1635.

41 J. Campos, E. Martínez, K. Marrero, Y. Silva, B. L. Rodríguez, E. Suzarte, T. Ledón and R. Fando, *Journal of Bacteriology*, 2003, **185**, 7231–7240.

42 K. M. Wheeler, G. Cárcamo-Oyarce, B. S. Turner, S. Dellos-Nolan, J. Y. Co, S. Lehoux, R. D. Cummings, D. J. Wozniak and K. Ribbeck, *Nature Microbiology*, 2019, **7**, 3–12.

Chapter 4

Synthesis and biological application of well-defined fluorescent polymer scaffolds

4.1 Background

Fluorescence is an extremely important photochemical property whereby fluorescent molecules (fluorophores) absorb light (for example in the UV region), and then emit at a different, lower energy, resulting in the emission of longer wavelengths, often in the visible region. Absorption (λ_{ex}) and emission (λ_{em}) wavelengths depend on, and are specific to the fluorophore in question, and light emitted from these molecules can be detected at very low abundance, down to single molecule detection depending on the brightness of the fluorophore and detector.[1,2] Fluorophore brightness, and thus the sensitivity of detection, governed by its molar extinction coefficient ε, and its quantum yield Φ, describes the amount of absorbed light by the fluorophore and the efficiency of the emission respectively.[3]

4.1.1 Fluorescence labelling in biology

In biochemical research, the properties of fluorescent molecules make them ideal probes or labels in chemical sensing and optical imaging applications. Such applications include mapping DNA sequences,[4,5] single molecule imaging of complex biological processes in real time,[6,7] activity and mechanism in drug delivery,[8,9] and in sensing of biomolecules.[10]

Linear polymers and nanoparticles are extensively researched for biological applications in the field of nanomedicine,[11] and as such, new ways of covalently attaching fluorophores to macromolecules are now widely reported.[12] Fluorescent labelling of macromolecules can reveal mechanisms of activity and location within a biological setting,[13] which can otherwise be hard to predict from first principles.[14] Macromolecules such as polymers are deemed especially well-suited to fluorescent labelling as the fluorescent label is considered to account for a small chemical and

physical “footprint” on the overall properties and activity of the macromolecule.[15] That being said, fluorescent labelling of shorter flexible polymers with bulky and hydrophobic fluorophores is predicted to have an unavoidable impact on the chemical and physical properties of the polymer as has been reported. [15,16] Therefore critically assessing the impact of the fluorescent label on the activity of the macromolecule is an important and often overlooked design parameter. With this in mind, quantifying and controlling the degree of polymer labelling as well as the location of the label with respect to the polymer is highly desired and can help towards standardising potential effects arising from heterogenous labelling.[16]

The preparation of fluorescent polymers is highly attractive given their potential biological applications, and can be accessed *via* a variety of synthetic routes. Fluorescent polymers can broadly be classed into three groups on account of the location of the fluorophore (**Figure 71**).

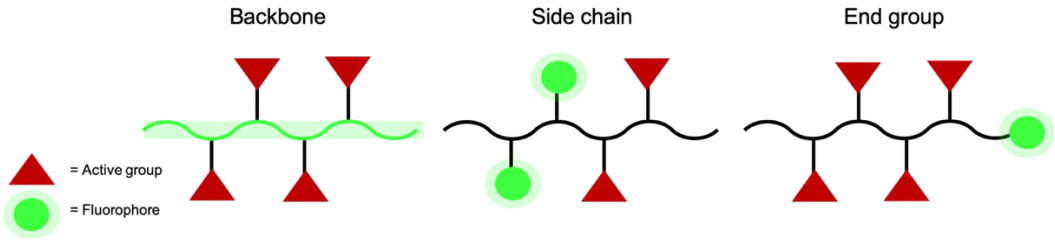

Figure 71. Simplified representative strategies for fluorescent polymer design.

4.1.2 Fluorescent conjugated polymers.

Polymers containing fluorescent conjugated backbones allow access to materials whereby fluorescence is an intrinsic property of the polymer without the need for further modification or evaluation. The first and simplest example of a fluorescent conjugated polymer backbone is that of poly(acetylene), however the synthesis of more extensively conjugated systems have led to the preparation of cationic polymers and glycopolymers capable of simultaneous bacterial imaging and clustering.[17-19]

There are inherent challenges associated with the synthesis of fluorescent conjugated polymers which can make them unsuitable in some applications. These include incompatibility with controlled polymerisation techniques used for alkene monomers, relying rather, on the use of transition metal catalysts such as W, Rh and Mo in their preparation,[20] and controlling both fluorescent and functional properties of the polymer independently.[21]

4.1.3 Side-chain modification

The modification of polymer side chains to incorporate a fluorescent molecule is a very popular labelling strategy, owing to its applicability to a wide range of polymers. This can be achieved by direct copolymerisation with a fluorescent monomer,[22] or employing monomers capable of undergoing subsequent chemo-selective post-polymerisation modification with a fluorescent compound possessing compatible conjugation chemistry, in co- and homo-polymerisations (**Figure 72**).[23,24]

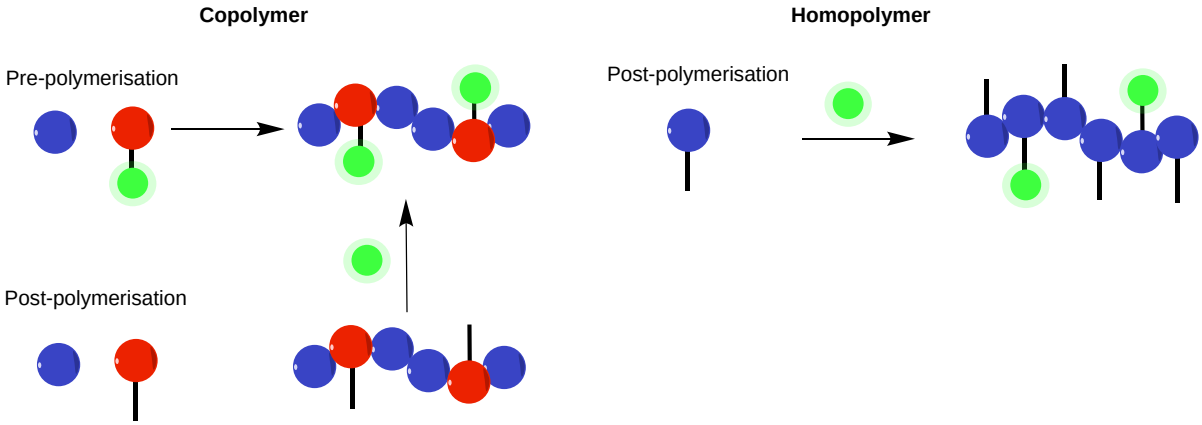

Figure 72. Polymer side-chain fluorescent labelling strategies.

Robin and O'Reilly recently described an elegant synthetic route to controlled and responsive side-chain fluorescence in polymethacrylates by the direct copolymerisation of monomers containing fluorescent dithiomaleimide or non-fluorescent dibromomalemide, the latter of which could be converted to fluorescent

dithiomaleimide *via* a thiol-exchange reaction.[25] To aid with polymer-bacteria colocalization, fluorescent cationic polymers have been prepared by the post-polymerisation modification of a tertiary amine containing homopolymer with a carboxylic acid coumarin dye, mediated by 2-bromo ethyl ester,[24] while fluorescent glycopolymers were prepared by CuAAc of an alkyne-containing homopolymer with azide-derivatized Fluorescein and mannose.[24,26]

4.1.4 End group modification

Polymer end groups are often chemically distinct from main chain monomer groups, and this can allow for specific fluorescent labelling of the end group, achieved either pre or post-polymerisation, in a similar way to side-chain modification (**Figure 73**).

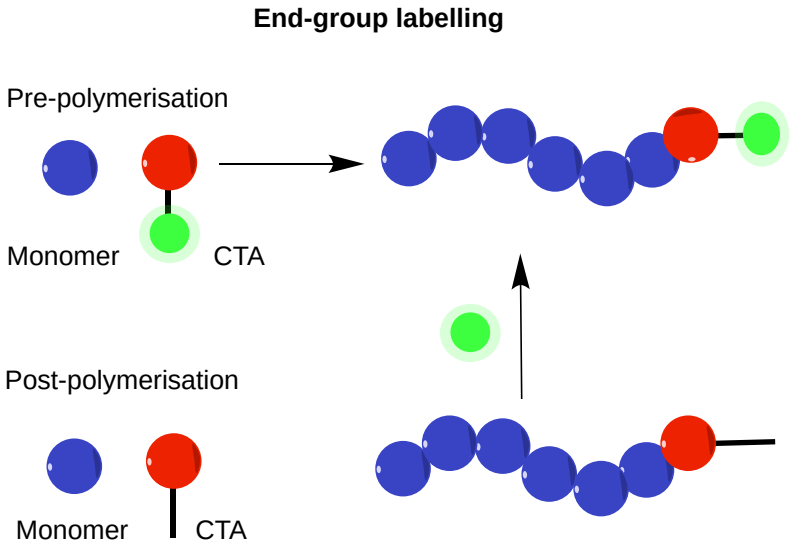

Figure 73. Polymer end group fluorescent labelling strategies.

Rather than the use of a fluorescent monomer (as with side-chain modification), pre-polymerisation strategies rely on the use of fluorescently modified chain transfer agents (CTA),[27] which control the polymer molecular mass and reside in the end groups of the resulting polymer. One of the most important classes of CTAs are

Reversible addition-fragmentation chain transfer (RAFT) agents which offer significantly improved control over the polymer dispersity and molecular mass, as well as affording very good retention of the fragmented RAFT agent at the end groups of the resulting polymer.[28,29] Employing a fluorescent RAFT agent is one strategy to achieve end group fluorescent labelling of a polymer, although this can be challenging due to stringent chemical requirements of the RAFT agent with respect to compatibility with the monomer to afford a controlled radical polymerisation process.[29,30] Despite this, fluorescent RAFT agents have been successfully synthesised,[31] and reported for some monomers, one example, in the polymerisation of poly tertbutyl acrylate, poly methyl methacrylate and triethyleneglycol monomethyl ether acrylate. In this case the RAFT agent was conjugated to dibromomaleimide and could be converted post-polymerisation to fluorescent dibromomaleimide by simple conjugate addition of a thiol.[32]

The alternative strategy to end group fluorescent labelling lies in post-polymerisation end group modification and provides a route to fluorescently label the end group without the need to modify the choice of CTA. Well-defined end-groups as is the case for RAFT derived polymers, can be modified to yield polymers with new chemical handles, for example, reduction of RAFT agents to give thiol functionality affords the potential to undergo subsequent modifications such as thiol-ene and disulfide formation.[33] McCormick and co-workers demonstrated end group labelling of polyNIPAM synthesised by RAFT after reduction of the trithicabonate with $NaBH_4$ to the thiol, and subsequent thio- maleimide coupling with *N*-(1-pyrenyl)Maleimide.[34] End group labelling *via* post-polymerisation modification suffers from additional reaction and purification steps, each requiring characterization. However, this strategy does

allow for greater versatility over the choice of fluorescent dye, and does not impact on the polymerisation process itself.

4.1.5 Summary

Aside from polymers possessing fluorescent backbones, fluorescent polymers can be prepared *via* covalent conjugation of fluorescent dyes with compatible chemical groups on the side-chain or end group of the polymer. Labelling can be carried out pre-polymerisation or post-polymerisation, the latter, extending the versatility of the material, but generally requiring additional synthetic and purification steps. Side-chain labelling benefits from the ability to tune the amount of fluorophore on the polymer, for example, increasing the number of fluorescent molecules with increasing degree of polymerisation (DP). However, side-chain modification can result in greater uncertainty over the precise location of the fluorophore on the polymer chain, which may have implication in regards to its application. End group modification affords the possibility to fluorescently label a polymer without impacting on the chemistry of the side-chain which can be particularly important for polymer scaffolds designed to undergo subsequent post-polymerisation modifications. A drawback of this strategy is the inability to tune the amount of fluorophore on the polymer, which in the case of higher DPs could result in lower relative brightness compared with polymers of smaller DP.

Independent of the labelling method, the purity, stability and impact that the fluorescent dye has on the activity of the compound needs to be taken into consideration. This is especially important if designing polymers for quantitative analysis by fluorescence. In all cases, efficient predictable chemistries such as click chemistry when matched with controlled polymerisations and robust characterisation

methods can negate some of the uncertainties associated with preparing these materials.

4.2 Objectives

The primary objective in this chapter was to develop a convenient synthetic route and assaying method for efficient and quantifiable end group labelling of previously reported poly(acryloyl hydrazide) ($\mathbf{P_x}$) scaffold. In this way, labelling of iterations of these scaffolds can be tightly controlled such that the loading degree of the fluorescent dye on the polymer can be quantified and easily reproduced. End group labelling of $\mathbf{P_x}$ offers a simple route to multi-coloured variants from the same parent polymer which are then able to undergo subsequent post-polymerisation modifications. Predictable end group labelling in this way will allow for quantifiable screening of polymer chemistries by fluorescence for a wide range of biological application.

A secondary objective was to demonstrate *via* fluorescence, the location the polymers involved with the aggregation of bacteria in biological assays, in order to better understand the role of the bacteria-polymer interaction.

4.3 Results and Discussion

Cationic polymers such as poly(*N*-(3-aminopropyl) methacrylamide) (**P1**) and poly(*N*-[3-(dimethylamino) propyl] methacrylamide) (**P2**) induce rapid clustering of *V. cholerae,*[35] which is driven by multivalent electrostatic interactions between the positively charged polymer and the negatively charged bacterial cell membrane.[36] The mechanism for the interaction between polymer and bacteria is unknown and it is not clear if the polymer exists solely between bacterial cells or whether it crosses the cell membrane. In order to identify the location of the cationic polymer within clusters of

bacteria, **P1** was synthesised and purified according to our previously reported methods,[35] and fluorescently side-chain labelled using commercially available CF405S (Biotium) used in biology for labelling proteins *via* amine linkage resulting in the random co-polymer **LP1 (Scheme 8)**.

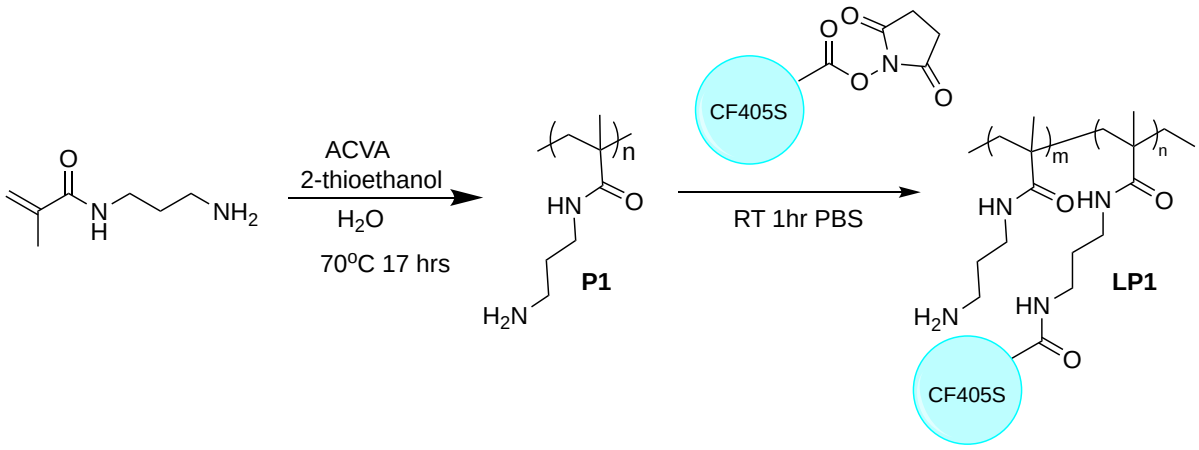

Scheme 8. Synthetic route for poly(N-(3-aminopropyl) methacrylamide) (**P1)** and resulting fluorescent random co-polymer after post-polymerisation modification with CF405S dye (**LP1**).

CF405S was employed here due to its ability to be excited by the 405 nm laser and emit in the blue region (461 nm), making it suitable to use alongside SYTO 9 and propidium iodide (PI) which are commonly used to stain live and dead bacteria. To this end, we evaluated the colocalisation of clusters of *V. cholerae* and cationic polymer **LP1 (Figure 74).**

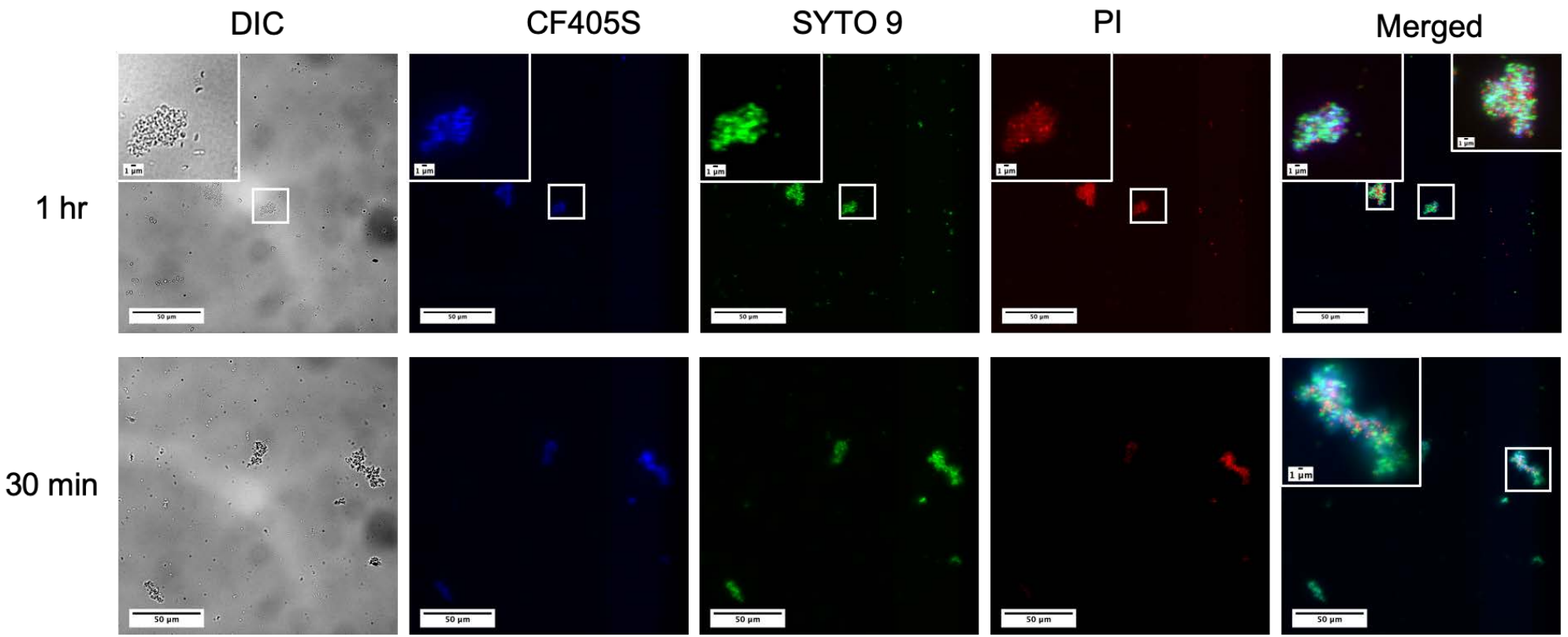

Figure 74. Optical images (63 x oil objective) of *V. cholerae* after incubation with 0.05 mg ml^{-1}**LP1** (Blue)**.** Bacteria were LIVE/DEAD stained with Propidium iodide (PI) (Red) and SYTO 9 (Green) prior to fixing onto the microscope slide.

Images displayed colocalisation of blue (CF405S) channel with green (SYTO 9) and red (PI) channels in the case of bacterial clusters, indicating that the labelled polymer is indeed associated with the formation of bacterial aggregates and supports the hypothesis that bacterial aggregates are mediated by cationic polymers.

Although using a dye labelling kit in this way can give very good results with regards to brightness and photostability, there is limited control available over the chemistry and quantification of the conjugation with **P1** and the exact chemical structure of CF405S is not freely available.

Having demonstrated the merit of employing fluorescence to determine polymer location in the case of polymer-mediated bacterial clustering, we next sought to fluorescently label Boc-protected poly(acryloyl hydrazide) **boc-P_x** in an efficient and quantifiable manner, so that better control over the labelling could be achieved, without impacting on the polymers ability to undergo aldehyde-hydrazide post-polymerisation modification on deprotection to **P_x**.

Building on our work in chapter 1 towards improving the control over the synthesis of **boc-P_x**, thus increasing its versatility further, we set out to develop an optimised synthetic route and characterisation assay in order to install a linker capable of conjugating different fluorescent dyes in a simple, controlled, and reproducible manner (**Scheme 9**).

4.3.1 Overall synthetic strategy.

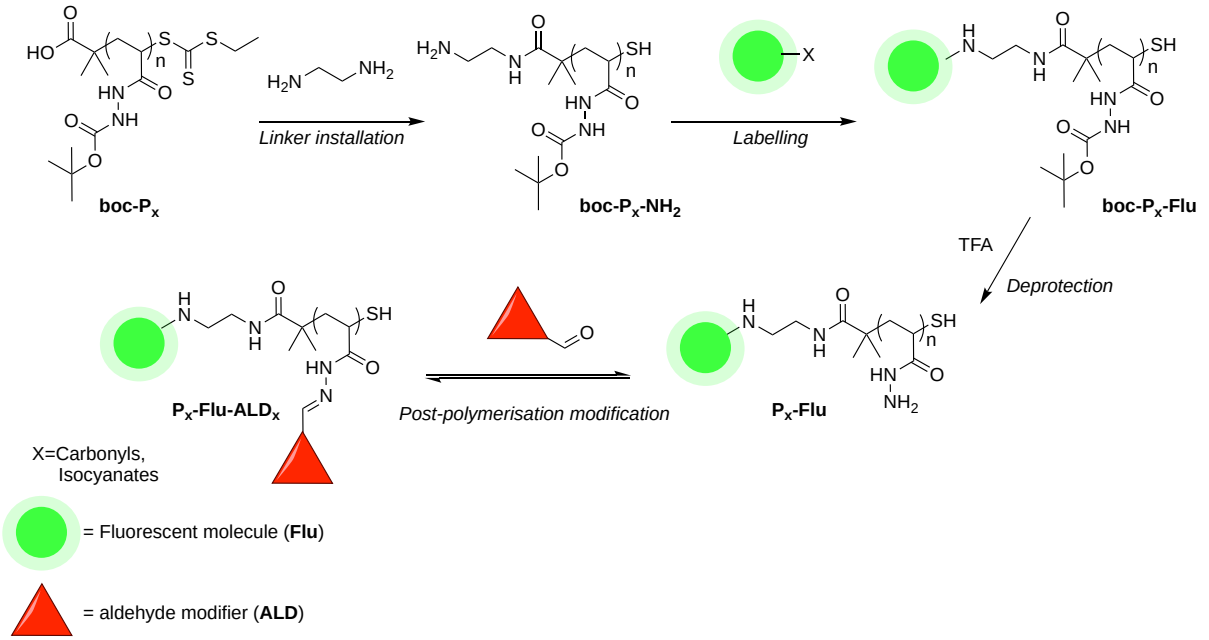

Scheme 9. Proposed synthetic route towards fluorescently labelled $\mathbf{P_x}$ ($\mathbf{P_x}$**-Flu**) and subsequent post-polymerisation modification of $\mathbf{P_x}$**-Flu** with aldehydes.

4.3.2 Installation of ethylene diamine (EDA) linker

The end group fidelity of polymers synthesised by RAFT, allowed for a convenient chemical handle for which to undergo further modification such as fluorescent labelling, and in the case of **boc-P$_x$**, The trithiocarbonate containing Z group of RAFT agent (**CTA**) can be easily reduced to yield a thiol end group which can be further modified *via* maleimide derivatives.[34] However, previous initial work in the group exploring this route demonstrated poor labelling efficiency, which was attributed to the reversibility of the maleimide-thiol conjugate bond during the deprotection step in TFA. Therefore, focus was set on an alternative labelling strategy towards transformation of the carboxylic acid end group functionality of **boc-P$_x$** to amine functionality **boc-P$_x$-NH$_2$** (**Scheme 9**), affording a route to labelling of the polymer with more readily available dyes such as those containing carboxylic acid and aldehyde group chemical handles. Another consideration was that by preservation of the thiol containing end-group, could

be this chemistry could be utilised in future applications for the modification of gold nanoparticles,[37,38] or surfaces (**Scheme 10**).[39]

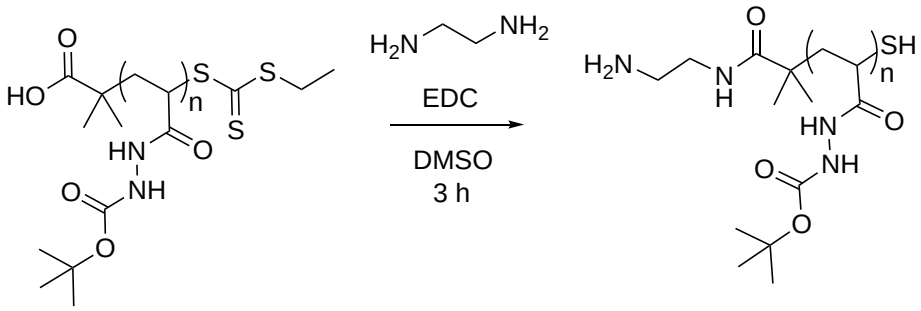

Scheme 10.Synthetic route for the installation of EDA linker group to the carboxylic acid end group of **boc-P_x** to afford **boc-P_x-NH_2**.

During the synthesis, of **boc-P_x-NH_2**, a large excess of EDA was used, typically 1000 equivalents, in order to avoid cross linking of the polymer chains, and purification of the compound was carried out by dialysis with a 1 kDa cut-off with regular water changes over the course of a week. The modified polymer was obtained by lyophilisation to yield a white powder with good mass retention (90 %). All traces of the pale-yellow colour of the starting material were lost which indicated that that the trithiocarbonate end group had been cleaved by addition of the EDA. It was important to assess the purity of the polymer for traces of EDA which had not removed during the dialysis step, in this regard proton NMR was carried out to evaluate the presence of the proton signal for EDA represented as a singlet (2.47 ppm) in DMSO-d6 (**Figure 75**).

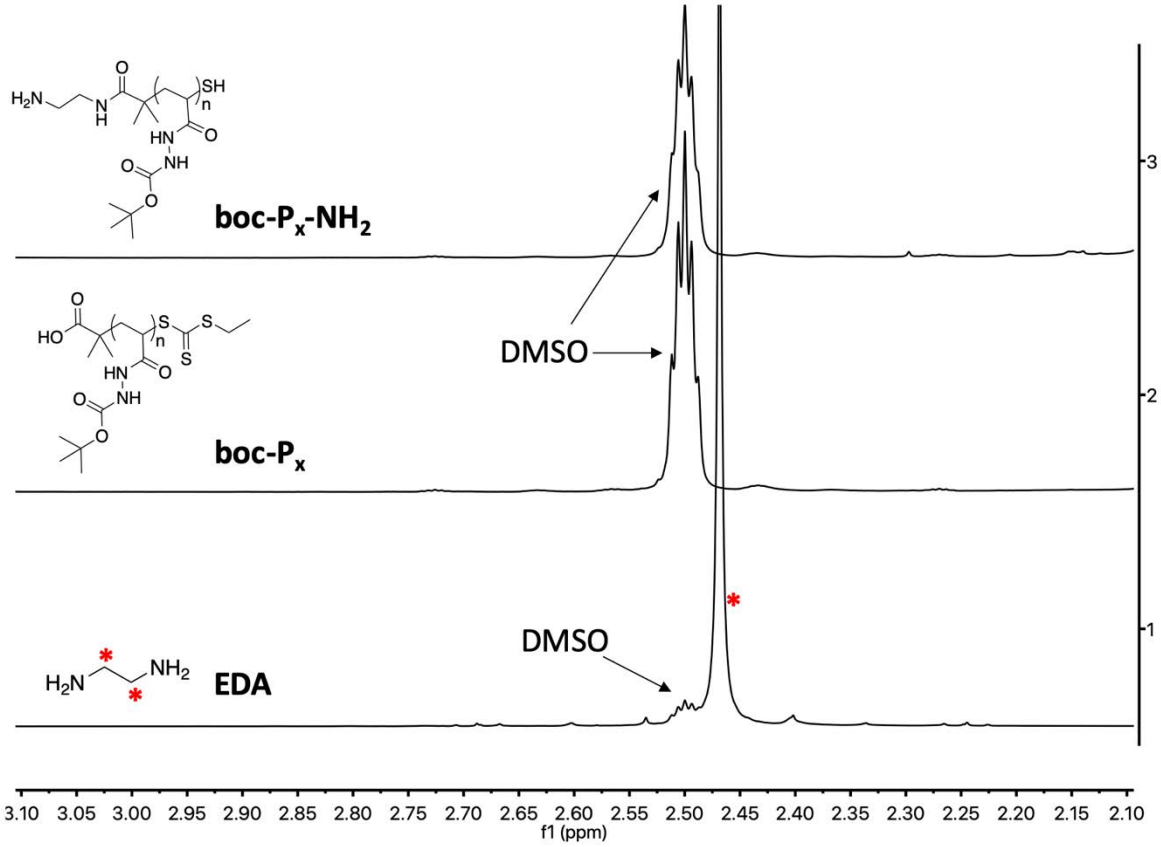

Figure 75. Proton NMR for EDA showing CH_2 signals at 2.47 ppm (bottom) and representative proton NMR for EDA modified **boc-P_x** after purification showing no trace of residual EDA protons (top). Representative NMR for the corresponding un-modified **boc-P_x-NH_2** (middle). * indicates proton signals for EDA.

No trace of unreacted EDA was observed at 2.47 ppm in the proton NMR for **boc-P_x-NH_2** after purification, suggesting complete removal of the free diamine by this method.

At this stage we evaluated whether treatment with EDA could cause structural changes in the polymer, possibly as a result of crosslinking between primary amines and carbonyls on the polymer backbone, or between modified and un-modified end-groups despite the use of excess amine. In order to evaluate this, purified **P_x**, was analysed by GPC, both prior to, and after reaction with EDA (**Figure 76**).

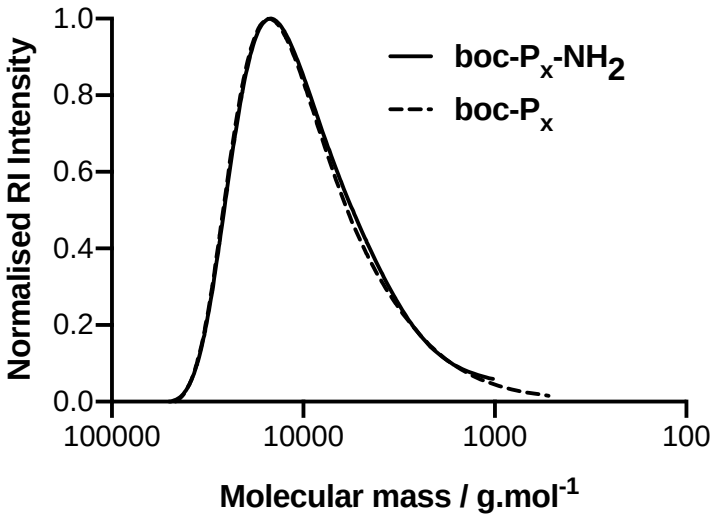

Figure 76. Representative GPC trace (DMF LiBr 0.05 M) for **boc-P$_x$** (DP55) before (dashed line) and after (solid line) reaction with EDA.

Modification with EDA is associated with a theoretical net loss of 62 g mol^{-1} due to the cleavage of the trithiocarbonate group, which was expected to be too small to be detected by gel permeation chromatography (GPC), however shifts in retention time towards larger molecular masses, and broader mass distributions ($Đ_m$), could indicate that cross-linking was occurring. Pleasingly, no change in the appearance of the GPC trace was observed for this modification step.

Table 10. Molecular mass data for **boc-P$_{55}$** and **boc-P$_{55}$-NH$_2$**.

Entry	^{a}DP$_{(NMR)}$	^{b}M$_{p(theo)}$	^{c}M$_{n(GPC)}$	^{c}Mw$_{(GPC)}$	$Đ_M$
boc-P$_{55}$	55	10468	9331	14877	1.59
boc-P$_{55}$-NH$_2$	55	10406	9383	14943	1.59

^{a}Degree of polymerisation calculated by proton NMR, ^{b} theoretical molecular mass estimated from monomer conversion, ^{c} Number average and weight average molecular mass calculated by GPC (DMF LiBr 0.05 M) (g.mol^{-1}).

GPC data indicated that no significant structural change had occurred during the synthesis of **boc-P$_{55}$-NH$_2$** and with this in mind we proceeded to investigate whether new peaks associated with the installation of EDA on the polymer could be detected and quantified by proton NMR (**Figure 77**).

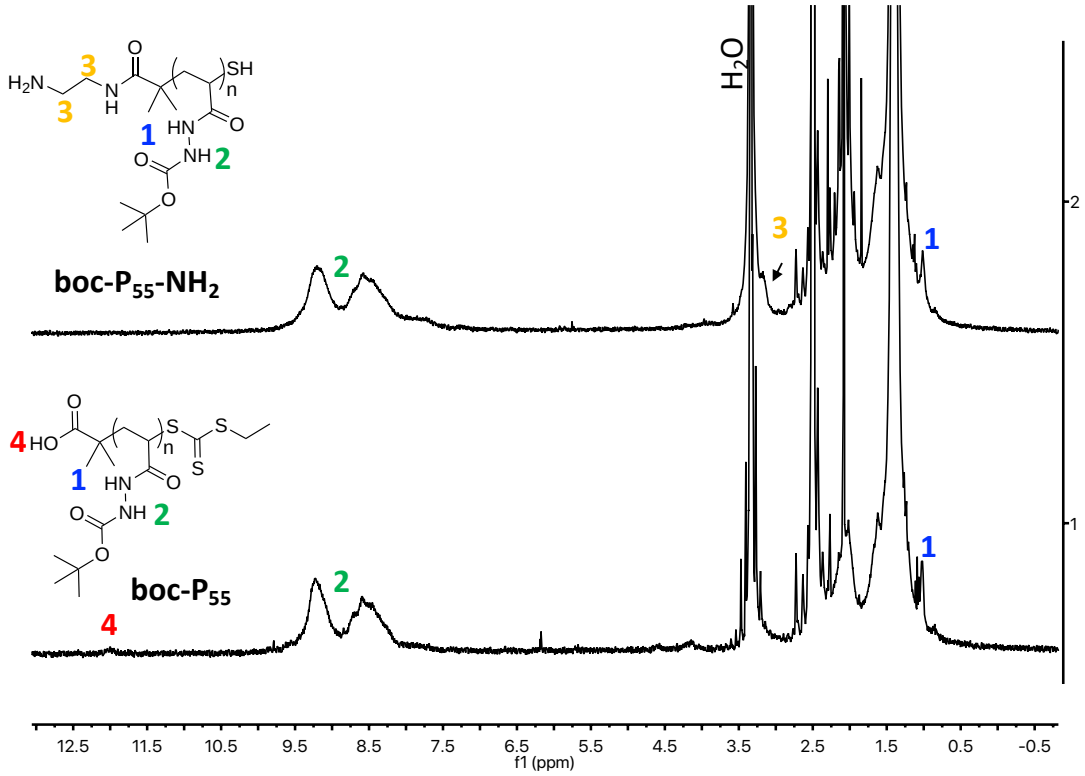

Figure 77. Proton NMR in DMSO 6d for unmodified **boc-P$_x$** (bottom) and EDA modified **boc-P$_x$-NH$_2$** (top) with new broad region visible at 3.17 ppm (3).

Proton NMR revealed new broad peaks for **boc-P$_{55}$-NH$_2$** at 3.17 ppm (**Figure 77**, top, 3) which was broadly in-line with predicted values for a small molecule analogue containing two peaks; 3.46 and 2.81 ppm. The new signal displayed an integration of 2.41 protons compared with the terminal dimethyl group at 1.0 ppm (**Figure 77**, 1) (6 protons). The disappearance of a smaller broad peak at 12 ppm (**Figure 77**, 4) visible in the proton NMR for **boc-P$_{55}$** was observed, which was assigned as the terminal hydroxyl proton, displaying an integration of 0.87 compared to the terminal dimethyl group at 1.0 ppm (6 protons). EDA modification could be better observed by proton NMR in $CDCl_3$ allowing for an estimate of EDA loading by integration of the broad signal at 3.2 ppm against the dimethyl end groups for a **P$_x$** with a theoretical DP44 (**Figure 78**).

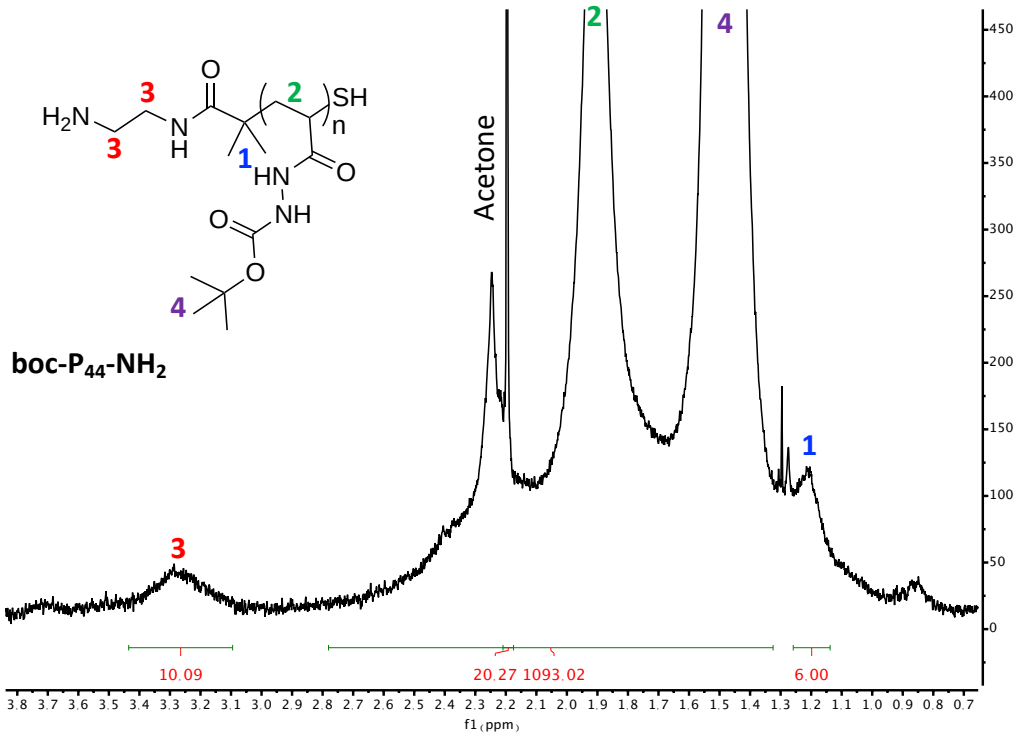

Figure 78. Proton NMR ($CDCl_3$) for **boc-P_{44}-NH_2**.

Integration of the new signal at 3.25 ppm (**3**) against the dimethyl end group of the polymer (**1**) appeared to overestimate the loading at over 250 %, and we reasoned that this was likely due to the broadness of the peaks and overlapping regions resulting in a high degree of error.

While proton NMR provided encouraging evidence that the end group modification with EDA had been successful given the appearance of a new broad signal around 3.2 ppm, it was concluded that NMR was not a reliable measure of the degree of EDA loading. With this in mind the use of an alternative method to quantify the number of amines on the polymer and hence, the efficiency of the end group modification reaction was explored. In this regard, a Fluram assay which employs fluorescamine (Fluram) as a chemical probe for amines, was explored as a potential route to quantify the number of primary amines on the polymer by fluorescence.

Fluram is commonly used to quantify primary amines present on proteins and amino acids in biology,[40] the detection of small biomolecules,[41] and more recently for the quantification of primary amines in polymers and polymer nanoparticles.[42,43] The Fluram assay relies on non-fluorescent compound fluorescamine, which reacts rapidly at room temperature with primary amines to yield highly fluorescent compounds (λ_{ex} 390 nm, λ_{em} 475 nm) (**Scheme 11**).[44]

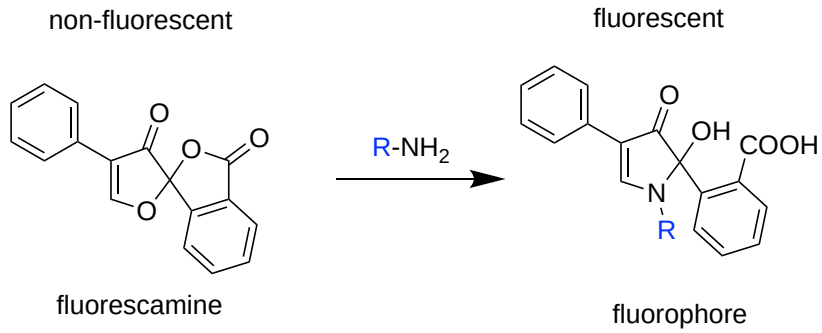

Scheme 11. Structural change in fluorescamine on reaction with primary amines to yield the corresponding fluorophore.

Primary amine concentration can be quantified in the picomole range with low background, owing the non-fluorescent starting material (Fluram) and hydrolysis products.[44] Fluorescamine is inexpensive and as such, the Fluram assay is a cost-effective tool which can be applied to high throughput style microplate assays.[45] Firstly, parameters such as a suitable calibration standard, reaction conditions and excitation and emission wavelengths were investigated so as to best apply this assay for our system and provide optimal reproducibility and accuracy. Calibration curves were carried out using a model amine containing small molecule, *tert*-Butyl N-(2-aminoethyl) carbamate (**boc-NH_2**), which displayed a linear relationship between [**boc-NH_2**] and emission intensity λ_{max} in the range 1 μM and 15 μM.

In order to be confident of optimal λ_{ex} and λ_{em} for our model amine **boc-NH$_2$**, emission was monitored using a spectrofluorometer at different excitation wavelengths for **boc-NH$_2$** after incubation with Fluram (**Figure 79**).

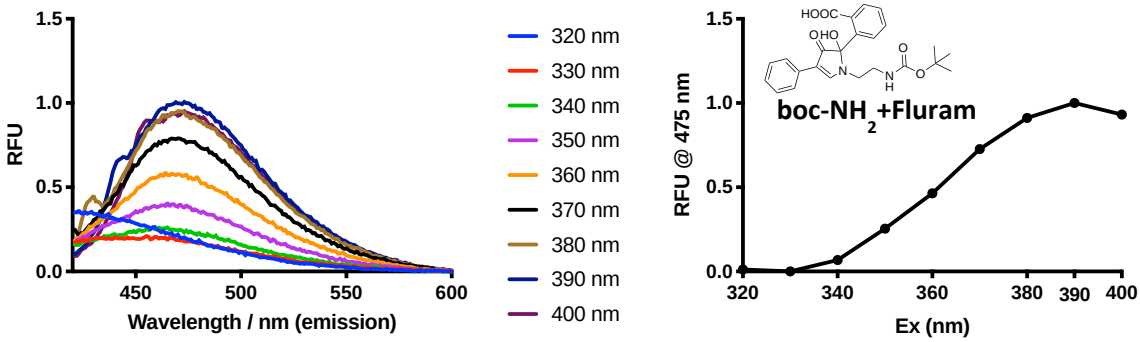

Figure 79. left: Fluram (12.4 μM) emission spectrum after reaction with **boc-NH$_2$** (6.22 μM) at varying emission wavelengths.

Optimal emission was observed at 475 nm with an excitation of 390, and these parameters were then reassessed using a CLARIOstar plus (BMG Labtech) microplate reader for both **boc-NH$_2$** and EDA modified polymer (**boc-P$_x$-NH$_2$**) to establish the suitability of the plate reader for this application and simultaneously evaluate differences between fluorescent signals originating from the small molecule model amine, and from the amine-containing polymer (**Figure 80**).

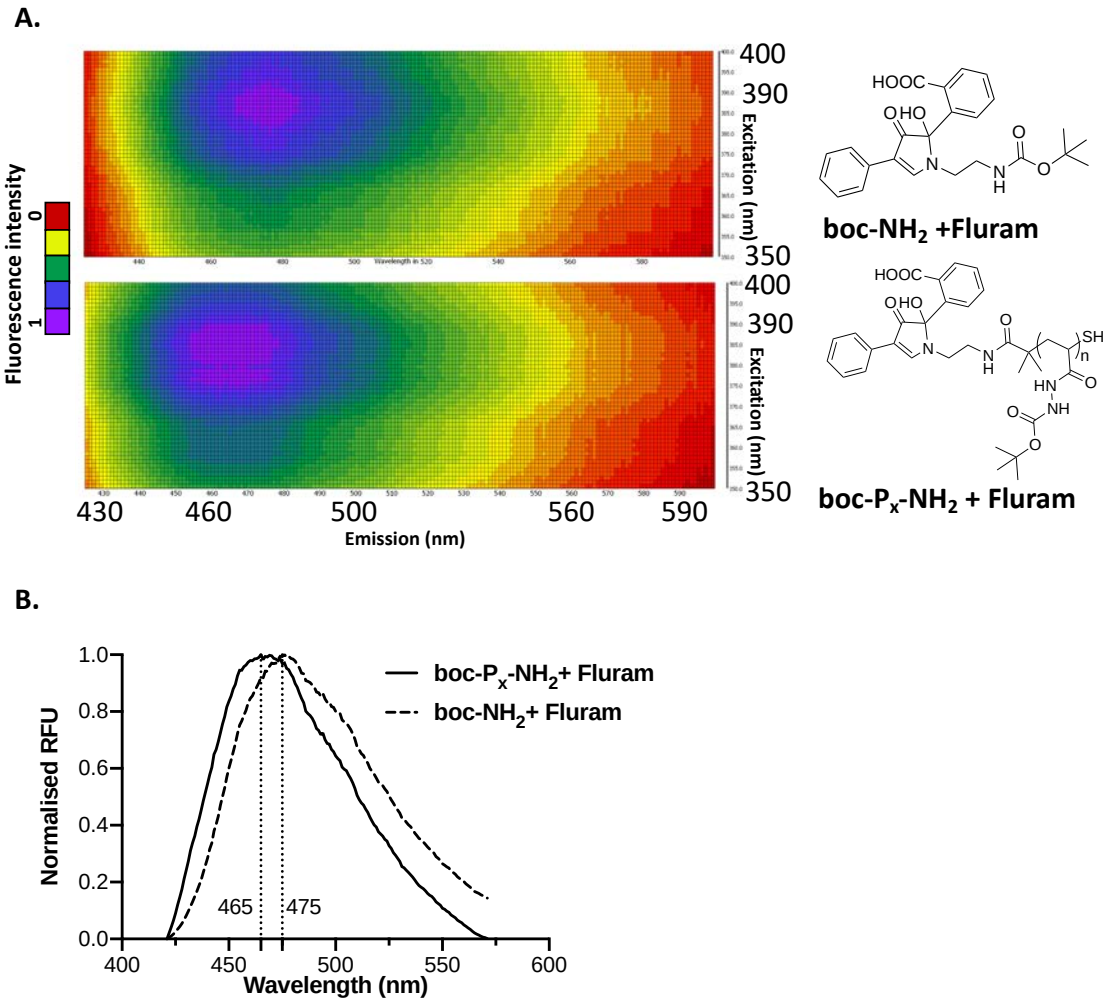

Figure 80. A) Heat map of the fluorescence intensity for **boc-NH$_2$** (6.22 μM) and **boc-P$_x$-NH$_2$** (5.92 μM) after reaction with Fluram (2 eq.) in dry DMSO, recorded using a CLARIOstar plus plate reader. B) fluorescent spectrum (λ_{ex} 390 nm) for **boc-NH$_2$** (6.22 μM) and **boc-P$_x$-NH$_2$** (5.92 μM) after reaction with Fluram (2 eq.).

Crucially, fluorescence intensity for these compounds revealed that while both were excited at the same wavelength (λ_{ex} 390 nm), emission maximum was shifted for **boc-P$_x$-NH$_2$** to λ_{em} 465 nm compared to λ_{em} 475 nm for **boc-NH$_2$**.

Next, optimal reaction time and conditions were assessed in order to establish the point of maximum conversion of Fluram to the fluorescent Fluram-amine conjugate for both model amine and polymer. 2 eq. of Fluram with respect to primary amine were employed in order to ensure an excess of the chemical probe, and reaction was

subsequently carried inside a plate reader at RT in a black 96 well plate and monitored by fluorescence (**Figure 81**).

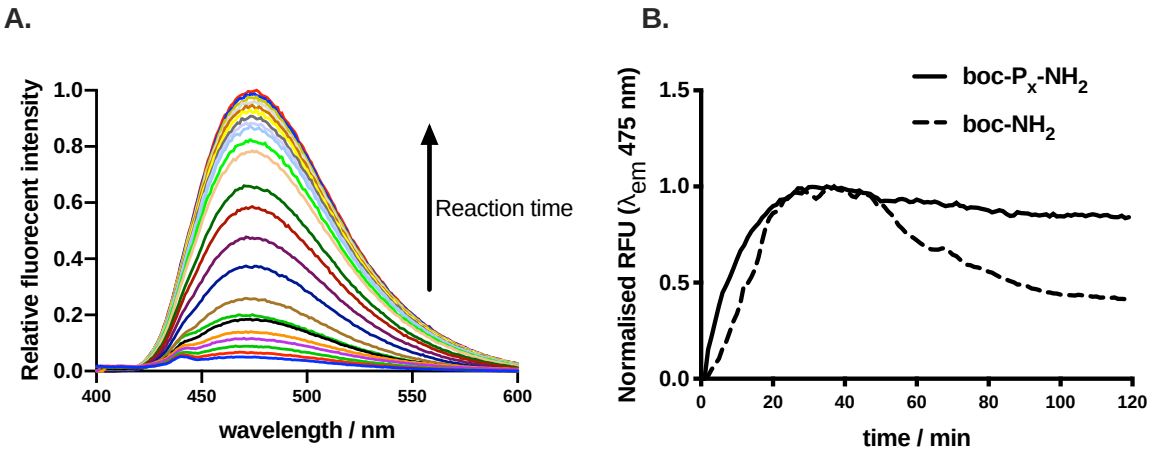

Figure 81. A) fluorescent spectra (λ_{ex} 390 nm) for **boc-NH₂** at increasing reaction time with fluram (2 eq. RT), and B), kinetic curves of fluorescent intensity (λ_{ex} 390 nm, λ_{em} 475 nm) for **boc-NH₂** ([NH_2] 6.22 μM) and **boc-P_x-NH₂**. ([NH_2] 5.92 μM) with reaction time (Fluram, 2 eq. RT), carried out in a black 96 well plate.

Both polymer and model amine initially displayed slightly different reaction rates with Fluram under these conditions, but reassuringly both compounds converged to a stable level of maximum fluorescence, and thus, maximum conversion to the Fluram-amine conjugate between 20 and 40 minutes. This observation confirmed that fluorescence for calibration standards and modified polymer could be measured simultaneously and compared at these timepoints. Interestingly, **boc-NH₂** displayed a gradual reduction of fluorescence after 50 minutes indicating that the small molecule analogue was more susceptible to hydrolysis and/or repeated cycles of excitation.

Based on evaluation of the parameters discussed above, the Fluram assay was carried out on sequential concentrations of **boc-P_x-NH₂** with a maximum theoretical [NH_2], and hence the efficiency of the EDA end group modification of the polymer was assessed by comparison of the theoretical and the experimental values for [NH_2]. The latter was determined by interpolation of the fluorescence intensity (λ_{ex} 390 nm) at λ_{em} 465 nm against a calibration curve of fluorescence intensity (λ_{em} 465 nm) for known

concentrations of **boc-NH_2**. For each condition, [Fluram] to [NH_2] was kept consistent at 2 eq. ([Fluram]/[NH_2]), and under these conditions, complete consumption of the amine to form the fluorescent Fluram-amine conjugate was achieved after 20 minutes at RT, and thereafter, produced stable levels of fluorescence for a further 20 minutes at which point measurements could be taken. [NH_2] between 2 μM and 15 μM were prepared by serial dilutions in DMSO, allowing for pipetting volumes compatible with 96 well plates.

Table 11. Representative experimental layout for a typical Fluram assay as described here.[a]

Sample	[b]	[c]	[d]	DMSO (μL)	[b] (μg·mL^{-1})	[d](μM)	[c] (μM)	[d](μM)	[Fluram]/ [NH_2]	Total volume
Blank		0	0	200						200
Cal 1		11.0	2.5	187			4.23	**2.00**	2.12	200
Cal 2		22.0	5.0	173			8.46	**4.00**	2.12	200
Cal 3		33.0	7.5	160			12.69	**6.00**	2.12	200
Cal 4		44.0	10.0	146			16.92	**8.00**	2.12	200
Cal 5		55.0	12.5	133			21.15	**10.00**	2.12	200
Cal 6		66.0	15.0	119			25.38	**12.00**	2.12	200
Cal 7		77.0	17.5	106			29.61	**14.00**	2.12	200
Pol 1	20	30		150	45.00	**5.35**	11.54		2.16	200
Pol 2	40	60		100	90.00	**10.70**	23.08		2.16	200
Pol 3	50	75		75	112.50	**13.38**	28.84		2.16	200

[a] Cal 1-7 represents conditions for the production of the standard curve using **boc-NH_2**, and Pol 1-3 represents sequential concentrations of **boc-P_x-NH_2**. [b] **boc-P_x-NH_2** (54 μM) (μL), [c] Fluram (80 μM) (μL) [d] **boc-NH_2** (160 μM) (μL).

Each calibration condition (Cal 1-7) and polymer condition (pol 1-3) was pipetted in triplicates with DMSO serving as a solvent only control in a 96 well plate which was covered in foil and gently rocked for 30-40 minutes before recording the data using a BMG CLARIOstar plus microplate reader (**Figure 82**).

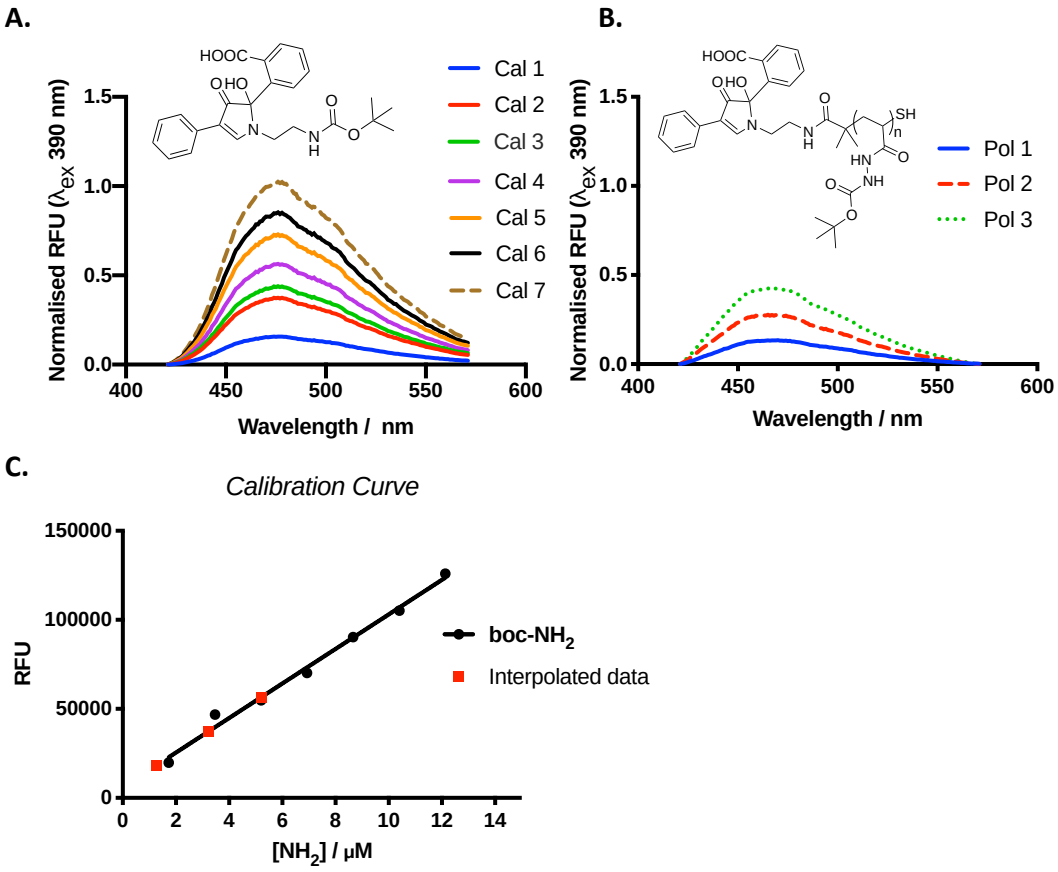

Figure 82. Data collected from a typical Fluram assay: A), standard concentrations with **boc-NH$_2$** B), emission of **boc-P$_x$-NH$_2$** C), example of interpolated values for **boc-P$_x$-NH$_2$** against a standard curve.

Employing the Fluram assay, EDA loading on the polymer was evaluated for a DP55 **boc-P$_{55}$-NH$_2$** (**Table 12**) and then repeated for **boc-P$_x$-NH$_2$** at a range of different DPs (**Table 13**).

Table 12. Experimental data from a Fluram assay, for **boc-P$_{55}$-NH$_2$** for calculated average loading based on three concentrations of the polymer.

[a][NH$_2$] theoretical	[b] [NH$_2$] experimental	% loading
2.30	1.26	55
4.61	3.24	70
6.91	5.21	75
Average loading (%)		67

[a] Calculated by estimated M_p of the polymer (monomer conversion) [b] Calculated by interpolation of a standard curve using a Fluram assay.

Table 13. Estimated loading efficiency of EDA on **boc-P_x-NH_2** prepared at different DPs by RAFT.

Entry	[a]$M_{p(theo)}$	[b]$M_{n(GPC)}$	[c]EDA loading
boc-P_{55}	10467	9200	67%
boc-P_{38}	7292	-	68%
boc-P_{162}	30342	21220	68%
boc-P_{44}	8408	8190	60%

[a] monomer conversion by H1 NMR (g.mol^{-1}), [b] number average molecular weight by GPC (DMF LiBr 0.05 M) [c] Determined by Fluram assay

An acceptable degree of consistency was observed between samples and loading of EDA appeared to be independent of DP, although the loading was not quantitative. The explanation for the observed lower than quantitative efficiency may be as a result of poor availability of the end group to react with the linker.

4.3.3 Synthesis of green fluorescent polymer scaffold: P_x-Flu

With evidence of predictable installation of EDA onto **boc-P_x**, the next step involved fluorescently labelling the polymer *via* the EDA linkage, and quantifying the labelling degree. Fluorescein isothiocyanate (FITC), which was readily available and capable of efficient conjugation to primary amines was chosen to explore fluorescently labelling the polymer. At this point It was important to consider the reaction of thiols with isothiocyanate groups,[46] which could lead to labelling at both the amine and thiol end groups of **boc-P_x-NH_2**. However, compared to the thiourea derivative formed with amines, the resulting dithiocarbamate is known to be reversible under physiological conditions,[47,48] and therefore it was hypothesised that dithcarbamate-linked FITC would likely be cleaved during the deprotection step with neat TFA.

To fluorescently label the polymer, **boc-P_x-NH_2** was mixed with an excess of FITC (6:1) in DMF with DIPEA as a non-nucleophilic base (**Scheme 12**).

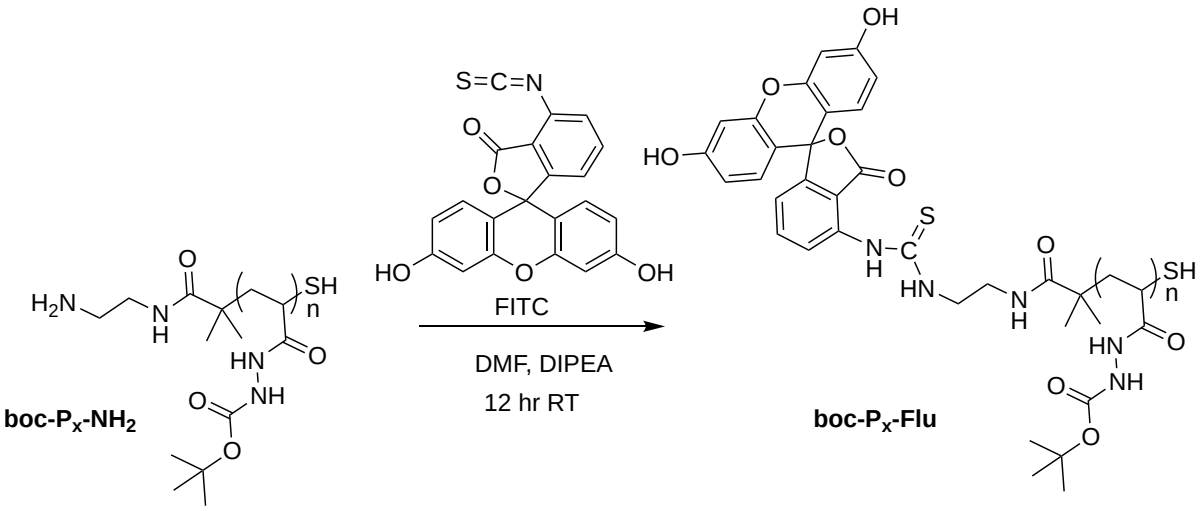

Scheme 12. Synthetic route to fluorescently labelled boc-P_x-Flu.

The reaction proceeded for 12 hours at RT while shielded from the light using foil. Following this, the crude was condensed using a high-pressure vac line and isolation of the labelled polymer from the free dye was carried out using a sephadex LH-20 column in DMF and fractions were analysed by fluorescence GPC (**Figure 83**).

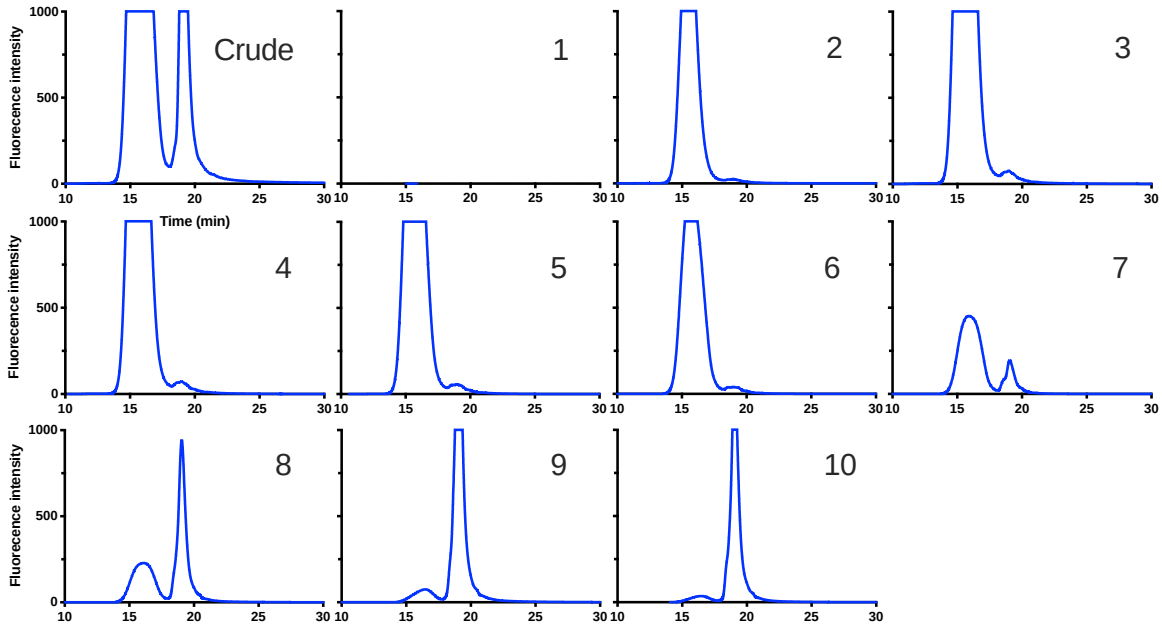

Figure 83. Fluorescent GPC (λ_{em} 510 nm) traces (DMF LiBr 0.05M) for fractions (numbered) collected after separation of **boc-P_{91}-Flu** from FITC using a sephadex LH-20 column (DMF).

Reasonable separation was observed at this point during the purification process as assessed by analysis of each fraction collected from the column; fractions 2-4 for a DP91 **boc-P_x** displayed a good degree of separation from FITC, with the appearance of small impurity at 18 minutes likely to be small oligomers of the polymer rather than the free FITC, justified by the decreases in the observed impurity between fractions 3 and fractions 6 and the observation of two peaks, impurity and FITC in fraction 7. Overlap between **boc-P_{91}-Flu** and FITC was apparent after fraction 7 which accounted for the reduced yield (22 %) upon combination of pure fractions (1-6).

Separation by this method was considerably worse for **boc-P_x** targeting lower DPs, and we therefore explored alternative methods of purification. By quenching unreacted FITC with further portions of EDA, and dialysing the crude until no traces of FITC were observed in the dialysis mixture, lyophilised **boc-P_x-NH_2** was isolated from free FITC at a significantly improved yield (70 %).

To affirm that the installation of the amine linker EDA was indeed crucial for labelling with FITC, a labelling reaction was carried employing both **boc-P_{55}-NH_2** and its unmodified parent **boc-P_{55}** as a control sample**,** crudes of the reaction were compared by fluorescence GPC in order to assess levels of non-EDA associated labelling (**Figure 84**).

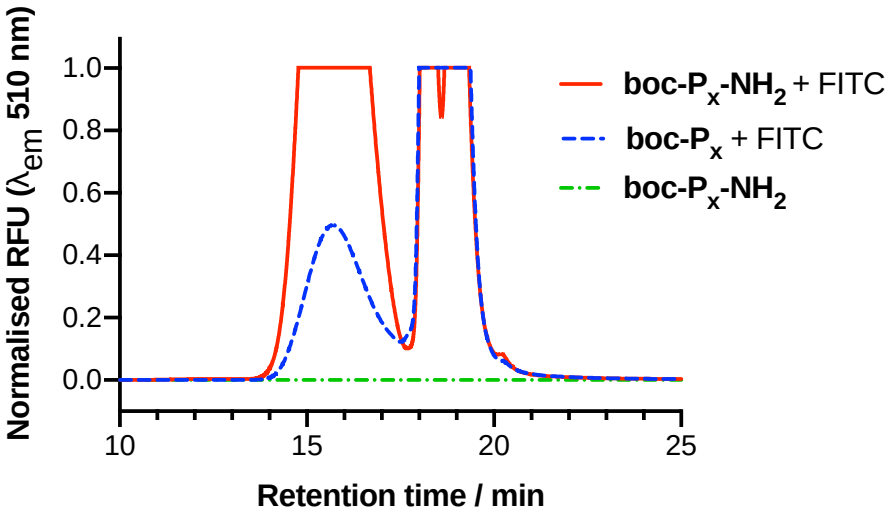

Figure 84. Fluorescent GPC (λ_{em} 510 nm) traces (DMF,LiBr 0.05M) of crude of reaction between **boc-P_{55}** and FITC, with (solid line) and without (dashed line) prior installation of EDA linker. Dot-dash line represents **boc-P_{55}-NH_2** without the addition of FITC. Concentration of polymer in each case was 2 mg ml^{-1}.

The GPC trace indicated a clear increase in loading of FITC in the polymer region (~14-17 minutes) in the case of the EDA modified polymer, and also revealed that FITC could be incorporated onto the polymer without this modification, although to a significantly lower degree. It was reasoned that "background" labelling could be due to a degree of cleavage of the trithiocarbonate end group and reaction of FITC with the resulting thiol. This observation brought to our attention the difficulty in quantifying the fluorescent labelling contribution from amine compared to the thiol at this stage of the reaction.

Despite the possibility of labelling with FITC occurring at both ends of **boc-P_x**, the purity of the dialysis-isolated polymer with respect to unreacted FITC was evaluated by proton NMR (**Figure 85**).

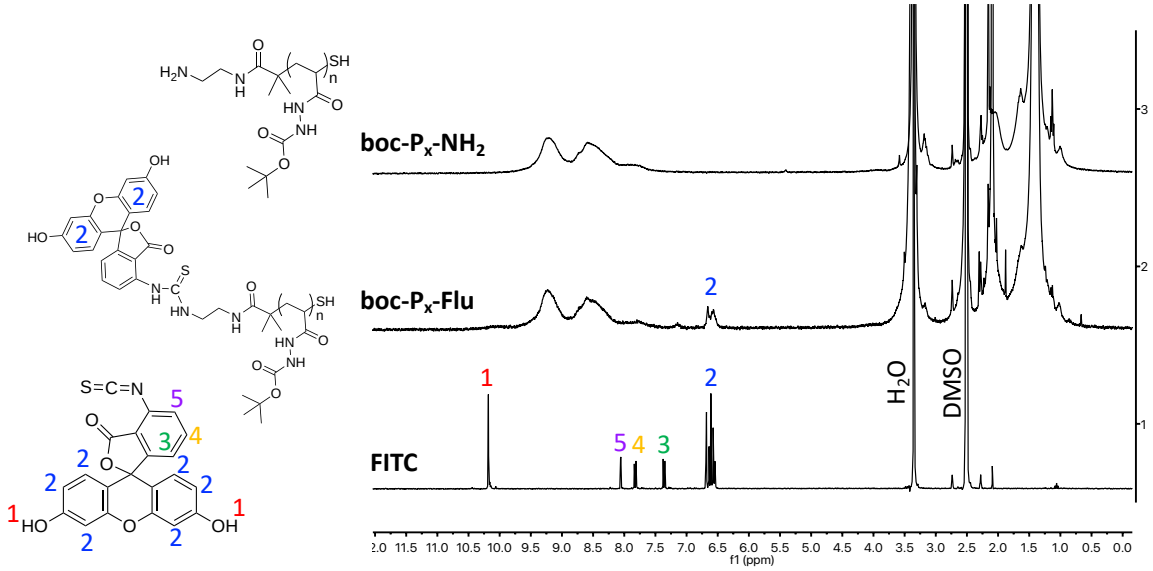

Figure 85. Proton NMR (DMSO d6) for **boc-P$_x$-FITC** after purification by dialysis (middle). And corresponding starting materials (top / bottom).

Proton NMR of **boc-P$_x$-Flu** displayed new broad signals around 6.6 ppm consistent with conjugated FITC protons. There was no evidence of sharp signals associated with FITC especially from hydroxyl protons (**1**) at 10.18 ppm which suggested that the polymer-FITC conjugate was isolated from unreacted FITC. The loading of FITC onto the polymer was quantified at this stage by proton NMR, by integration of the FITC signal at 6.7ppm (6 protons) against the hydrazide region on the polymer backbone in accordance with theoretical DP (**Figure 86**).

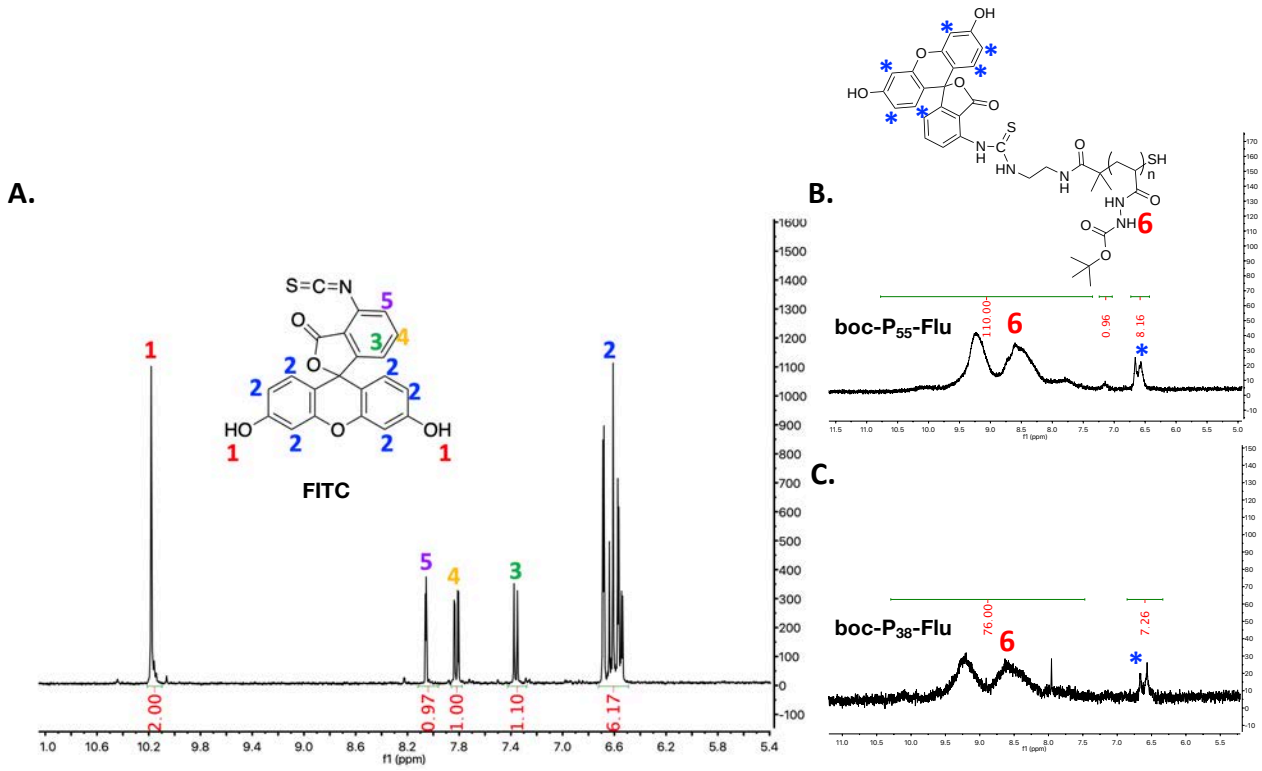

Figure 86. Proton NMR (DMSO d6) for A) FITC B) **boc-P$_{55}$-Flu** and C) **boc-P$_{38}$-Flu**, highlighting key proton signals involved with calculation of FITC loading.

Table 14. Quantification data for **boc-P$_x$-Flu** described in this section.

Entry$_{DP}$	[a]M$_{p(Theo)}$	[b]M$_{n(GPC)}$	[c]EDA loading %	[d]FITC loading %
boc-P$_{55}$	10467	9199	67	140
boc-P$_{38}$	7292	-	68	121

[a] Theoretical polymer molecular weight based on monomer conversion (g.mol^{-1}) [b] Number average molecular weight determined by GPC (DMF, LiBr 0.05 M) (g.mol^{-1}), [c] Calculated using a Fluram assay, [d] calculated by proton NMR.

Values obtained for the loading of FITC by proton NMR were roughly double the estimated loading of EDA (**Table 14**), which could be rationalised as a result of FITC labelling *via* the thiol end group as was predicted and could account for a theoretical maximum loading *via* this quantification method of ~170%. Given the uncertainty over the contribution of the thiol end group with respect to the labelling step, we assessed the labelling of the polymer with FITC using a model **boc-P$_x$**, lacking thiol functionality

but possessing end group analogous to **boc-P_x-NH_2** in order to evaluate labelling strictly *via* the amine linkage. A model **boc-P_{FRP}** was then prepared by free radical polymerisation (FRP) targeting a DP50 **P_x**, but substituting of the RAFT agent for cysteamine as a chain transfer agent (CTA) (**Scheme 13)**.

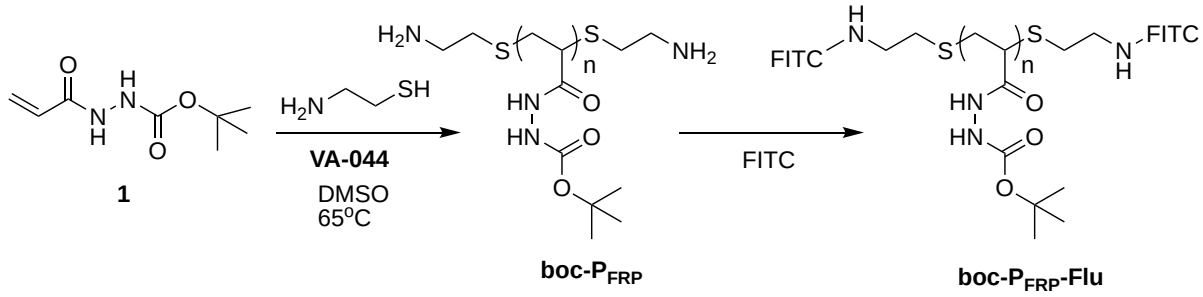

Scheme 13. Synthetic route taken in the synthesis of **boc-P_{FRP}** by free radical polymerisation, and subsequent labelling with FITC under identical conditions as for **boc-P_x-NH_2**.

The resulting polymer was expected to be capped by two primary amine-containing cysteamine groups. In this way the total concentration of NH_2 on the polymer would be determined by the ratio of [monomer]:[CTA]:[initiator] ([100][2][0.4]) with no contribution from thiol end groups or uncertainty over installation of the linker. In accordance previously described experimental conditions FITC was allowed react with **boc-P_{FRP}** at different molar equivalents with respect to [NH_2], and crudes of the reaction mixture were analysed by GPC ($Abs_{495\ nm}$) prior to the addition of the polymer, and after 24 hours (**Figure 87**). Polymer absorption at 495 nm around 12 minutes retention time and quantification of the purified compounds by proton NMR demonstrated the ability of FITC labelling *via* amine terminating end groups (**Figure 87**).

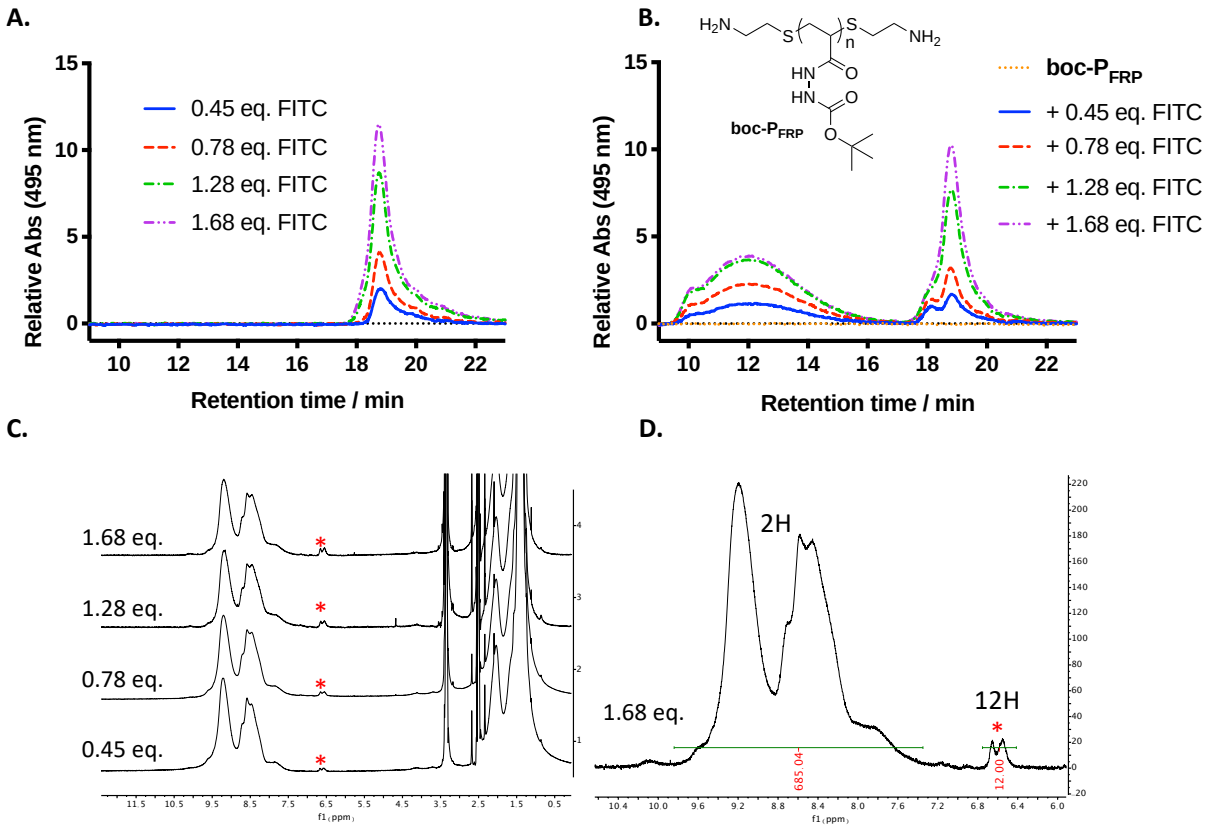

Figure 87. A) GPC trace (DMF LiBr 0.05M) of FITC before and B) after addition of **boc-P$_{FRP}$**. C) Proton NMR (DMSO) for isolated **boc-P$_{FRP}$** after reaction with increasing equivalents of FITC and D) Expanded proton NMR displaying integrals used to calculate number of monomer units per FITC molecule from integrating FITC signal at 6.5 ppm (2 X 6 protons) and hydrazide protons ~9.0 ppm (DP/2 protons).

Polymer absorption at 495 nm (10-16 minutes retention time) indicated increased loading of the dye onto the polymer with increasing FITC equivalents with respect to the theoretical end group functionality afforded by cysteamine. Maximum loading was observed between 0.78 eq. and 1.68 eq with little to no increase in loading observed when increasing from 1.28 to 1.68 eq. These observations were corroborated by integrating the hydrazide backbone signals against the FITC signals (highlighted *) for purified **boc-P$_{FRP}$-Flu** which followed a similar pattern to the GPC trace, allowing for an estimation of monomer units of the polymer per FITC molecule (**Table 15**).

Table 15. Calculated ratios of FITC to monomer unit for **boc-P_{FRP}-Flu** described in this section

[a] eq. FITC added	[b] No. monomer units per FITC molecule
0.45	1036
0.78	648
1.28	362
1.68	343

[a] With respect to estimated moles of NH_2 available for reaction on the polymer, [b] calculated by integration of FITC signal (2X6H) against hydrazide region in the polymer backbone (3H).

These results confirmed the ability to label the boc-protected polymer scaffold with FITC *via* amine containing end-groups, and with this in mind the focus was set to establishing whether FITC remained conjugated to the polymer after the critical deprotection step with TFF.

Deprotection of **boc-P_x** yields **P_x**, capable of undergoing post-polymerisation modification with aldehydes and sugars and as such, retention of the fluorescent label during this step is critical for the primary application of **P_x** as a screening platform.

Deprotection of **boc-P_x-Flu** was carried out in the dark on addition of neat TFA and isolation of the purified fluorescent polymer was carried out in the dark *via* purification by dialysis. Despite the removal of FITC from the protected polymer during the previous step, it was apparent during the dialysis step that free FITC was present in the dialysis water indicating a degree of cleavage of the fluorescent dye. It was rationalised that this was expected and represented cleavage of the FITC molecule from the thiol end group of the polymer the linker on account of the unstable nature of the linkage under acidic pH. Despite some loss of FITC during dialysis, reassuringly, a water-soluble fluorescent orange powder was recovered (55%) after lyophilisation and GPC analysis of the compound using refractive index, absorbance and fluorescence, confirmed that FITC was still bound to the polymer (**Figure 88**).

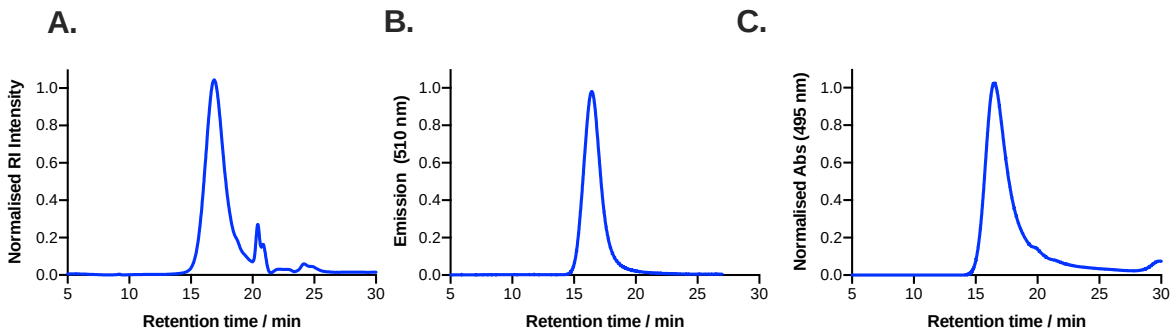

Figure 88. Representitive GPC trace (Lonza DPBS) for purified **P_{91}-Flu** recorded by A) refractive index, B) emission (λ_{ex} 490 nm, λ_{em} 510 nm) and C) absorption (λ_{abs} 495 nm).

GPC analysis confirmed isolation of the deprotected polymer, although a small non-fluorescent impurity was observed at a retention around 20 minutes which may indicate the presence of small oligomers of **P_x** without the required chemistry to undergo fluorescent labelling. Absorption at 495 nm confirmed that FITC was still conjugated to the polymer, and emission (510 nm) confirmed that the fluorophore was still able to fluoresce after excitation at 495 nm.

At this stage, the loading of FITC on **P_x-Flu** was assessed by proton NMR (**Figure 89**).

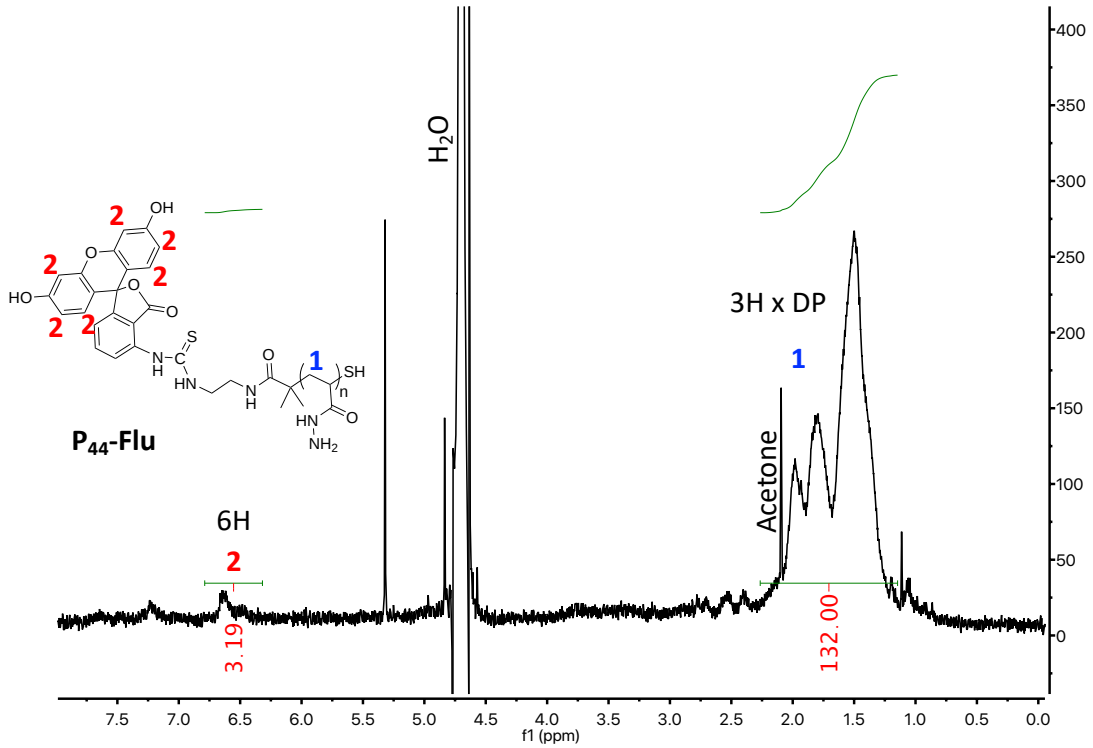

Figure 89. Proton NMR (D_2O) for a **P_{44}-Flu** highlighting the key proton signals involved with quantifying the loading of FITC

For a DP44 **P_x-Flu**, FITC loading after deprotection was calculated as 53% total loading with respect to moles of the polymer, or 88% with respect to the respective estimated EDA installation. The calculated loading was in-line with expected FITC loading *via* the EDA linker compared with the previously discussed over labelling for the boc-protected polymer, further supporting our rational that FITC conjugation *via* the thiol had been cleaved during the deprotection step. In order to further corroborate the NMR results, the loading of FITC on **P_x-Flu** was characterised by interpolation of a calibration curve of FITC absorbance (**Figure 90**).

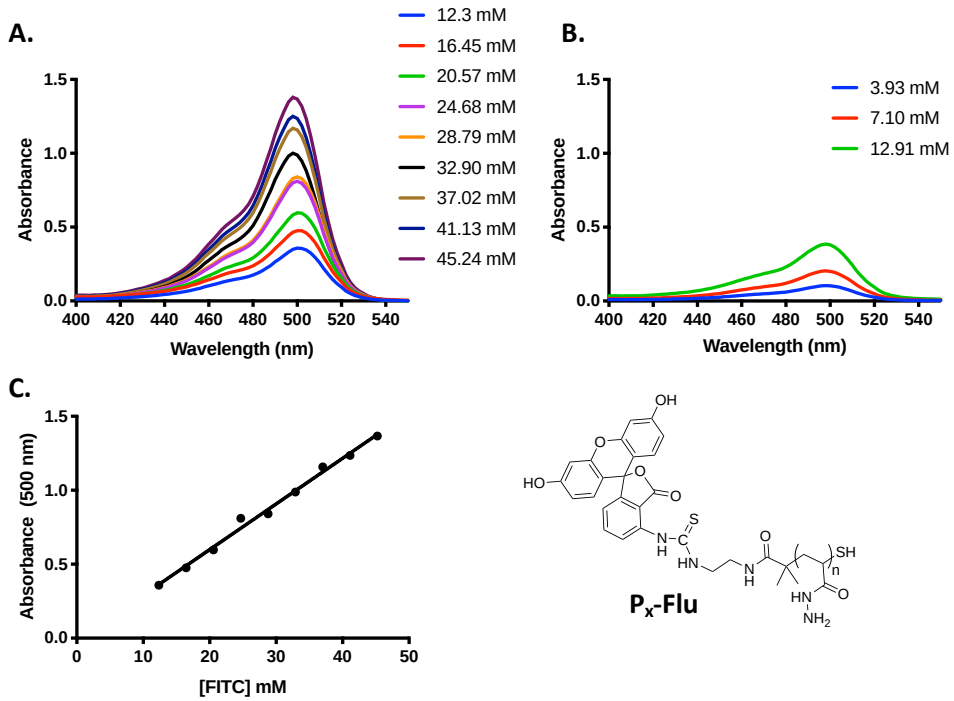

Figure 90. A) Absorbance spectrum for FITC and B) **P_x-Flu** at increasing concentrations. C) Corresponding standard curve for FITC concentrations at 500 nm.

UV-Vis was chosen here to measure the amount of FITC on **P_x-Flu** rather than fluorescence to better negate the effects of photobleaching, and encouragingly, the values obtained by this method were generally in agreement with the calculated loading of EDA and in this regard were "quantitative" for two of the three samples analysed (**Table 16**).

4.3.4 Post polymerisation of P_x-Flu

Finally, and in accordance with the primary objectives set out in this chapter, we investigated the ability of **P_x-Flu** to undergo post-polymerisation modification reactions, in order to access and screen new polymer chemistries originating from the fluorescent scaffold. In this regard, imidazole-4-carbaldehyde (**IMI**) was employed as model aldehyde due its previously-studied reaction with **P_x**.[49] On addition of the aldehyde under mildly acidic conditions (100 mM acetic acid), a new broad region between 8.5

and 6.4 ppm was observed as well as a decrease in the aldehyde signal (9.6 ppm) and corresponding hydrate (6.0 ppm) indicating that **P_x-Flu** was able to undergo post-polymerisation modification with **IMI**. Loading was calculated by integration of the sharp aldehyde signals of the free aldehyde and hydrate compared to the entire imidazole region (3H) (**Figure 91**).

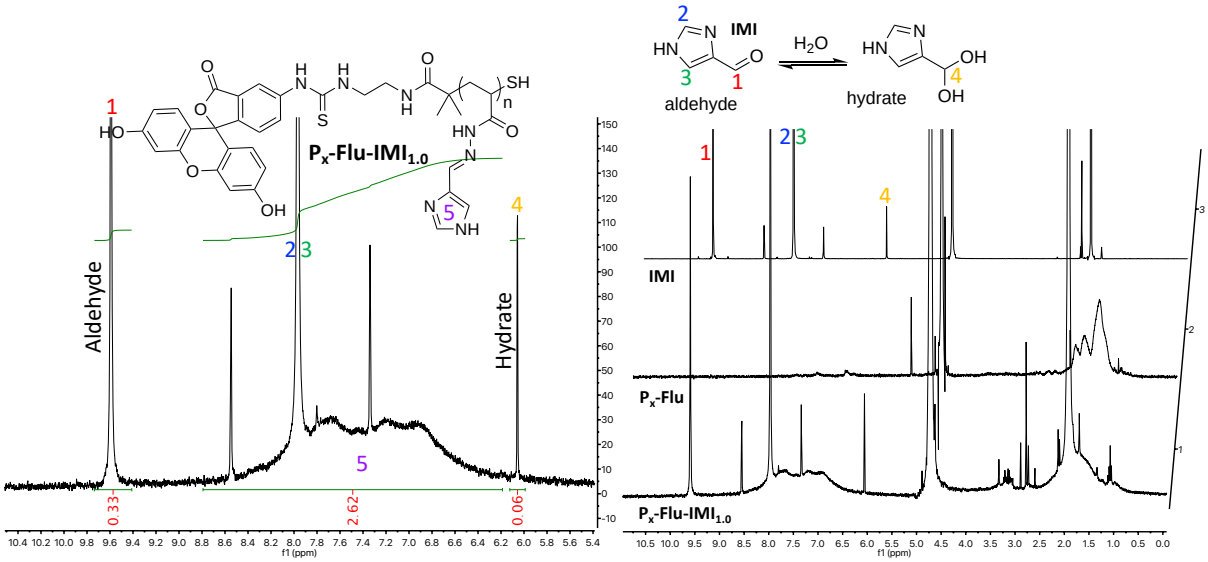

Figure 91. Proton NMR (D_2O) for **P_x-Flu-IMI$_{1.0}$** A), highlighting integrals used to calculate conversion of the aldehyde onto the polymer and B), stacked NMR spectrum for **P_x-Flu-IMI$_{1.0}$** and corresponding starting materials; **IMI**, **P_x-Flu**.

After incubation of **P_x-Flu** with 1.1 equivalent of **IMI**, the loading of the aldehyde was calculated at 68% and 59 %. by proton NMR. Equivalence of the aldehyde was calculated with respect to moles of hydrazide side chains, accounting for the molecular weight contribution of FITC, RAFT agent and EDA linker (12% for a DP55 **P_x-Flu**). Reassuringly, these values were consistent with those previously reported for **P_x-IMI** (66%),[49] indicating that fluorescent end group modification did not impact on the ability to undergo subsequent side-chain modification. A summary of the transformations discussed thus far for the modification of **boc-P_x** at different calculated molecular masses can be found below (**Table 16**).

Table 16. Summary data for **P_x-Flu-IMI** described in this study.

Entry	[a] $M_{p(theo)}$	[b] $M_{n(GPC)}$	[e] EDA loading	M_p **P_x-Flu** ($g.mol^{-1}$)	[c] M_n	[d] FITC loading	[f] IMI coupling
P_{91}-Flu-IMI	17150	10749	225%	8396	5213	109 %	67 %
P_{55}-Flu-IMI	10467	9199	67%	5229	9753	91 %	59 %
P_{38}-Flu-IMI	7292	n/a	68%	3837	8694	38 %	n/a %

[a] **boc-P_x**, $g.mol^{-1}$(1H NMR), [b] **boc-P_x**, $g.mol^{-1}$, (GPC, DMF, LiBr 0.05 M). [c] **P_x-Flu** (SEC, Lonza DPBS) [d] determined by UV-Vis standard curve, [e] calculated by Fluram assay [f] calculated by 1H NMR.

4.3.5 Synthesis of blue polymer scaffold: P_x-MCCA

After synthesis and characterisation of fluorescent FITC labelled polymer scaffold **P_x**, with good control and reproducibility over fluorescent loading, this synthetic route was further evaluated towards synthesis of different "coloured" scaffolds. Our focus then turned to preparing **P_x** capable of emission in the blue/violet region. A dye capable of emitting in this region was especially important for work with bacteria in order to distinguish between polymer emission and emission of a green fluorescent protein (GFP) producing strain of *V. cholerae* which was a strain predominantly used for assessment of growth.

The fluorophore; 7-methoxycoumarin-3-carboxylic acid (MCCA) which absorbs in the UV-region (330 nm) and emits in the blue/violet region (402 nm) was chosen for the labelling of **P_x-NH_2**. Furthermore, MCCA had been previously reported in the labelling of polymers containing amines and for similar applications involving clustering of bacteria by polymers. [36] MCCA has a lower molar extinction coefficient compared to FITC (20,000 vs 77,000 cm^{-1} M^{-1}),[50] therefore efficient labelling and extra care to avoid photobleaching needed to be considered for biologically useful materials. In addition, compared to reactions with isocyanates (FITC), carboxylic acid conjugation with amines require more forcing conditions due to the lower reactivity of the carbonyl group. Despite this, successful conjugation had been reported for MCCA and polymers containing primary amine side chains, and thus a synthetic route was targeted based

that reported in the literature,[51] but employing DMF rather than propinonitrile to maintain solubility of **boc-P$_x$** (**Scheme 14**).

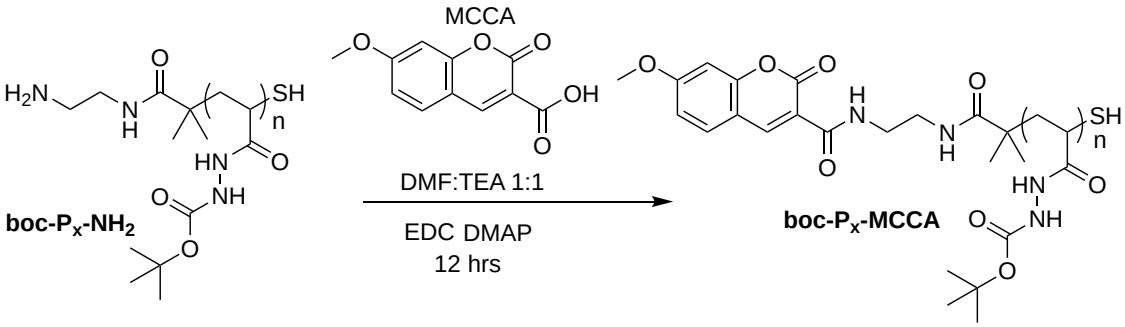

Scheme 14. Synthetic route for the preparation of **P$_x$-MCCA** and subsequent post polymerisation modification with a model aldehyde (IMI).

To assess whether MCCA had been successfully conjugated to **boc-P$_x$-NH$_2$** *via* this method, crudes of **boc-P$_x$-NH$_2$** after reaction with MCCA, and respective unmodified control **boc-P$_x$** were analysed by fluorescence GPC. (**Figure 92**).

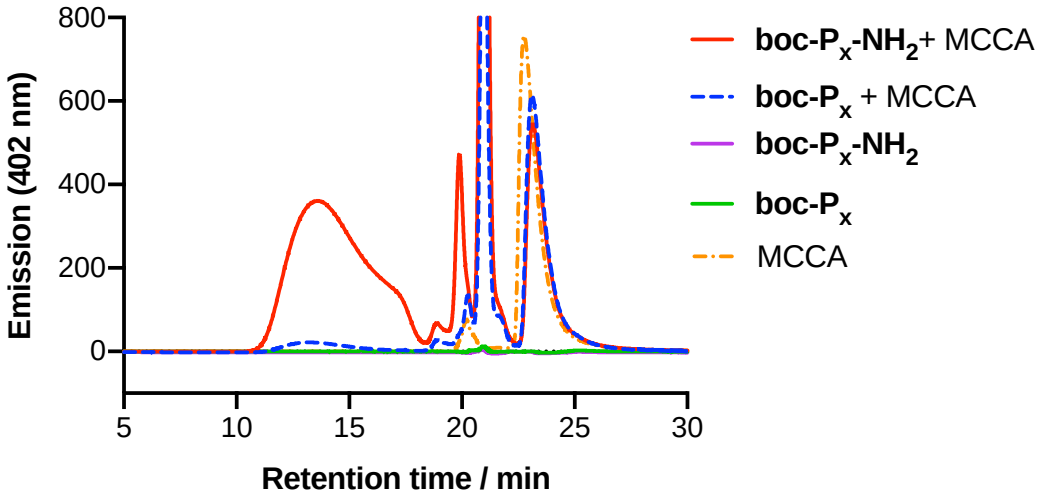

Figure 92. GPC trace (DMF LiBr 0.05 M) for crude of **boc-P$_x$** and **boc-P$_x$-NH$_2$** after reaction with MCCA (4 eq.).

As with FITC labelling, a control whereby MCCA was reacted with **boc-P$_x$** lacking the EDA end group confirmed that the linker was crucial for this reaction (EDA modification efficiency by Fluram = 68%). Under these conditions, the thiol is not amenable to reaction with the carboxylic acid of MCCA,[52] however a degree of background labelling

of the polymer which lacked the EDA linker was observed and accounted for 5% of the total fluorescent signal by GPC.

Purification of crude **boc-P$_x$-MCCA** was initially carried by dialysis as before, and lyophilised to a brown powder (51%), however analysis of the purified compound by proton NMR revealed sharp peaks, presumably from a mixture of small molecule derivatives of unreacted MCCA (**Figure 93**).

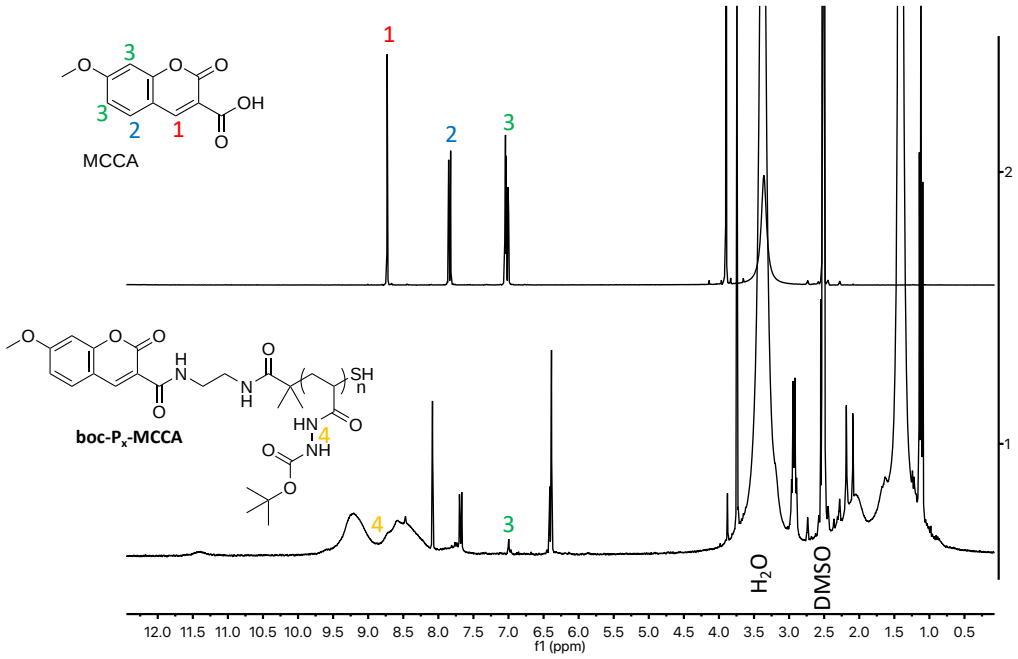

Figure 93. Proton NMR (DMSO d6) for unreacted MCCA (top) and **boc-P$_x$-MCCA** after dialysis (bottom).

It was rationalised that the presence of these impurities was likely due to the very low solubility of MCCA in water, and as such, it was concluded that dialysis was not a suitable method for isolation at this stage despite being the only purification method reported in the literature protocol.[51]

Given, the previously low yields afforded on purification by column chromatography, and the inability to perform a liquid separation due to the incompatible solubilities of both MCCA and boc-protected polymer, boc-deprotection was carried out without further purification of **boc-P$_x$-MCCA** at this stage**.** Deprotection was carried

out in neat TFA as before, and this time an acidic work up was carried out to extract unreacted MCCA into chloroform. Washing was repeated in this way until no further fluorescent compound could be detected in the organic phase. The aqueous phase containing **P_x-MCCA** was then dialysed and lyophilised to a pale brown powder (50%), purity and fluorescent labelling of the compound was confirmed by SEC (**Figure 94**).

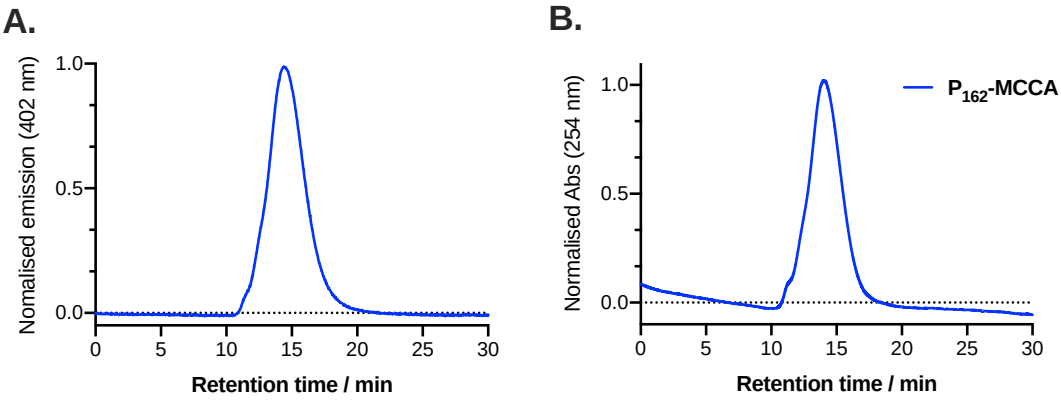

Figure 94. SEC trace (Lonza DPBS) for purified **P_{162}-MCCA** (2 mg ml^{-1}) A), Normalised emission at 402 nm, representative of polymers containing MCCA and B), Normalised absorbance at 254 nm, associated with carbonyl absorption of **P_x**.

Emission SEC confirmed the presence of the MCCA fluorophore on the polymer and the emission trace was consistent with the absorbance trace at 254 nm, associated with the absorption at this wavelength by carbonyl groups present in **P_x** side chains. There was no presence of free MCCA in the proton NMR after deprotection, however, although MCCA is detectable by NMR in D_2O, this method cannot be used as a conclusive indication of purity due to the low solubility of MCCA in H_2O. Furthermore, the presence of new peaks indicative of MCCA conjugated to the polymer were not detected by proton NMR which may have been as a result of their low abundance on the polymer, or possibly due to shielding of the hydrophobic fluorophore in the proton NMR (**Figure 95**).

At this point no further assessment of purity of **P_x-MCCA** or degree of MCCA loading was carried out, and focus was moved towards evaluating the ability to conjugate imidazole- **IMI** to the **P_x-MCCA** scaffold (**Figure 95**).

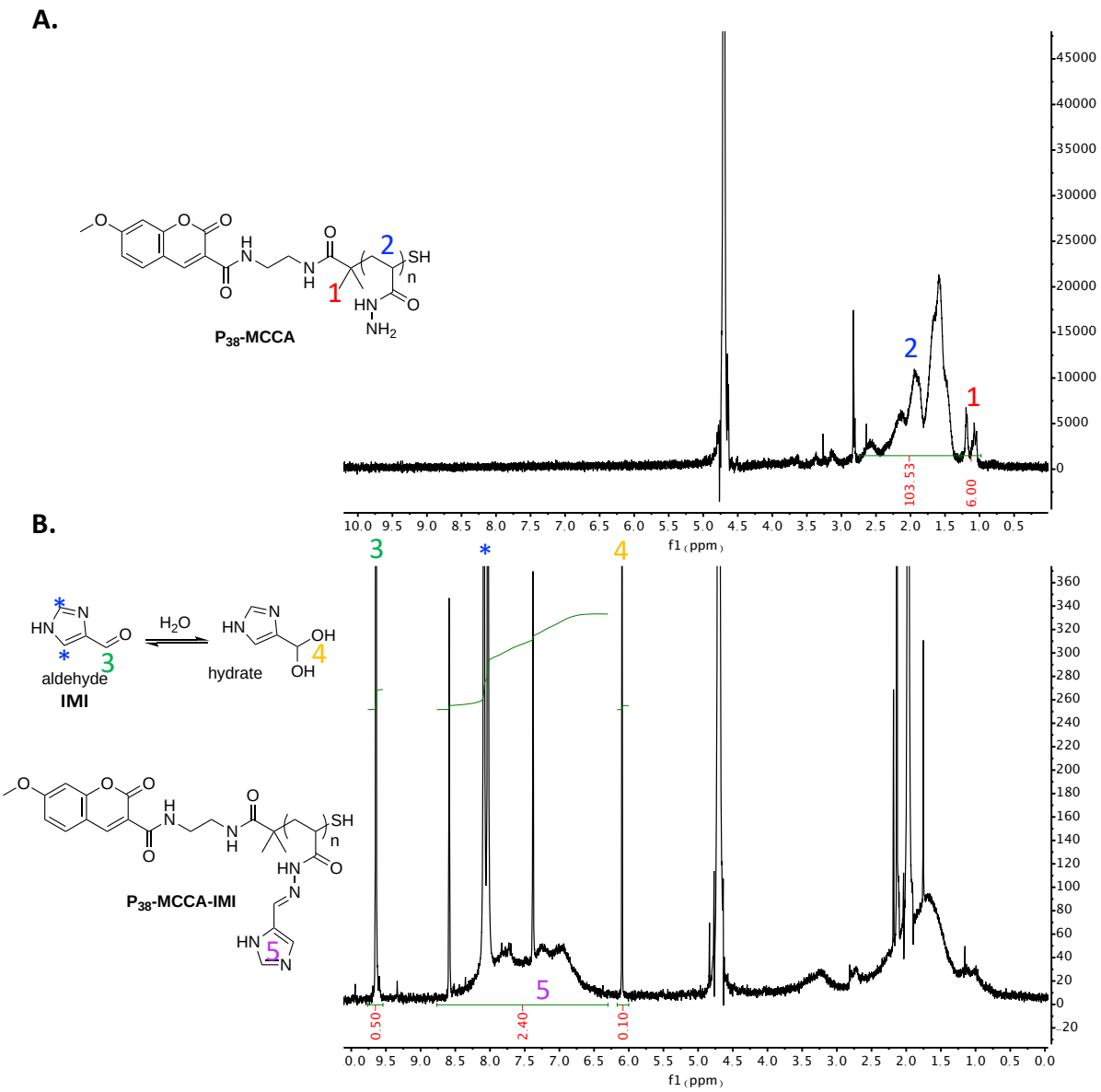

Figure 95. Proton NMR (D_2O) for A) **P_{38}-MCCA** and B) crude **P_{38}-MCCA-IMI** (right) after reaction with 1.1 equivalent of Imidazole-4-carbaldehyde.

Pleasingly P_x-MCCA was able to undergo post-polymerisation modification with **IMI**, although a lower degree of loading of 44% was observed on incubation with 1.1 equivalent of aldehyde to hydrazide. It was rationalised that reduced **IMI** loading may have been due to free MCCA reacting with the hydrazide side-chain during the

deprotection step. With this in mind purifying **boc-P_x-MCCA** by SEC may therefore offer a more attractive means of purifying this compound.

4.3.6 Biological testing with P_x-MCCA

To assess whether labelling of **P_x** with MCCA had yielded a fluorescent polymer sufficiently bright enough for use in standard biological applications, **P_{38}-MCCA-IMI** was incubated with GFP expressing *V. cholerae* under standard bacterial clustering conditions (covered in more detail in Chapter 2) to evaluate polymer-bacteria colocalisation by fluorescence (**Figure 96**).

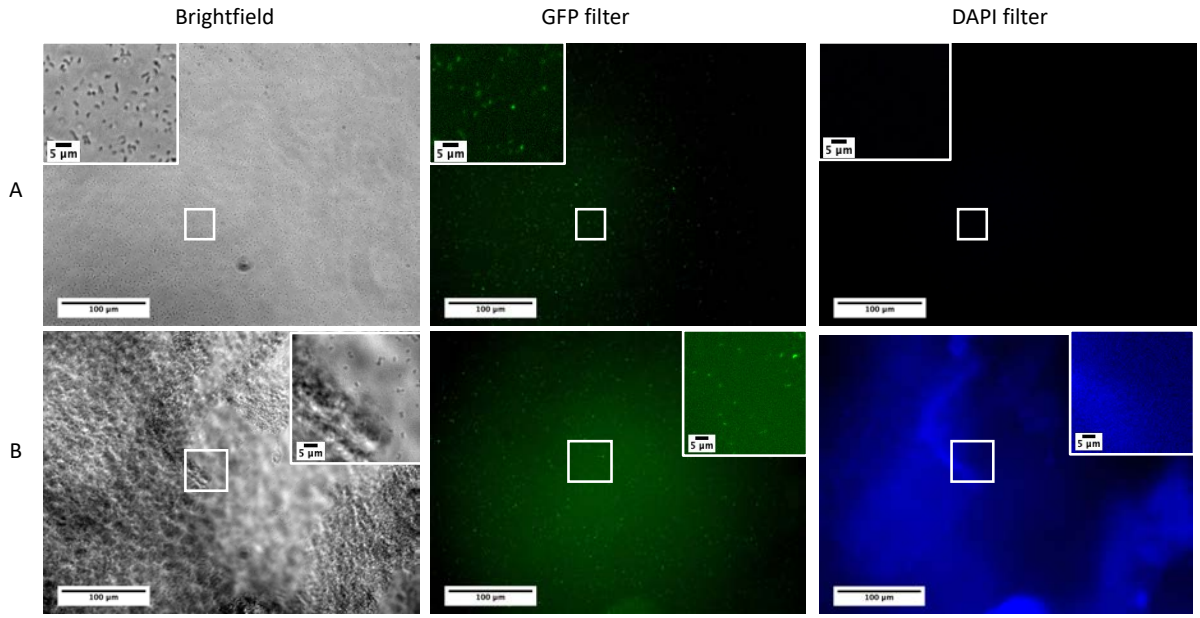

Figure 96. Optical images (20 x magnification) captured after 0 hours incubation of A) untreated *V. cholerae* and B) *V. cholerae* + 0.5 mg ml^{-1} **P_{38}-MCCA-IMI$_{1.1}$** (OD_{600} = 0.02). To the end, images were captured in brightfield, and fluorescence using the GFP and DAPI filter set at 0- and 5-hours incubation at 37°C

Images identified that **P_{38}-MCCA-IMI$_{1.1}$** initially formed mucus-like precipitates in the growth media (clear DMEM) as was routinely observed for **P_x-IMI** (**Chapter 3**) and these precipitates were easily distinguishable by fluorescence (DAPI) from the bacteria (GFP), confirming that there was no overlap between these fluorescent

channels. After 5 hours of incubation, *V. cholerae* were observed predominantly adhered to the polymer precipices (**Figure 97**).

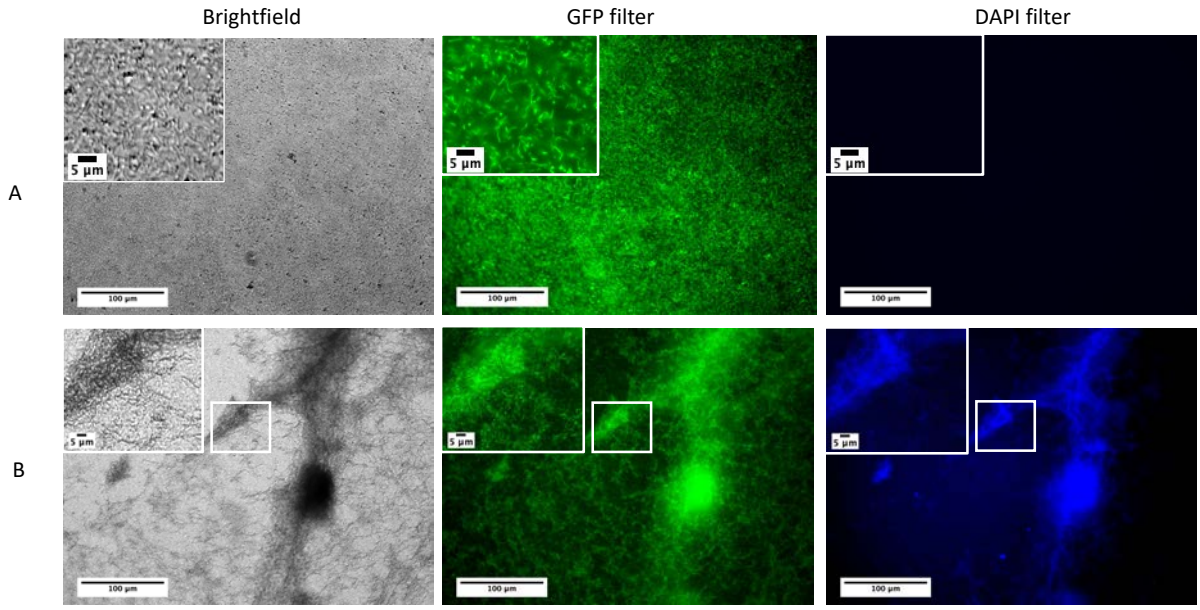

Figure 97. Optical images (20 x magnification) of A), untreated *V. cholerae* and B), *V. cholerae* + 0.5 mg ml^{-1} **P_{38}-MCCA-IMI** captured after 5 hours incubation at 37^{o}C.

After 5 hours incubation at 37 ^{o}C, colocalisation of *V. cholerae* on the **P_{38}-MCCA-IMI$_{1.1}$** precipitate was clearly apparent. Fluorescence of **P_{38}-MCCA-IMI$_{1.1}$** allowed for a more detailed evaluation of the complex 3D polymer network. Z-stacks in the GFP channel further demonstrated the 3-dimensional nature of the bacteria-polymer aggregates which we hope may be explored in future work using confocal microscopy (**Figure 98**).

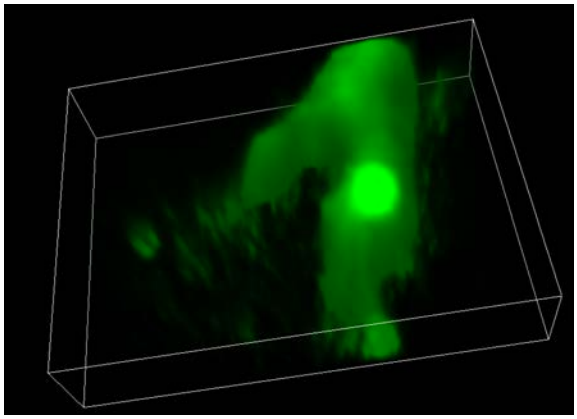

Figure 98. Z-Stacked GFP fluorescent images from conditions described in **Figure 25** showing location of *V. cholerae* adhered to **P_{38}-IMI$_{1.1}$**. Images were taken every 3 µm though 90 um and rendered in 3D using NIS elements (Nikon) using the AlphaBlend render mode.

4.4 Conclusions

Fluorescently labelling macromolecules is a key step to understanding their mechanisms of action in biological settings. However, evaluation into the location and purity, stability and degree of labelling of the labelled nanomaterial is often overlooked and can lead to uncertainty over the observed activity.

The primary aim was to synthesise a fluorescently labelled polymer scaffold **P_x** with a quantifiable and reproducible degree of fluorophore loading, in order to investigate the mechanism of polymer-driven aggregation of bacteria. To this end, a synthetic and characterisation strategy for fluorescently labelling poly(acryloyl hydrazide) (**P_x**), has been developed, with a particular focus on the installation and characterisation of an amine linker *via* end group modification to afford the option of labelling with a wide variety of fluorescent dyes depending on the application. It was demonstrated that the installation of the linker can be quickly and efficiently assessed using a Fluram assay which was optimised for use in microtiter plates. The labelling of **P_x-NH_2** with FITC correlated well with the calculated loading of EDA although quantitative labelling of **P_x-NH_2** was not realised, and **P_x-Flu** was able to undergo

subsequent post-polymerisation reactions to the same degree as the non-fluorescent **P_x**. **P_x-Flu** prepared using this strategy.

As an example of the versatility of this screening platform, **P_x-NH_2** was labelled with a blue fluorescent dye and subsequently further modified with cationic aldehyde imidazole-4-carbaldehyde in order to co-localise cationic polymer with GFP expressing *V. cholerae*. Fluorescent microscopy revealed that the mucus-like precipitate was indeed as a result of precipitating polymer, confirming the polymers role in the sequestration of *V. cholerae.*

4.5 Future work

Work should be carried out to quantify and optimise the loading of MCCA after reaction with **P_x-NH_2**, which has not been covered yet in this research, and to explore the use of alternative blue dyes. MCCA is significantly less bright than FITC, and initial work to synthesise **P_x-MCCA-IMI** suffered from an inability to detect fluorescent emission when taking the polymer forward into biological experiments. Poor brightness of the material was most likely as a result of photobleaching, but may in part have been influenced by DP. There may also be scope to optimise the reaction for labelling with MCCA, and this would be aided by quantification of fluorophore loading, which could then be assessed in the same as for **P_x-Flu** by UV-vis or fluorescence standard curves. Alternative blue dyes with greater photostability and more amenable chemical handles (for example, isothiocyanates or isocyanates) for conjugation *via* the amine linker may also be usefully explored.

Initial biological work with **P_x-MCCA-IMI** revealed a complex 3-dimentional matrix of polymer fibers, capable of sequestering *V. cholerae*. Further investigations could be carried out using fluorescent polymers with a variety of different side-chain

chemistries to probe the impact chemistry has on the nature of this matrix and whether this influences the polymers' ability to aggregate bacteria. There would be benefit in carrying out future imaging using super resolution confocal microscopy, so that Z-stacks can be represented with greater fidelity and a detailed evaluation of the bacteria-polymer interaction can be established.

There would be merit in preparing a red fluorescent $\mathbf{P_x}$ using the same method, to demonstrate the strengths of linking colour to polymer functionality. In future screening assays, the use of RBG (red blue green) polymers may be employed to differentiate between different binding efficiencies for certain polymer parameters; for example, polymer molecular weights and chemical nature of the side-chain. This methodology would open up the potential for using these materials in a biosensing capacity and to aid high-throughput screening for bacterial clustering (**Figure 99**).

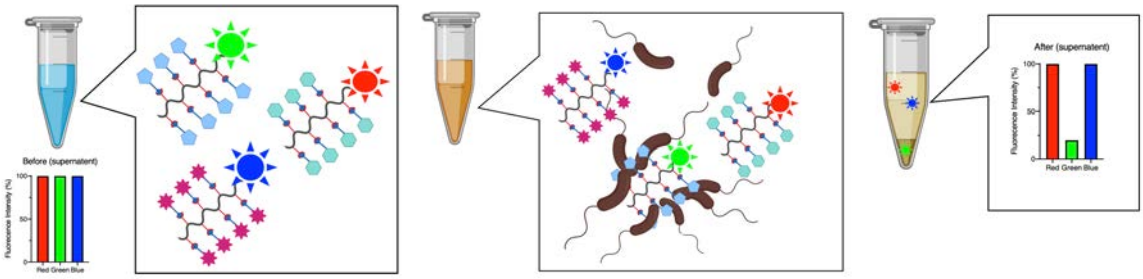

Figure 99. Potential route to screen polymer side group chemistry for affinity to bacteria by measuring concentration of fluorescently labelled polymers with differing fluorescent emission.

4.6 References

1 J. Chen, Z. Zhang, L. Li, B.-C. Chen, A. Revyakin, B. Hajj, W. Legant, M. Dahan, T. Lionnet, E. Betzig, R. Tjian and Z. Liu, *Cell*, 2014, **156**, 1274–1285.

2 H. S. Rye, J. M. Dabora, M. A. Quesada, R. A. Mathies and A. N. Glazer, *Analytical Biochemistry*, 1993, **208**, 144–150.

3 V. I. Martynov, A. A. Pakhomov, N. V. Popova, I. E. Deyev and A. G. Petrenko, *Acta Naturae*, 2016, **8**, 33–46.

4 R. K. Neely, P. Dedecker, J.-I. Hotta, G. Urbanavičiūtė, S. Klimašauskas and J. Hofkens, *Chem. Sci.*, 2010, **1**, 453–9.

5 G. Kaur, J. Lewis and A. van Oijen, *Molecules*, 2019, **24**, 491–20.

6 A. Revyakin, Z. Zhang, R. A. Coleman, Y. Li, C. Inouye, J. K. Lucas, S.-R. Park, S. Chu and R. Tjian, *Genes Dev.*, 2012, **26**, 1691–1702.

7 S. Shashkova and M. C. Leake, *Biosci. Rep.*, 2017, **37**, BSR20170031–19.

8 N. White, *Advanced Drug Delivery Reviews*, 2005, **57**, 17–42.

9 J. M. Dubach, C. Vinegoni, R. Mazitschek, P. Fumene Feruglio, L. A. Cameron and R. Weissleder, *Nature Communications*, 2014, **5**, 10345–20.

10 T. Ueno and T. Nagano, *Nature Publishing Group*, 2011, **8**, 642–645.

11 B. L. Banik, P. Fattahi and J. L. Brown, *WIREs Nanomed Nanobiotechnol*, 2015, **8**, 271–299.

12 M. P. Robin and R. K. O'Reilly, *Polym. Int.*, 2014, **64**, 174–182.

13 A. K. Pearce, B. E. Rolfe, P. J. Russell, B. W. C. Tse, A. K. Whittaker, A. V. Fuchs and K. J. Thurecht, *Polym. Chem.*, 2014, **5**, 6932–6942.

14 E. P. Magennis, A. L. Hook, M. C. Davies, C. Alexander, P. Williams and M. R. Alexander, *Acta Biomaterialia*, 2016, **34**, 84–92.

15 S. F. Hedegaard, M. S. Derbas, T. K. Lind, M. R. Kasimova, M. V. Christensen, M. H. Michaelsen, R. A. Campbell, L. Jorgensen, H. Franzyk, M. Cardenas and H. M. Nielsen, *Sci Rep*, 2018, 1–14.

16 M. A. van Dongen, C. A. Dougherty and M. M. Banaszak Holl, *Biomacromolecules*, 2014, **15**, 3215–3234.

17 P. Zhang, H. Lu, H. Chen, J. Zhang, L. Liu, F. Lv and S. Wang, *Anal. Chem.*, 2016, **88**, 2985–2988.

18 P. Zhang, S. Li, H. Chen, X. Wang, L. Liu, F. Lv and S. Wang, *ACS Appl. Mater. Interfaces*, 2017, **9**, 16933–16938.

19 M. D. Disney, J. Zheng, T. M. Swager and P. H. Seeberger, *J. Am. Chem. Soc.*, 2004, **126**, 13343–13346.

20 J. Liu, J. W. Y. Lam and B. Z. Tang, *Chemical Reviews*, 2009, **109**, 5799–5867.

21 S. Hayashi, S.-I. Yamamoto and T. Koizumi, *Sci Rep*, 2017, 1–8.

22 S. Uchiyama, P. Remón, U. Pischel, K. Kawamoto and C. Gota, *Photochem. Photobiol. Sci.*, 2016, **15**, 1239–1246.

23 S. Kumar, B. Maiti and P. De, *Langmuir*, 2015, **31**, 9422–9431.

24 E. P. Magennis, N. Francini, F. Mastrotto, R. Catania, M. Redhead, F. Fernandez-Trillo, D. Bradshaw, D. Churchley, K. Winzer, C. Alexander and G. Mantovani, *PLoS ONE*, 2017, **12**, e0180087.

25 M. P. Robin and R. K. O'Reilly, *Chem. Sci.*, 2014, **5**, 2717–7.

26 V. Ladmiral, G. Mantovani, G. J. Clarkson, S. Cauet, J. L. Irwin and D. M. Haddleton, *J. Am. Chem. Soc.*, 2006, **128**, 4823–4830.

27 M. L. Coote and I. Degirmenci, *Chapter 6. Theory and Applications of Thiyl Radicals in Polymer Chemistry*, Elsevier Inc., 2018.

28 G. Moad, E. Rizzardo and S. H. Thang, *Aust. J. Chem.*, 2012, **65**, 985–92.

29 S. Perrier, *Macromolecules*, 2017, **50**, 7433–7447.

30 M. Destarac, *Polymer Reviews*, 2011, **51**, 163–187.

31 R. Guo, X. Wang, C. Guo, A. Dong and J. Zhang, *Macromol. Chem. Phys.*, 2012, **213**, 1851–1862.

32 M. P. Robin, M. W. Jones, D. M. Haddleton and R. K. O'Reilly, *ACS Macro Lett.*, 2011, **1**, 222–226.

33 H. Willcock and R. K. O'Reilly, *Polym. Chem.*, 2010, **1**, 149–157.

34 C. W. Scales, A. J. Convertine and C. L. McCormick, *Biomacromolecules*, 2006, **7**, 1389–1392.

35 N. Perez-Soto, L. Moule, D. N. Crisan, I. Insua, L. M. Taylor-Smith, K. Voelz, F. Fernandez-Trillo and A. M. Krachler, *Chem. Sci.*, 2017, **8**, 5291–5298.

36 I. Louzao, C. Sui, K. Winzer, F. Fernandez-Trillo and C. Alexander, *European Journal of Pharmaceutics and Biopharmaceutics*, 2015, **95**, 47–62.

37 B. Ebeling and P. Vana, *Macromolecules*, 2013, **46**, 4862–4871.

38 M. Takara, M. Toyoshima, H. Seto, Y. Hoshino and Y. Miura, *Polym. Chem.*, 2014, **5**, 931–939.

39 C. I. Biggs, M. Walker and M. I. Gibson, *Biomacromolecules*, 2016, **17**, 2626–2633.

40 A. Lorenzen and S. W. Kennedy, *Analytical Biochemistry*, 1993, **214**, 346–348.
41 W. L. Baker, *Antimicrob Agents Chemother*, 1983, **23**, 26–30.
42 M. Monajati, A. Tamaddon, G. Yousefi, S. S. Abolmaali and R. Dinarvand, *New J. Chem.*, 2019, **43**, 11564–11574.
43 H. Wang, J. Zhuang and S. Thayumanavan, *ACS Macro Lett.*, 2013, **2**, 948–951.
44 S. Udenfriend, S. Stein, P. Bohlen, W. Dairman, W. Leimgruber and M. Weigele, *Science*, 1972, **178**, 871–872.
45 T. B. Toro and T. J. Watt, *Protein Science*, 2015, **24**, 2020–2032.
46 G. Swoboda and W. Hasselbach, *Z. Naturforsch., C, Biosci.*, 1985, **40**, 863–875.
47 X. Wu, Q.-H. Zhou and K. Xu, *Acta Pharmacol Sin*, 2009, **30**, 501–512.
48 C. H. Kaschula and R. Hunter, Elsevier, 2016, vol. 50, pp. 1–43.
49 D. N. Crisan, O. Creese, R. Ball, J. L. Brioso, B. Martyn, J. Montenegro and F. Fernandez-Trillo, *Polym. Chem.*, 2017, **8**, 4576–4584.
50 R. W. Sabnis, *Handbook of Fluorescent Dyes and Probes*, John Wiley & Sons, Inc, Hoboken, NJ, USA, 2015.
51 I. Louzao, C. Sui, K. Winzer, F. Fernandez-Trillo and C. Alexander, *European Journal of Pharmaceutics and Biopharmaceutics*, 2015, **95**, 47–62.
52 S. Iimura, K. Manabe and S. Kobayashi, *Chem. Commun.*, 2001, 94–95.

Final conclusions and future work

5.1 Final conclusions

The use of synthetic linear polymers as bacterial antiadhesives is a growing but as yet undeveloped field, this is due in part to complexities in controlling both biological and chemical systems as well as a lack of continuity between synthesis and biological testing. Despite this, recent work outlined in the introduction of this thesis demonstrates the potential that synthetic polymers have as multivalent biological mimics to bind to, and interfere with normal bacterial processes. The focus of this work has been towards the development and application of a simple polymer screening platform based on poly(acryloyl hydrazide) to allow the efficient discovery of new chemistries for sequestering pathogens *via* convenient post-polymerisation modification of the polymer backbone with aldehydes and sugars which can be tested for activity *in-situ*. This thesis represents efforts towards understanding and controlling both polymer chemistry and microbiology assays in order to lay the foundation for a larger scale high throughput screening in future work.

Controlled radical polymerisation techniques, such as RAFT can reduce uncertainty with respect to polymer structure and the observed biological activity and allow for “tuning” of the polymer system. In Chapter 1, the RAFT polymerisation of acryloyl hydrazide was optimised through choice of polymerisation temperature and radical initiator. Optimisation resulted in the synthesis of poly(acryloyl hydrazide) with a lower molecular weight dispersity and an ability to synthesise larger polymers with only a small loss of control. As a result of these optimisations, the effect of molecular weight of poly(acryloyl hydrazide) on the response of *Vibrio cholerae* could be better evaluated (Chapter 2). In Chapter 2, poly(acryloyl hydrazide) was functionalised with aromatic cationic groups, 2-amino-3-formylpyridine and imidazole carbaldehyde, which possess similar protonation states and hydrophobicity, to yield cationic polymers

with well-defined degrees of functionalisation. Time-lapse microscopy revealed how increasing degree of functionalisation with imidazole carbaldehyde increased the hydrophobility of the resulting polymer and also resulted in a material to which *V. cholerae* could be observed binding to. Poly(acryloyl hydrazide) with ≥ 75% imiadazole moieties installed was able to sequester and greatly reduce the concentration of planktonic *V. cholerae* in liquid media and also induced a phenotypic change, whereby it was observed that the production of the Cholera toxin was downregulated and the production of biofilm was upregulated.

The versatility of poly(acryloyl hydrazide) owing to the hydrazide chemistry allowed for a small library of glycopolymers to be prepared in order to compare glycopolymers bearing lectin recognition motifs to cationic polymers (Chapter 3). Such direct comparisons from the same parent polymer are traditionally difficult to achieve without chemical manipulation of the polymer backbone or the ligating group. It was found that, while stable glycoconjugate were able to be formed under optimised conditions, no evidence for irreversible bacterial clustering was observed. Despite this, flocculation assays indicated a sharp but short-lived increase in optical density at 20 minutes post incubation which may indicate bacterial interaction with the glycopolymer. It was noted that treated *V. cholerae* with mannose displaying glycopolymers increased the production of biofilm over those treated with free mannose alone, and to a greater extent than glucose, galactose glycopolymers or poly(acryloyl hydrazide).

Finally, a systematic approach to installing a green or blue fluorescent probe onto the end group of poly(acryloyl hydrazide) was developed, allowing for a good estimation of fluorescent labelling degree and purity (Chapter 4). Here, a fluorescent poly(acrlyolyol hydrazide) emitting in the blue region was functionalised with imidazole carbaldehyde revealing the location of the polymer within the clusters of bacteria.

5.2 Future work

Controlled synthesis of polymers is important for determining structure-activity relationships. Higher molecular weight poly(acryloyl hydrazide) with lower dispersity may be possible with further optimisation of the RAFT polymerisation conditions. This could be achieved through the use of a photoinitiator and UV irradiation, for the rapid generation of radicals at room temperature and should be explored as a follow-up to work carried out in Chapter 1.

The experiments set out in this work have laid the foundation for a more thorough exploration of the polymer chemical space *via* hydrazone linkage and may be useful in determining a general set of “ideal” chemistries and polymer architectures to sequester a variety of different pathogens as well as triggering interesting and useful bacterial phenotypes. Future work should focus on developing a larger scale high-throughput process for screening arrays of modified poly(acryloyl hydrazide) under identical experimental conditions for a number of different pathogens. This methodology will be better suited for determining trends in polymer chemistry and biological activity and may help identify compositions which can increase specificity for a particular pathogen. Polymers possessing fluorescent probes of different colours may offer a convenient way of quickly identifying which chemistries are preferable for bacterial clustering using fluorimetry (Chapter 4, Figure 99).

Cell work should be carried out to determine the potential protective effect of these polymers against pathogenic bacteria verses their possible cytotoxicity to host cells which was not carried out in this work. Poly(acryloyl hydrazide) modified with imidazole may be a good initial candidate for this given the observed rapid adherence of *V. cholerae* to the polymer precipitates.

In Chapter 3, evidence of aggregation of *V. cholerae* remained inconclusive with the prepared glycopolymers. Future work with glycopolymers should focus on purifying these materials to avoid background interference of excess carbohydrate which may reduce the ability of the glycopolymer to bind bacterial lectins. Furthermore, the stability of the glycoconjugate in purified polymers should be assessed as the glycoconjugate formed between sugars and hydrazides is expected to be less favourable compared with that with aldehydes.

Given the lack of evidence for bacterial clustering with the glycopolymers reported in this work, there may be merit in preparing poly(acryloyl hydrazide) with a longer spacer group between the hydrazide and the polymer backbone in order to reduce steric hindrance and increase degrees of freedom when binding lectins. This is something that has been shown to benefit the binding of glycopolymers with model lectins as discussed in the introduction chapter. Indeed, studies using model lectins such as Concanavalin A (ConA) may help initially identify ideal carbohydrate densities and combinations for poly(acryloyl hydrazide) before testing with bacteria.

Appendix

Materials and methods

6.1 Materials

2-((Ethylthio)carbonothioyl) thio-2-methylpropanoic acid (**CTA**) was synthesised according to protocols described in the literature.[1,2] t-Butyl carbazate and N-3(-dimethylaminopropyl)-N'-ethylcarbodiimide hydrochloride (**EDC**) was purchased from Fluorochem. 2,2′-Azobis[2-(2-imidazolin-2-yl)propane] dihydrochloride (**VA-044**) was purchased from Fluorochem and used without further purification. N-[3-(dimethylamino)propyl]methacrylamide (**DMAPMAm**) and N-(3-aminopropyl)methacrylamide (**APMAm**) were purchased from Sigma®, and used without further purification. 4,4'-azobis(4-cyanovaleric acid) (**ACVA**) and 2,2'-azobis(2-methylpropionitrile) (**AIBN**) were purchased from Sigma® and used without further purification. Ethylene diamine (**EDA**) was purchased from Sigma-Aldrich. **D-Mannose** was purchased from Alfa Aesar®, **D-Glucose** was purchased from Fisher Scientific® and **D-Galactose** was purchased from Acros®, all were used without further purification. Imidazole-4-carboxaldehyde (**IMI**) and 2-amino-3-formyl pyridine (**2A3FP**) were purchased from Fluorochem and used without any further purification. Crystal violet was purchased from VWR and used as a 1% solution in H_2O. 2-Nitrophenyl β-D-galactopyranoside (**ONPG**) was purchased from Sigma-Aldrich®. Fluorescein isothiocyanate (**FITC**) and 7-methoxycoumarin-3-carboxylic acid (**MCCA**) was purchased from Sigma®, Flourescamine was purchased from VWR. All solvents were Reagent grade or above, purchased from Sigma-Aldrich®, Fisher Scientific® or VWR®, and used without further purification. LB and clear DMEM used in growth and maintenance of *Vibrio cholerae* was purchased from Sigma® Tetracycline and spectinomycin were purchased from Sigma®. All solvents were Reagent grade or above, purchased from Sigma-Aldrich®, Fisher Scientific® or VWR®, and used without further purification.

6.2 Bacterial strains used in this study

Strains of *Vibrio cholerae* O1 Inaba serotype used in this study were kindly donated by Dr. Perez-Soto:

Strain	*Description*
NPMW1	A1552 carrying pMW-*gfp* plasmid; $Spect^R$
NP5001	A1552 pRW50-oriT promoterless; Tet^R
NP5003	A1552 pRW50-oriT containing upstream region of *ctxAB* promoter; Tet^R
NP5008	A1552 pRW50-oriT containing upstream region of *vspR* promoter; Tet^R
NP5009	A1552 pRW50-oriT containing upstream region of *rbmA* promoter; Tet^R
NP5010	A1552 pRW50-oriT containing upstream region of *rbmC* promoter; Tet^R

Strains were supplemented with antibiotics; Tetracycline (10 µg mL^{-1}), NP5001-010 or Spectinomycin (50 µg mL^{-1}), NPMW1.

Media LB (Sigma): 10 g/L tryptone, 10 g/L NaCl and 5 g/L yeast extract**, clear DMEM (Sigma)**: 0.265 g/L $CaCl_2$, 0.0001 g/L $Fe(NO_3)_3$, 0.09767 g/L $MgSO_4$, 0.4 g/L KCl, 3.7 g/L $NaHCO_3$, 6.4 g/L NaCl,0.109 g/L NaH_2PO_4, 0.084 g/L L-Arg, 0.0626 g/L L-Cys, 0.03 g/L Gly, 0.042 g/L L-His, 0.105 g/L L-Iso, 0.105 g/L L-Leu, 0.146 g/L L-Lys, 0.03 g/L L-Met, 0.066 g/L L-Phe, 0.042 g/L L-Ser, 0.095 g/L L-Thr, 0.016 g/L L-Trp, 0.12037 g/L L-Tyr, 0.094 g/L L-Val, 0.004 g/L choline chloride, 0.004 g/L folic acid, 0.0072 myo-inositol, 0.004 g/L niacinamide, 0.00404 g/L pyridoxine, 0.004 g/L D-pantothenic acid, 0.0004 g/L riboflavin, 0.004 g/L thiamine, 4.5 g/L glucose and 0.584 g/L L-Glu.

6.3 Characterisation

Nuclear Magnetic Resonance (NMR) spectra were recorded on either a Bruker Avance III 300 MHz or a Bruker Avance NEO 400 MHz spectrometer. Chemical shifts are reported in ppm (units) referenced to the following solvent signals: dimethylsulfoxide (DMSO)-d6 H 2.50 and deuterium oxide (D_2O) H 4.79. Gel Permeation Chromatography (GPC) was performed with a Shimadzu Prominence LC-20A fitted with a Thermo Fisher Refractomax 521 Detector and a SPD20A UV-vis Detector. poly(N'-(*tert*-butoxycarbonyl)acryloyl hydrazide) (**boc-P_x**) was analysed using 0.05 M LiBr in dimethylformamide (DMF) at 60 °C as the eluent, and a flow rate of 1 mL min^{-1}. The instrument was fitted with a Polymer Labs PolarGel guard column (50 × 7.5 mm, 5 µm) followed by two PLGel PL1110–6540 columns (300 × 7.5 mm, 5 µm). Molecular weights were calculated based on a standard calibration method using polymethylmethacrylate standards (Agilent®). Poly(acryloyl hydrazide) **P_x** and glycopolymers **P_x-MAN, P_x-GAL P_x-GLU** were analysed using Dulbecco's Phosphate Buffered Saline 0.0095 M (PO_4) without Ca and Mg at 35°C as the eluent and a flow rate of 1 mL min^{-1}. The instrument was fitted with a PL aquagel-OH guard column (50 × 7.5 mm, 8 µm) followed by two Agilent PL aquagel-OH columns (300 × 7.5 mm, 8 µm). Molecular weights were calculated based on a standard calibration method using poly(ethylene glycol) and poly(ethylene oxide) standards (Agilent®). **P_x-IMI** and **P_x-2A3FP** were analysed using 100 mM AcOH/ deionised water at 40 °C as the eluent and a flow rate of 0.6 mL min^{-1}, the instrument was fitted with a guard column (Shodex Asahipak GF-1G 7B) followed by a Shodex Asahipak GF-510 HQ and a Shodex Asahipak GF-310 HQ. UV and Fluorescence data was recorded on a BMG Labtech FLUOstar omega plate reader. Dialysis was carried out in deionised water at room temperature for a minimum of 48 hours using a Spectra/Por 6 1000 Molecular weight

cut-off (MWCO) 38 mm width membrane. Optical images and time-lapse images for **P_x-IMI** and **P_x-2A3FP** were captured using a Nikon Eclipse Ti inverted microscope with a 100 X oil objective or 20 X air objective in DIC (30 ms exposure) or fluorescence (800 ms exposure) incubation at 37 ^oC was used in the case of time-lapse images. Time-lapse imaging of *V. cholerae* incubated with **P1** and **P2** was carried out using an oCelloScope (BioSense solutions) at 37^oC and the respective growth curves were generated using the inbuilt software. Fluorescent time-lapse imaging of *V. cholerae* in the presence of **IMI** was carried out using a JuLI Stage (NanoEntek) using the GFP filter set. Fluorescent images were captured with 800 ms exposure time.

6.4 Methods

6.4.1 Synthesis of p(APMAm) (P1)

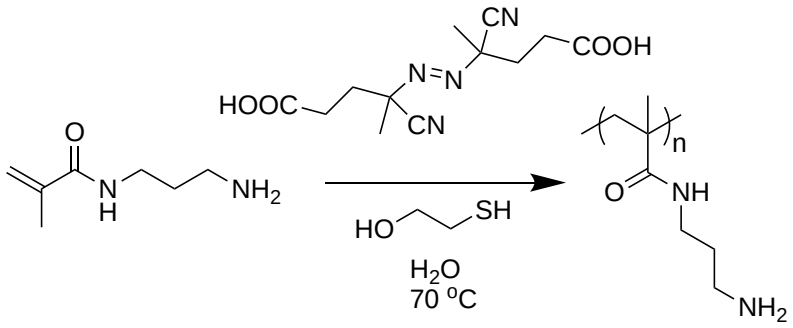

N-(3-aminopropyl)methacrylamide (APMAm) hydrochloride (505.0 mg, 2.770 mmol), 4,4'-azobis(4-cyanovaleric acid) (ACVA) (12.4 mg, 0.033 mmol) and 2-mercaptoethanol (1.0 µL, 0.014 mmol) were dissolved in MilliQ water (2.2 mL). This solution was degassed under argon for 10 minutes and then heated at 70 °C under stirring for 17 hours. After this time, the reaction flask was opened to the air and the crude was precipitated three times into diethyl ether (50 mL). The precipitate was freeze-dried and a crystalline white solid was obtained (70.0 mg, 14% yield). 1H-NMR (300 MHz, D2O) δ (ppm): 3.11 (br, 3H, CH3 backbone), 2.93 (br t, J= 7.0 Hz, 2H, CO-NH-CH2), 1.78 (br, 2H, -CH2-NH2), 1.63 (br, 2H, -CH2-CH2-NH2), 0.98 (br, 1H, CH2 backbone), 0.83 (br, 1H, CH2 backbone). M_n (GPC) 46997, $Đ_M$ (GPC) 1.16.

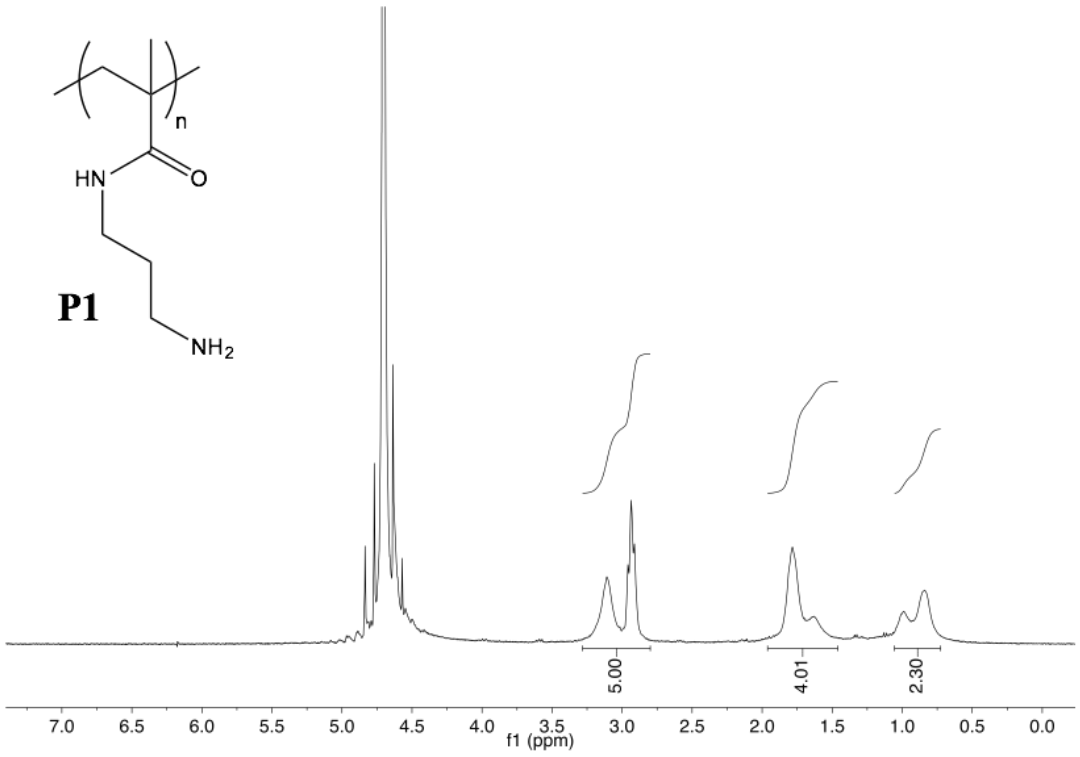

6.4.2 Synthesis of p(DMAPMAm) (P2).

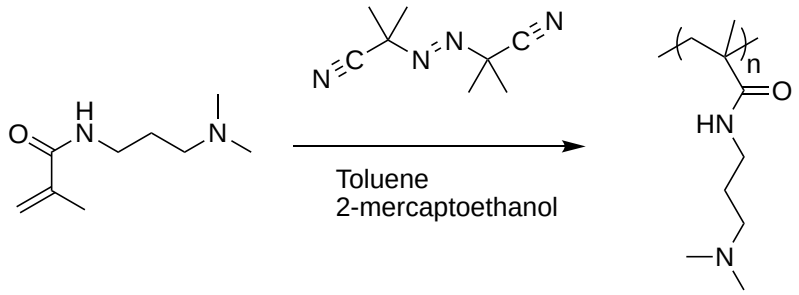

N-[3-(dimethylamino)propyl]methacrylamide (DMAPMAm) (2.2 mL, 12.025 mmol), 2,2'-azobis(2-methylpropionitrile) (AIBN) (19.6 mg, 0.117 mmol) and 2-mercaptoethanol (4.0 µL, 0.056 mmol) were dissolved in toluene (9.5 mL). This solution was degassed under argon for 10 minutes and then heated at 70 °C under stirring for 18 hours. After this time, the reaction flask was opened to the air and the crude was precipitated twice: first into diethyl ether (200 mL) and then into a diethyl ether/ hexane mixture (1:1) (100 mL). The precipitate was freeze-dried and a crystalline white solid was obtained (1.66 g, 87% yield). 1H-NMR (300 MHz, DMSO-

d6) δ (ppm): 7.51 (br, 1H, CO-NH), 2.96 (br, 2H, CO- NH-CH2), 2.19 (br, 5H, CH2-N-(CH3)2 + CH3 backbone), 2.11 (br, 6H, N-(CH3)2), 1.50 (br, 2H, CH2-CH2-N), 0.78 (br, 2H, CH2 backbone). M_n (buffer GPC) 46331, $Đ_M$ (buffer GPC) 1.14.

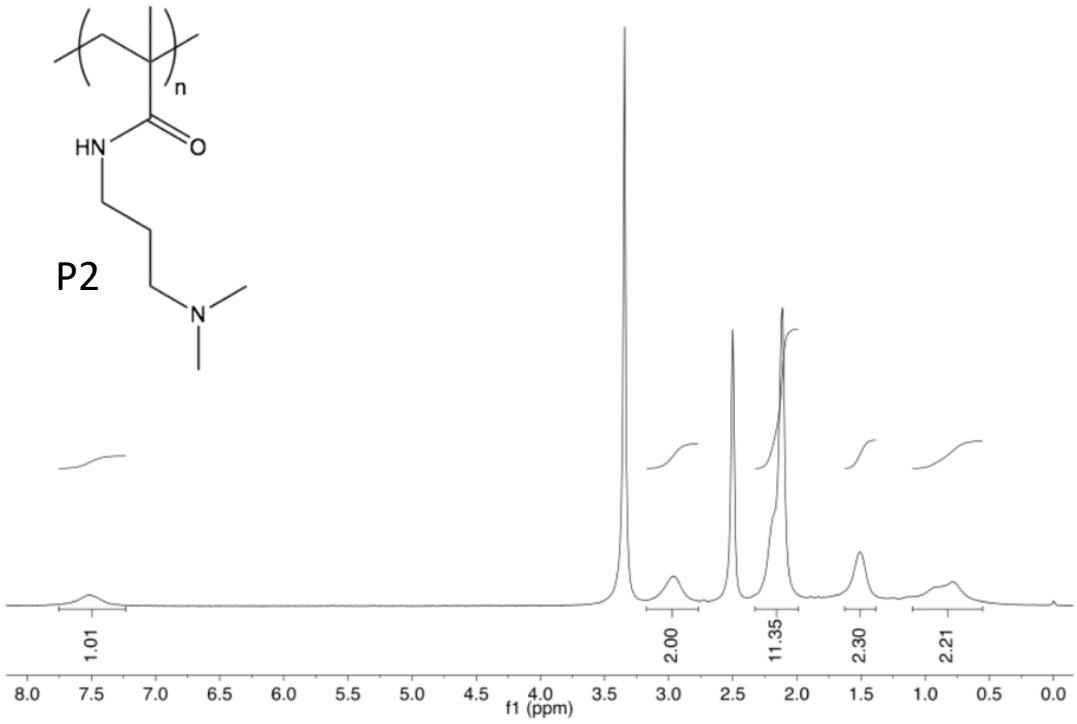

6.4.3 Labelling P1 with CF405S

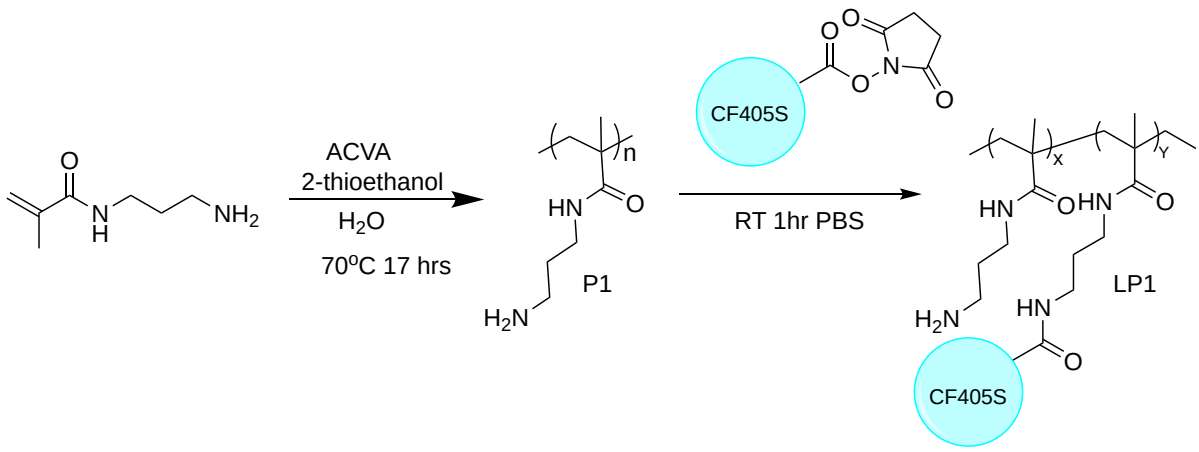

poly(*N*-(3-aminopropyl) methacrylamide) (P1) (5 mg) was dissolved in 0.1 M $NaHCO_3$ (2 mL) meanwhile, anhydrous DMSO (0.1 mL) was to a defrosted vial of CF405S (Biotium) and vortexed to form a 10 mM stock solution of the dye. To the solution containing P1, 50 uL of the dye stock solution was added dropwise and the resulting mixed rocked for 1 hours at room temperature. Purification was carried out firstly using a sephadex G-25 column followed by a sephadex G-10 column. Separation was confirmed by TLC (H_2O) and the material was used without any further purification or characterisation.

6.4.4 Synthesis of tert-Butyl-2-acryloylhydrazine-1-carboxylate (1)

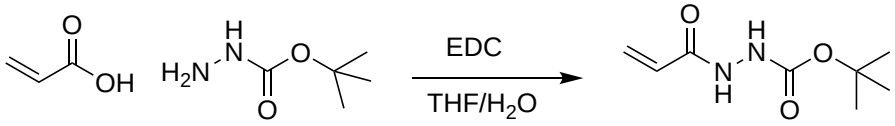

Acrylic acid (3.77 mL, 54.96 mmol), t-Butyl carbazate (6.00 g, 45.00 mmol) was dissolved in 2:1 H_2O:THF mixture (180 ml). N-3(-dimethylaminopropyl)-N'-ethylcarbodiimide hydrochloride (EDC) (12.29 g, 64.11 mmol) was added in portions over 15 minutes and the stirred at RT for 3 hrs. The resulting mixture was extracted

with EtOAc (3 x 75 ml) and the organic layer washed with saturated $NaHCO_3$ (3 x 75 ml) and water (1 x 50 ml) and dried with $NaSO_4$. The solvent was removed under reduced pressure to afford a crude product as an off-white solid which was purified by recrystallisation from hot EtOAc (70°C to r.t.) to afford a white crystalline powder (4.5 g, 49%). ^{1}H-NMR (300 MHz, DMSO-*d6*) δ (ppm) 9.77 (s, 1H), 8.74 (s, 1H), 6.18-6.20 (m, 2H), 5.69 (dd, $^{3}J_{H,H}$= 7.5, 4.5 Hz, 1H), 1.42 (s, 9H) . ^{13}C-NMR (400 MHz, DMSO-*d6*) δ (ppm) 164.5, 155.8, 129.3, 126.1, 79.2, 28.0.

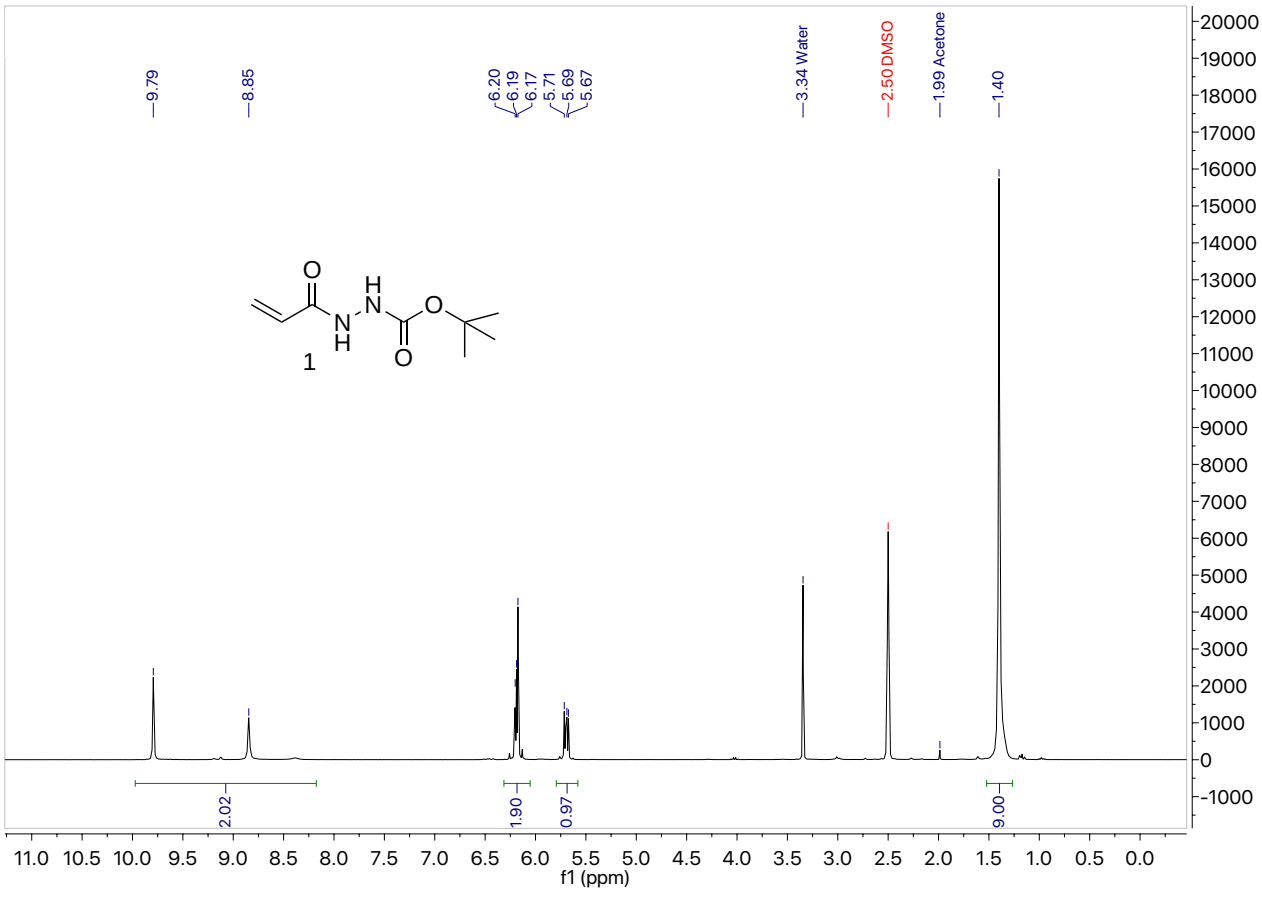

6.4.5 Representative synthesis of Poly(tert-butyl-2-acryloylhydrazine-1-carboxylate) (boc-P_x)

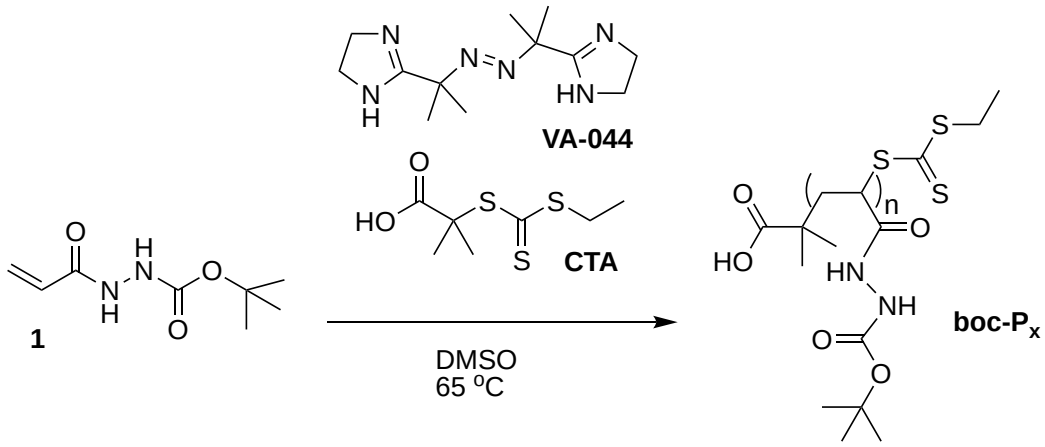

2,2'-azobis[2-(2-imidazolin-2-yl)propane]dihydrochloride (**VA-044**) (3.0 mg, 0.01 mmol), 2-ethylthiocarbonothioylthio-2-methylpropanoic-acid (**CTA**) (10.0 mg, 0.045 mmol) and N'-(tert-butoxycarbonyl)acryloyl hydrazide (**1**) (1.666g, 8.950 mmol) were dissolved in DMSO (10.0 mL) and a 100 µL sample was taken at this stage to calculate conversion (ρ). The solution vessel was sealed with a septum and electrical tape, and degassed by bubbling with argon for 25 minutes. The sealed solution was then left to react at 65°C for 2 hours. The reaction was stopped by allowing the tube to cool using a water bath and exposing it to air. A 100 µL aliquot was taken at this stage to calculate conversion (ρ) and for GPC analysis. The resulting mixture was diluted with H_2O before transferring to dialysis tubing (100 kDa) and dialysed against H_2O. The resulting precipitate was firstly dried by lyophilisation and then in a desiccator with P_2O_5 to afford an off-white solid (835 mg) (**boc-P_x**), monomer conversion 62% by proton NMR, 80% yield. ^{1}H-NMR (300 MHz, DMSO-*d6*) δ (ppm) 1.4 (br,11H, 9H in C(C*H*$_3$)$_3$, 2H in CHC*H*$_2$), 2.1 (br, 1H, CH$_2$C*H*), 8.5 (br, 1H, N*H*) 9.3 (br, 1H, N*H*) GPC (DMF 0.05M LiBr): M_n = 31.63 kg.mol^{-1} $Đ_m$ = 1.23

6.4.6 Representative synthesis of poly(tert-butyl-2-acryloylhydrazine-1-carboxylate) N-(2-aminoethyl) propionamide (boc-P_x-NH_2)

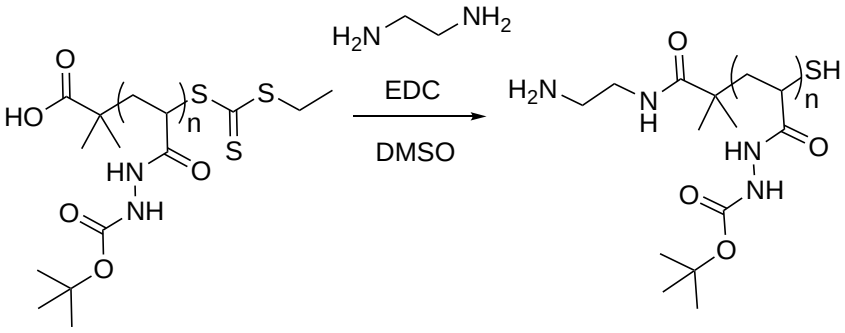

boc-P_x (1 g, 0.13 mmol), and ethylene diamine (5 ml, 150 mmol) were dissolved in DMSO (10 ml). EDC (4 g 20.87 mmol) was added in portions at 0 hr 1hr and 2hr and the mixture stirred at r.t for 3 hours. The resulting mixture was purified by dialysis against H_2O and lyophilized to a white powder (90 %) ^{1}H-NMR (300 MHz, DMSO-*d6*) δ (ppm) 1.4 (br,11H, 9H in C(C*H*$_3$)$_3$, 2H in CHC*H*$_2$), 2.1 (br, 1H, CH$_2$C*H*), 3.17 (br, 4H, NC*H*$_2$C*H*$_2$N) 8.5 (br, 1H, N*H*) 9.3 (br, 1H, N*H*). Loading efficiency ~60-80% (fluram assay).

6.4.7 Representative synthesis of FITC-poly(tert-butyl-2-acryloylhydrazine-1-carboxylate) N-(2-aminoethyl) propionamide (boc-P_x-NH_2-Flu)

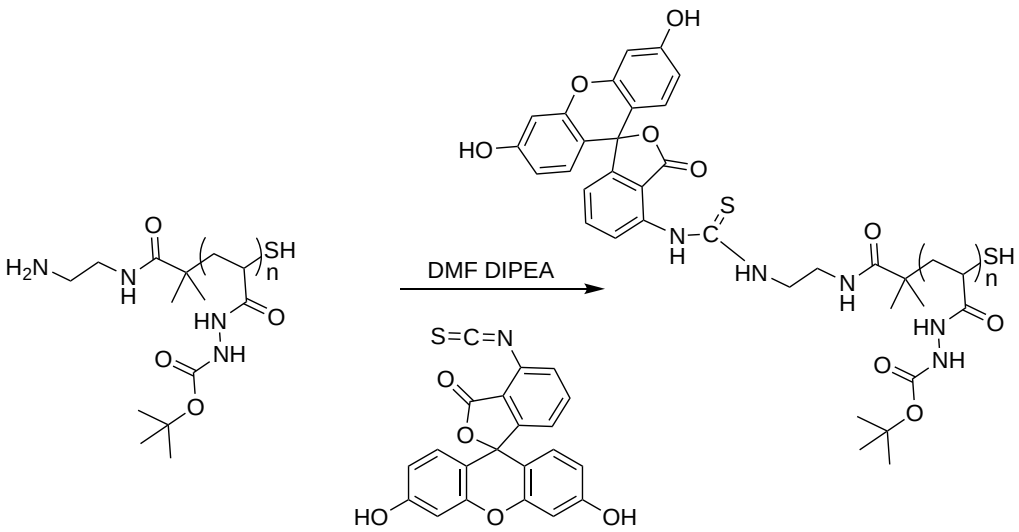

boc-P_x-NH_2 (201 mg), fluorescein isothiocyanate (FITC) (50 mg 0.128 mmol) and DIPEA (50 uL 0.286 mmol) were dissolved in DMF (5 ml) and stirred at RT. After dissolution, a further portion of DMF (5 ml) was added and the resulting mixture was reacted for 18 hours in the dark. An aliquot (100 uL) of the resulting crude mixture was taken for fluorescent GPC analysis before purification of the fluorescent polymer by dialysis against H_2O (5 liters) and lyophilization to yield an orange/yellow solid (70 %). The labelling was confirmed by UV-vis (λ_{max}495 nm) and fluorescence GPC, (λ_{ex},490 nm λ_{em} 510 nm) ^{1}H-NMR (300 MHz, DMSO-*d6*) δ (ppm) 1.4 (br,11H, 9H in C(C*H*$_3$)$_3$, 2H in CHC*H*$_2$), 2.1 (br, 1H, CH$_2$C*H*), 8.5 (br, 1H, N*H*) 9.3 (br, 1H, N*H*) 6.6 (m, 6H, FITC) 7.2 (br, 1H FITC) 10.13 (br, s 2H FITC).

6.4.8 Representative synthesis of FITC-poly(acryloyl hydrazide) N-(2-aminoethyl) propionamide (P_x-MCCA)

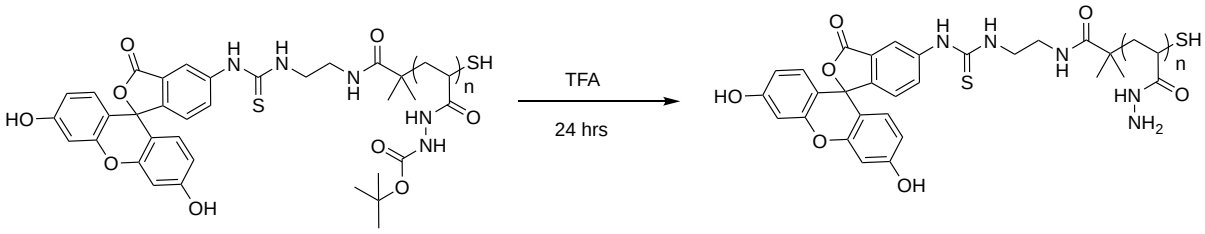

Working in the dark, Trifluoroacetic acid (TFA) (5 mL) was added dropwise to FITC-N'-(tert-butoxycarbonyl) acryloyl hydrazide **boc-P_x-FITC** (200 mg) and stirred at RT for 24 hrs. Excess TFA was evaporated by blowing a steady stream of argon over the solution to a viscous oil which was further diluted with H_2O (5 mL), neutralised with $NaHCO_3$ until effervescence was no longer observed and dialysed against H_2O (5 L) for one week. The purified compound was obtained as an orange, water soluble powder after lyophilization (55%). Presence of the fluorophore was confirmed by fluorescence emission (λ_{em} 510 nm)

^{1}H-NMR (300 MHz, D_2O) δ (ppm)6.5 (br m, 6H) 1.19-2.28 (br m, (3·DP) H), 0.97 (s, 3H) 0.92 (s, 3H).

6.4.9 Representative synthesis of MCCA-poly(tert-butyl-2-acryloylhydrazine-1-carboxylate) N-(2-aminoethyl) propionamide (boc-P_x-MCCA)

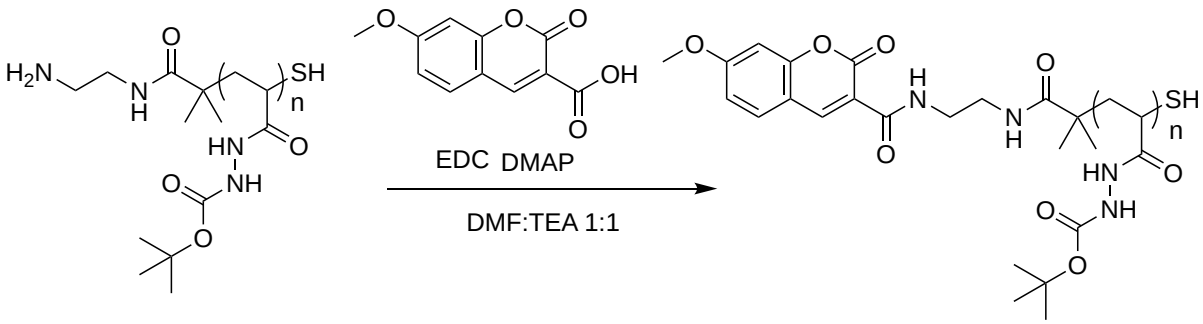

Working in the dark, **boc-P_x-NH_2** (100 mg, 0.011 mmol), 7-methoxycoumarin-3-carboxylic acid (10 mg, 0.045 mmol) and EDC (10 mg, 0.052 mmol) was dissolved in DMF/triethylamine (10 mL 1:1, v/v). In an ice bath and with stirring, DMAP (1 mg, 0.01 mmol) was added and the resulting mixture was left to react overnight. The crude mixture was purified by dialysis against H_2O (5 liters) and lyophilised to yield a light brown solid (70 %).

6.4.10 Representative synthesis of MCCA-poly(acryloyl hydrazide) N-(2-aminoethyl) propionamide (P_x-MCCA)

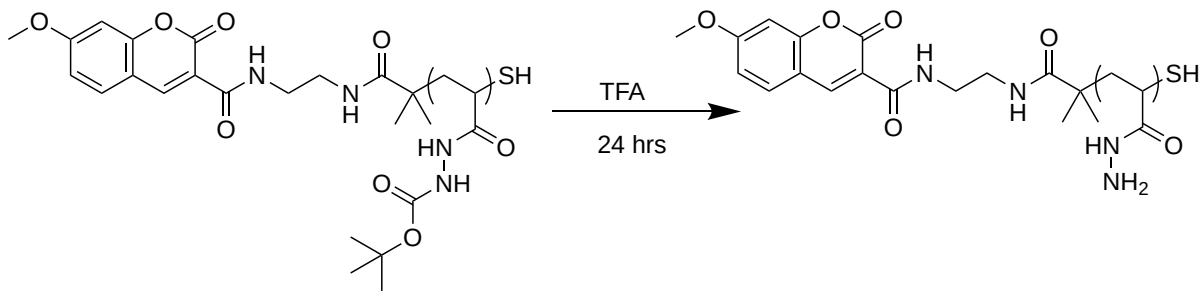

Working in the dark, Trifluoroacetic acid (TFA) (2 mL) was added dropwise to MCCA-N'-(tert-butoxycarbonyl) acryloyl hydrazide **boc-P_x-MCCA** (100 mg) and stirred at RT for 24 hrs. Excess TFA was evaporated by blowing a steady stream of argon over the

solution to a viscous oil which was further diluted with H_2O (5 mL) and washed with chloroform (10 x 5 mL) until no traces of MCCA could be detected in the organic phase. The washed aqueous phase was neutralised with $NaHCO_3$ until effervescence was no longer observed and dialysed against H_2O (5 L) for one week. The purified compound was obtained as a brown, water soluble powder after lyophilization (50%). Presence of the fluorophore was confirmed by fluorescence emission (λ_{em} 402 nm). ^{1}H-NMR (300 MHz, D_2O) δ (ppm) 1.19-2.28 (br m, (3·DP) H), 0.97 (s, 3H) 0.92 (s, 3H)

6.4.11 Representative synthesis of poly(tert-butyl-2-acryloylhydrazine-1-carboxylate) (boc-P_{FRP}) by free radical polymerisation

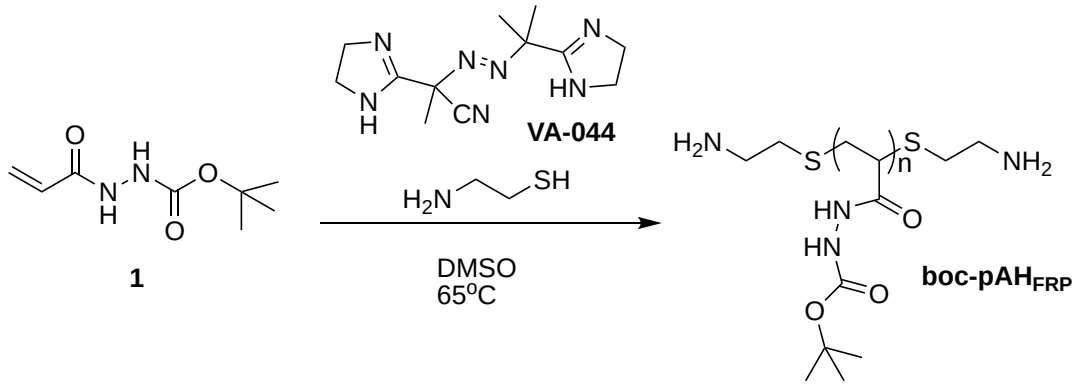

In a typical experiment 2,2'-azobis[2-(2-imidazolin-2-yl)propane]dihydrochloride (**VA-044**) (27.0 mg, 0.07 mmol), cysteamine (27.6 mg, 0.36 mmol) and N'-(tert-butoxycarbonyl)acryloyl hydrazide (**1**) (3.333g, 17.900 mmol) were dissolved in DMSO (20.0 mL) and a 100 µL sample was taken at this stage to calculate conversion (ρ). The solution vessel was sealed with a septum and electrical tape, and degassed by bubbling with argon for 25 minutes. The sealed solution was then left to react at 65°C for 2 hours. The reaction was stopped by allowing the tube to cool using a water bath and exposing it to air. A 100 µL aliquot was taken at this stage to calculate conversion

(ρ) and for GPC analysis. The resulting mixture was diluted with H_2O before transferring to dialysis tubing (100 kDa) and dialysed against H_2O. The resulting precipitate was firstly dried by lyophilisation and then in a desiccator with P_2O_5 to afford an off-white solid (835 mg), monomer conversion 90% by proton NMR, 80% yield. ^{1}H-NMR (300 MHz, DMSO-*d6*) δ (ppm) 1.4 (br, 2H in CHC*H*$_2$), 2.1 (br, 1H, CH$_2$C*H*), 8.5 (br, 1H, N*H*) 9.3 (br, 1H, N*H*) GPC (DMF 0.05M LiBr): M_n =59.63 kg.mol^{-1} $Đ_m$ = 3.43

6.4.12 Representative synthesis of poly(acryloyl hydrazide) (P_x)

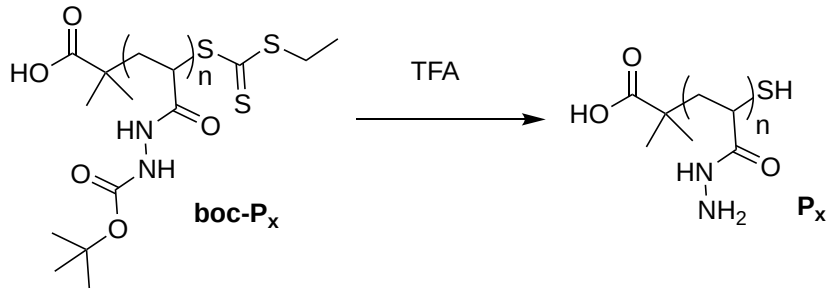

boc-P_x **P_x**

Trifluoroacetic acid (TFA) (6 mL) was added dropwise to N'-(tert-butoxycarbonyl) acryloyl hydrazide (**boc-P_x**) (600 mg) and stirred at RT for 24 hrs at which point excess TFA was evaporated by blowing a steady stream of argon over the solution until an oil had formed. The oil was diluted with H_2O (6 mL) and neutralised with $NaHCO_3$ until effervescence was no longer observed, at which point the solution was transferred to a dialysis membrane, dialysed against H_2O and freeze-dried to a white powder (139 mg 50%) ^{1}H-NMR (300 MHz, D_2O) δ (ppm) 1.19-2.28 (br m, (3·DP) H), 0.97 (s, 3H) 0.92 (s, 3H) SEC (Lonza DPBS 0.0095 M (PO4)): M_n = 15.91 kg.mol^{-1} $Đ_m$ = 1.22

6.4.13 Representative conjugation of P_x with aldehydes: Synthesis of P_x-IMI_x and P_x-$2A3FP_x$

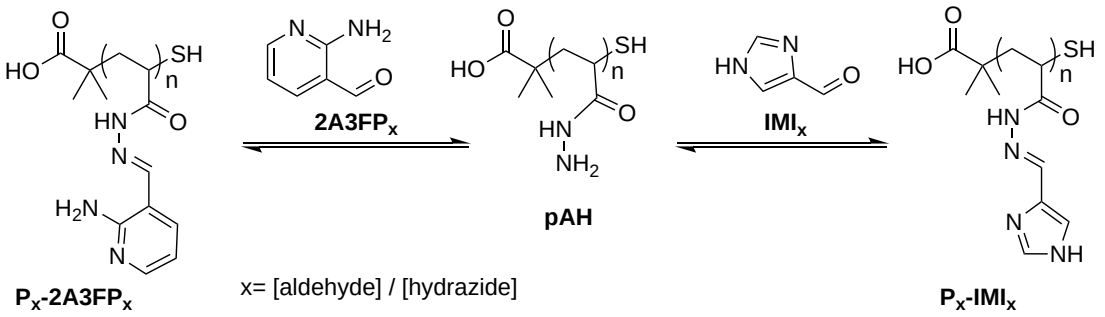

In a typical experiment, a solution of **P_x** (300 µL, 0.116 M, 0.0348 mmol) in AcOH/D_2O (100 mM pH 2.9), was added to either 75 µL (0.25 eq. 0.0088 mmol), 150 µL (0.5 eq. 0.0175 mmol), 175 µL (0.75 eq. 0.0261 mmol) or 300 µL (1.0 eq. 0.0348 mmol) of **IMI** (0.116 M) or **2A3FP** (0.116 M) in AcOH/D_2O (100 mM pH 2.9) and the final volume made was up to 600 µL in the same buffer. Samples were stirred at 60 ^oC for 24 hours. At this point samples were transferred to NMR tubes for calculation of degree of modification by proton NMR. The compounds were used in biological experiments described in this study without further purification.

6.4.14 Representative synthesis of Glycopolymers: P_x-MAN, P_x-GLU and P_x-GAL

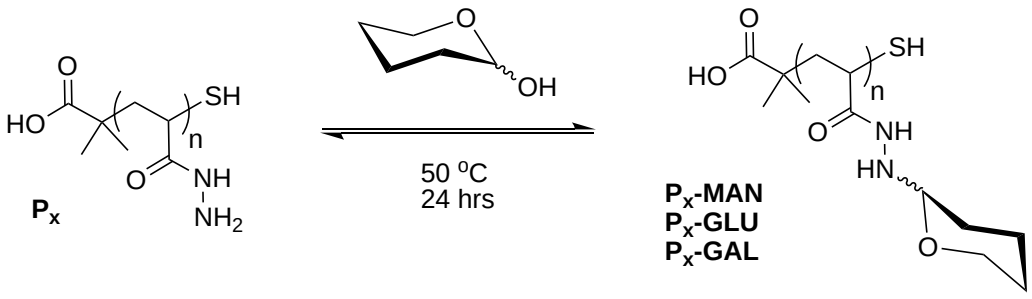

In a typical experiment, in a 96 well plate, a solution of **P_x** (150 µL 0.075 mmol) in acetate buffer (100 mM pH 5.5), was added to 50 µL (2 eq. 0.15 mmol), 100 µL (4 eq. 0.3 mmol) or 150 µL (6 eq. 0.45 mmol) of D-mannose, D-glucose or D-galactose (3 M) in acetate buffer (100 mM pH 5.5) and the final volume made was up to 300 µL. The

plate was sealed and incubated at 50 °C for 24 hours. The compounds were used in biological experiments without further purification.

6.4.15 Fluram Assay

To serial dilutions of **boc-P_x-NH_2** and *tert*-Butyl N-(2-aminoethyl)carbamate **boc-NH_2** in DMSO was added fluorescamine in DMSO (2 eq.). The resulting mixtures were left to react for 30 minutes in the dark with shaking. Fluorescence was recorded using a BMG ClARIOstar plate reader (λ_{ex} 390 nm). Concentration of NH_2 (**boc-P_x-NH_2**) was calculated by interpolation of fluorescence (λ_{em} 465 nm) against a standard curve for **boc-NH_2** (λ_{em} 475 nm).

6.4.16 FITC determination by absorbance

Stock solutions of fluorescein isothiocyanate (FITC) (isopropanol:DPBS 50:50 v/v, 0.4 mmol) and **P_x-Flu** (isopropanol:DPBS 50:50 v/v, 510 µg ml^{-1}) were serially diluted in the same solvent at ranges 12 mM - 45 mM and 25 -102 ug ml^{-1} respectively.Absorbance was recorded on a BMG clariostar plate reader

[FITC] for **P_x-Flu** was calculated by interpolating absorbance values at 490 nm against a standard curve for FITC (abs 490 nm).

6.4.17 Imaging V. cholerae bacterial clustering by LP1

V. cholerae WT were grown in LB overnight and diluted to an OD_{600} of 1.0 in clear DMEM **LP1** was added at a concentration of 0.05 mg mL^{-1}. Images of the clustering were taken after 30 and 60 minutes by mounting 10 µL of sample on microscopy slides, staining with LIVE/DEAD *Bac*Light™ kit (Thermo Scientific) as per the manufacturer's instructions and visualizing using a Zeiss Axio Observer.Z1 microscope with 63X/1.4 Plan Apocromat objective coupled with Apotome2 (Zeiss) using SYTO 9 ($\lambda_{ex}/\lambda_{em}$

485/495), PI ($\lambda_{ex}/\lambda_{em}$ 535/617) and DAPI ($\lambda_{ex}/\lambda_{em}$ 385/617) filter set. Image acquisition was carried out using Zen Pro Software (Zeiss) and further processed in imageJ.

6.4.18 General procedure for 96 well plate imaging assays

V. cholerae NPMW1 (A1552 containing pMW-*gfp* plasmid) were grown overnight in LB + 50 mg ml^{-1} spectinomycin and diluted to an OD_{600} of 0.02 in clear DMEM + 50 µg mL^{-1} spectinomycin. Bacterial suspensions were transferred to a black 96 well plate with a clear bottom and mixed with polymers (0.5 mg ml^{-1} or 0.05 mg ml^{-1}). At this point wells were incubated at 37 ^{o}C imaged every 30 minutes using a Nikon-Eclipse ti microscope with a 20x objective in DIC (30 ms exposure time) and fluorescence (800 ms exposure time) with either GFP or DAPI filter set. Image acquisition was carried out using Nikon NIS-Elements software and final images processed with ImageJ.

6.4.19 V. cholerae growth curves

In a costar clear-bottomed black 96 well plate, colonal overnight cultures of GFP-expressing *V. cholerae* were diluted in clear DMEM with 50 µg ml^{-1} spectinomycin to an OD_{600} of 0.02 for a final volume of 200 µL, to which glycopolymer solutions (0.47 µL) prepared as described above, were added to give a final polymer concentration of 0.05 mg ml^{-1}. All conditions were made up to 200 µL with clear DMEM + 50 mg ml^{-1} Spectinomycin. The 96 well plate was sealed with a BEM-1 breathe easy gas-permeable membrane (Sigma) and incubated at 37 ^{o}C with shaking at 200 rpm (double orbital) inside an FLUOstar Omega plate reader. OD_{600} and GFP fluorescence intensity was recorded every 30 minutes for 15-24 hours using a FLUOstar Omega plate reader.

6.4.20 V. cholerae flocculation assay

Colonal overnight cultures of GFP-expressing *V. cholerae* were diluted in clear DMEM with 50 µg ml^{-1} spectinomycin to an OD_{600} of 1.0 inside plastic cuvettes polymer condition were added at and cuvettes were sealed with parafilm. Turbidity was measured (OD_{600}) using a benchtop spectrophotometer at varying timepoints. between timepoints cuvettes were secured in a cuvette holder at room temperature without shaking.

6.4.21 Crystal Violet Assay

As described by O'Toole[3], non-adhered *V. cholerae* were firstly removed by turning over the plate and dumping the liquid followed by submerging the whole plate in a small tub of distilled water and gently shaking out the water into a separate container. This was repeated until no further loose bacterial debris could be removed.

200 µL of 1% w/v crystal violet solution in dH_2O was added to each condition and left at room temperature for 30 minutes to ensure complete staining of the biofilm. Crystal violet was removed by submerging the plate in dH_2O and washing until no more crystal violet could be visibly washed from the plate. 200 µL of 95% ethanol was added to each condition to solubilise the crystal violet and the plate was stood for 10 minutes at room temperature. Finally, sonication of the plate was carried out for 10 seconds in a water bath to ensure homogeneous mixing of the crystal violet and dislodging of any remaining adhered biofilm. CV staining was quantified by absorbance at 550 nm in a FLUOstar Omega plate reader with 95% ethanol as a blank.

6.4.22 Transcriptional assay: β-galactosidase assay

To monitor the expression of genes related to virulence, adhesion factors and biofilm formation, various reporter strains of *V. cholerae* A1552 containing the pRW50 oriT plasmid were constructed and kindly donated by Dr. Perez-Soto.[4]

-Buffer and reagent preparation

Prior to the assay, Z-Buffer and ONPG (O-Nitrophenyl-β-D-galactopyranoside) solution were prepared according to a protocol used in the Grainger group (Birmingham). Z-buffer was prepared according to the following recipe: 0.80 g $Na_2HPO_4.7H_2O$ (0.06M) 0.28g $NaH_2PO_4.H_2O$ (0.04M) 0.5 mL 1M KCl (0.01M)0.05 mL 1M $MgSO_4$ (0.001M) were dissolved in 40 mL deionised water, adjusted to pH 7.0 and finally made up to 50 mL.

ONPG solution was prepared by dissolving 160 mg ONPG in 200 mL Z-buffer with 270 µL 2-mercaptoethanol. The bottle was covered in foil to protect from light and stored at 4 ^oC for a maximum of a week.

-Assay protocol

Overnight cultures (1 mL) of the desired reporter strains grown in LB were pelleted by centrifugation (7000 rpm, 5 minutes) and the supernatant replaced 1 mL DMEM + Tetracycline (10 µg ml^{-1}). The concentration of the bacterial suspension was measured in each case and adjusted to a starting OD_{600} of 0.2 in 1 mL of supernatant + polymer in Eppendorf tubes. Each condition was prepared in a separate tube and incubated at 37^oC with shaking. At the desired timepoint, the OD_{600} was measured for each condition and cells were lysed by adding 10 µL toluene, 10 µL 1% sodium deoxycholate and vortexing. Tubes were left open to allow excess toluene to evaporate for 20 minutes, after which each condition was vortexed and 100 µL of the lysate added to 5 mL developing tubes in triplicates. Using a timer, 2500 µL of ONPG solution was added

to each developing tube every 10 seconds. After 20 minutes the reaction was quenched by addition of 1 mL of 1M Na_2CO_3 to each tube every 10 seconds as before. 300 µL of each condition was transferred into a 96 well plate and the absorbance at 420 nm was measured. ONPG solution was used as a blank and care was taken to avoid transferring bacterial debris to the well plate which would interfere with the reading. Growth adjusted readings were reported in miller units using the equation:

$$\beta - galactosidase\ activity\ (Miller\ Units) = \frac{1000 * 2.5 * total\ reaction\ volume * Abs_{420}\ nm}{4.5 * time * lysis\ volume * OD_{600}}$$

1000/4.5 is a conversion factor to convert the absorbance at 420 nm into moles of o-nitrophenol. 2.5 is used to convert OD_{600} into mg of dry protein based on an assumption that OD_{600} of 1.0 corresponds to 0.4 mg/mL of dry bacterial mass. Time is expressed in minutes and volumes are in mL.

6.5 References

1 J. Skey and R. K. O'Reilly, *Chem. Commun.*, 2008, **31**, 4183.

2 D. N. Crisan, O. Creese, R. Ball, J. L. Brioso, B. Martyn, J. Montenegro and F. Fernandez-Trillo, *Polym. Chem.*, 2017, **1**, 1392–9.

3 G. A. O'Toole, *JoVE*, 2011, 1–2.

4 N. Perez-Soto, L. Moule, D. N. Crisan, I. Insua, L. M. Taylor-Smith, K. Voelz, F. Fernandez-Trillo and A. M. Krachler, *Chem. Sci.*, 2017, **8**, 5291–5298.